Investigation and Characterization of Off-Focus Radiation Peaks from a Digital Breast Tomosynthesis System

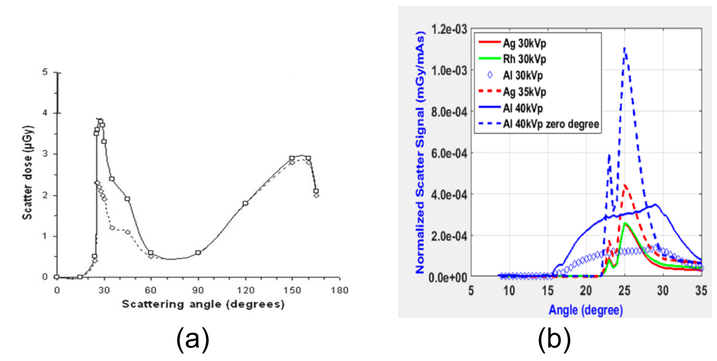
Maiar Abdelwahab[1,2], Dr Paola Baldelli[2]

[1]School of Physics – University College Dublin. [2]BreastCheck – The National Breast Screening Programme, Ireland

Introduction

Digital breast tomosynthesis (DBT) is an advanced form of mammography that acquires multiple low-dose X-ray projections to improve breast cancer detection by reducing tissue overlap. During imaging, scatter radiation is produced when X-rays interact with tissue and equipment, while off-focus radiation originates within the X-ray tube and collimator assembly.

Previous studies by Judge *et al.* (2013) and Yang *et al*. (2016) **(Fig 1.)** reported unexpected radiation peaks at ~25–30° around Hologic mammography systems, which were attributed to off-focus radiation but were not experimentally characterised.



(a) (b)

Figure 1: (a) Unexpected scatter peak at ~30° from 2D Hologic Selenia unit, (b) Unexpected scatter peak at ~25° from Hologic DBT unit [1][2].

This study investigates and characterises anomalous radiation peaks in a Hologic 3D DBT system under different fields of view, acquisition settings, and target/filter combinations, and assesses their impact on imaging performance.

Method

System & Dosimetry:

- Hologic 3Dimensions DBT system (a-Se detector).
- RaySafe X2 MAM sensor (threshold: 1 μGy).

Experimental Setup:

- Detector positioned 1m below breast table centre.
- Measurements acquired over 0–360°.

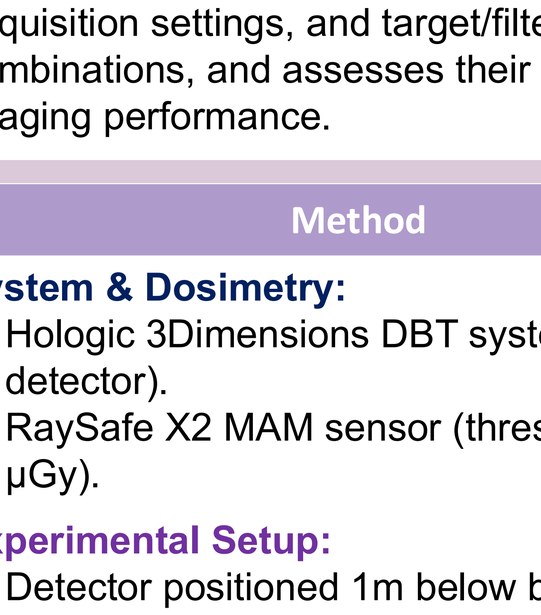


Figure 2: Experimental setup for angular radiation measurements around the breast table (2D and 3D DBT modes).

Exposure Conditions:

- 2D mode: W/Rh, W/Ag (35 kVp, 200 mAs).
- 3D mode: W/Al (30 kVp, 100 mAs).

Investigations:

- Fields of view: 15×15, 18×24, 24×29 cm².
- Acquisition positions: −30°, 0°, +30°.



Figure 3: Different acquisition positions (−30°, 0°, +30° relative to the breast table)

- Target/filter combinations.
- Spatial dose distribution mapping.

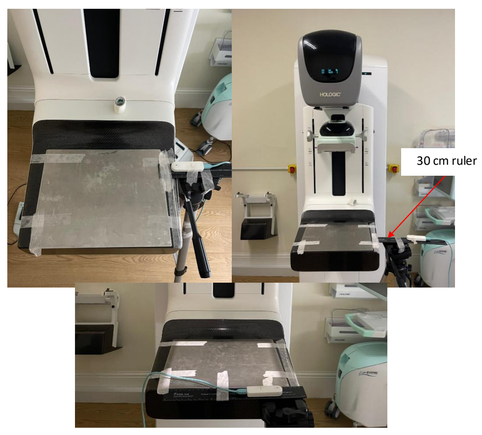
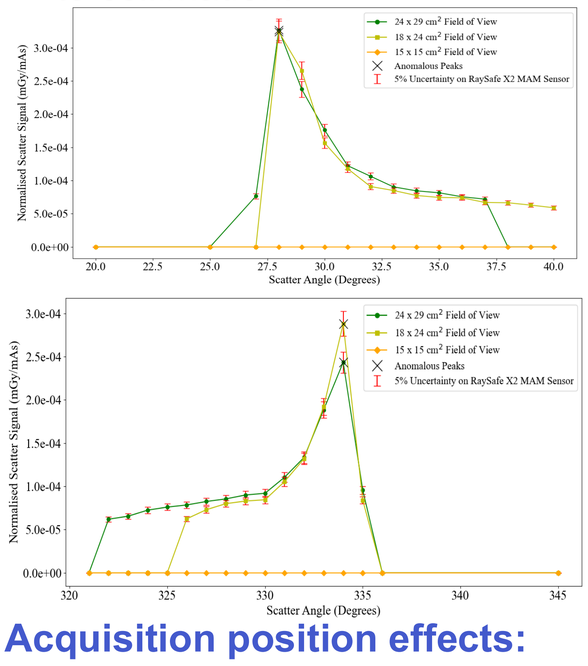


Figure 4: Experimental setup for spatial dose measurements around the detector (heatmap generation)

Results

Two consistent anomalous peaks were observed at ~28° ± 1° and ~334° ± 1° across most configurations.
These peaks were:

- Present for 24×29 cm² and 18×24 cm² fields of view.
- Absent for the 15×15 cm² field of view due to collimation.



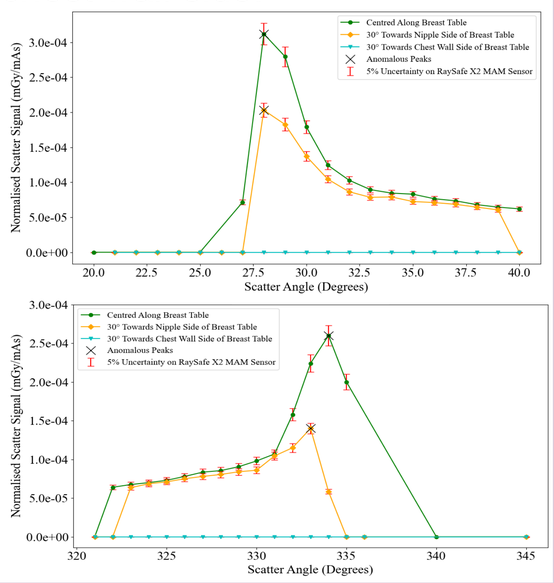
(a)

(b)

Figure 5: Scatter signals for all fields of view (W/Rh, 35 kVp, 200 mAs): (a) 20–40° range, (b) 320–345° range.

Acquisition position effects:

- The two consistent anomalous peaks were observed when the detector was centred and towards the nipple side.
- No peaks detected when positioned towards the chest wall side.



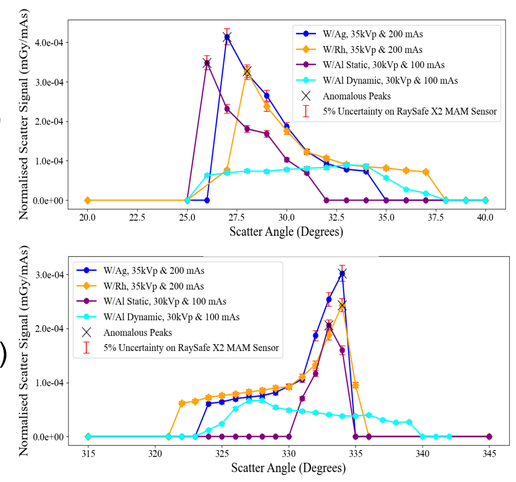
(a)

(b)

Figure 6: Detailed scatter signals across acquisition positions (W/Rh, 35 kVp, 200 mAs): (a) 20–40°, (b) 320–345°.

Target/filter combinations:

- W/Ag produced higher scatter signals than W/Rh.
- W/Al (3D dynamic mode) showed no distinct peaks.



(a)

(b)

Figure 7: Detailed scatter signals for all target/filter combinations showing anomalous peak regions: (a) 20–40°, (b) 320–345°.

Spatial dose distribution:

- Dose decreased smoothly with distance from the detector.
- Elevated dose regions observed at ~28° and ~334° outside the primary field; consistent with previously observed anomalous peaks.

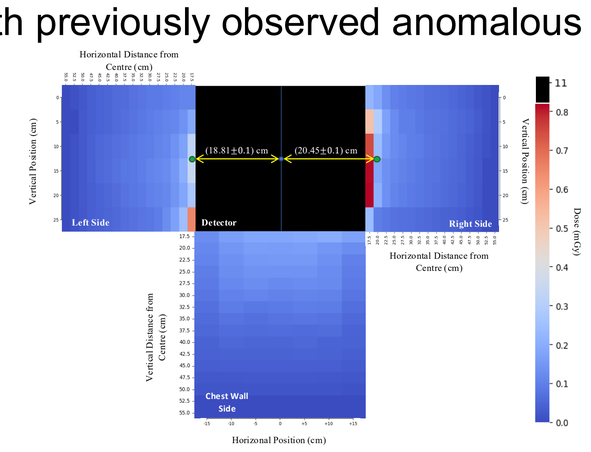


Figure 8: Spatial dose distribution around the breast table used to identify locations of anomalous peaks.

Discussion & Conclusion

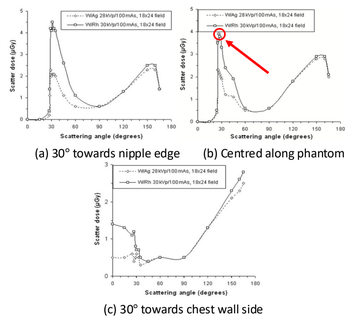
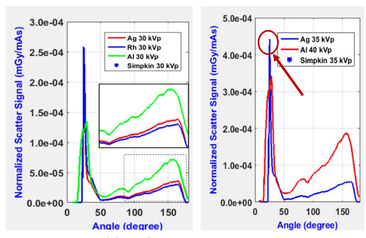


Figure 9: Scatter dose distributions from Judge *et al*. (2013) showing peaks at ~30° for nipple-side (a) and centred acquisitions (b), with no peak at the chest wall position (c) [1].



(a) (b)

Figure 10: Normalised scatter signals from Yang *et al*. (2016) showing peaks at ~25–30° across different acquisition settings [2].

- The consistent presence of anomalous peaks at ~28° and ~334° demonstrates a non-random, system-specific radiation pattern.
- Strong agreement with Judge *et al.* (2013) and Yang *et al.* (2016) confirms their origin from the X-ray tube and collimator assembly.
- These findings indicate that the peaks are due to off-focus radiation, not conventional scatter.
- Spatial dose mapping supports this, showing localised elevated regions outside the primary field.
- Off-focus radiation contributes minimally to dose but may affect image quality in extreme cases.

References

[1] Judge, M.A., Keavey, E. and Phelan, N. (2013). Scatter radiation intensities around full-field digital mammography units. *The British Journal of Radiology*, 86(1021), pp.20120130–20120130. doi: https://doi.org/10.1259/bjr.20120130.

[2] Yang, K., Li, X. and Liu, B. (2016). Scatter radiation intensities around a clinical digital breast tomosynthesis unit and the impact on radiation shielding considerations. *Medical Physics*, 43(3), pp.1096–1110. doi:https://doi.org/10.1118/1.4940352.

Radiation Protection Requirements for Ducts and Penetrations through Shielding Barriers

Mícheál John Ó Colla[1], David Lavin[2], Brendan Tuohy[2]
[1]Medical Physics, University of Galway, Ireland
[2]Department of Medical Physics & Clinical Engineering , University Hospital Galway, Ireland

Background

Ducts and service penetrations passing through X-ray room shielding barriers for ventilation, plumbing and electrical services require additional shielding to ensure the integrity of the barriers are not compromised. The main aim of this project was to determine the minimum level of shielding required for such penetrations to maintain adequate radiation protection. Current practice by some Radiation Protection Advisors is to recommend an arbitrary length of shielding equal to three times the widest dimension of the penetration, despite limited experimental evidence to support this approach. Figure 1. illustrates that the required shielding overlap can be determined using the equations W + 2W or W + 2H, depending on whether the duct has a greater width (W) or height (H). Overlapping the duct with three times the widest duct dimension should satisfy the equation in most cases.

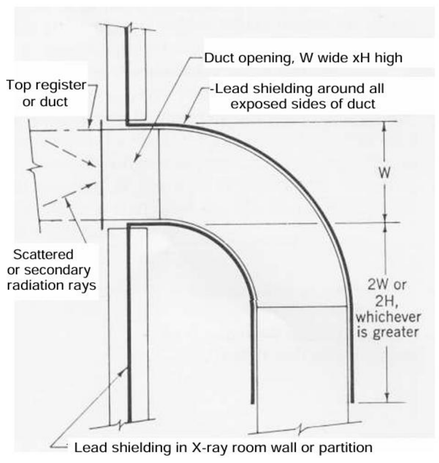


Figure 1: Plan view of radius elbow in ductwork running through partition of X-ray room, exposed to secondary or scattered radiation (Lead Industries Association, Inc., 1979).

Methodology

Measurements were performed in a fluoroscopy room. The X-ray tube was positioned above a 20cm Perspex phantom to generate scatter, while a Code 4 lead shielding barrier containing a penetration was placed a fixed distance from the phantom. Various circular duct configurations were attached to the penetration. Dose rates through the duct were measured with a Fluke 451P survey meter for increasing lengths of Code 4 lead wrap on the duct. These were compared to reference measurements taken behind an intact section of the shielding barrier. Parameters investigated included duct type (plastic or metal; straight or with a 90° bend), lead wrap thickness and width, scatter energy (81 kVp and 102 kVp), distance from the scatter source and angle of incidence. Three table positions relative to the phantom were defined as Left, Centre and Right with the table at 0 cm, 42.5 cm, and 85 cm respectively. Additional measurements were also acquired with the phantom at greater distances from the duct. The general set-up is shown in Figure 2a & 2b.

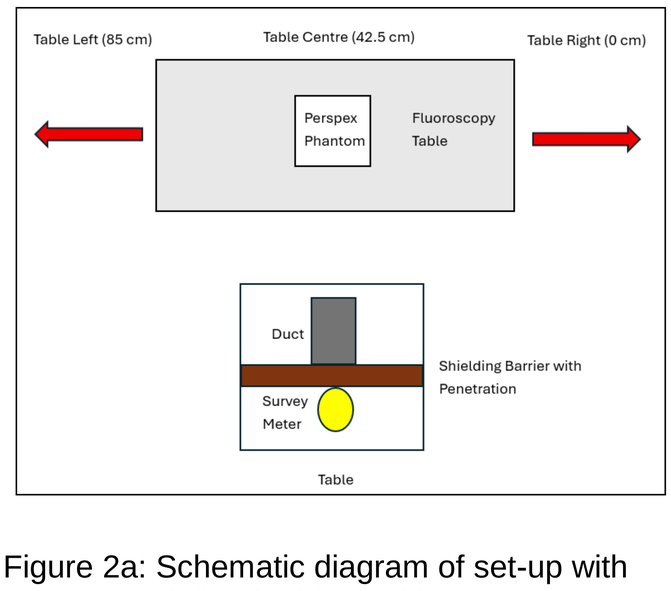


Figure 2a: Schematic diagram of set-up with defined table positions



Figure 2b: Side-view image of set-up

Results and Discussion

Results demonstrated that reduced lead wrap lengths provided equivalent shielding to current recommendations in certain cases. It was found that straight ducts were adequately shielded with a wrap 2.5x the diameter in many configurations. This is illustrated in Figure 3, which compares dose rate measurements for different lengths of lead shielding wrap on the duct with those obtained for fully shielded measurements. The measurements were taken for a 100 mm diameter circular duct at 102 kVp with the phantom in the Table Right position. 90˚ angled ducts required substantially less lead wrapping to meet the design goal. For a 100 mm lead overlap (i.e. 1x diameter wrap), it was found that adequate shielding was provided at each of the 3 table positions. At 81 kVp and 102 kVp the dose rate readings for the 100 mm lead overlap were lower than the shielded reference data. The results for 102 kVp are shown in Figure 4.

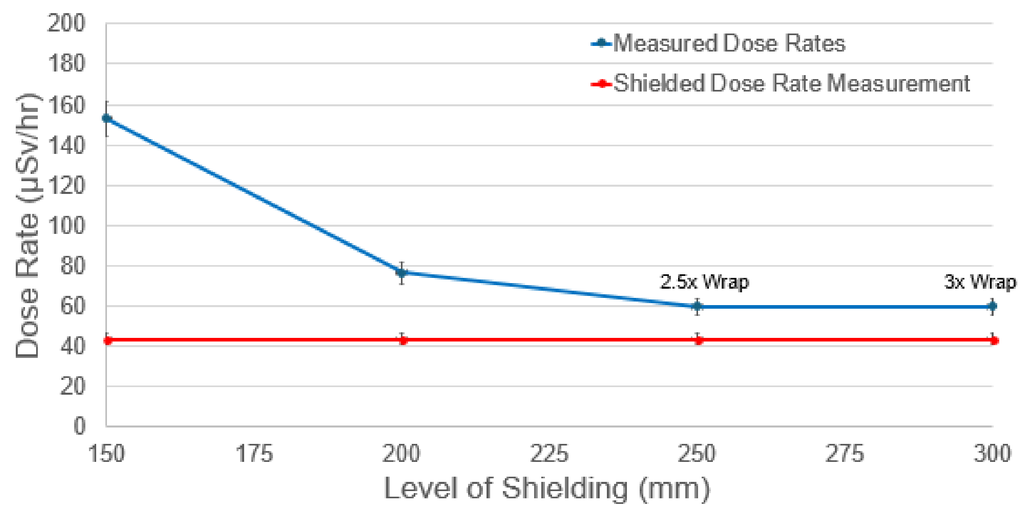


Figure 3: Comparison of measured dose rates through a straight 100 mm diameter duct versus shielded dose rate measurements at 102 kVp in the Table Right position.

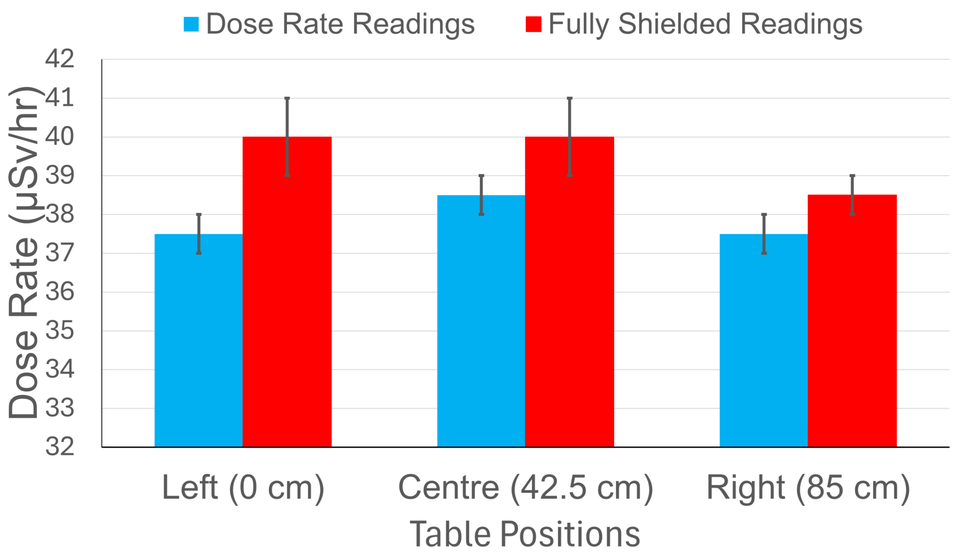


Figure 4: Comparison of measured dose rates through a 90˚ duct (100 mm diameter) with a 100 mm lead shielding overlap, versus shielded dose rate meaurements at 102 kVp in each of the defined table positions.

Conclusion

These findings support an evidence based shielding approach for ducts and penetrations that maintains radiation safety while reducing unnecessary material use, cost and construction complexity for diagnostic imaging facilities. Implementing these recommendations at design stage could lead to significant resource savings without compromising staff or public radiation safety. Further work required for different duct types and angulations.

References

Lead Industries Association, Inc. *A guide to the use of lead for radiation shielding. New York: Lead Industries Association, Inc.*
British Institute of Radiology (2012) *Radiation Shielding for Diagnostic Radiology*. British Institute of Radiology.
National Council on Radiation Protection and Measurements (2004) *Structural Shielding Design for Medical X-ray Imaging Facilities. NCRP Report No. 147, Bethesda, Maryland:*
Radiological Protection Institute of Ireland (RPII) (2009). *The Design of Diagnostic Medical Facilities where Ionising Radiation is used. Dublin: Radiological Protection Institute of Ireland.*

Making High-Resolution Tractography for Neurosurgical Guidance Practical with SMS

Michael O'Neill*[1], Jess Fitzpatrick[1] , Alan Stone[1], Aisling O'Driscoll[2], Seamus Looby[2]

1 Medical Physics & Clinical Engineering, Beaumont Hospital 2 Department of Radiology, Beaumont Hospital

**Corresponding author: michaeloneill@beaumont.ie*

Introduction

- Tractography uses multi-directional diffusion weighted MR imaging (DWI) and a mathematical model to image pathways in the brains network.
- Tractography is used in neurosurgical planning to help identify and avoid eloquent brain regions during resection.
- Constrained Spherical Deconvolution (CSD) models have recently replaced Diffusion Tensor (DTI) models as the gold standard mathematical model[1].
- CSD provides more accurate Tractography (see Figures 1 & 2) but increases scan times (~15mins) due to the need for isometric voxels and more diffusion directions[1].
- Simultaneous Multi-Slice (SMS) techniques allow two or more slices to be acquired at the same time.
- SMS reduces scan time proportional to the SMS factor without affecting image distortion or SNR[2].
- This study investigates the optimal SMS factor for fulfilling CSD requirements (isometric voxels and more diffusion directions) while maintaining scan time and image quality

Fig 1.

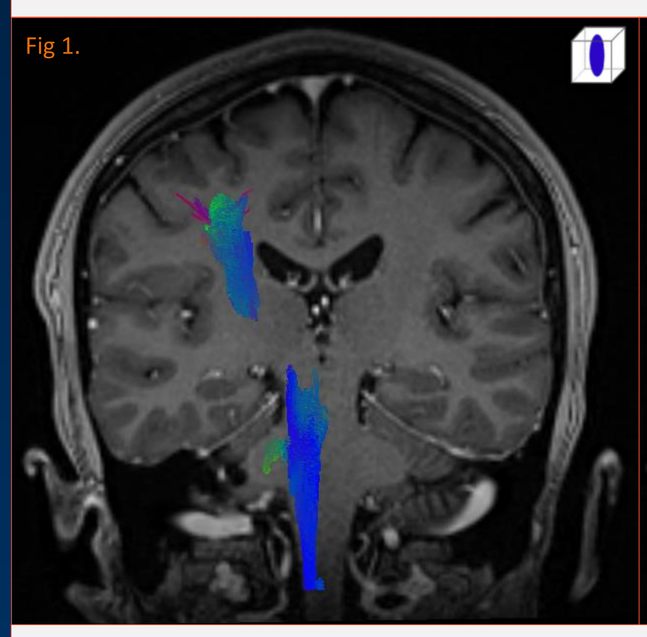


Fig 2.

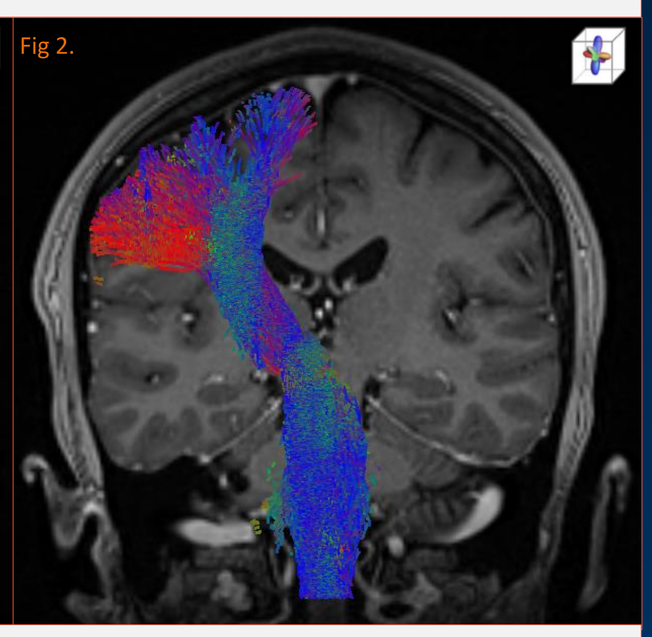


Fig. 1–2: Right motor corticospinal tract generated from (Fig. 1) a DTI model and (Fig. 2) a CSD model. Fiber colours indicate direction: inferior–superior (blue), left–right (red), and anterior–posterior (green).

Methodology

- A 3% agar gel phantom was used as a uniform test object (Fig 3).
- All scans were acquired using a 20 channel Head/Neck coil (Fig 4) on a Siemens 1.5T Sola MRI.

Fig 3.



Fig 4.



Fig. 3: 3% agar gel phantom stored in a container to provide a stable, uniform medium for MRI acquisition.
Fig. 4: Siemens 20-channel head/neck radiofrequency coil used with the 1.5T Siemens Sola system.

- Phantom images were acquired using the protocols listed in Table 1.

Protocol	TR (ms)	Voxel sizes (mm)	Slices	b0 vols	b1000 vols	Diffusion Directions	SMS factor	Scan time
Current Base	3900	1.8x1.8x5.0	25	12	60	20	0	4:58
3mm³_s0	8300	3.0x3.0x3.0	68	2	60	30	0	9:17
3mm³_s2	4200	3.0x3.0x3.0	68	2	60	30	2	4:47
3mm³_s3	2700	3.0x3.0x3.0	66	2	60	30	3	3:10
2mm³_s0	12000	2.0x2.0x2.0	94	2	60	30	0	14:10
2mm³_s2	6100	2.0x2.0x2.0	94	2	60	30	2	6:55
2.5mm³_s0	9900	2.5x2.5x2.5	80	2	60	30	0	11:06
2.5mm³_s2	5000	2.5x2.5x2.5	80	2	60	30	2	5:40

Table. 1: Summary of the current base protocol and proposed protocols that meet CSD requirements. Protocols highlighted in red were found to have clinically unfeasible TR & scan times and were excluded.

- The following image quality measurements were performed on slices in the middle of the phantom:
  - Image Integral Uniformity (IU).
  - Signal-to-noise ratio (SNR).
  - Ghosting ratio (GR).
  - Qualitative artefact assessment

Results

- Measurements of SNR, Image Integral Uniformity & Ghosting ratios yielded the following results (see Figure 5, 6, 7 and 8).

Fig 5 (A)

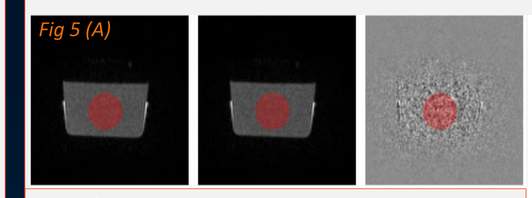


Fig 5 (A): Placement of ROIs for SNR measurement on each slice. Mean signal and standard deviation were extracted from the raw and subtracted images, respectively.
Fig 5 (B) 3mm³_S0 and 3mm³_S2 produced similar SNR values, followed by the Base, 2.5 mm³, 3 mm³, and 2 mm³ protocols.

Fig 5 (B)

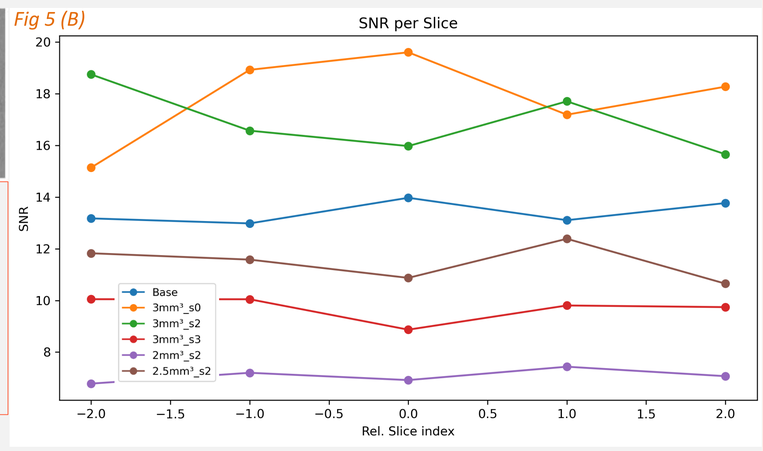


Fig 6 (A)

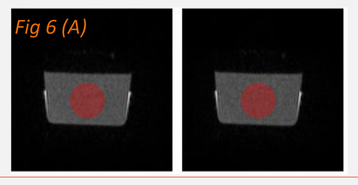


Fig 6 (A): Placement of ROIs for Integral Uniformity (IU) measurement on each slice. Max and min signal values were extracted from the raw images for calculation.
Fig 6 (B): 3 mm³_S2 produced the highest and most consistent IU, followed by 3 mm³_S0, the Base, 2.5 mm³, 3 mm³, and 2 mm³ protocols.

Fig 6 (B)

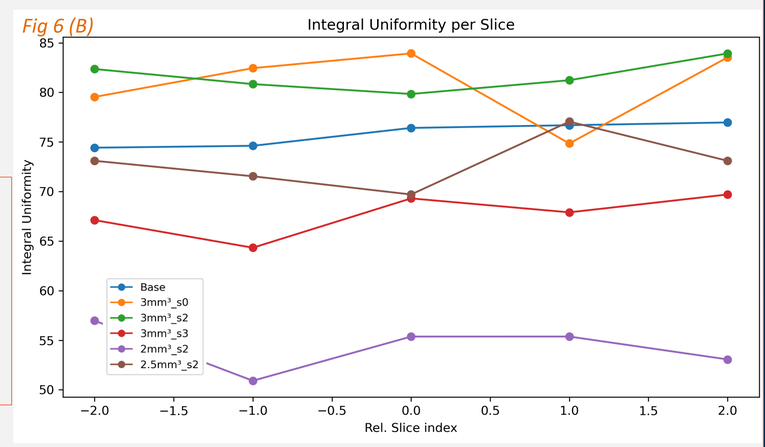


Fig 7 (A)

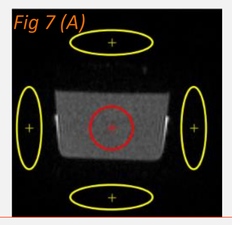


Fig 7 (A): Placement of ROIs for Ghosting Ratio (GR) measurement on each slice. Mean signal values from the red and yellow ROIs were extracted for calculation.
Fig 7 (B): The dotted line indicates the acceptable clinical threshold for GR (<2.5%)[3]. All protocols, except 3 mm³_S0, produced acceptable ghosting levels.

Fig 7 (B)

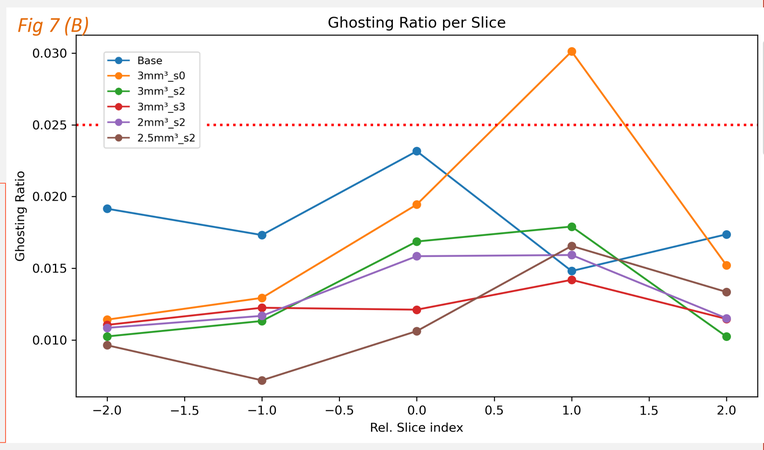


Fig 8

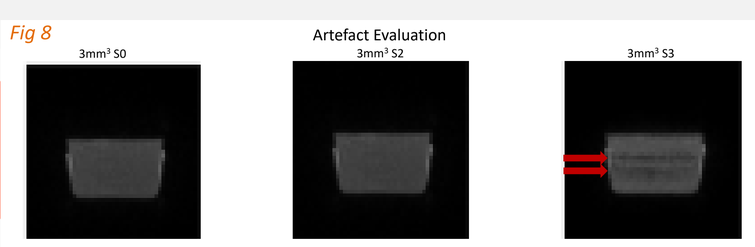


Fig 8 (A): Image Artefacts were observed in the 3mm³_S3 protocol. The images here show the central slice of the agar phantom for the 3mm³_S0, 3mm³_S2 and 3mm³_S3.

Discussion

- All proposed protocols increased the diffusion directions to 30, which is more suitable for Constrained Spherical Deconvolution (CSD).
- Proposed protocols were compared against the standard Base protocol. Protocols with image quality measurements substantially below the Base were excluded from further consideration.
- The **2 mm³_S2** and **3 mm³_S3** protocols performed poorly for Integral Uniformity (IU) and Signal-to-Noise Ratio (SNR) relative to Base. The smaller voxel volume of the 2 mm³_S2 protocol (less than 50% of the Base) contributes to reduced SNR and IU.
- The **3 mm³_S3** protocol exhibited aliasing artefact due to the limited number of coil elements in the head-foot direction of the 20-channel head coil. This means an SMS factor of 3 is unachievable.
- The **3 mm³_S0** protocol demonstrated excellent SNR and IU but produced unacceptable GR results. Because of this and with its near 10-minute scan time, it was excluded.
- **3 mm³_S2** outperformed **2.5 mm³_S2** in SNR, IU, and GR but provided reduced in-plane resolution.
- The **2.5 mm³_S2** protocol was selected for future patient studies as a balanced option between image quality and scan time.
- If higher SNR is required for radiological assessment or CSD algorithms, **3 mm³_S2** may be considered.

Clinical Impact

This phantom testing informed the creation of a high angular resolution DWI protocol. This new protocol will be used in future patient studies where CSD based tractography will be applied.

References

[1]. Radwan, A. M., Emsell, L., Vansteelandt, K., Cleeren, E., Peeters, R., de Vleeschouwer, S., Theys, T., Dupont, P., & Sunaert, S. (2024). Comparative validation of automated presurgical tractography based on constrained spherical deconvolution and diffusion tensor imaging with direct electrical stimulation. Human Brain Mapping. 10.1002/hbm.26662

[2]. Barth, M., Breuer, F., Koopmans, P. J., Norris, D. G., & Poser, B. A. (2016). Simultaneous multislice (SMS) imaging techniques. In Magnetic Resonance in Medicine (Vol. 75, Issue 1, pp. 63–81). John Wiley and Sons Inc. https://doi.org/10.1002/mrm.25897

[3]. American Association of Physicists in Medicine (2010). Acceptance Testing and Quality Assurance Procedures for Magnetic Resonance Imaging Facilities. Report of MR Subcommittee Task Group I. https://www.aapm.org/pubs/reports/rpt_100.pdf

Seeing the Unseen

A Critical Look at Detecting Defective Detector Elements in Digital Mammography

Ali Asghar Ayaz, Colin Walsh, Evon Smyth

Medical Physics and Bioengineering Department (MPBE), St James' Hospital aayaz@stjames.ie

INTRODUCTION

During routine quality assurance of a digital mammography system, a subtle image artefact raised concerns regarding a potential defective detector element.

This study aimed to critically evaluate the effectiveness of ImageJ based methodologies (for implementing EFOMP and EUREF tests) in identifying defective detector elements that are not apparent on routine clinical images.

METHODOLOGY

- Isolating detector performance from other system components.
- A 4cm PMMA uniformity phantom across five imaging configurations was tested.

Image Configurations Assessed

- Rhodium filter
- Phantom Rotation (90°)
- No paddle
- Silver filter
- Grid Out



Fig. 1: Testing setup using standard 4cm acrylic slab

- Images were analyzed using the ImageJ Mammo_QC plugin across four QA methodologies, identifying flagged ROIs that prompted service intervention and detector remapping.
- All tests were repeated post-mapping to enable direct comparison with pre-mapping performance.

Image Analysis Performed

- EFOMP Uniformity
- EUREF Homogeneity
- Artefact Evaluation
- Uncorrected Defective Elements

RESULTS

Uniformity:

	Rh Standard		Rotate Phantom 90°		Rh no comp paddle		Ag Standard		Ag Standard		Rh Grid Out		Rh Standard Post Mapping	
	Local	Global	Local	Global	Local	Global	Local	Global	Local	Global	Local	Global	Local	Global
Number of Deviating ROI:	0	0	0	0	0	0	0	0	0	0	0	0	0	0
Maximum Deviation:	0.08%	0.43%	0.09%	0.38%	0.08%	0.46%	0.10%	0.34%	0.10%	0.34%	0.80%	3.89%	0.08%	0.00%
Limiting Value:	5%	10%	5%	10%	5%	10%	5%	10%	5%	10%	5%	10%	5%	10%
Decision:	Pass	Pass	Pass	Pass	Pass	Pass	Pass	Pass	Pass	Pass	Pass	Pass	Pass	Pass

Fig. 2: Table showing results from Uniformity test for all tested configurations.

- Test passed in all configurations with no significant variation between Pre & Post Mapping.
- Not a viable option to look for the defective elements in the detector.

Homogeneity:

- No noticeable variation observed between results from Pre and Post-Mapping images.
- Test yielded inconclusive results for identifying the defective elements.

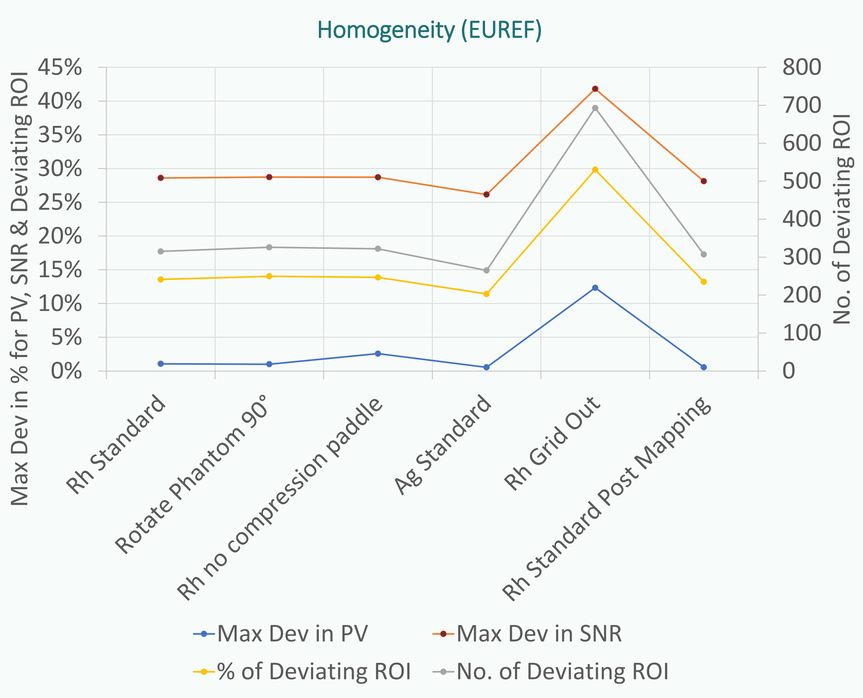


Fig. 3: Graph showing results obtained from Homogeneity test.



Fig. 4: Flagged pixels marked on detector surface 3328x4096 (X,Y)

Artefact Evaluation:

- Consistently flagged abnormal ROIs across all configurations.
- Strong spatial correlation of detected regions.
- Post-mapping: no flagged ROIs observed.
- Highly sensitive in detecting defective elements.

Uncorrected Defective Elements:

- Defective ROI consistently detected pre-mapping.
- Strong agreement with artefact evaluation test.
- Post-mapping: defect resolved.
- Effective for defect localization.

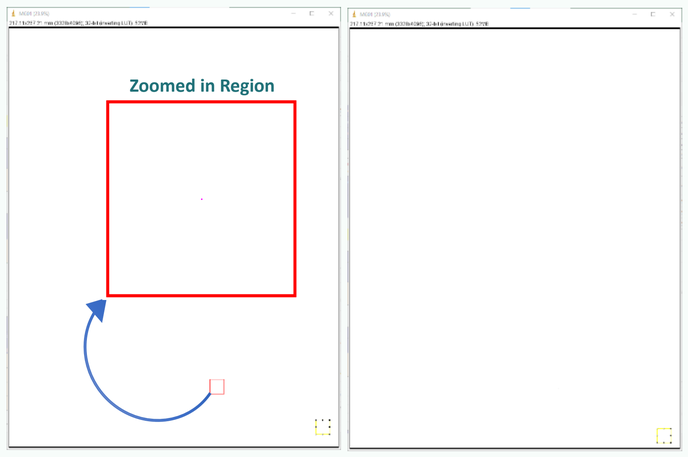


Fig.5: Rh Standard Pre Mapping Rh Standard Post Mapping

CONCLUSION

The tests performed helped in identifying a subtle defect in the detector element that was not visible on clinical images but was confirmed by the vendor when service was called. Furthermore, the information regarding the location of defective element was very helpful for the service engineer to perform required corrective actions which included detector remapping. This highlights the importance of including uncorrected defective element and artifact evaluations in Annual Mammography QA protocols for early detection and timely resolution of issues.

FUTURE WORK

- Establish action thresholds for:
  - Number of flagged ROIs
  - Spatial distribution of defects
- Define criteria for detector remapping vs replacement
- Standardize implementation within QA protocols

TAKE HOME MESSAGE

- Standard QA tests (uniformity & homogeneity) may miss subtle detector defects.
- Artefact and Uncorrected defective element analysis provide higher sensitivity.

References

- Porzio, Massimiliano; Konstantinidis, Anastasios (2020), "Plugins for QC compliant with the European guidelines and EUREF/EFOMP protocols for digital mammography and digital breast tomosynthesis", Mendeley Data, V5, doi: 10.17632/8jj7865wfn.12

iapm Irish Association Of Physicists In Medicine

OSPIDÉAL SAN SÉAMAS ST JAMES'S HOSPITAL

A 3D Printed Phantom for Measuring Geometric Accuracy in MRI

Alan Stone[1,2*], George Spathis[2], Jess Fitzpatrick[1], Deborah Jacob[1], Paul Davenport[3], Michael O'Neill[1]

[1]*Medical Physics & Clinical Engineering, Beaumont Hospital*
[2]*Centre for Physics in Health and Medicine, School of Physics, University College Dublin*
[3]*St. Lukes Radiation Oncology Network at Beaumont Hospital, Dublin, Ireland*

**Corresponding author: alanstone@beaumont.ie*

INTRODUCTION

- Magnetic Resonance Imaging (MRI) is becoming increasingly important for stereotactic neurosurgery and radiotherapy [1]. However, MRI images are inherently prone to geometric distortion which can cause significant deviation from the intended surgical location [2] or dose delivery site [3]

- For stereotactic MRI, guidelines recommend correction of images using distortion correction (DC) filters and monitoring of geometric distortion [4]. Measurement of geometric distortion can be performed using phantoms that provide limited information[5] or are prohibitively expensive [6].

- The aim of this study is to present a cost-effective, 3D printed phantom with an automated analysis pipeline for measuring MRI geometric distortion and to demonstrate its use for assessing the performance of MRI DC filters

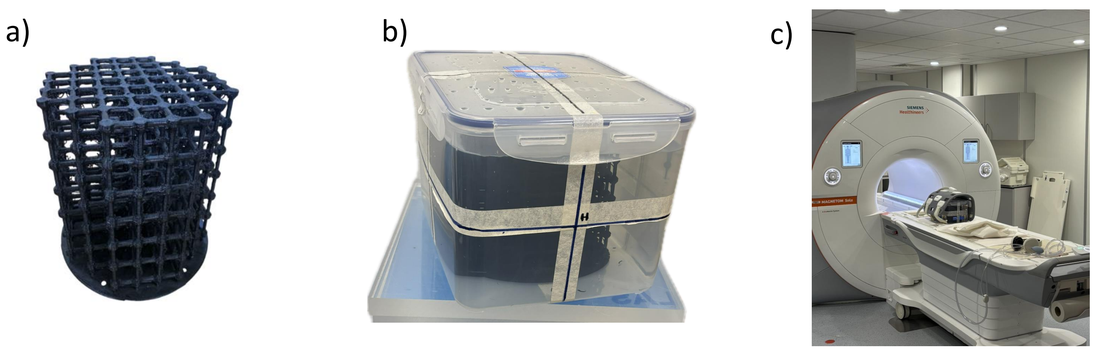


Figure 1: a) 3D printed grid containing 364 control-points, b) final phantom with 3D printed grid submerged in water and c) phantom positioned for scanning with body receive-coil

METHODS

- A custom phantom was fabricated from a 3D printed grid, placed in a plastic container and filled with water (see **Figure 1b**)

- The 3D printed grid contains 364 control-points arranged three dimensionally (dimensions 15cm × 15cm × 13cm) (see **Figure 1a**)

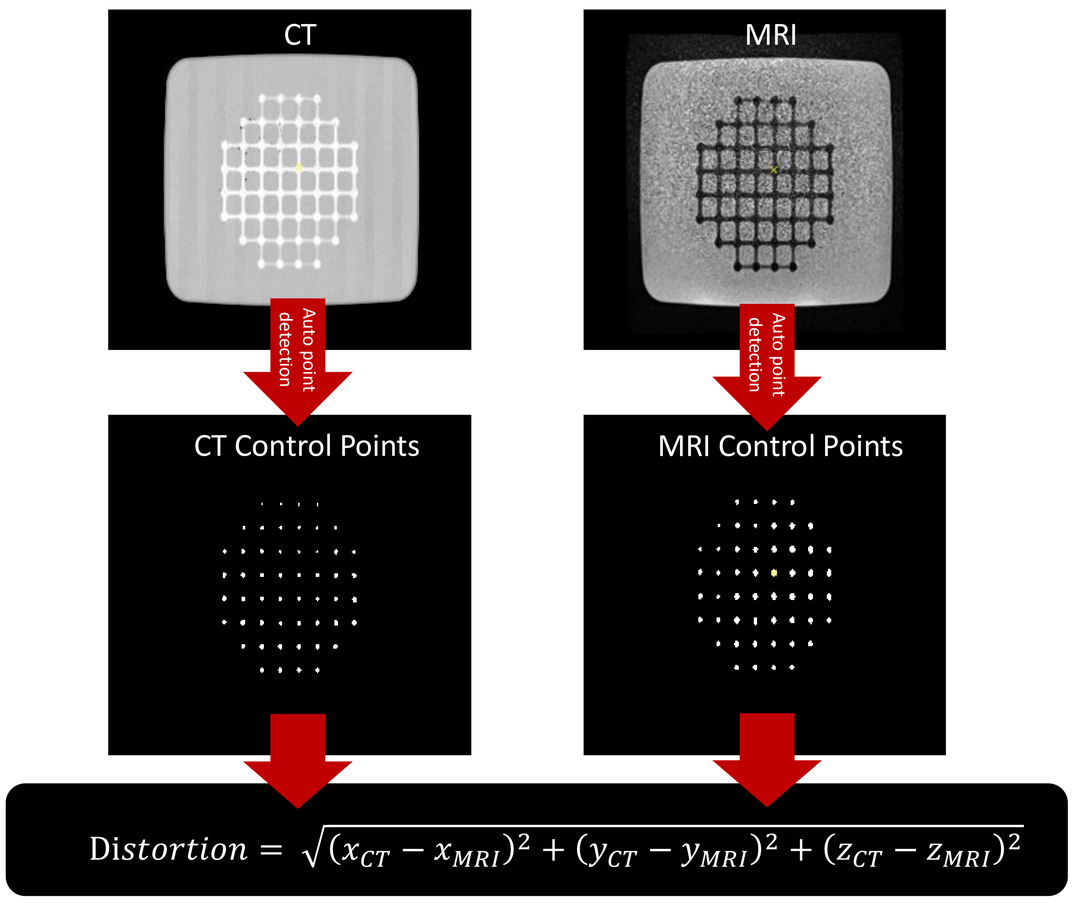


Figure 2: Geometric distortion calculation. CT and MRI images are rigidly aligned, control points automatically detected using template matching and distortion calculated using the equation shown

- To measure geometric distortion, MR images of the phantom were compared to a CT of the phantom (see **Figure 2**) as CT is considered to provide a ground truth geometry

- MR images were acquired at 1.5T using a spoiled gradient-echo with distortion correction (DC) filters On and Off (see **Figure 1c**).

- MRI and CT images were aligned using rigid body registration. Phantom control-points were automatically identified using normalised cross correlation [7] (see **Figure 2**)

- Geometric distortion of each MRI control-point was obtained by calculating the Euclidean distance to the same control-point in CT (see **Figure 2**)

RESULTS

- MR images acquired with the distortion correction (DC) filter Off differed geometrically when compared to CT and MR images with DC filter On (see **Figure 3**)

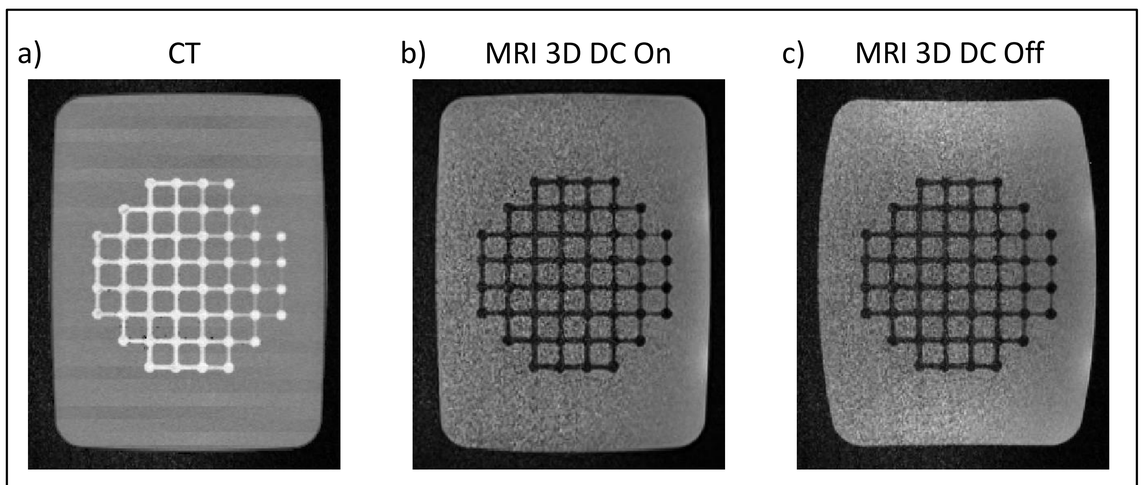


Figure 3: Comparison of (a) CT, (b) MRI with 3D distortion correction (DC) filter On and (c) 3D DC filter off. MR images acquired with DC off demonstrate largest deviation in geometry from CT

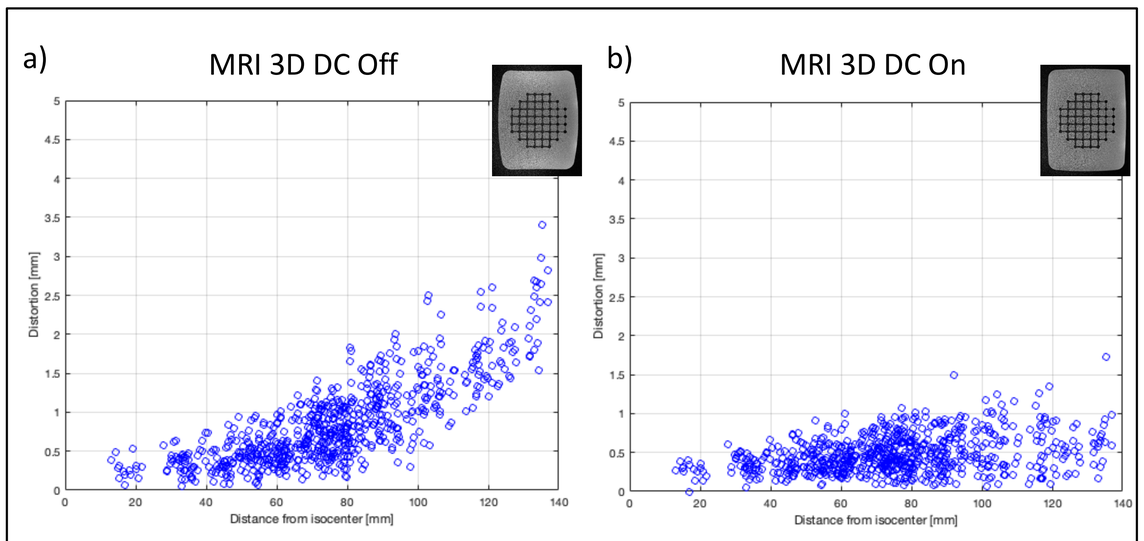


Figure 4: Distortion as a function of distance from isocenter for MRI images acquired with (a) 3D DC filter Off and (b) 3D DC filter On. The application of the 3D DC filter demonstrates a reduction in geometric distortion particularly at locations further from isocenter

- MRI geometric distortion measurements showed a trend of increasing distortion with distance from MRI isocentre as expected [8] (see **Figure 4**)

- Geometric distortion measured in non-DC MRI were found to have statistically (t-test, $p<0.05$) greater geometric distortion (max=3.4mm) when compared to distortion corrected images (max=1.7mm) as expected [9]

CONCLUSION

- In this study we demonstrate a cost-effective tool for measuring geometric distortion using a 3D printed phantom and automated analysis pipeline

- MRI geometric distortions were found to be greater at further distances from iso-centre and without distortion correction filters

- Future work will apply this phantom to investigate geometric distortions at different field strengths and the optimisation of stereotactic MRI acquisitions

CLINICAL IMPACT

- This study presents an accessible solution for measuring geometric distortion in MRI and highlights the role of careful patient positioning and distortion correction filters when acquiring MRI for stereotactic planning.

References

[1] Putz et al. Strahlenther Onkol. 2020 May;196(5):444-456.
[2] Balachandran et al. IEEE Trans Biomed Eng. 57(7):1729-35 (2010)
[3] Pappas et al. Technol Cancer Res Treat;16(6):1120-1129 (2017)
[4] Putz et al. Strahlenther. Onkol. 200, 1–18 (2024).
[5] https://www.sunnuclear.com/products/acr-mri-phantom
[6] https://www.sunnuclear.com/products/large-field-mr-distortion
[7] Jafar et al.. Journal of Imaging. 2017;3(3):28.
[8] Torfeh et al. J. Appl. Clin. Méd. Phys. 22, 149–157 (2021).

An Audit of Image Rejection in General X-Ray

aogaffney@stjames.ie

Aoife Gaffney[1], Hannah Reilly[1], Elaine Doyle[2], Dr. Geraldine O'Reilly[1]

[1] MPBE, St. James's Hospital, Dublin 8

[2] DIAGIM, St. James's Hospital, Dublin 8

Introduction

In diagnostic radiology, x-ray images may need to be repeated for a number of reasons including:

- Patient motion,
- Incorrect positioning
- Metal artefacts etc

This can lead to an increase in radiation exposure for patients. Minimising the amount of rejected images follows the *ALARA* principle - keeping the dose *as low as reasonably achievable*.

AIM

To evaluate image rejection rates in five general rooms against a local KPI of less than 5% and to identify the primary causes to minimize unnecessary patient radiation exposure.

Methods & Results

Clinical Audit Methods

- 5 general rooms were analysed to determine if the locally established KPI of less than 5 % rejection was met.

Results

- All rooms exceeded the local KPI. (Fig. 1)
- The rejection rates ranged from 7% to 11%.

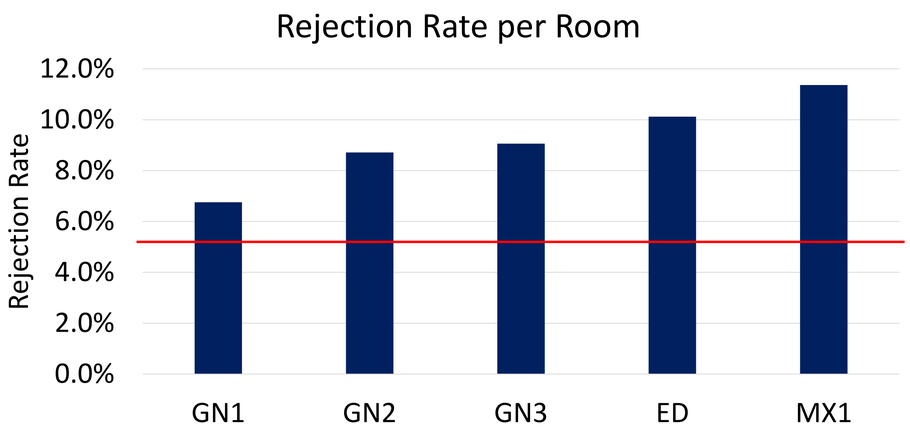


Fig. 1: Rejection Rate per Room

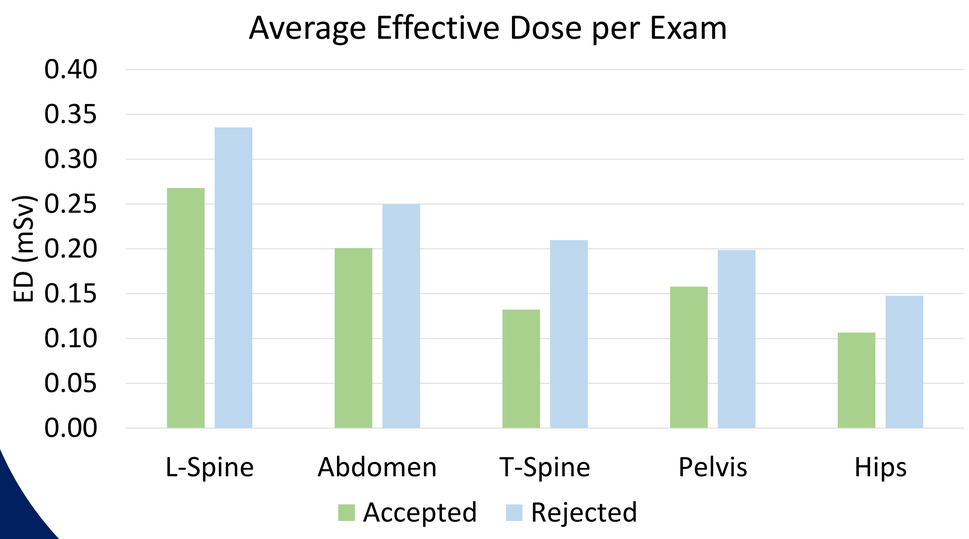


Fig. 3: Average Effective Dose for 5 types of exams

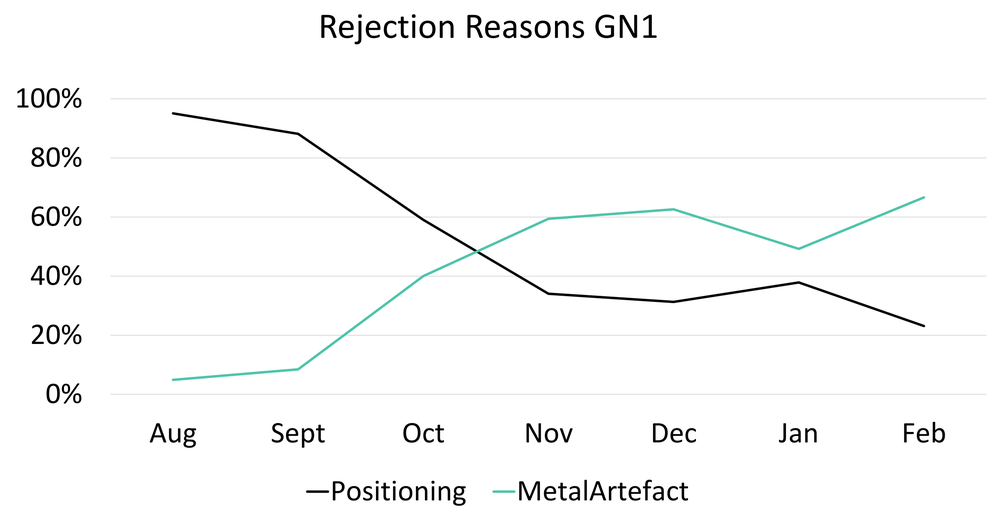


Fig. 2: Rejection Reasons GN1 (change made in October)

Analysis Method

- The reasons for rejection were analysed.
- The effective dose for each view was calculated using the conversion factors from Wall et al [1].
- For the purpose of this poster the data was sorted by anatomical region instead of views so the maximum conversion factor was taken and applied.
- The dropdown list of rejection reasons was reordered in one room and the data was collected after a few months.

Results

- Positioning was the rejection reason 95% of the time. However, this was the first reason in the dropdown in all rooms.
- To identify if the order within the dropdown was biasing selection, it was re-ordered in one room and the main reason changed to metal artefacts (Fig. 2).
- Rejected images contributed to ~12% of the overall effective dose for relevant body parts.
- Fig. 3 shows the anatomical regions with the highest average effective dose (ED) per scan. The dose associated with a rejected image was generally higher than that of an accepted image.

Follow – Up/ Conclusion

- An information session was carried out to share findings.
- Posters including the rejection rate and percentage rejection per body part were placed in each general x-ray room.
- The dropdown list of rejection reason in all rooms will be reordered and reanalysed after a few months.
- Minimising the need for image rejection improves both patient safety and departmental efficiency.
- The data gathered allowed us to identify some potential causes of higher rejection rates (Fig. 4) and to determine which areas require increased effort or training to reduce the rejection rate.

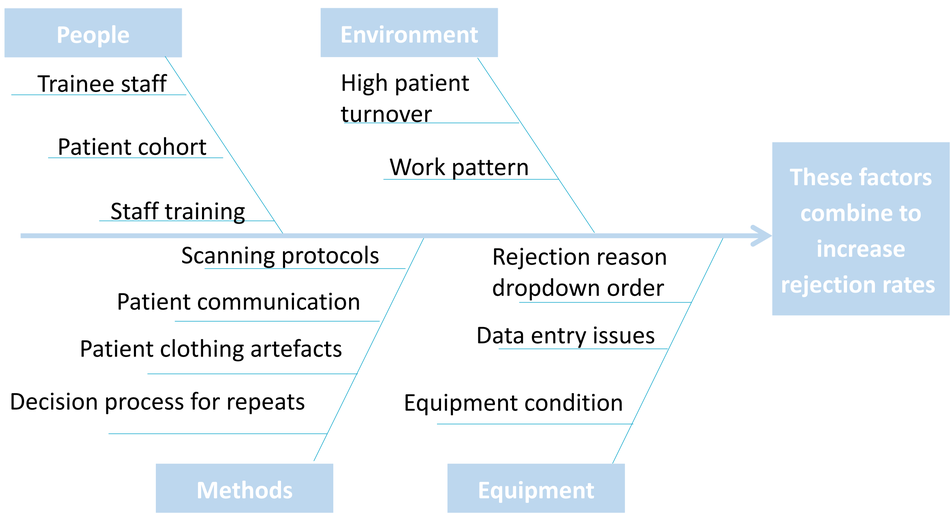


Fig. 4: Root-Cause Analysis Diagram

REFERENCES

1. Wall BF, Haylock R, Jansen JTM, Hillier MC, Hart D, Shrimpton PC. Radiation risks from medical X-ray examinations as a function of the age and sex of the patient. Published October 1, 2011.
2. Radiation Control Program Management Conference (CRCPD'S) Quality Assurance Committee (QA): 10% (CRCPD, 2020; WHO, 2006).
3. "Reject and effective dose analysis in digital radiography – a Finnish imaging department case study" (2025)
4. "Radiation risks from Medical X-Ray Examinations as a Function of the age and Sex of the Patient" (2011).

OSPIDÉAL SAN SÉAMAS

ST JAMES'S HOSPITAL

Assessing scatter-corrected planar CZT imaging for lung shunt fraction estimation using anthropomorphic and 4D digital phantoms.

Bríana Fennell[1], Niamh McArdle[2], Seán Cournane[1,2], Jackie McCavana[1,2]

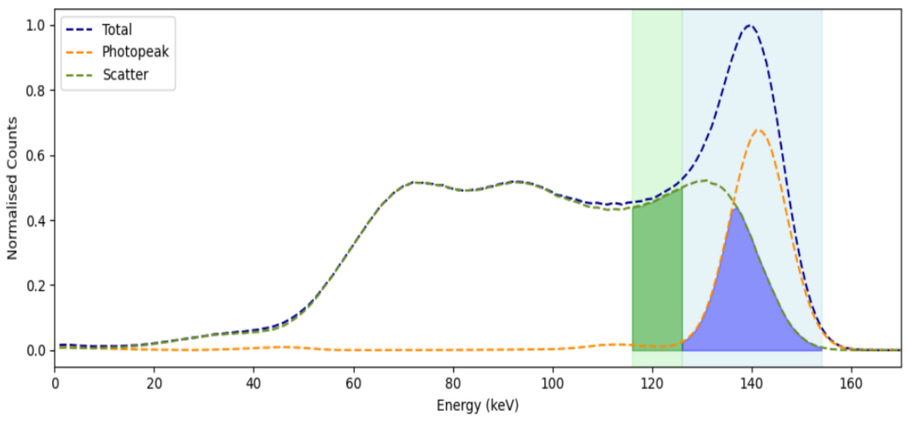
(1) Centre for Physics in Health & Medicine, University College Dublin, (2) St. Vincent's University Hospital, Ireland.

Introduction

Accurate lung shunt fraction (LSF) estimation is needed for reliable lung and liver dose assessment in Selective Internal Radiation Therapy (SIRT). Scatter contributions affecting LSF accuracy can be mitigated using energy window–based scatter correction (SC), validated through Monte Carlo (MC) simulation. While such approaches have been explored for sodium iodide (NaI(Tl)) gamma cameras, their applicability to modern cadmium zinc telluride (CZT) systems remains insufficiently characterised [1]. This work aimed to evaluate the accuracy of LSF estimation using CZT imaging and to assess the performance of a spectrally optimised SC method under realistic, patient-dependent conditions [2].

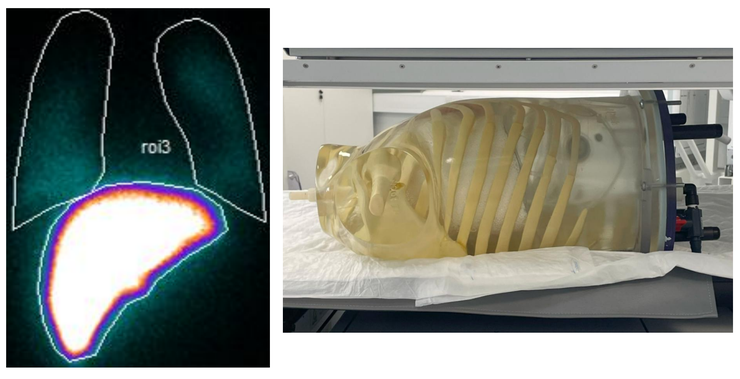
Method

Validation of SIMIND



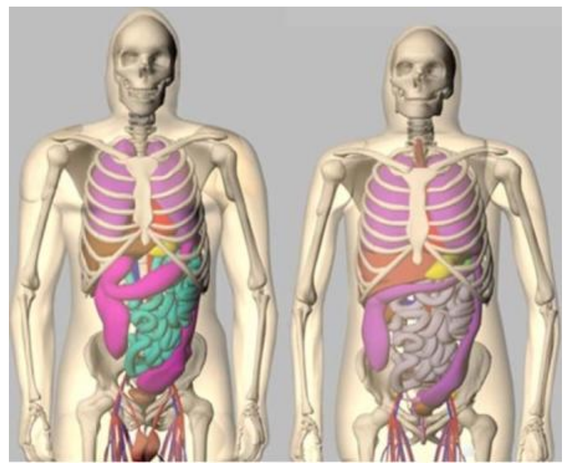
The CZT system and SC window were characterised using SIMIND MC simulations and validated with water-phantom point-source measurements, showing ≤6% AUC differences in the photopeak window and enabling optimisation of the scatter window.

Anthropomorphic Phantom Validation



Phantoms with varying known LSFs, ranging from 2.77% to 11.87%, were imaged on a GE 870 CZT system and compared with simulations (***Figure 4***). LSFs and energy spectra were quantified, with Dice coefficients (***Figure 3***) assessing ROI agreement.

XCAT Digital Phantoms



4D XCAT phantoms incorporating respiratory motion and a range of BMIs (20.64–37.96 kg m^{-2}) were used to evaluate patient-specific effects on LSF estimation and SC (***Figure 5***).

Results

RSD Phantom Dice Evaluation

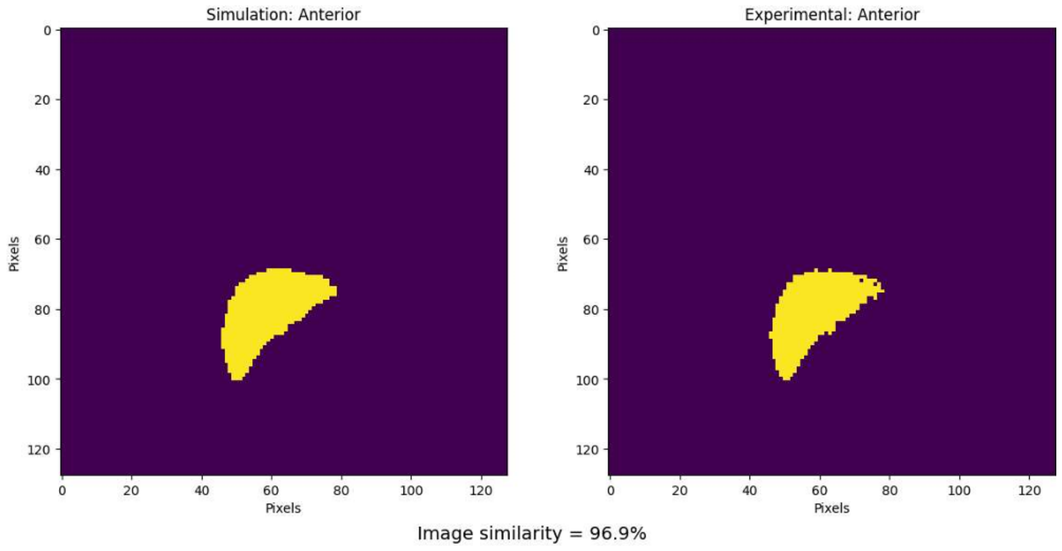


Figure 3: Comparison of experimental and simulated images in the anterior view. Image similarity was assessed using the Dice similarity coefficient.

LSF Results – RSD Phantoms

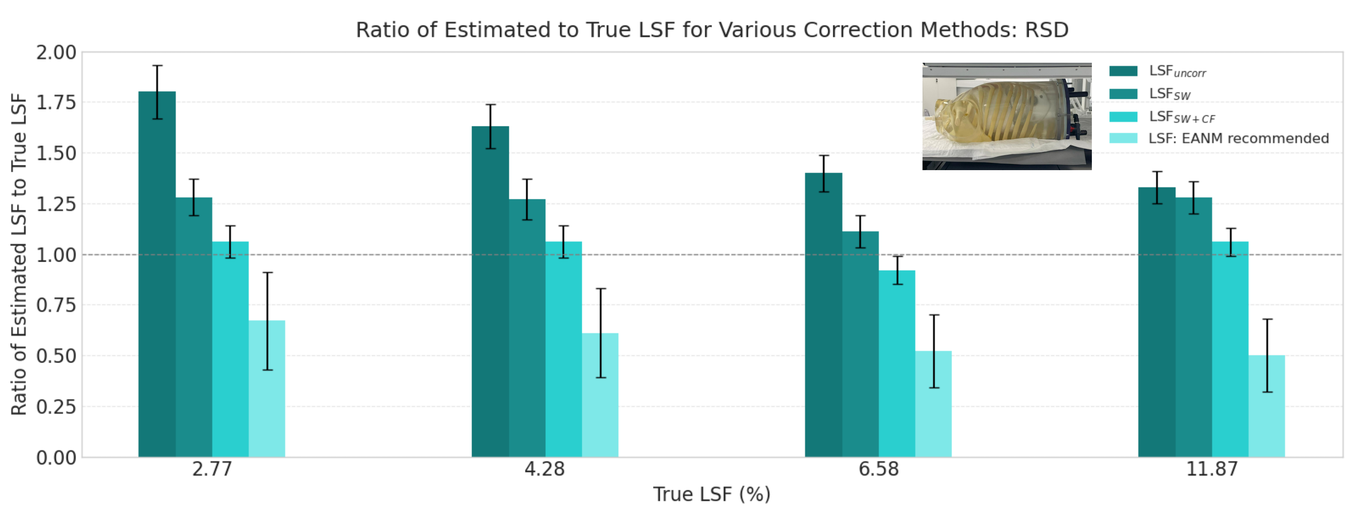


Figure 4: SC improved accuracy in planar RSD LSFs, whereas uncorrected measurements consistently overestimated true values. The SW estimates scatter from a lower-energy window, while SW+CF applies an additional correction factor to account for residual scatter.

XCAT Results – Patient-Specific Effects

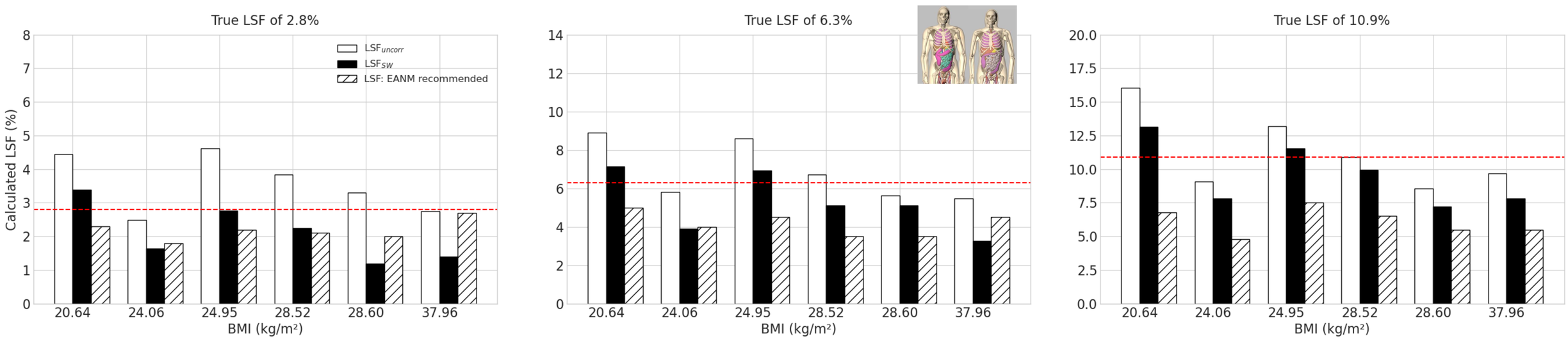


Figure 5: LSFs derived from 4D XCAT phantoms show that SC tends to underestimate values across most BMI categories, emphasizing the need to account for patient-specific anatomy and respiratory motion when estimating LSF [3].

Conclusions

CZT-specific SC improves LSF estimation (to within 8% of the true value) compared with uncorrected planar imaging for the RSD phantom; however, this was not replicated for the patient phantoms due to factors such as varying tissue densities and body habitus. Results from realistic XCAT digital phantoms demonstrate that simplified phantom validation may not fully reflect clinical conditions, with potential for underestimation in higher BMI cases. These findings underscore the importance of more patient-specific SC strategies to ensure reliable and accurate pre-SIRT dose assessment.

References

1. McArdle N, et al. Phys. Med. 2022;99: 94-101.
2. Segars W, et al. Medical Physics. 2008;35.8:380-8.
3. Chiesa C, et al. EJNMMI Phys. 2021; 8.1: 77

Any Questions?
briana.fennell@childrenshealthireland.ie

ST. VINCENT'S HEALTHCARE GROUP
Advancing Healthcare Since 1834
JCI Accredited

An Alternative Approach to Reassurance Monitoring of Uncategorised Staff working in Controlled Areas.

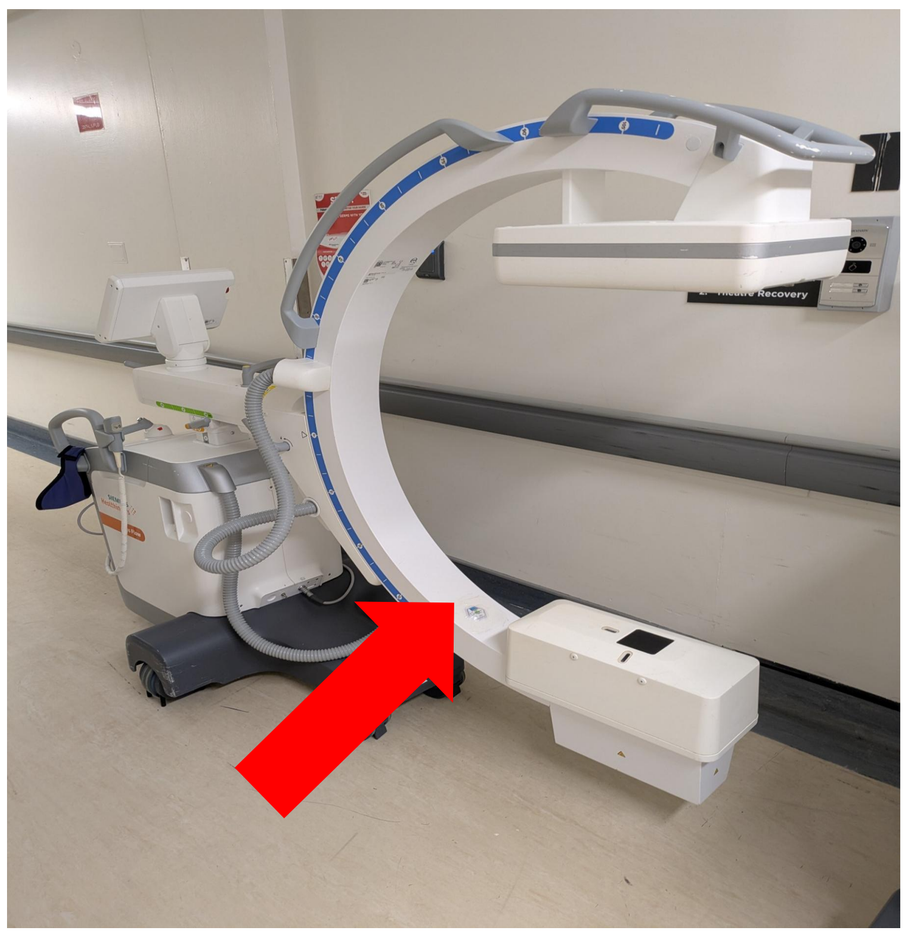
J. McCullagh, James Dolan.
Radiology Physics Department
Cork University Hospital

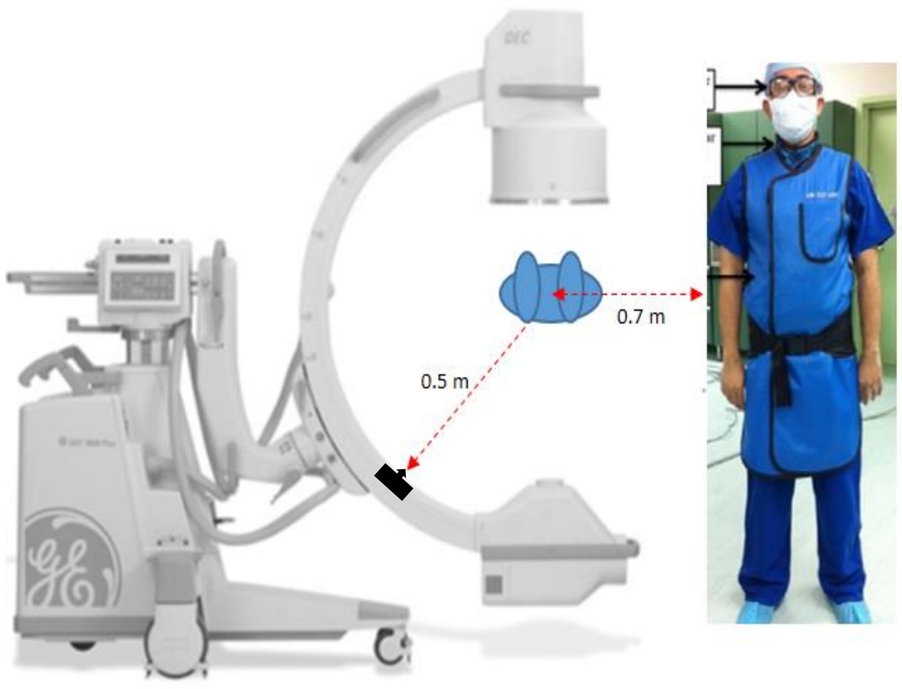
Introduction

Radiation risk assessment of mobile C-Arm use in theatre has led to the removal of dosimeter badges from over 100 staff. While no legal requirement exists to provide a dosimeter for uncategorised workers it should still be possible to demonstrate that staff exposures are ALARA and not exceeding dose limits.

Aim

Evaluate an alternative approach to individual monitoring whereby dosimeters attached to mobile C-Arms are used to give an indirect measure of theatre staff exposure.





Methods

Ambient dosimeters were attached at the 30° position of seven mobile C-Arm X-Ray units used across 10 theatres, primarily for orthopaedic, plastic, neurosurgical and urological procedures. The cumulative dose record from bi-monthly badge readings compiled over a one year period were then used to derive estimates of staff exposure, which were evaluated by comparing with calculated dose estimates based on DAP workloads obtained from PACS.

Results

Depending on C-Arm use annual badge readings ranged from only 0.1 mSv up to 17.6 mSv. Staff exposure estimates derived from these readings indicated that exposure levels were lowest in Plastics and Orthopaedics (0.01 – 0.04 mSv) and highest in Urology (0.01 – 0.2 mSv). The adjoining table shows how these compared with estimates derived from patient DAP workloads.

		Theatre Role	Calculated Annual Body Dose (mSv)	Indirectly Measured Annual Body Dose (mSv)	Δ%
Neurology Theatre	1	Primary Surgeon	48	154	224%
	3	Anaesthetist	52	56	8%
	4	Scrub Nurse	52	34	-35%
	6	Radiographer	19	12	-35%
Orthopaedic Theatre	1	Primary Surgeon	62	40	-36%
	3	Anaesthetist	54	35	-36%
	4	Scrub Nurse	32	21	-36%
	6	Radiographer	12	7	-36%
Plastics Theatre	1	Primary Surgeon	0.4	0.4	3%
	3	Anaesthetist	0.2	0.2	3%
	4	Scrub Nurse	0.1	0.1	3%
	6	Radiographer	0.0	0.0	3%
Urology Theatre	1	Primary Surgeon	79	203	156%
	3	Anaesthetist	52	44	-15%
	4	Scrub Nurse	52	26	-49%
	6	Radiographer	19	10	-49%

Discussion

The table shows how well staff dose estimates derived from C-Arm badges compared with estimates derived from DAP workloads. Poor reporting of patient DAP on PACS, as required by some C-Arms, is blamed for the larger differences found for some staff roles as shown above. The issue of poor DAP reporting has been addressed since this study was carried out and it is expected agreement between measured and calculated in future evaluations will be improved.

Conclusion

The results provide convincing evidence that staff exposure levels are being maintained ALARA and the study has shown C-Arm badging is a realistic alternative for reassurance monitoring of uncategorised staff.

Further Work

Repeat the evaluation following the improved reporting of patient DAP on PACS.

For further information contact: james.mccullagh@hse.ie

Characterisation of a commercially available tungsten-filled polymer filament for use in image quality testing and radiation safety solutions.

L.Oonan[1], Dr E.Kenny[1,2], Dr B.Gibney[1,2]

(1) Mater Misericordiae University Hospital (2) University College Dublin

INTRODUCTION

In 2023, Prussia Research released a polyethylene terephthalate glycol (PET-G) filament containing tungsten, offering enhanced attenuation properties over more traditional filaments such as polylactic acid (PLA). The development of filaments such as these is particularly significant in the context of medical imaging, where the attenuation of the material is critical.

The ability to produce relatively low-cost 3D printed tungsten test objects and bespoke safety solutions in a short time frame is highly advantageous for research purposes. However, limited data exists describing their imaging characteristics across different imaging modalities.

The purpose of this study is to experimentally assess the characteristics of a commercially available tungsten-filled PET-G filament using x-ray and computed tomography (CT).

METHODS

Test objects were fabricated using a Prusa i3 MK3S 3D printer (Prusa Research) and Prussiament tungsten filled PET-G (75% 1Kg*)*. Due to the abrasive nature of the material used for printing a hardened steel nozzle (0.4 mm) was required alongside a print bed with high adhesion such as powder coated satin. Print parameters were provided by Prussia though a dedicated printing profile downloadable on their website however these needed to be modified slightly to produce consistent print quality with our printer.

Stepwedges, MTF targets and CT inserts were designed using Computer Aided Design (CAD) software (Autofusion 360) and prepared for printing using PrusaSlicer. X-ray images were taken using a GE Optima 220 mobile x-ray system under RQA 5 beam quality conditions (2.5 uGy, 6.8 mm Al). CT Images were acquired using a Siemens DRIVE dual-tube system. Image analysis was performed using ImageJ.

Material attenuation was evaluated using a tungsten stepwedge with step heights ranging between 1 - 5 mm. To evaluate print consistency, three identical stepwedges were printed and evaluated. Spatial resolution was assessed by calculating the Modulation Transfer Function (MTF) of a 40 by 40 mm square target with a 4 mm thickness. Finally CT number (HU) value and uniformity were assessed using a 13 mm x 150 mm tungsten rod positioned within the centre chamber of the $CTDI_W$ phantom.

The test object generation and assessment pipeline can be observed in *figure 1* below.

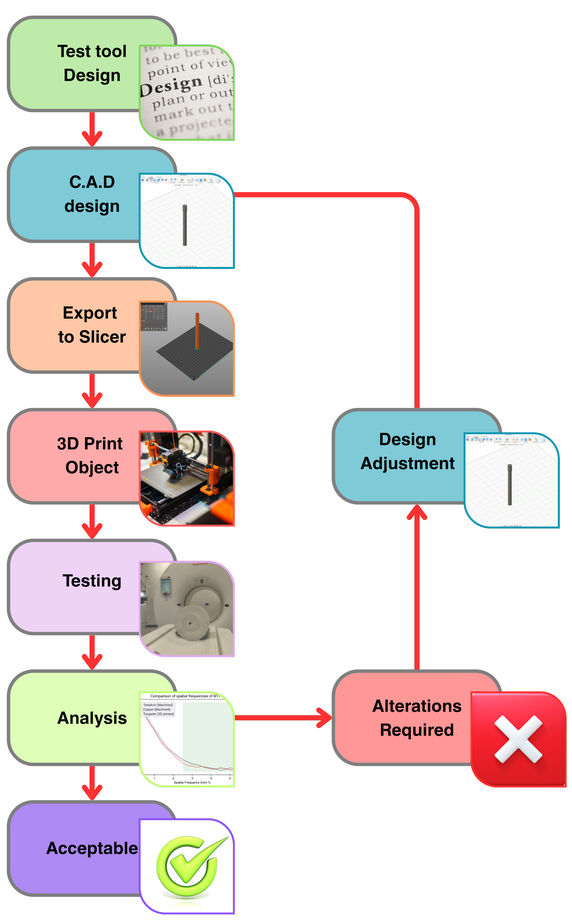


Figure 1: Pipeline for design and fabrication of 3D printed tungsten test objects.

RESULTS

Material Thickness:

Analysis of pixel values (PV) recorded using general x-ray demonstrated that 4 mm of tungsten attenuated approximately 98% of incident x-rays (67 kVp and 12.5 mAs - RQA 5 beam quality). Repeated measurements across two additional step wedges returned similar results showing good print reproducibility. Results of this assessment can be observed in *figure 2*.

RESULTS

Spatial Resolution Assessment:

Modulation Transfer Function (MTF) values recorded were comparable to those obtained using traditional machined materials. *Figure 3* shows the comparison between Tantalum, Copper and 3D printed tungsten objects. An MTF_{50} value of 1.18 lp/mm was recorded for the tungsten printed object while a value of 1.24 lp/mm was measured for the tantalum. While tantalum demonstrated the superior performance, with further refinement the 3D printed tungsten shows potential.

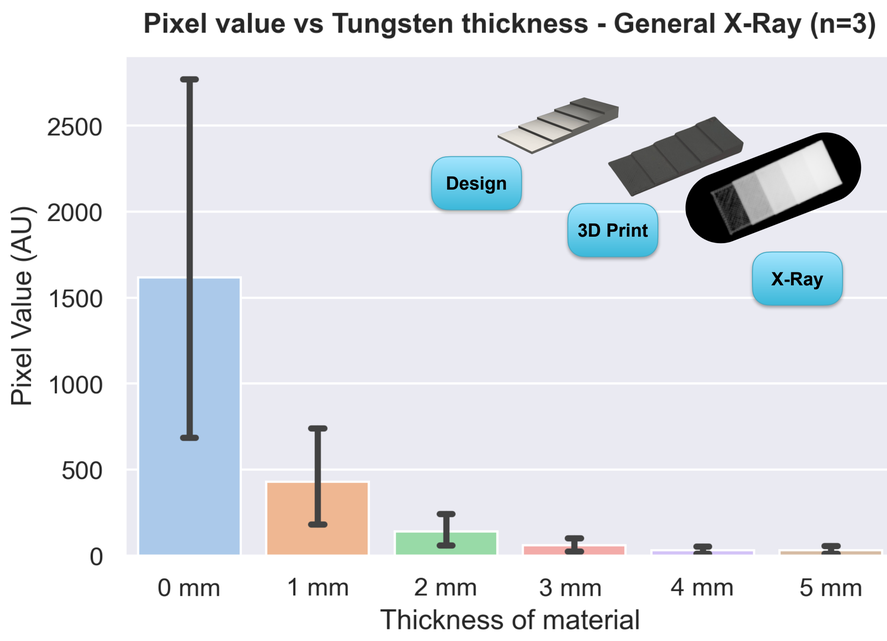


Figure 2: Pixel value vs stepwedge thickness (mm). Based on these results it was determined that 4 mm of tungsten was sufficient to attenuate 98% of incident x-rays.

Hounsfield Unit (HU) assessment and uniformity:

The CT numbers were evaluated across 10 central slices at varying tube potentials between 80 and 120 kVp. The mean HU value obtained was 3071.81 ± 0.25, which corresponds to the upper limit of the scanners standard HU scale. Longitudinal uniformity was assessed across 36 continuous slices with a slice thickness of 4 mm. At 80 kVp, a maximum deviation of 0.21 HU was noted across the volume of the test object. This indicates a good printing consistency with little layer variation at 100% infill.

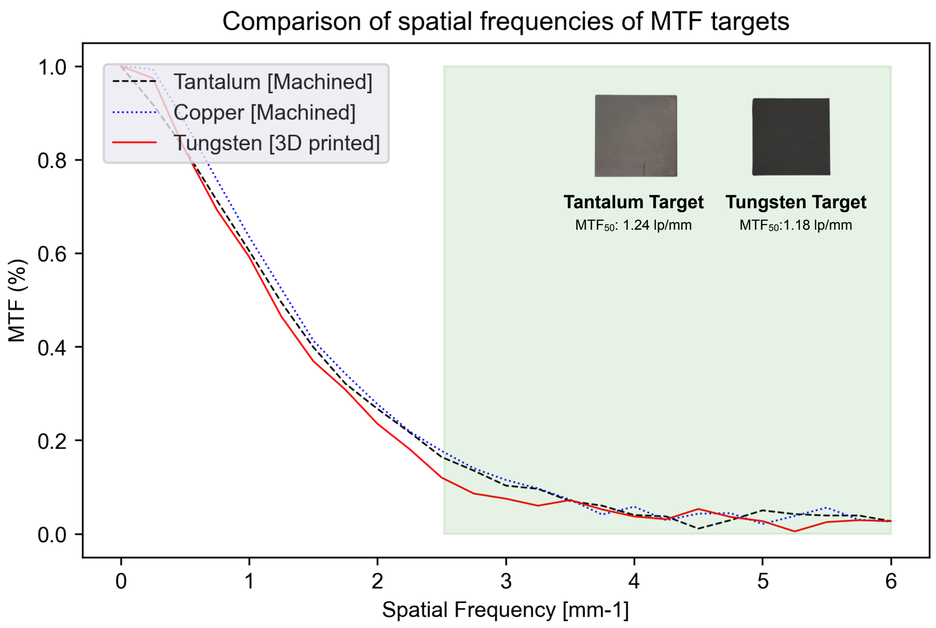


Figure 3: Measured MTF values of different targets. Tantalum (shown in black) is the “gold standard” used for regular image quality assessment in the Mater Hospital.

DISCUSSION

Our assessment of tungsten filled PET-G filament from Prusa Research demonstrates that these materials can be manufactured with adequate consistency for use in image quality assessment. These test objects have also been shown to have good reproducibility which is important for ensuring reliable and reproducible measurements during routine QA testing. The ability to acquire MTF, X-ray attenuation and CT uniformity data confirms the feasibility of rapidly producing low cost, test specific test tools for use in routine Medical Physics testing. While MTF_{50} values for the printed tungsten target was lower than the tantalum reference, it remains sufficient for routine testing and trend analysis. The adoption of 3D printing alternatives for test objects has the potential to deliver substantial cost savings to departments.

The findings of this study particularly regarding attenuation properties provide a foundation for future work in areas such as Nuclear Medicine, where bespoke radiation protection solutions may be required for both therapeutic and diagnostic applications.

References:

•Prusament PETG Tungsten 75% 1kg (NFC) | Original Prusa 3D printers directly from Josef Prusa. Prusa3D by Josef Prusa. Available from: https://www.prusa3d.com/product/prusament-petg-tungsten-75-1kg

•Yoon MS, Jang HM, Kwon KT. Influence of parameters and performance evaluation of 3D-Printed Tungsten Mixed filament shields. Polymers [Internet]. 2022 Oct 13;14(20):4301. Available from: https://pmc.ncbi.nlm.nih.gov/articles/PMC9609353/

A CT Topogram–Based Methodology for Periodic Screening and Transmission Assessment of X-ray Personal Protective Equipment

Darragh McCague[1] , Danielle Maguire[1] , Jackie McCavana[1,2]

(1) St. Vincent's University Hospital, Ireland (2) School of Physics, University College Dublin, Ireland

Introduction & Aim

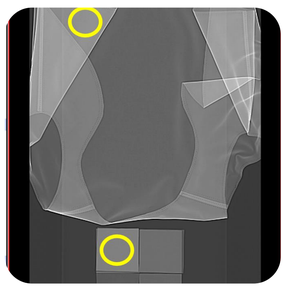
Recent concerns regarding the integrity of X-ray personal protective equipment (PPE) barrier materials have highlighted the importance of routine PPE testing. Routine testing includes structural defect screening and attenuation performance assessment. While fluoroscopic imaging is commonly used for defect detection, transmission testing is difficult to implement in clinical environments due to the need for specialist set up and calibrated detectors. This work aimed to develop a practical method for qualitative and quantitative PPE assessment using CT topogram imaging.



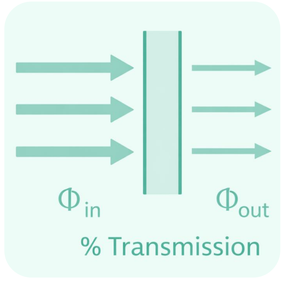
CT Topogram
- 120 kV
- 20 mAs



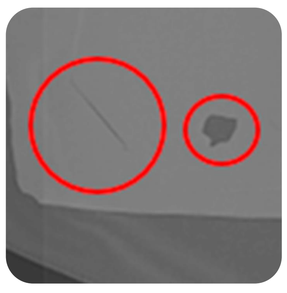
Setup
- Low μ board
- Isocentre
- Tube at 0°



Acquisitions
- PPE items
  - Seams offset
- Reference Panels



Transmission Testing
- Compare MPVs



Structural Screening
- Defects
  - Tears
  - Thinning
  - Rips



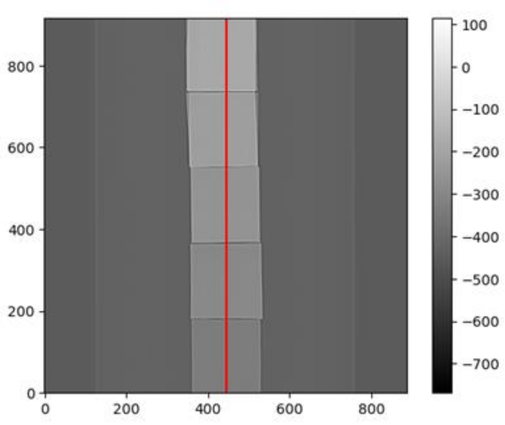
Pass / Fail
- Combined Uncertainty Comparison
- BIR Criteria[1]

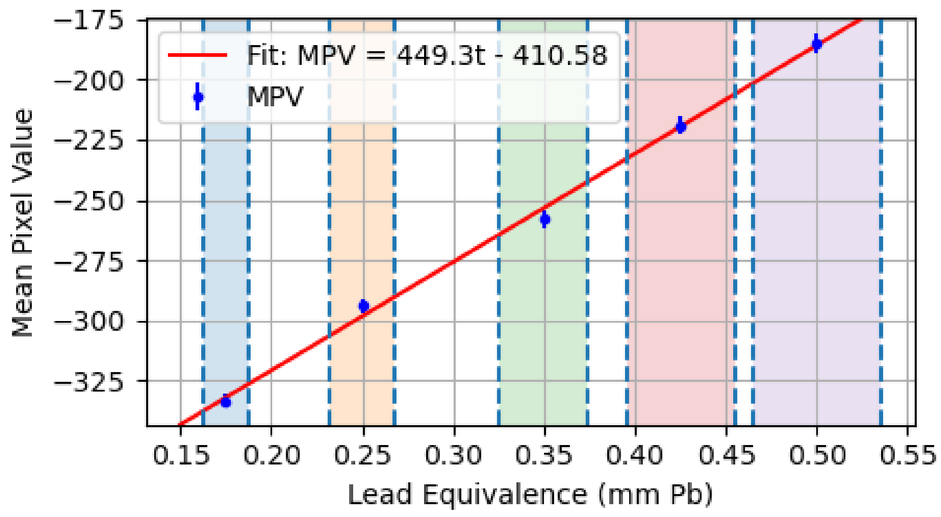
Methods

PPE positioning and acquisition parameters were optimised to minimise statistical uncertainty. Method validation included assessment of field-of-view uniformity and ROI mean pixel value (MPV) sampling uncertainty. A spreadsheet was developed to automatically analyse results.

Results

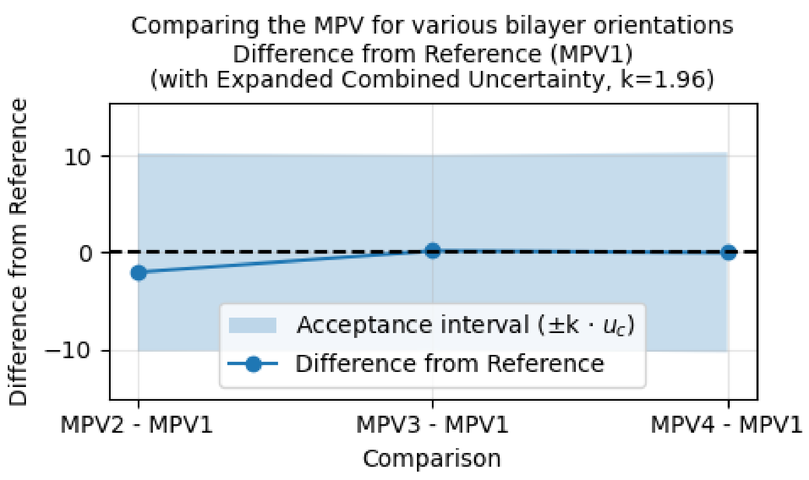
Resolving Lead Equivalence Thicknesses





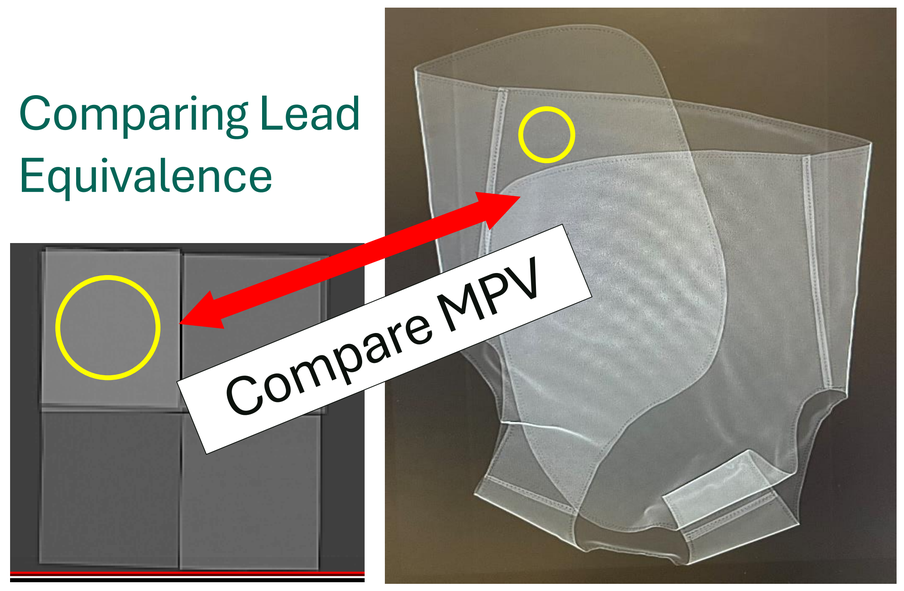
The measurement uncertainty was significantly less than the ±7% manufacturing tolerance for lead equivalence, indicating that the method has sufficient sensitivity to identify PPE that does not meet specification.

Comparing Bilayer Orientations



All differences were smaller than the expanded combined uncertainty, indicating statistical equivalence at 95% confidence.

Comparing Lead Equivalence



The measured and reference MPVs are considered equivalent if:

$$|MPV_{panel} - MPV_{ref}| \leq k \cdot u_c$$

Where:

$$u_c = \sqrt{SD_{panel}^2 + SD_{ref}^2} \text{ and } k = 1.96$$

for 95% C.I.

Advantages	Limitations
Ergonomic workflow with minimal PPE handling	Requires reference material of comparable composition
Combined defect and attenuation assessment	Bilayer orientation effects are not distinguishable
Reduced occupational radiation dose	CT access may limit implementation

Request file access

Conclusion

A rapid, reproducible, and sensitive method for acceptance testing and periodic X-ray PPE quality assessment was developed

[1]Personal Protective Equipment for diagnostic x-ray use, Report of the BIR working party, 2016, P. Hiles et al.

ST. VINCENT'S HEALTHCARE GROUP
Advancing Healthcare Since 1834

UCD DUBLIN

JCI Accredited

SureStart Bolus Tracking: CTPA Optimisation

Lauren Reilly, Dara O Gallchobhair, Aidan Meehan, Patrick Monnelly
Medical Physics & Clinical Engineering, Beaumont Hospital

Introduction

Pulmonary embolism (PE) is a blood clot that blocks and stops blood flow to an artery in the lung and can become life-threatening [1]. It is important to diagnose PE in a timely manner. CT Pulmonary Angiogram (CTPA) is performed on patients with suspected PE as it is a fast, highly accurate and widely available [2]. A contrast agent is used to detect any blockages within the pulmonary arteries.

SureStart is a bolus-tracking feature that automates scan acquisition by monitoring contrast attenuation within a ROI in real time [3] [4]. A low dose planning scan (scanogram) (Figure 1.) is obtained first to define the start and end of the spiral scan as well as the ROI for the vessel of interest, usually the descending aorta for CTPA due to fewer motion artefacts (Figure 2.). Careful planning of the scan is essential for achieving an optimal result while minimising radiation exposure [4].

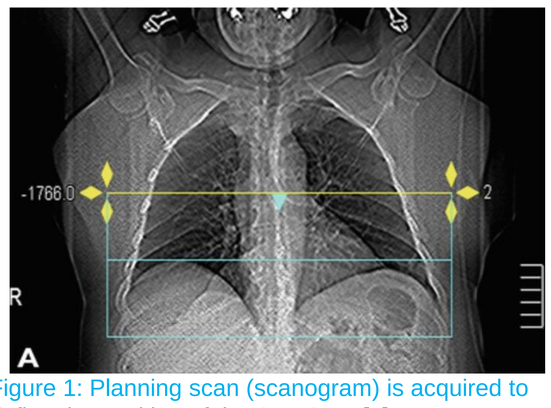


Figure 1: Planning scan (scanogram) is acquired to define the position of the SureStart [4]

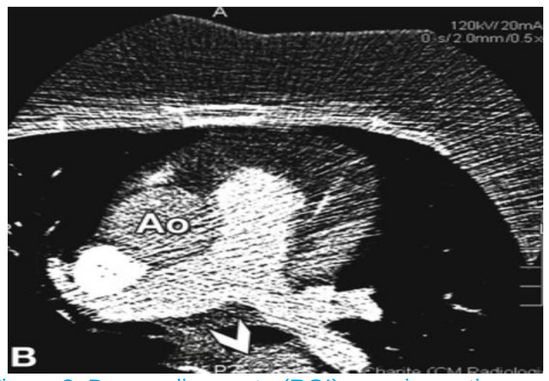


Figure 2: Descending aorta (ROI) seen in continuous low-dose scan [4]

A HU threshold is selected for this ROI, and low-dose monitoring scans are acquired every 2 seconds until the threshold is reached as seen in figure 3 below [4]. Alternatively, the scan can be started manually by the operator when signs of contrast filling is noted.

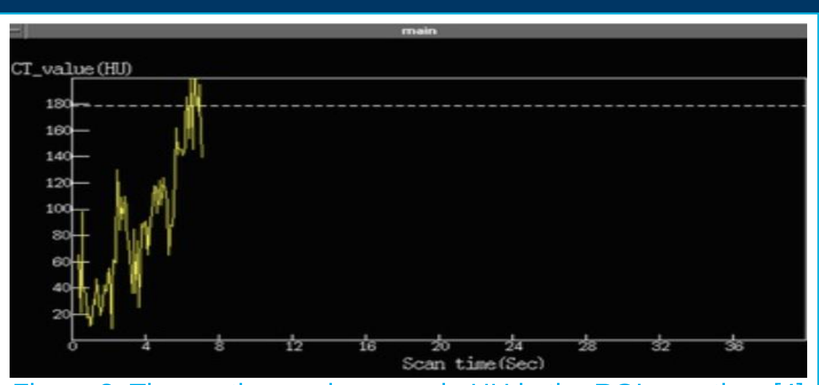


Figure 3: The continuous increase in HU in the ROI over time [4]

Motivation

A substantial amount of CTPA scans in Site A were repeated due to poor image quality, they contacted the medical physics team to review. The aim of this study is to investigate the factors that influence SureStart and contribute to image quality issues.

Methodology

- A review of published literature was conducted to investigate which factors influence SureStart performance
- A survey of CTPA examination image quality from four hospitals was conducted in the context of these factors
- The following factors were researched, based on the survey:
  - Different HU trigger levels
  - Needle gauge size
  - Contrast volume
  - Vessel of interest used for ROI
  - Exposure parameters
- Comparison of SureStart protocols provided insight into leading factors that contribute to the image quality issues.

Results

- Multiple failed scans occurred at one hospital (Site A) who contacted the medical physics team.
- Table 1 and 2 below shows the different levels of contrast, HU trigger level used, and the thickness of the cannula found during research and between sites respectively

Table 1: Contrast levels, gauge sizes, and HU trigger levels seen in research

Contrast (mL)	Gauge	HU	Ref.
70	18/20	180	[4]
50-65	18	180	[5]
60	20	220 (absolute)	[6]
-	20/22	>100	[7]
60	18	150-170	[8]
60	18/20	180	[9]
80	-	120	[10]

Table 2: Contrast levels, gauge sizes, and HU trigger levels compared across 3 hospitals

Contrast (mL)	Gauge	HU	Site
-	18	**210**	A
75	18/20	160	B
50 min.	18/20	180	C

Discussion

- It was seen in research the injection rate should be increased for larger patients as well as adjusting tube voltage and current based on the patients BMI.
- One paper states “The scan parameters used for any cardiac CT should be tailored to the individual patient but also the intended application” [9].
- Site A was found to be using a higher HU trigger level (220 HU) compared to other sites (160-180 HU) and published research.
- Other sites demonstrated greater protocol flexibility, including manual triggering, increased exposure for large patients, and repeat planning scans when anatomy was unclear
- Collaboration with other hospitals was recommended to Site A and findings were shared with Site A
- A substantial amount of CTPA scans in Site A were repeated due to poor image quality and by adapting the changes to their protocol, a decrease in repeat scans and patient dose has been seen.

Conclusion

After implementing changes, an audit was conducted showing that 5% of cases were found to be inadequate, a decrease from 17.5%. This study highlights the importance of optimising the protocol and protocol flexibility when using SureStart to achieve diagnostic image quality.

Before
17.5 %
Inadequate and repeated scans

→

After
5%
Inadequate and repeated scans

References

[1]. Mayo clinic, Pulmonary embolism (https://www.mayoclinic.org/diseases-conditions/pulmonary-embolism/symptoms-causes/syc-20354647)
[2]. G. Zantonelli et al. (2022). “Acute Pulmonary Embolism: Prognostic Role of Computed Tomography Pulmonary Angiography (CTPA)”.
[3]. N.C. Dalyrmple (2009). “Multidetector Computed Tomography”.
[4]. TOBISHA (2012). “The ONE Guides: Cardiac Imaging”. One Aquilion dynamic volume CT.
[5]. S Gang et al. (2012). “Evaluation of CT coronary artery angiography with 320-row detector CT in a high-risk population”. The British Journal of Radiology, 85 (2012), 562–570, DOI:10.1259/bjr/90347290
[6]. D. Grob et al. (2018). “Imaging of pulmonary perfusion using subtraction CT angiography is feasible in clinical practice”. European Radiology (2019) 29:1408–1414, DOI: 10.1007/s00330-018-5740-4.
[7]. K. Ogawa (2021). “Visualization of small visceral arteries on abdominal CT angiography using ultrahighresolution CT scanner”. Japanese Journal of Radiology (2021) 39:889–897, DOI: 10.1007/s11604-021-01124-6.
[8]. A. Bernard et al. (2021). “Deep learning reconstruction versus iterative reconstruction for cardiac CT angiography in a stroke imaging protocol: reduced radiation dose and improved image quality”. Quant Imaging Med Surg. 2021 Jan; 11(1):392–401. DOI: 10.21037/qims-20-626.
[9]. HeartFlow (2019). “Acquisition and Reconstruction Techniques for Coronary CT Angiography”. Canon Medical Systems Scanner Platforms.
[10]. C. Otgonbaatar et al. (2024), “Superresolution deep learning image reconstruction: image quality and myocardial homogeneity in coronary computed tomography angiography”, Journal of Cardiovascular Imaging (2024) 32:30, DOI: 10.1186/s44348-024-00031-4

Reject Rate Analysis as a Tool for Patient Dose Optimisation in General Radiography

Authors: Clare Corbally, Mairéad Hyland, Aibhilinn McHugh, Bethany Mahady, Anton Tan, Nicko Mendoza, Jardine Paul Inocencio, Chloe Merritt, Patricia Egan, Dr. Niall Sheehy

INTRODUCTION

The aim of this project was to identify general radiography protocols associated with high reject rates and use these protocols, in conjunction with high-dose alert frequencies, to tailor focused staff education sessions.

The aim of these sessions was to reduce the percentage of alerts and rejected images in order to keep doses to patients As Low As Reasonably Achievable (ALARA).

METHODS

- Data was analysed from the GE XR656 X-ray system to identify protocols with particularly high reject rates. Reasons for rejected images were also reviewed for these protocols.
- Data was also extracted from the dose management software, Dosewatch, to assess which protocols had higher numbers of high dose alerts.
- Based on these results focused education sessions were held and a target of 5% was established for reject rates and dose alerts post-intervention.

RESULTS

Repeat/ Reject Reasons	Hip	Lumbar Spine	Pelvis
Patient positioning	82	65	108
Incorrect Collimation	6	7	19
Patient Jewelry/ Clothing	0	13	16
Noisy Image	4	6	10
Patient motion	3	7	9
Incorrect technique selected	0	1	4
Image Artefact	1	1	1
Poor Inspiration	0	0	0
Patient Habitus	1	0	0
Incorrect/ Missing view markers	0	0	0
Incomplete Acquisition	0	1	3

Table 1: *Reasons for repeat/rejected images 2024*

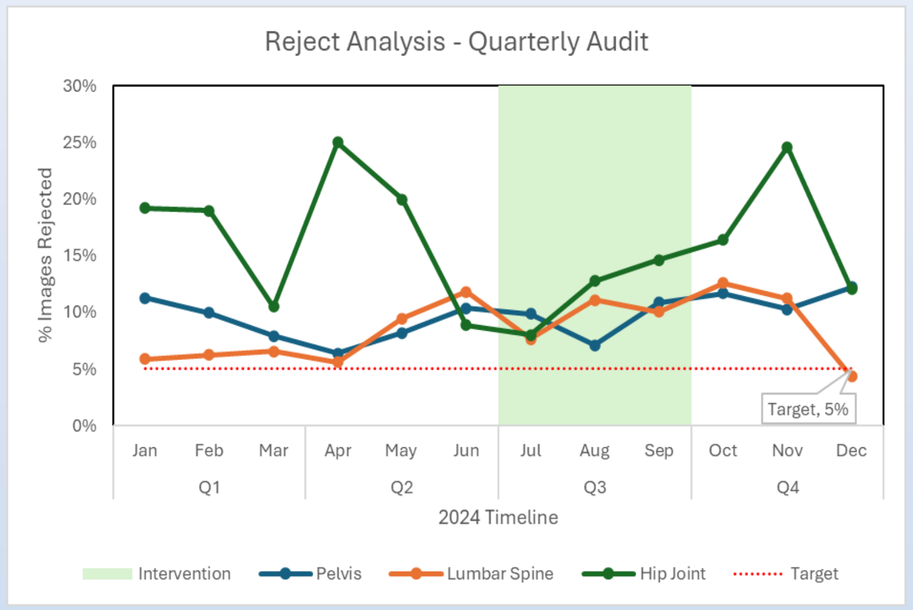


Figure 1: *Reject analysis 2024. Intervention period is shown in green.*

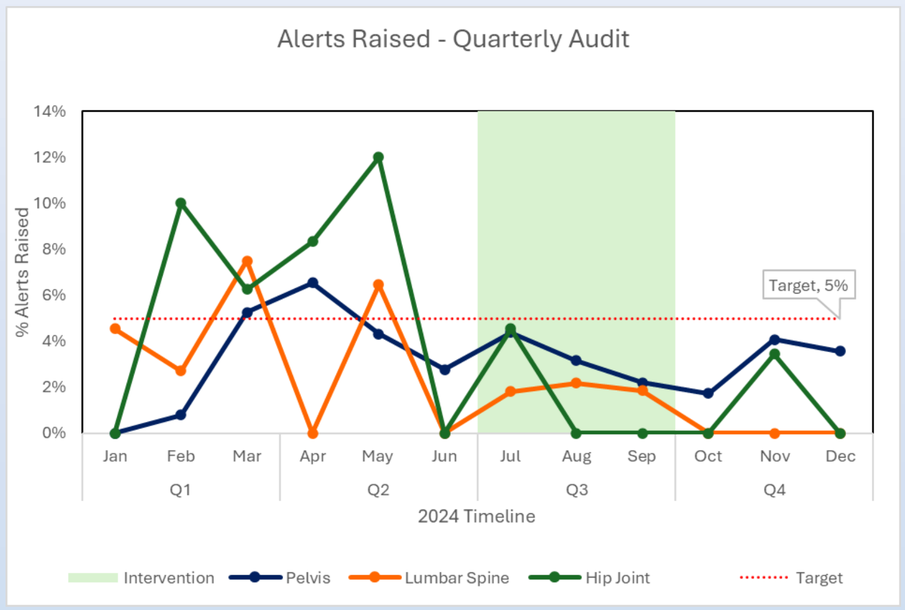


Figure 2: *Dose alerts 2024. Intervention period is shown in green.*

Repeat/ Reject Reasons	Hip	Lumbar Spine	Pelvis
Patient positioning	32	44	118
Incorrect Collimation	2	5	24
Noisy Image	2	11	12
Patient Jewelry/ Clothing	0	8	7
Incorrect technique selected	0	3	0
Poor Inspiration	0	0	0
Image Artefact	0	2	2
Patient motion	0	2	4
Patient Habitus	0	0	0
Incorrect/ Missing view markers	0	0	2
Incomplete Acquisition	0	0	1

Table 2: *Reasons for repeat/rejected images 2025*

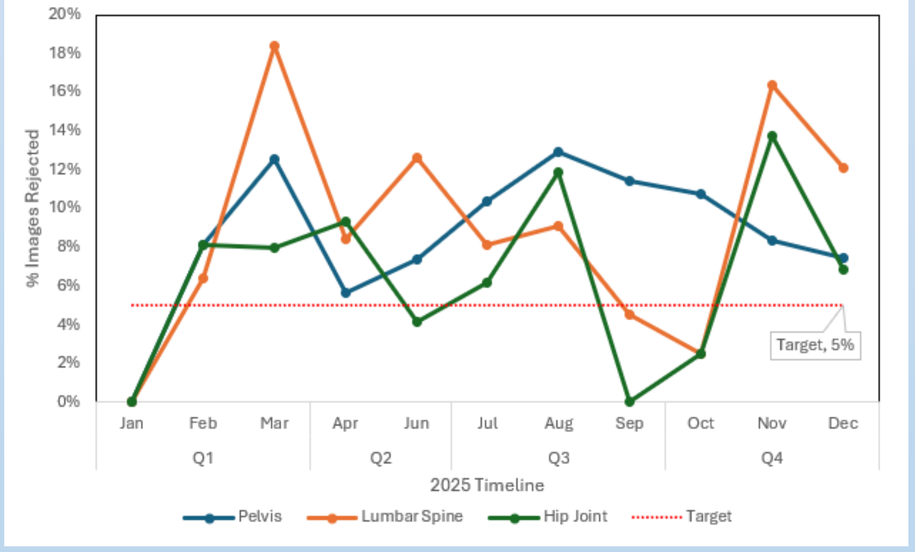


Figure 3: *Reject analysis 2025.*

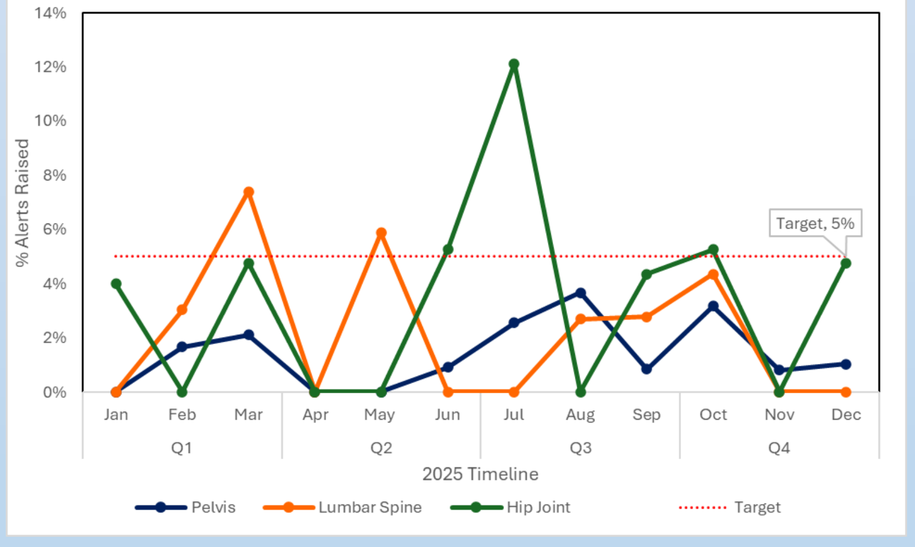


Figure 4: *Dose alerts 2025.*

- Initial data analysis indicated highest reject rates for pelvis, lumbar spine, and hip joint. Dosewatch data showed a agreement with high dose alerts and also showed inconsistent use of Automatic Exposure Controls (AECs) for these protocols.
- The most frequently selected reasons for rejecting images for all three protocols were found to be ‘collimation’, ‘patient positioning’ and ‘patient jewelry/clothing’. (See Table 1 and Table 2)
- Education sessions were held in conjunction with clinical specialist radiographers focusing on these three protocols and tailored around patient set-up and AECs.
- Dose alerts showed a decrease during intervention for all examinations, meeting the target of 5%. Reject rates decreased during intervention but did not reach the target of 5%. (See Figure 1 and Figure 2)
- Post-intervention, dose alerts increased with only pelvis examinations remaining below target (4%). Reject rates for all examinations increased post-intervention. (See Figure 3 and Figure 4)

CONCLUSIONS AND FURTHER WORK

- Overall reject rates in the department are between 5% - 7%, this meets the guidance of AAPM TG 305 which recommends ≤ 8% - however when these reject rates are further analysed for specific protocols there is an increase to as high as 25%. This indicates a need to further investigate reject rates at an individual protocol level.
- A decrease in reject rates and dose alerts was observed during intervention, however both increased again post-intervention. This is due to staff turnover in the area and complacency post-education, this highlights a requirement for continuous education rather than once-off interventions.
- This information has informed the recurring practice of education sessions by senior members of the radiography team in the domain of patient positioning, use of collimation and standardised use of AEC.

REFERENCES

1. JCI Joint Commission International (2021) Accreditation Standards for Hospitals 7th Edition, Illinois, USA
2. S.I. No. 256/2018 – European Union (Basic Safety Standards for Protection Against Dangers Arising from Medical Exposure to Ionising Radiation) Regulations 2018.
3. S.I. No. 30/2019 – Radiological Protection Act 1991 (Ionising Radiation) Regulations 2019
4. Aibhilinn McHugh, Patricia Egan, “Dose Optimisation Team – A practical implementation”, Physica Medica, 2018.
5. GE Dosewatchhttps://www.gehealthcare.com/en-ph/products/dose-management_old/ dosewatch-dose-monitoring-software-ge-healthcare. Accessed 7th June 2024
6. IAEA https://www.iaea.org/resources/rpop/health-professionals/radiology/diagnostic-reference-levels. Accessed 15th July 2024
7. https://www.hiqa.ie/sites/default/files/2022-11/Diagnostic%20Reference% 20Levels_ Undertaking%20guidance_Oct%202022.pdf. Accessed 15th July 2024
8. AAPM task group report 305: Guidance for standardization of vendor-neutral reject analysis in radiography, 2023

Beacon Hospital



Shaping the Future: Lessons Learned from Tin Filtration on the SOMATOM Go.Top

Authors: Aibhilinn McHugh, Clare Corbally, Mairéad Hyland, Cathal McShane, Laura Clowry, Patricia Egan, Dr. Niall Sheehy

Background and Aims

Tin (Sn) filtration is increasingly used in dual-source CT systems to reduce patient radiation dose and improve spectral separation. The Siemens Go.Top is a Twin Beam Dual Energy (TBDE) CT, which is a single source CT with a specialised filter. This project evaluates the clinical implementation and initial outcomes of Tin Filtration (Sn) on the SOMATOM Go.Top platform, focusing on dose reduction strategies and image quality optimization.



Fig 1: Siemens Somatom go.Top CT Scanner[3]

Methods and Materials

Using a Catphan QA phantom, standardised scan protocols were acquired using equivalent imaging parameters, with and without tin filtration. We optimised tin-filtered (Sn) CT protocols to reduce patient radiation exposure while maintaining diagnostic image quality, using equivalent effective mAs and kV. Performance was evaluated against baseline protocols, comparing scan duration, CTDIvol, DLP, and image quality.

Results

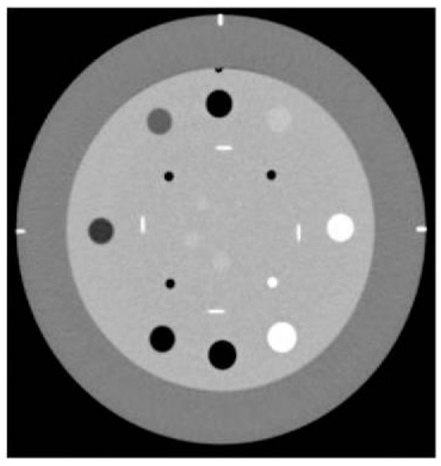


Fig 2: Catphan HU phantom[5]

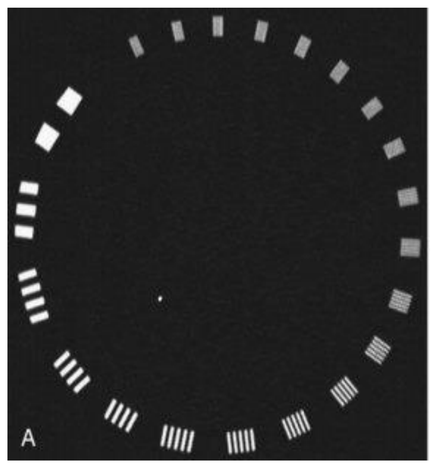
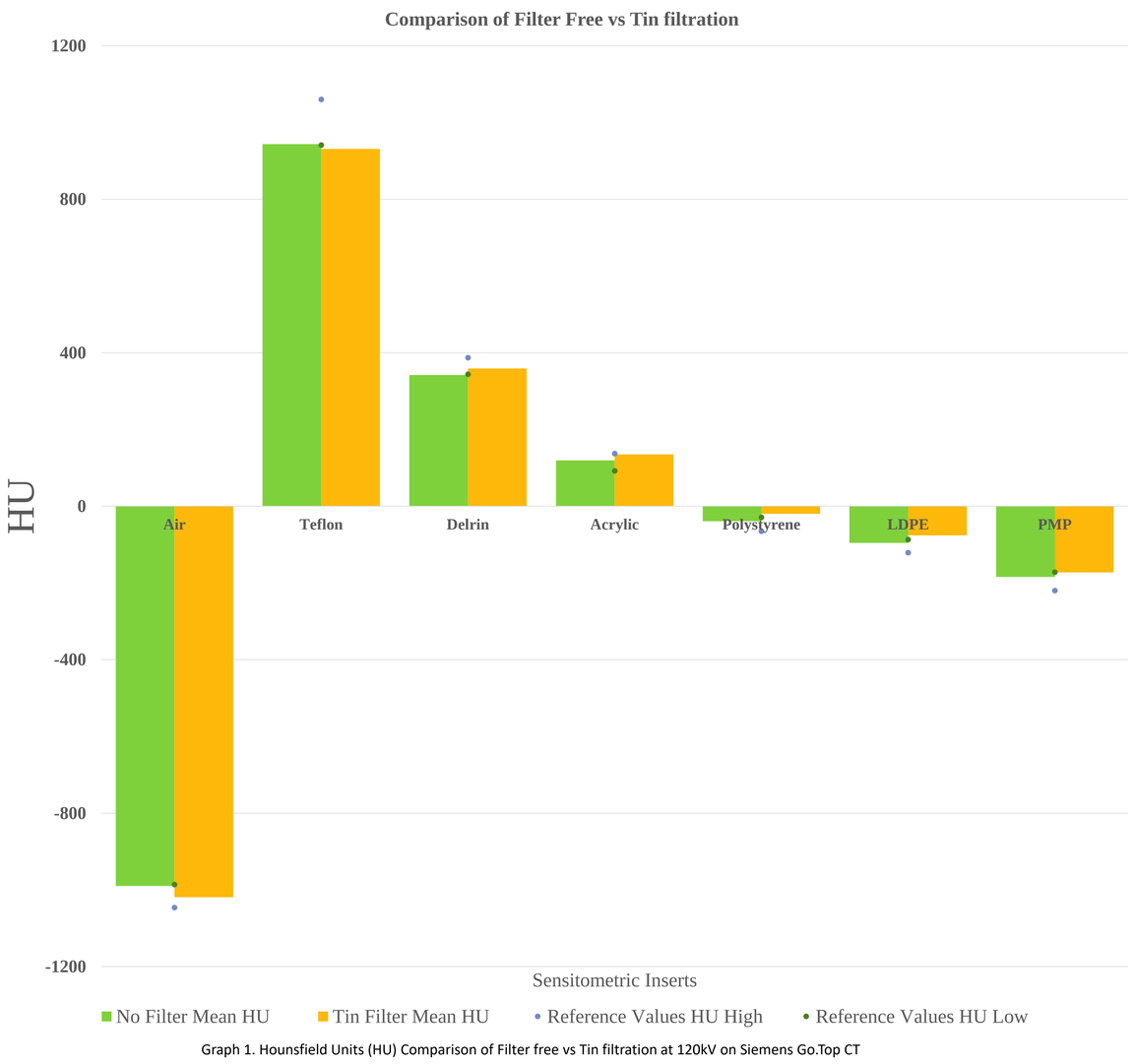


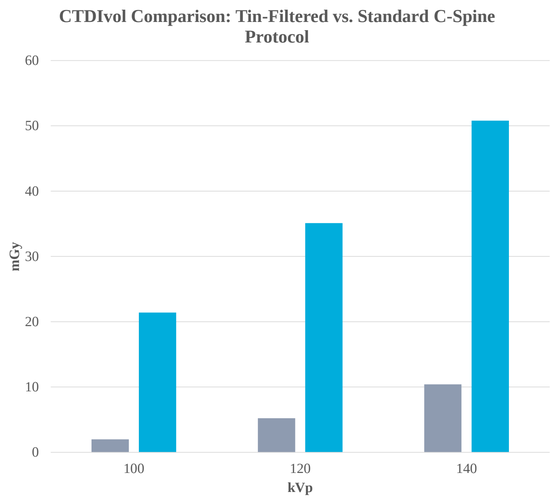
Fig 2: Catphan High spatial resolution phantom[5]



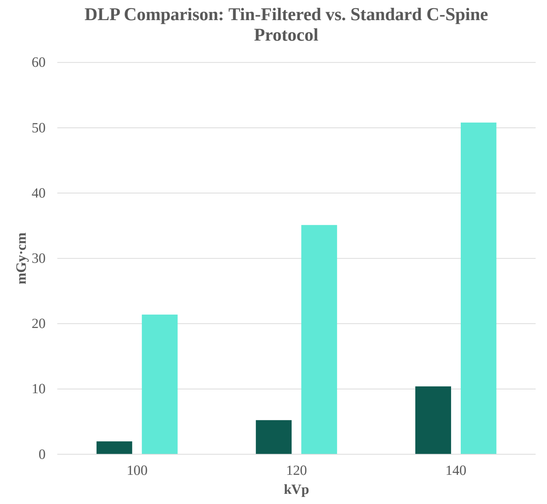
Graph 1. Hounsfield Units (HU) Comparison of Filter free vs Tin filtration at 120kV on Siemens Go.Top CT

Results

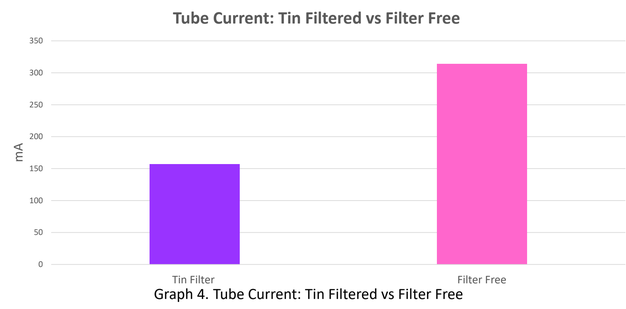
High Spatial Resolution test ,resulted in 10lp/mm for filter free and 11lp/mm for tin filtration.



Graph 2. CTDIvol Comparison: Tin-Filtered vs. Standard C-Spine Protocol Across Varying kVp with Fixed mAs

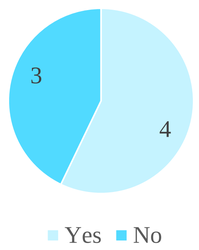


Graph 3. DLP Comparison: Tin Filtered vs Standard C-Spine protocol across varying kVp with fixed mAs

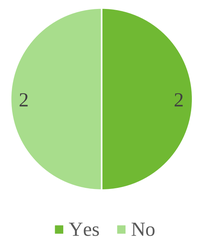


Graph 4. Tube Current: Tin Filtered vs Filter Free

Does your CT have a Tin Filter



Do you use the Tin Filter



Graph 5. Survey Results from IAPM Newsgroup

Graph 5. Survey results from IAPM newsgroup
Three centres had Siemens CT systems but no tin filtration capability.
One CT had yet to be commissioned and one was used for radiotherapy – where they wanted the kV spectrum to be the same across all protocols. The only protocol mentioned for use with tin filtration was Sinus.

Discussion

	Tin Filter	Non- Tin Filter
Dose Efficiency	★★★★★ (Excellent)	★★★☆☆ (Moderate)
Soft-Tissue Contrast	★★☆☆☆ (Limited)	★★★★★ (Excellent)
Image Noise	★★★☆☆ (Depends on patient)	★★★★★ (Low noise)
Artifacts	★★★★★ (Reduced)	★★★☆☆ (More artifacts)
Scan Duration	★★★☆☆ (Longer scan time)	★★★★★ (Quick scan time)
Best Use Cases	Lung, bone, sinus, low-dose	Abdomen, pelvis, contrast studies
Limitations	Soft tissue, large patients	Higher dose, more artifacts

Table 1. Pros and Cons of Tin Filtration Protocol vs Standard Protocol

	Twin Beam Dual Energy (TBDE)	Dual Source Dual Energy (DSDE)
FOV	★★★★★ (Large)	★★★★☆ (Medium)
Spectral Separation	★★★☆☆ (Good)	★★★★★ (Excellent)
Quantitative Imaging	★★★☆☆ (Moderate)	★★★★★ (Excellent)
Scan Duration	★★☆☆☆ (Requires cooling time)	★★★★☆ (Similar to filter free)
Best Use Cases	Lung, Ortho	Renal Stone, Iodine maps

Table 2. Pros and Cons of TBDE vs DSDE

Our results demonstrate that tin-filtered CT achieves a 50% radiation dose reduction, although it also decreases the CT attenuation for materials like Teflon, Polystyrene, and LDPE. This effect can cause an underestimation of calcium attenuation, presenting challenges for accurate cardiovascular risk classification. Therefore, specific reconstruction algorithms are required for accurate risk assessment. Notably, TBDE is more vulnerable to this than Dual Source Dual Energy (DSDE), which provides better quantitative imaging and relies less on vendor-specific post-processing. Tin filtration can increase image noise, resulting in a grainier image, which can require an adjustment period for diagnostic interpretation / reporting.

Conclusion

Although it could require specialised reconstruction algorithms and additional training for diagnostic image interpretation, the associated benefits in radiation dose reduction and spectral performance make it a valuable tool for selected clinical applications. Careful protocol selection is necessary to balance patient safety with operational efficiency.

Next Steps

For this work:

- More in-depth review of image quality across varying scan protocols
- Comparison of Siemens Go.Top (TBDE) vs Siemens Pro Pulse (DSDE)
- Use of an anthropomorphic phantom for increased dosimetric accuracy and improved clinical relevance

References

1. S.I. No. 256/2018 - European Union (Basic Safety Standards for Protection Against Dangers Arising from Medical Exposure to Ionising Radiation) Regulations 2018.
2. Report No. 233 - Performance Evaluation of Computed Tomography Systems - The Report of AAPM Task Group 233 (2019)
3. https://www.siemens-healthineers.com/en-ie/computed-tomography/somatom
4. C a t p h a n ® 500 and 600 M a n u a l
5. “How to measure CT image quality: Variations in CT-numbers, uniformity and low contrast resolution for a CT quality assurance phantom” PhysicaMedica. Vol.30 Issue.4.
6. “The Importance of Spectral Separation. An Assessment of Dual-Energy Spectral Separation for Quantitative Ability and Dose Efficiency”
Krauss B, Grant KL, Schmidt BT, Flohr TG. Invest Radiol 2015 Feb;50(2):114-8.
7. “Implementing tin-prefiltration in routine clinical CT scans of the lower extremity: impact on radiation dose”
Marth T, Kajdi G W, Stern C, Sutter R.

Evaluation of the Eggnest radiation protection device in a cardiac catheterisation lab

Keith Scully[1], Eilís O'Halloran[1], Emerald House[1], Brendan Tuohy[1], Phillip Doyle[2]

1. Department of Medical Physics and Clinical Engineering, University Hospital Galway
2. Letterkenny University Hospital

Introduction

Cardiologists are of particular interest in the monitoring of occupational radiation exposure doses due to their relatively close proximity to the patient, the source of scatter, coupled with generally high workload procedures.

This work compares the scatter protection provided by the EggNest XR (Egg Medical) radiation protection device with that of standard shielding. The standard room shielding consists of the table lead skirts and a ceiling suspended lead screen. The added protection device consists of a carbon fibre base secured to the patient couch from which flexible shielding skirts wrap the patient couch and tube head along with retractable flip shielding side panels along the side and around head of the patient bed provide additional scatter shielding.

Methodology

To compare the additional protection provided by the system, occupational doses for both the primary and secondary operators, in this case the Cardiologist and Specialist Registrar were measured during multiple procedures carried out on a Phillips Azurion 7 M12 image guidance C-arm system.

Doses were measured for a sampling of coronary angiography and PCI procedures of varying complexities and screening durations. Accumulated doses for each case were recorded using Raysafe i3 real time dosimeters, measuring the scatter dose outside of the lead apron and thyroid collar shield at hip and collar level, representative of body and eye dose.

The typical locations of the 1st and 2nd operator within the catheterisation lab and the placement of the real time dosimeter badges are presented in Fig. 1.

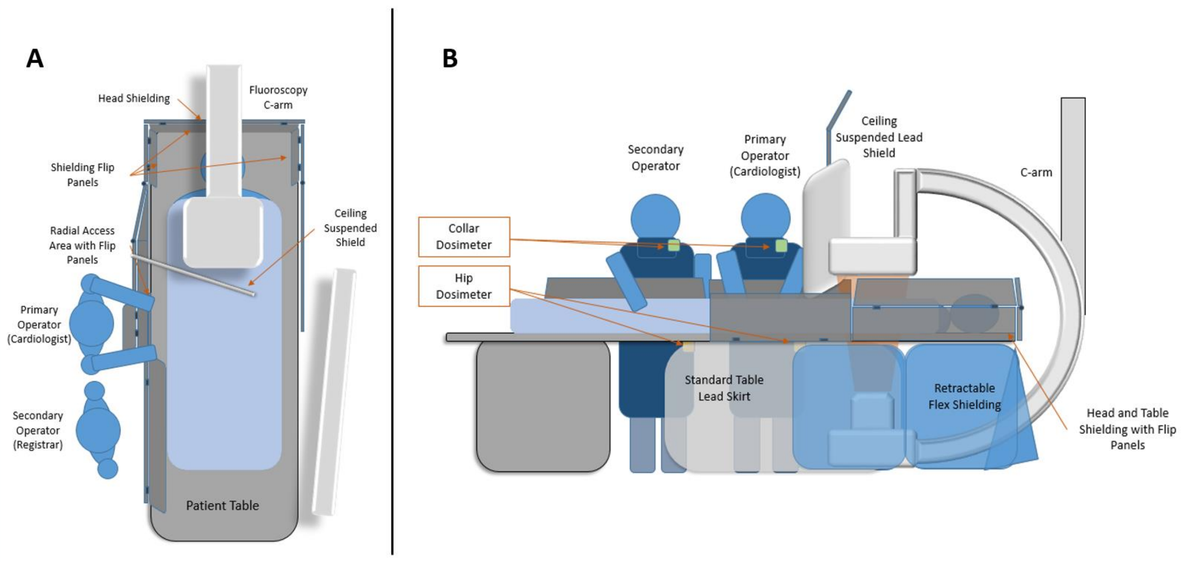


Fig. 2. Diagrams showing plan view of operator positions during a Cath lab case (A) and Side view showing operator positions along with C-arm (B), including real time dosimeter locations and both standard and additional device shielding protection provided by EggNest.

The 4 recorded doses, at hip and collar level for both operators were normalised by the total procedure dose-area-product (DAP) for each case to account for case complexity and patient variation. This provided a dose conversion factor ($\mu Sv/Gy \cdot cm^2$) for each dosimeter location for each operator. The mean, median and distribution of these DAP normalised doses were compared to assess the dose reduction capabilities of the device at different locations for both operators.

It should be noted that the Raysafe i3 dosimeters measure dose in terms of $H_p(10)$ and so are not a direct operational quantity for eye dose. However, for the purposes of considering the relative dose reductions provided by the system rather than absolute dose measurements, this was not considered an issue under the assumption that the relationship between $H_p(10)$ and $H_p(3)$ is consistent for the scatter energies measured throughout these cardiac procedures.

Results

The dose distributions for both operators at collar and hip level, with and without the additional shielding, are presented in Fig. 2. and Fig. 3.

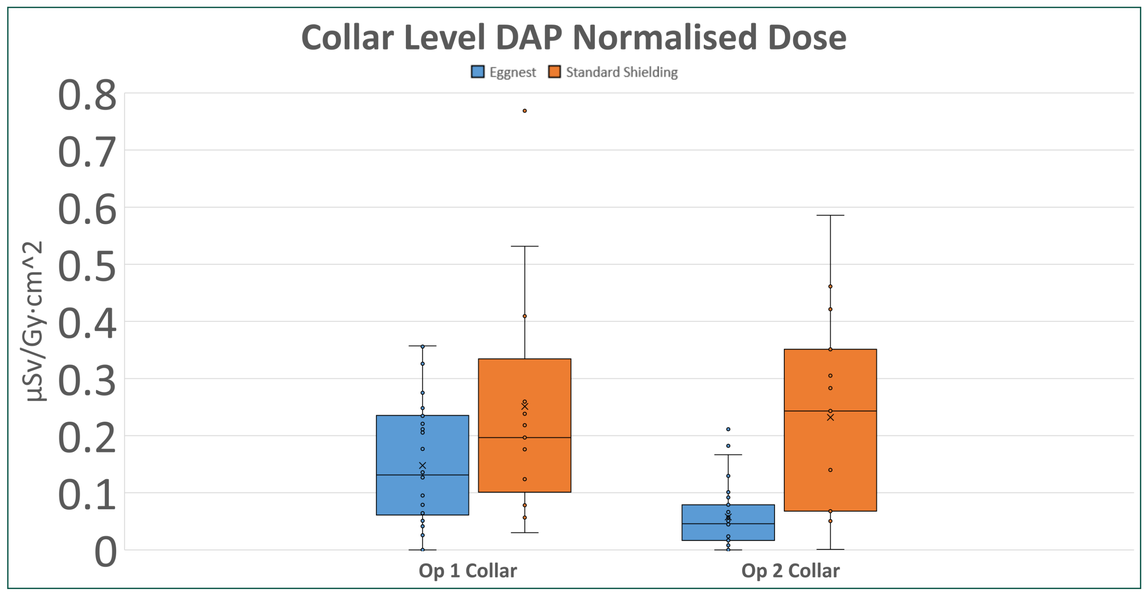


Fig. 2. Boxplots showing the distribution of normalised dose distributions measured at collar level for the primary and secondary operator, for cases with and without the protection device in the place.

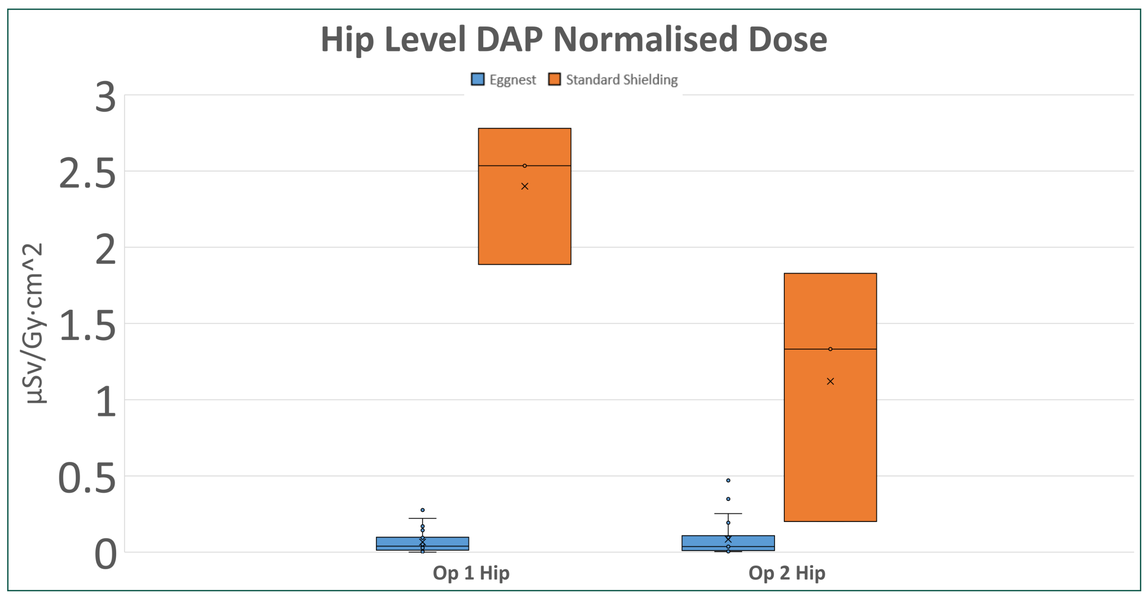


Fig. 3. Boxplots showing the distribution of normalised dose distributions measured at hip level for the primary and secondary operator, for cases with and without the protection device in the place.

Table 1. shows the percentage reduction in the average and median DAP normalised doses for cases with and without the shielding device in place.

	Primary Operator Hip Level	Primary Operator Collar Level	Secondary Operator Hip Level	Secondary Operator Collar Level
% Reduction in Mean Dose/Dap	96.4 %	41.2 %	86.5 %	75.2 %
% Reduction in Median Dose/Dap	98 %	33.3 %	83.7 %	81.1 %

Table 1. Percentage reductions in the measured mean and median normalised dose values at hip and collar levels for the primary and secondary operator.

A greater than 95% dose reduction was observed for the primary operator at hip level and over 80% reduction for the secondary operator. The collar level reduction was greater than 70% for the secondary operator. The measured reduction in collar level doses for the primary operator was less significant, approximately 41% reduction in the average and 33% reduction in the median doses.

Conclusion

This work highlights the potential dose reductions that can be achieved using this device, but with a strong dependency on the correct use of existing shielding. Most shielding at collar level for operator 1 is provided by the existing ceiling suspended lead shield in either setup. The potential eye dose reductions for the secondary operator are more significant, as the use of EggNest allows for positioning of the ceiling suspended shield in a way that provides increased protection to the secondary operator.

Body doses, as measured at hip level, would be heavily attenuated by the user's lead apron, meaning the high relative dose reductions at those areas would translate into less of an effect in absolute dose terms. Yet, assuming an approximate annual dose of 3 mSv to a Cardiologist with the standard shielding setup, the EggNest could provide body dose reductions of the order of 90%, or 2.7 mSv in annual dose savings to the operator.

Evaluation of a Local ^{18}F-PSMA-1007 PET/CT Protocol Against EANM Guidelines

D. Caldwell, M. Dooley, J. Burns, N. Fitzsimons
Mater Misericordiae University Hospital, Eccles Street, Dublin 7, Ireland

Purpose

Our hospital provides PSMA PET/CT using the ^{18}F-PSMA-1007 radiotracer. European Association for Nuclear Medicine (EANM) guidelines for PSMA PET/CT were published in 2023[1]. As our imaging protocol for PSMA PET/CT had remained unchanged since it's inception in 2022, the objectives of this study was to compare our protocol to these guidelines, identify discrepancies, and assess their impact on image quality, radiation dose, clinical practice and workflow.

Methodology

A retrospective chart review of the 123 ^{18}F-PSMA PET/CT studies in a one year period was performed. All patients were imaged on the Siemens Healthineers Biograph Vision 450 digital PET/CT scanner in our department. Data were gathered through patient notes, radiologists' reports or via Siemens *Teamplay* dose management software. Radiotracer administration was assessed by analysing injected activity per body weight and deviations from the target activity.

Uptake times were recorded and demonstrated a bimodal distribution, reflecting real-world workflow constraints. This prompted comparison of PET image quality between shorter uptake (60–70 minutes) and guideline-recommended uptake (90–100 minutes). Image quality was evaluated by three registrar radiologists for 30 patients in each uptake time group using a five-point Likert scale assessing overall image quality, lesion conspicuity, and perceived noise.

CT acquisition parameters were analysed, including scan range, patient positioning and dose-length product (DLP). Effective doses were derived for both PET and CT components, and local diagnostic reference levels (DRLs) were compared with national benchmarks.
Protocol modifications implemented during the study period, particularly changes in patient arm positioning, were also evaluated for their impact on dose metrics.

Main Differences

Parameter	EANM Guidelines	Local Practice
Injected Activity	3-4 MBq/kg	2.6 MBq/kg
Uptake Time	90-120 minutes	Varied – but 65% < 90 mins
Scan Range	Vertex to mid-thigh	Vertex to mid/distal tibia
CT Component	Attenuation correction CT	Diagnostic quality CT
Arm Position	Above head	Varied

Table 1: Summary of main differences between EANM Guidelines and local practice.

Injected Activity

The median injected activity was found to be 2.6 MBq/kg, lower than EANM guidelines. This is due to the increased sensitivity and improved resolution of a digital PET/CT system. However, significant variability was observed, with deviations of up to 66% from the intended activity (Fig. 1). Only 58% of patients received the intended 2.5 MBq/kg This highlights the practical challenges of manually dispensing low radiotracer volumes and suggests a role for automated dispensing systems to improve accuracy as well as reducing radiation exposure.

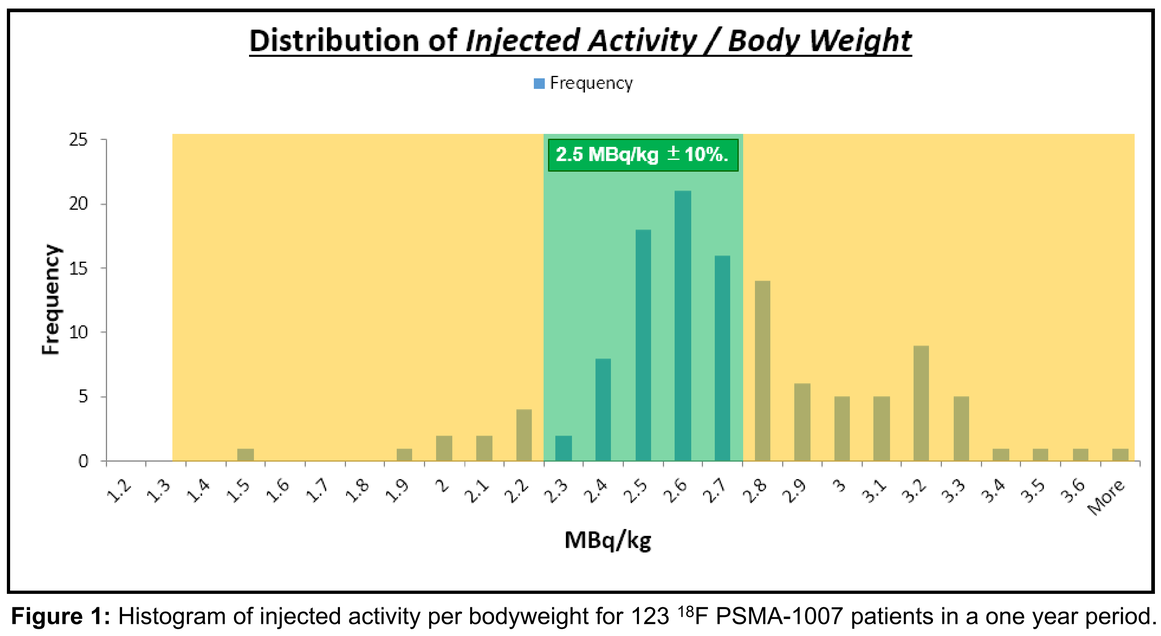


Figure 1: Histogram of injected activity per bodyweight for 123 ^{18}F PSMA-1007 patients in a one year period.

Uptake Time

Further investigation found that differences in uptake times was due to delayed PSMA delivery times and staffing/funding issues. Despite a large proportion of scans being acquired before the recommended 90-minute uptake time, no statistically significant difference in image quality was observed between early and standard uptake groups (p = 0.686). All examinations were deemed diagnostically acceptable. This suggests that, in this setting, uptake times of ≥ 60 minutes are sufficient for maintaining diagnostic image quality, providing flexibility for workflow optimisation without compromising clinical utility.

Scan Range and CT Component

In our hospital, ^{18}F-PSMA PET/CT scans can extend from the vertex to the ankles, influenced by local experience and incidences of tibial metastases (n=2) in our patient population. Compared with EANM guideline ranges (Fig. 2a), this broader coverage increases dose-length product (median = 967 mGy·cm) and scan time. The CT component contributed a median 14.2 mSv (74%) to the whole-body effective dose, versus 4.8 mSv from the PET component (Fig. 2b). The protocol incorporates a full diagnostic CT to provide comprehensive, contrast-enhanced "one-stop" staging, reducing the need for additional appointments and dual read-outs. All studies are interpreted by radiologists with nuclear medicine training within MDT reviews, improving diagnostic confidence and workflow efficiency. This approach is driven by limited radiotracer access and the need to streamline patient pathways. Our local DRL for the CT component significantly exceeds the national DRL, however, full diagnostic CT scans cannot be directly compared to protocols where ^{18}F PSMA is paired only with an attenuation correction CT.

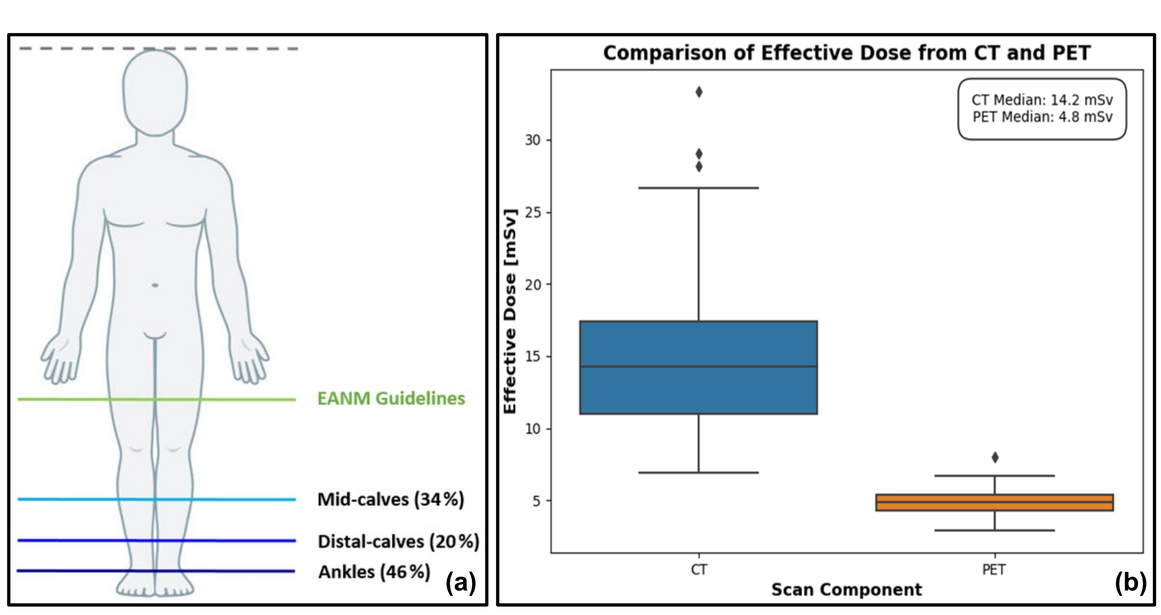


Figure 2: (a) Percentage distribution of local scan ranges vs. EANM guidelines (b) Boxplot of effective doses of CT and PET components of local PET/CT PSMA scans over a one year period.

Patient Positioning

Arm position varied depending on patient's ability to tolerate arms above their head. Higher CT doses and instances of streaking artefacts were associated with arms down. Post-audit, bed speed was increased from 1 mm/s to 1.4 mm/s from vertex to mid-thigh and 1.7 mm/s from mid-thigh to ankle to facilitate patients keeping their arms up for the duration of the scan. Median DLP for the CT component has decreased by 21% to 765 mGy·cm. Radiologists are satisfied with PET image quality and no artefacts have been reported. Fig. 3 shows the difference in median DLP between various arm positions.

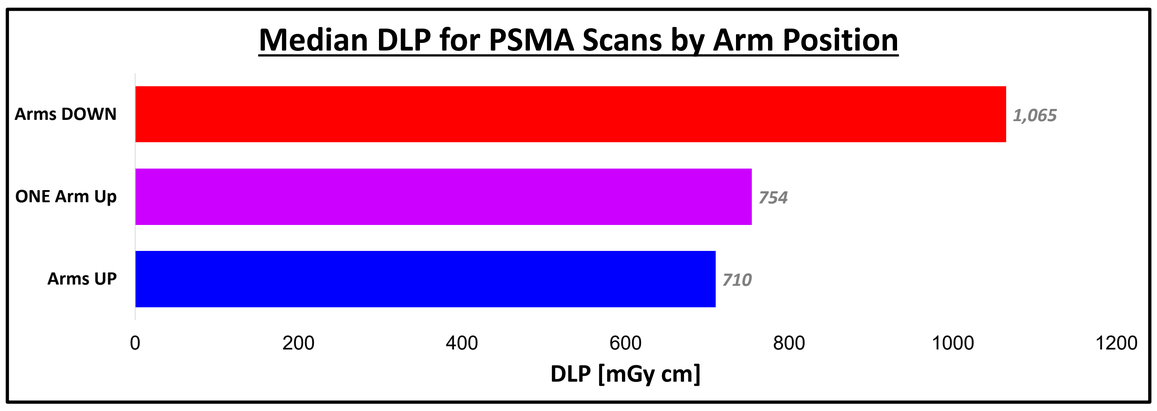


Figure 3: Median DLP for the CT component by arm position.

References

1. **Fendler, W. P., et al.** (2023). PSMA PET/CT: Joint EANM procedure guideline/SNMMI procedure standard for prostate cancer imaging 2.0. *European Journal of Nuclear Medicine and Molecular Imaging, 50*(5), 1466–1486. https://doi.org/10.1007/s00259-022-06089-w

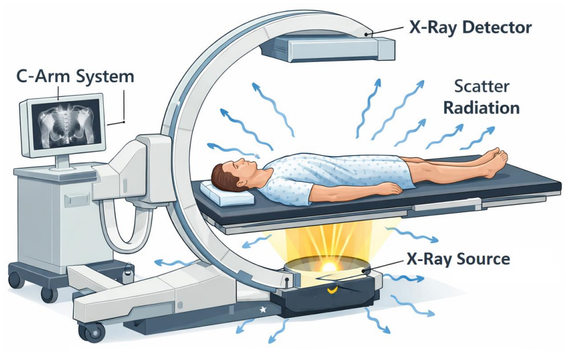
Radiation Risk Assessment of Mobile C-Arm Use in Operating Theatres: Implications for Occupational Dose Monitoring

Niyati Kamalasanan, Julie Lucey, Qudus Yusuf , Mohamed Galal

BLACKROCK HEALTH
HERMITAGE CLINIC

Objectives

The objectives of the study are to estimate occupational radiation exposure to theatre staff from mobile C-arm systems in the operating theatre across the different specialties - Orthopaedics, Vascular, Pain Management, and Urology, both with and without control measures, including reasonably foreseeable incidents and workloads on other sites. Additionally, the objectives include evaluating the necessity of ongoing routine personal dose monitoring and to estimate radiation doses across different staff roles in order to inform decisions regarding dosimeter use.



Background

Mobile C-arm fluoroscopy is widely used in operating theatres to provide real-time imaging during surgical procedures, resulting in occupational exposure to scattered radiation. There is significant disparity between different specialties, not only in terms of dose area product (DAP) and associated scattered radiation, but also with respect to tube orientation, pulse rate proximity of staff to the X-ray tube, all of which influence exposure levels. While personal dose monitoring is routinely implemented, dosimetry badge readings may be unreliable in many cases due to poor compliance with wearing the issued dosimeters. As a result, a more accurate approach to estimating occupational dose may be achieved through analysis based on patient DAP readings.

In accordance with SI No. 30/2019 – European Union (Basic Safety Standards for Protection Against Dangers Arising from Medical Exposure to Ionising Radiation) Regulations, the Undertaking is required to assess and optimise occupational exposures in consultation with the Radiation Protection Adviser (RPA), and Radiation Protection Officer (RPO). Advances in imaging technology and the routine use of protective measures may have reduced exposure levels compared to historical estimates. This study therefore evaluates occupational radiation doses among theatre staff and the necessity for continued routine personal dose monitoring in line with regulatory requirements.

Methodology

Data collection (4months in 2025).

Following details were gathered and analysed:

- Procedure type
- Theatre in use (T1 – T7)
- C-arm system used :GE OEC 1, GE OEC 1 –Big detector , BV Pulsera
- Consultant performing procedure
- Dose Are Product (DAP) recorded

Case selection & scatter measurements.

- Annual DAP calculated for each procedure type
- Representative “worst-case” scenarios selected (smallest theatre – T7, typical clinical settings)
- Scatter measurements performed

Dose estimation.

- Calculation of Dose per procedure derived from measured scatter dose – scaled to weekly and annual: considering workload.
- Staff group involved – Radiographers, Consultants, Anesthetic staff, scrub nurse and circulating nurse.

Control measures (Defined & Applied).

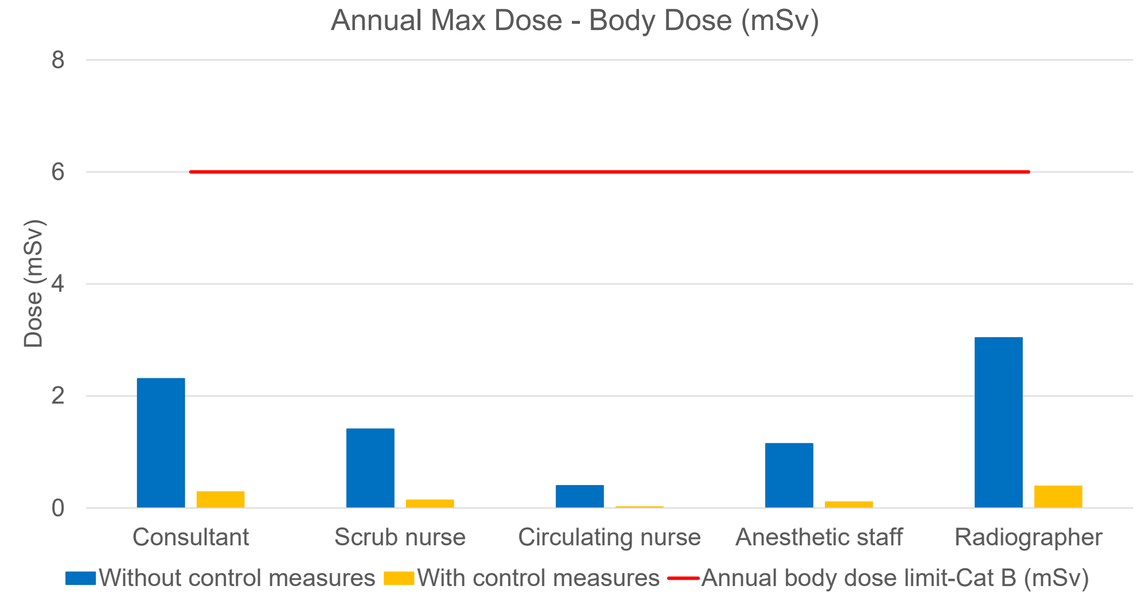
- Control measures included: Lead gown, thyroid shields and lead screen;
- Working practices: staff positioning, distance from source.
- Dose reduction factors involved:
  - ➢ Lead attenuation factors
  - ➢ Distance correction

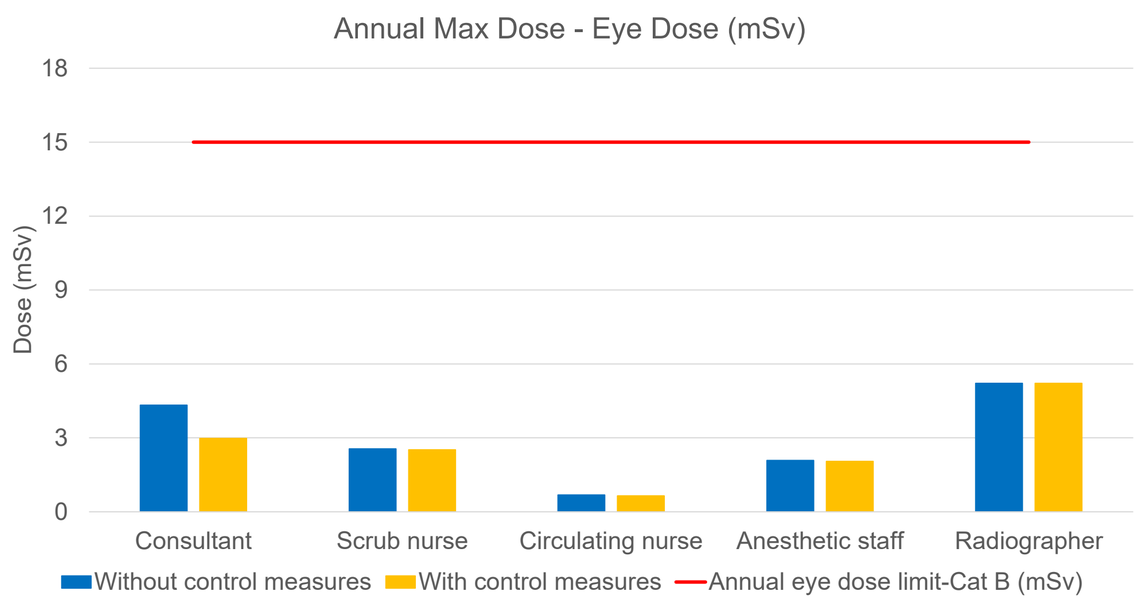
Comparison & categorisation.

- Estimated staff dose calculated and compared to With and without use of control measures
- Staff - categorized into category A & B and non-exposed workers based on limits under regulation, SI 30/2019

Results

Estimated occupational dose – Well below public dose limits !
Weekly & Annual exposure – minimal to all staff.
Use of PPE justified to reduce dose to negligible levels.





Conclusion

The risk assessment was successfully completed in accordance to the legislation and EPA guideline for undertaking on the application of the ionising radiation regulation (IRR19).

- The theatre occupational eye and body dose was estimated by utilising the scatter dose rate measurements at different dose modes, equipment magnification modes and c-arm orientations at different procedures.
- Considering estimated dose with and without operational control measures in place and including foreseeable incidents.
- All theatre staff (excluding the radiographers) working directly with the c-arm in theatre are now considered as uncategorised radiation workers.
- External shared dose for theatre staff is no longer required following current classification.
- Staff will no longer be badged for routine personal dose monitoring, electronic personal dosimeters (EPD) is available upon request by staff for reassurance/comfort purposes.

ACTION PLAN FOR CONTINUED COMPLIANCE:

- Provide re-education to theatre staff following outcome from the risk assessment regarding new monitoring arrangements.
- Annual review of risk assessment as prescribed in the Statutory Instruments Radiological Protection Act 1991 (Ionising Radiation) Regulation 2019.

Measured Dose rate:

Distance from tube (m)	Exposure Mode	Field Size	C-arm position	Dose Rate (mSv/hr)	
				Eye level	Body
1.0 from centre of px distance from detector to px - 9cm	Normal	Norm	Vertical	0.560	0.579
		Mag2		0.139	0.169
	High	Norm		0.754	0.821
		Mag 2		0.207	0.260
	Normal	Norm	Lateral	2.506	0.856
		Mag 2		0.525	0.246
	High	Norm		3.529	1.271
		Mag 2		0.790	0.367
	Normal	Norm	LAO Oblique 10degree	0.426	0.813
		Mag2		0.703	0.227
	High	Norm		2.497	1.088
		Mag 2		1.053	0.365

Dose per procedure calculated:

Procedure	C-arm in Vertical position	C-arm in Lateral position	Eye (mSv)	Body (mSv)
Angioplasty	100%	-	0.056	0.062
Disectomy	100%	-	0.001	0.001
Ortho	50%	50%	0.014	0.007
Urology	100%	-	0.001	0.001
Painblock Injection	50%	50%	0.003	0.001

Vio Buchete © 2007
http://buchete.googlepages.com

Systematic Comparison of Foetal Radiation Risk with Selected Modifiable Risk Factors; Risk Magnitude, Evidence Certainty & Communication Style

Emer Kenny[1,2] | John Legge[3] | Paddy Gilligan[1,2] | Seán Cournane[2,3]

[1]Mater Misericordiae University Hospital [2]University College Dublin [3]St. Vincent's University Hospital

BACKGROUND

CT Foetal Risk

CT foetal doses remain well below deterministic thresholds (<20 mGy vs 100 mGy). Stochastic risk is quantified using the conservative LNT model (odds ratio (OR) ~1.4 at 10 mGy) [1]

Modifiable Risk Factors

Published meta-analyses report comparable or higher childhood cancer ORs for maternal exposures (smoking, alcohol, coffee, etc) — yet these are rarely framed using the same quantitative frameworks applied to radiation.

Aim

Systematic comparison of childhood cancer risk estimates from CT exposure with selected non-radiation pregnancy exposures, examining alignment between risk magnitude, evidence certainty, and communication style.

METHODS

1 Study Design

Literature-based review. OR estimates for 10 mGy CT foetal exposure were compared with ORs for modifiable risk factors (selected where published meta-analyses reporting childhood cancer ORs were available) from systematic reviews (2014–2025) [4,5,6,7,8,9].

2 Evidence Certainty

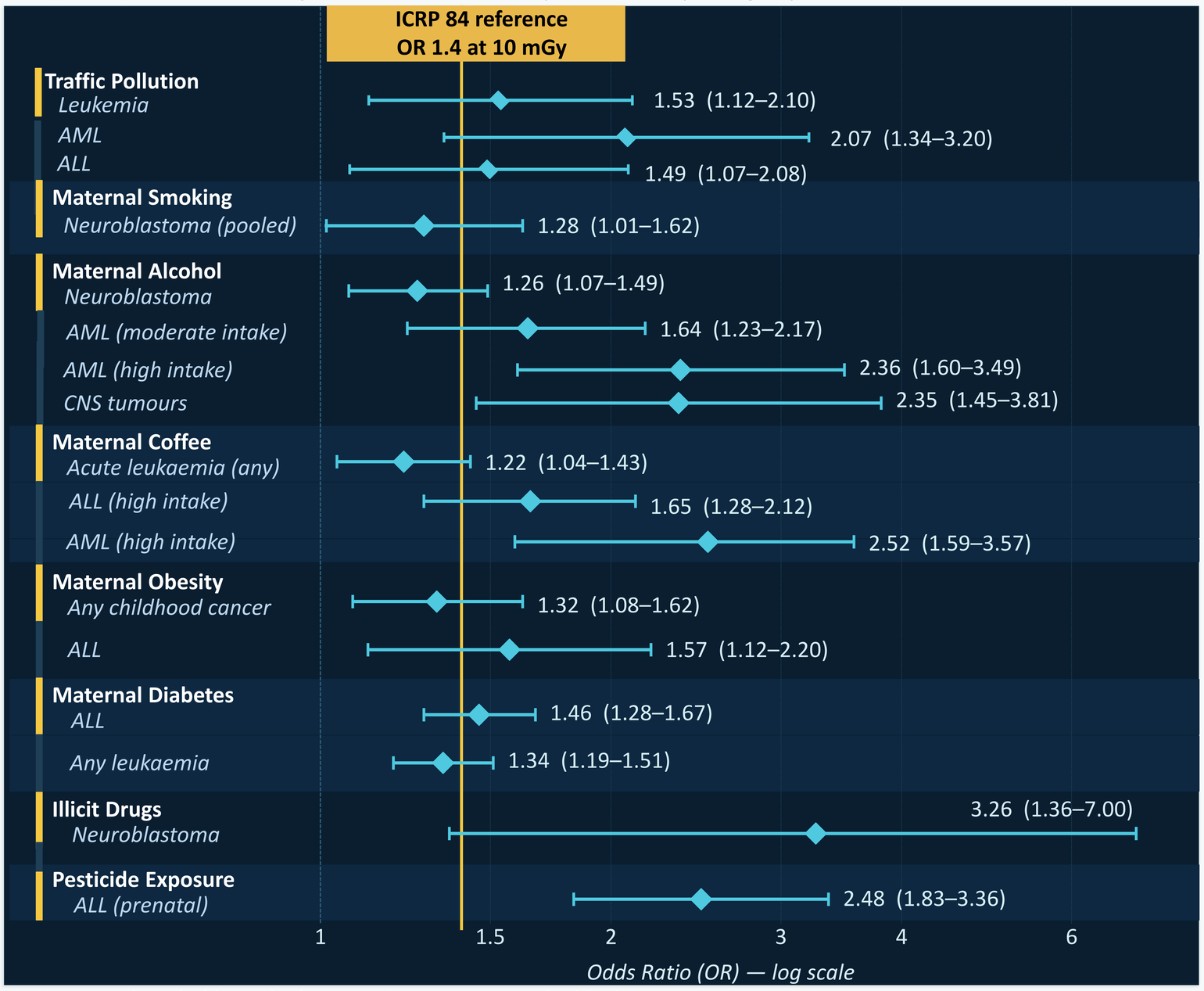
Risk factors were assessed for strength of evidence supporting association with childhood cancer, rated qualitatively based on study design, consistency, whether higher exposure increases risk, and whether evidence is direct or extrapolated. No formal grading tool applied.

3 Word Frequency Analysis

Irish and international guidance documents analysed for risk communication language. Word frequency results visualised as word clouds, where font size reflects term frequency.

CONTEXTUALISATION: ODDS RATIOS — MODIFIABLE RISK FACTORS vs. CT FOETAL RADIATION

Reported effect size (OR) ranges from published meta-analyses. Vertical solid line = ICRP 84 reference for 10 mGy foetal CT dose (OR 1.4). OR — the ratio of outcome likelihood in exposed vs. unexposed groups.



ALL = acute lymphoblastic leukaemia; AML = acute myeloid leukaemia

CONTEXTUALISATION: EVIDENCE CERTAINTY

CT Radiation — LNT — Low–Moderate

Modelled from high-dose atomic bomb survivor data [10,11]. Not directly measured at CT doses. LNT is a conservative assumption — actual risk at low doses may be lower [1]

Maternal Smoking — Moderate–High

Consistent results across multiple large studies. Clear biological mechanism (carcinogens cross the placenta) [4,7].

Maternal Alcohol — AML — Moderate–High

Large evidence base (39 studies, >16,000 cases) [6]. Clear dose–response: higher intake = higher risk. Effect seen across multiple cancer types [5].

Maternal Coffee — Moderate

Multiple studies show dose–response (higher intake = higher risk). However, other factors may partly explain the association [4,5]

Maternal Obesity — Moderate

Large studies show consistent association [9]. Plausible biological mechanism, but other contributing factors not fully excluded.

Maternal Diabetes — Moderate

Consistent findings in large studies [9]. Plausible biological pathway, but confounding factors not fully excluded.

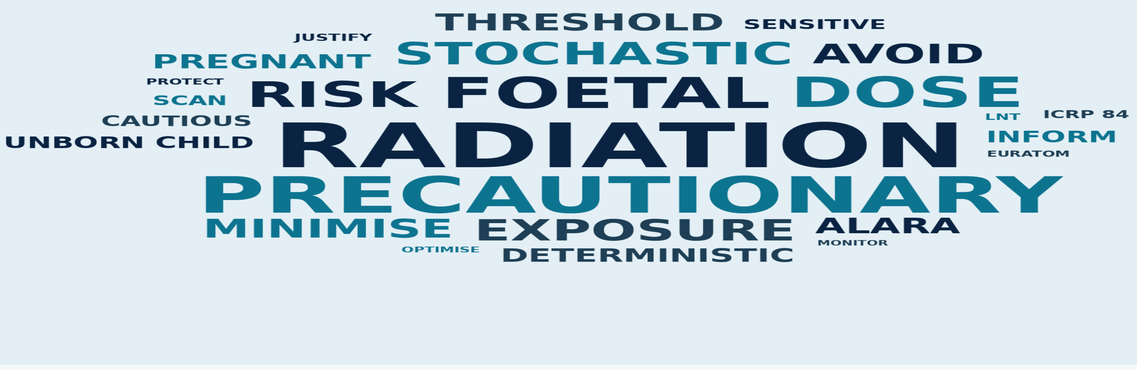
Pesticide Exposure — High

Umbrella review [8] — rated 'convincing' evidence. Consistent across multiple independent study types with clear dose–response

PATIENT-FACING MATERIALS: COMMUNICATION ANALYSIS

RADIATION / CT SOURCES

IAEA RPoP · HSE CT Leaflets · EPA · ICRP 84 · HIQA



MODIFIABLE RISK FACTOR SOURCES

HSE My Pregnancy Book 2020 · WHO · NHS Inform



DISCUSSION & CONCLUSIONS

Perception vs Evidence

The asymmetry is in framing, not evidence. CT foetal dose receives quantified and precautionary language; comparable modifiable risks are communicated qualitatively.

Clinical Concerns

Radiation concerns in pregnancy may delay time-critical imaging. In pulmonary embolism, trauma — delayed diagnosis may carry greater risk than the stochastic foetal dose.

Standardised Framing

Patient-facing materials should present all pregnancy-related risks using consistent frameworks, enabling proportionate informed consent.

Medical Physicist's Role

Physicists are uniquely placed to bridge dosimetry and clinical communication — providing contextualised risk data, not only dose quantification.

Study Limitation

CT is clinically indicated; modifiable exposures are not. This study's comparison contextualises childhood cancer risk magnitude but does not assess benefit/risk ratio.

Future Work: Evaluate clinician risk perception of childhood cancer from foetal CT versus medication and hospital interventional risks in pregnant patients.

KEY REFERENCES

[1] ICRP Publication 84 (2000). Pregnancy and Medical Radiation. Ann ICRP 30(1):1–43.

[2] HIQA (2023). National Diagnostic Reference Levels for CT Examinations. Dublin: HIQA.

[3] HSE (2020). My Pregnancy. Health Service Executive, Ireland.

[4] Emeny RT et al. (2025). Causes of Childhood Cancer Part 2: Pregnancy & Birth Factors. Cancers 17:2499.

[5] Emeny RT et al. (2025). Causes of Childhood Cancer Part 3: Environmental & Occupational Factors. Cancers 17:3516.

[6] Karalexi MA et al. (2017). Parental alcohol consumption and risk of childhood leukaemia. Eur J Cancer 78:48–62.

[7] Müller-Schulte E et al. (2018). Tobacco, alcohol & illicit drugs in pregnancy and neuroblastoma risk. Arch Dis Child Fetal Neonatal Ed 103:F467–F473.

[8] Onyije FM et al. (2022). Risk factors for childhood ALL: umbrella review. Cancers 14:382.

[9] Marley AR et al. (2022). Prepregnancy BMI, gestational weight gain, maternal diabetes and childhood cancer. JNCI Cancer Spectrum 6(2).

[10] Pearce MS et al. (2012). Radiation exposure from CT scans in childhood and subsequent leukaemia/brain tumour risk. Lancet 380:499–505.

[11] Linet MS et al. (2012). Cancer risks associated with external radiation from diagnostic imaging. CA Cancer J Clin 62:75–100.

[12] IAEA RPoP. Radiation Protection of Patients. iaea.org/rpop

IAPM Annual Scientific Meeting 2026

Keywords: radiation protection · foetal risk · CT foetal dose · pregnancy · risk communication

Image quality assessment of clinically-applied CBCT protocols using a QRM Cone Beam phantom

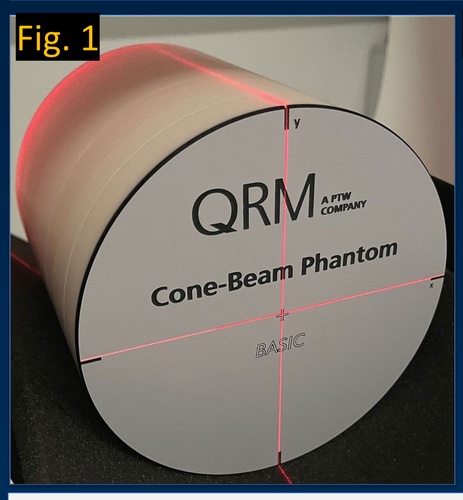
Alexandra Pericica*[1], Ronan Faulkner[1], Thomas Heary[1]

1 Medical Physics & Clinical Engineering, Beaumont Hospital

**Corresponding author: alexandrapericica@beaumont.ie*

Introduction

- Cone beam CT (CBCT) is implemented across a range of interventional, surgical, and diagnostic systems, with image quality characteristics varying between platforms and clinical protocols.
- Our hospital employs four CBCT-capable systems for diverse applications:
  - Artis Icono (interventional head/abdominal procedures)
  - Artis Pheno (neuro/vascular interventions)
  - Multitom RAX (orthopaedic extremities)
  - O-Arm (spine/trauma navigation)
- The purpose of this study is to (a) establish baseline image quality metrics to support quality assurance and optimisation and (b) perform a cross-platform assessment of CBCT image quality using clinically applied protocols.



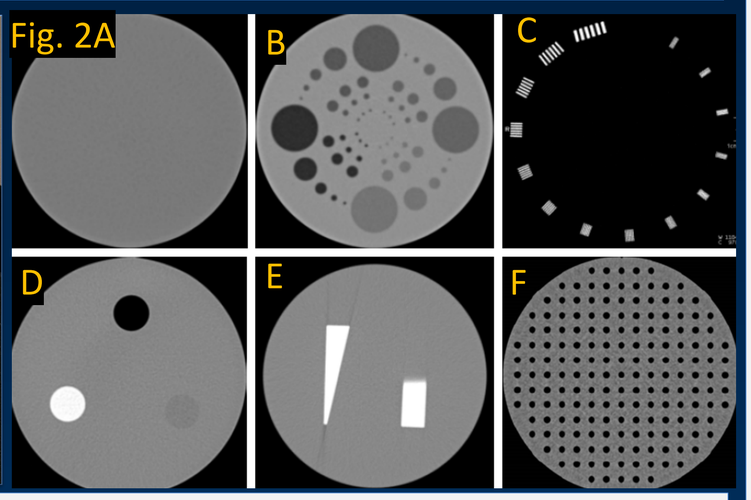


Fig 1 & 2: QRM Cone Beam phantom (PTW) and its respective modules

A. Uniformity B. Low contrast C. Spatial Resolution D. Scaling and noise E. MTF Wedges F. Geometric distortion

Methodology

- For each system, clinical protocols were selected to ensure results reflected day-to-day practice.

Device	Protocol	kV	mA	s
Artis Icono, Room A	8sDCT Head	109	400	8
Artis Icono, Room B	5sDCT Body	90	122	5
Multitom Rax	3D U Knee HQ	117	1	6
Medtronic O-Arm	Body 32	120	40	13
Artis Pheno (Hybrid)	4s DR Head	70	400	4

Table 1: CBCT Devices and protocols analysed

- Image quality assessment was conducted in accordance with EFOMP–ESTRO–IAEA guidelines[1]. Metrics include contrast-to-noise ratio (CNR), image uniformity index, signal-to-noise ratio (SNR), image noise index, MTFs, and geometric linearity.
- **Contrast to noise ratio (CNR)** was obtained using module D seen in Fig 2[1]:

$$CNR = \frac{\left|\mu_{\text{insert}} - \mu_{\text{background}}\right|}{\sigma_{\text{background}}}$$

where μ_{insert} and $\mu_{\text{background}}$ are the mean pixel values of an ROI in the insert and background respectively, and $\sigma_{\text{background}}$ is the corresponding standard deviation of the pixel value in the background region.

- **Image uniformity** was obtained using five homogeneous ROIs throughout module A of the phantom[1]:

$$Uniformity = \frac{|\text{CNR}|}{D_{\max}}, where\ D_{\max} = \max(|\mu_i - \bar{\mu}|)$$

Where μ_i = mean pixel value of each ROI and $\bar{\mu}$ = average mean pixel value over all ROIs

- **Signal-to-noise Ratio (SNR)** was defined as[2]:

$$SNR = \frac{\mu_{\text{ROI}}}{\sigma_{\text{ROI}}}$$

- **Image noise index** was defined as the mean standard deviation across the five homogeneous ROIs, representing pixel-value variability in a uniform region[1].
- **Spatial resolution** was quantified via modulation transfer function (MTF) measurements using the Slanted Edge MTF plugin in ImageJ. Five ROIs were analysed per dataset, with final MTF values reported as mean ± standard deviation.
- **Geometric linearity** was measured on module F using automated centroid detection in ImageJ. Neighbour spacings were calculated within rows/columns, with $error = \frac{\sigma(d)}{\bar{d}} \times 100\%$ (std/mean spacing).

References

[1] Heras Gala, H. et al. (2019) Quality control in cone-beam computed tomography (CBCT) EFOMP-ESTRO-IAEA protocol.

[2] Elkhateeb, S.M., Torgersen, G.R. and Arnout, E.A. (2016). Image quality assessment of clinically-applied CBCT protocols using a QAT phantom. Dentomaxillofacial Radiology, 45(5)

Results

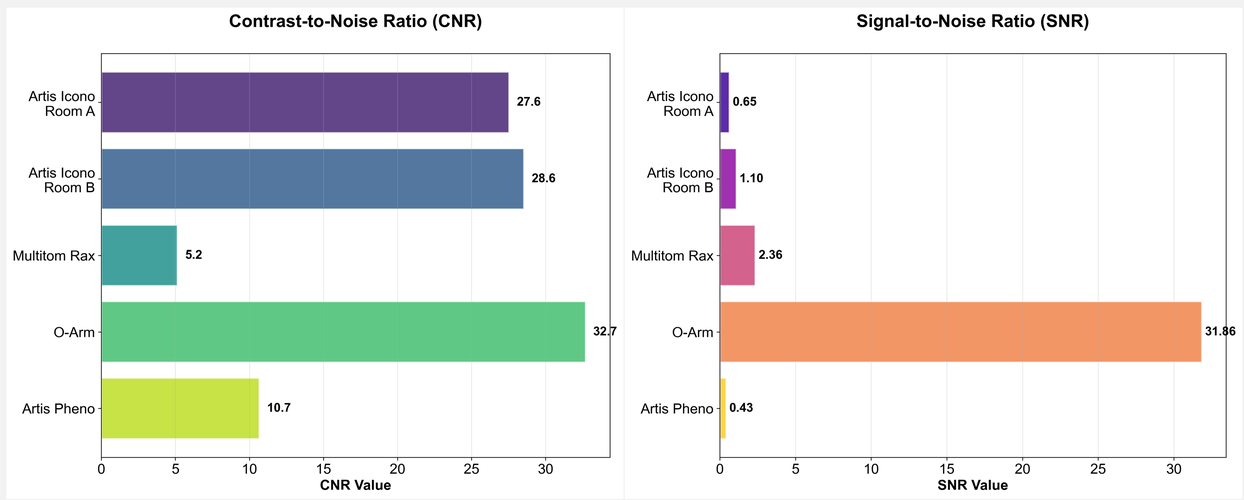


Fig 3: CNR and SNR for CBCT devices. O-Arm is the strongest according to both metrics, reflective of the high mAs and kV used in comparison to the Siemens systems.

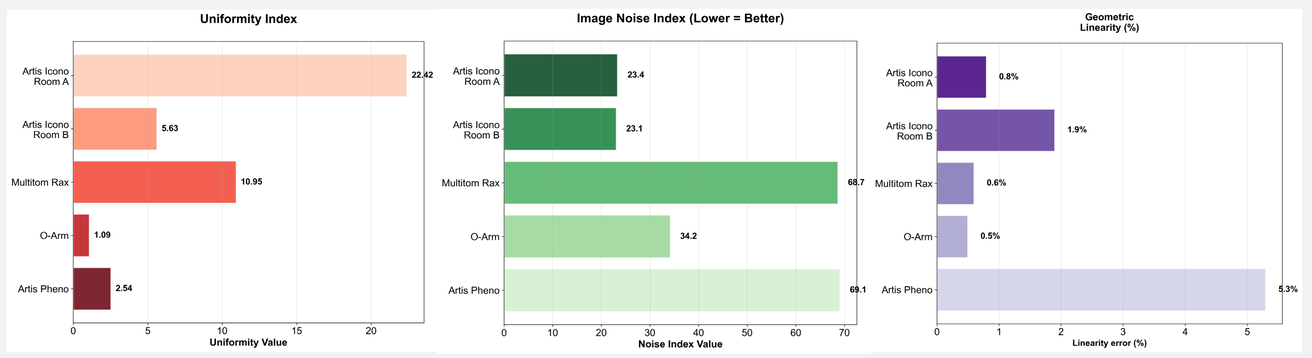
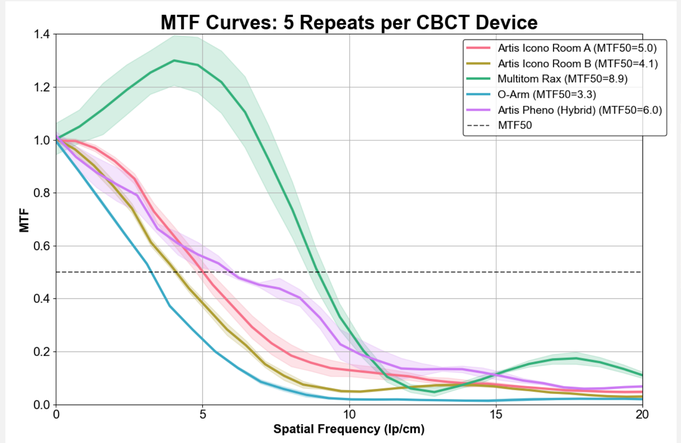


Fig 4: Uniformity, Image Noise Index and Geometric linearity error for each CBCT device. Artis Icono A demonstrates superior performance across these 3 stability metrics.



Device	MTF 50% (lp/cm)	S. Dev	MTF 10% (lp/cm)	S. Dev
Artis Icono, Room A	5.02	0.25	12.17	8.64
Artis Icono, Room B	4.10	0.09	8.64	1.03
Multitom Rax	8.91	0.31	18.60	3.22
Medtronic O-Arm	3.26	0.03	6.77	0.11
Artis Pheno (Hybrid)	6.00	0.23	14.67	1.07

Fig 5: MTF curves along with MTF 50 % and MTF 10 % values. Multitom Rax displayed highest MTF values, demonstrating superior spatial resolution. Note: The Multitom uses sharpening algorithms that increase contrast edges which can boost the MTF curve above 1.

Discussion

- This study successfully establishes baseline image quality metrics for five CBCT systems using their clinically applied protocols.
- Differences in image quality mainly reflected protocol settings and device design rather than a direct apples-to-apples comparison. The results highlight application-specific strengths as shown in the table below.

Device	Key Design	Suited For	IQ Metrics
Artis Icono	Fast 2.5-8s CBCT, 95°/s rotation, small focal spots	Head/abdomen interventions	High uniformity (22.42) for quick 3D planning; low SNR tolerable in high-contrast vascular.
Multitom Rax	Twin-robotic, Real3D Hi-Res/weight-bearing, high spatial resolution	Orthopedic extremities	Peak MTF (18.6 lp/cm) for trabeculae/bone detail; high noise ok for bony anatomy.
O-Arm	360° mobile CT, large FOV	Spine/trauma navigation	Superior CNR/SNR for soft-tissue/alignment verification
Artis Pheno (Hybrid)	Robotic hybrid, low-kV DR Head, precise positioning	Neuro/Vascular interventions	Good MTF10% (14.7 lp/cm) for vessel roadmaps

Table 2: CBCT Devices, their features, and respective IQ metrics

- **Artis Icono:** High uniformity (22.42) for fast DynaCT angiograms; low SNR (0.65) acceptable with vessel contrast.
- **Multitom Rax**: Top MTF resolves trabeculae; high noise (68.7) tolerable for bone work.
- **Medtronic O-Arm:** Superior CNR/SNR (32.71/31.86) for spine navigation despite low MTF (0.33).
- **Artis Pheno:** Strong MTF 10% (14.7 lp/cm) for vascular roadmaps; subtraction overcomes low SNR (0.43).

- **Optimisation Potential and future work:** Baselines reveal room for dose-efficient tweaks. For example, reduce mA/kV where noise dominates (e.g., Rax/Pheno) or adopt low-dose modes preserving QA metrics. Future work includes normalising future tests to DAP for fair comparison between IQ metrics and analysing unprocessed images.

Modelling Foetal Thyroid Dose Following I-131 Uptake Procedures Using a Gestation Dependent Biokinetic Model

Bill Kamtchou[a], Sean Cournane[a,b]

a. St. Vincent's University Hospital, b. Centre for Physics in Health Medicine (University College Dublin)

Introduction

Diagnostic I-131 uptake studies are routinely performed prior to radioiodine therapy. In pregnant patients, foetal effective doses are reportedly low due to the low activities (~1 MBq) employed. However, models suggest that foetal thyroid dose levels may approach or exceed the 300 mGy thresholds for physiological effects[1]. Around the onset of foetal thyroid function when there may be uncertainty of pregnancy status, limited modelled estimates exist on the potential foetal thyroid doses. Thus, the objective of this work was to develop a model for estimating early and mid-gestation foetal thyroid doses as a result of I-131 uptake for hyperthyroid patients.

Methods

A gestation-dependent maternal–foetal iodine biokinetic model based on ICRP 88[2] was implemented in Python to estimate foetal thyroid dose following acute maternal ingestion of I-131. An extensive compartmental model simulating iodine transport using gestational-age-dependent transfer coefficients was validated against published maternal thyroid doses and foetal % uptake (<1%)[3]. The model was subsequently modified to simulate increased 24 h maternal thyroid uptake in a hyperthyroid cohort by scaling thyroid uptake rates; this approach represents a first-order approximation of altered thyroid physiology.

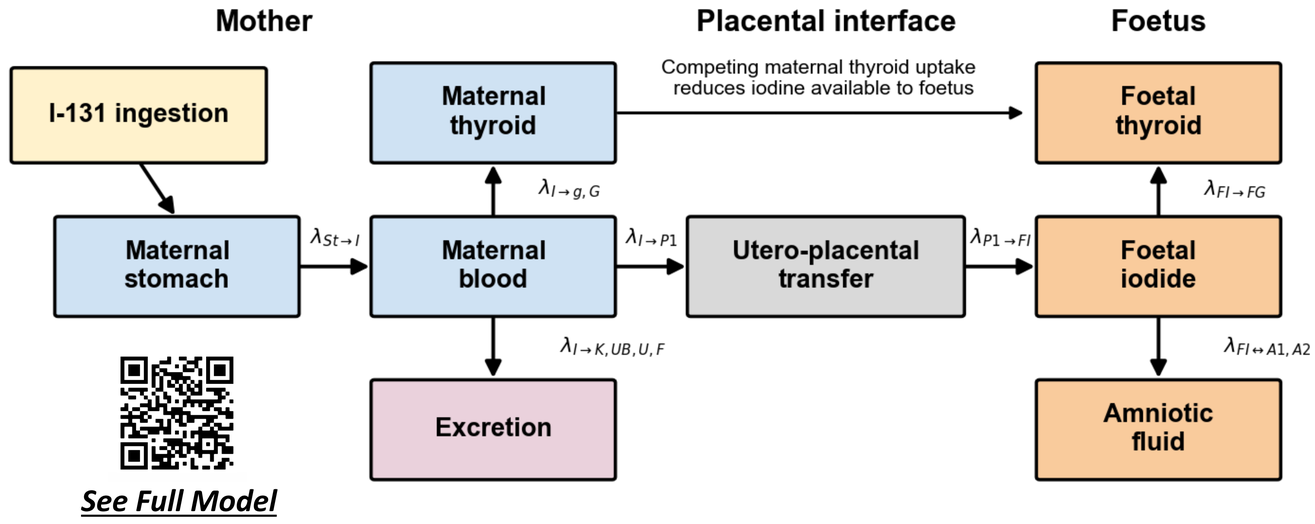


Fig1. Simplified gestation dependent maternal-foetal iodine model based on ICRP-88.

Results

For normal uptake ranges (<30%)[4], estimated foetal thyroid doses per MBq administered were <4 mGy prior to approximately 10–12 weeks' gestation, reflecting the absence of functional foetal thyroid tissue. Following this, foetal thyroid dose increased rapidly, approaching ~300 mGy at 20–21 weeks' gestation (±1 week). Modelled increased hyperthyroid maternal uptake substantially reduced foetal thyroid dose and delayed the gestational age at which this level was approached, to 26–27 weeks for moderate uptake (~55%) and 34–35 weeks for high uptake (~75%) scenarios.

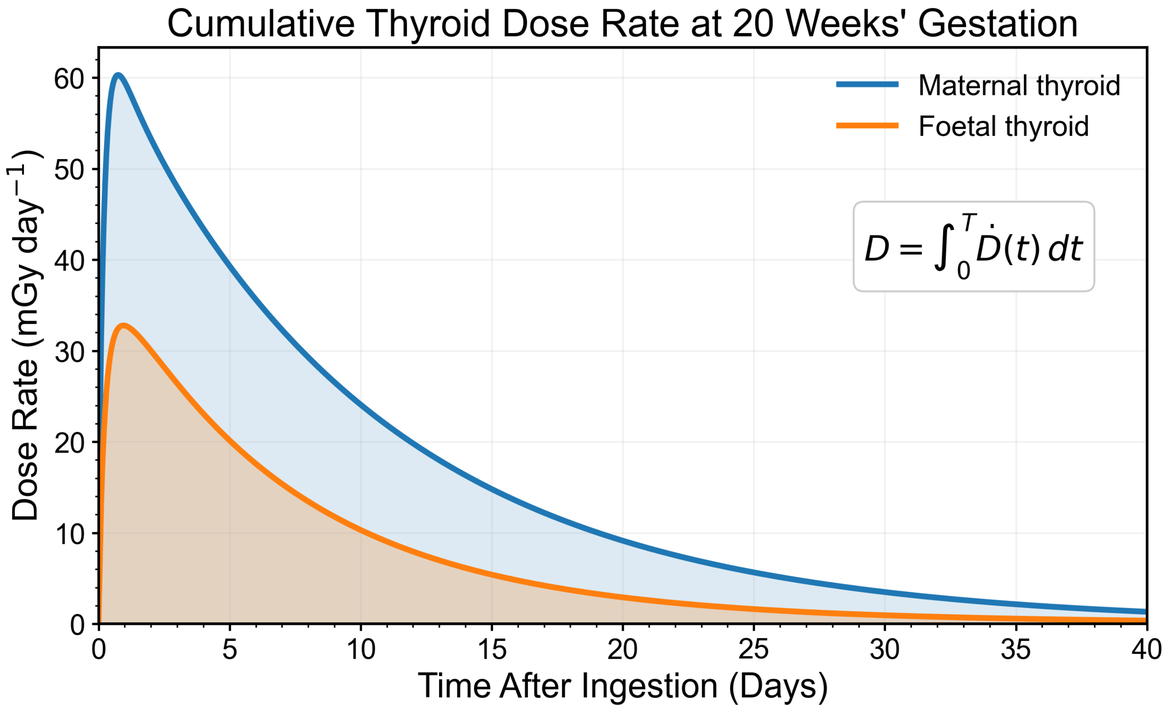


Fig2. Time-dependent absorbed dose rate in the maternal and foetal thyroid following ingestion of 1 MBq I-131 at 20 weeks' gestation. The shaded area under each curve represents the time-integrated absorbed dose.

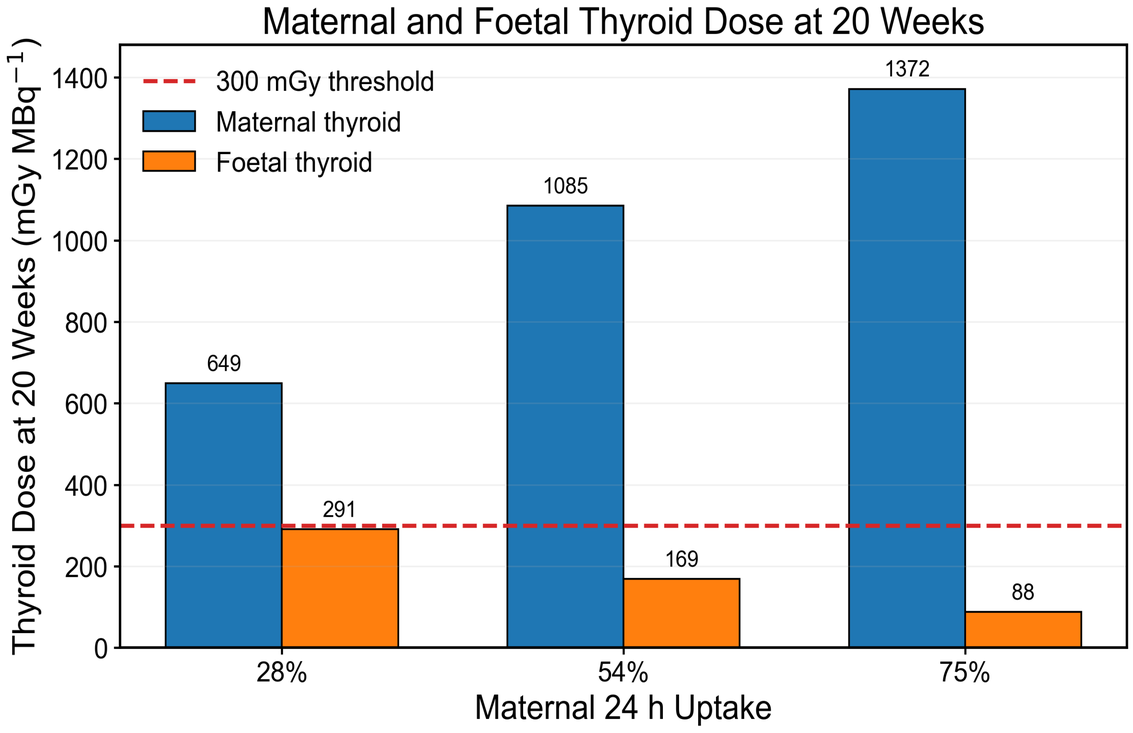


Fig3. Comparison of maternal and foetal thyroid absorbed dose coefficients at 20 weeks' gestation for three maternal uptake scenarios. Increasing maternal thyroid uptake substantially decreases foetal thyroid dose while increasing maternal thyroid dose due to enhanced thyroidal sequestration of radioiodine.

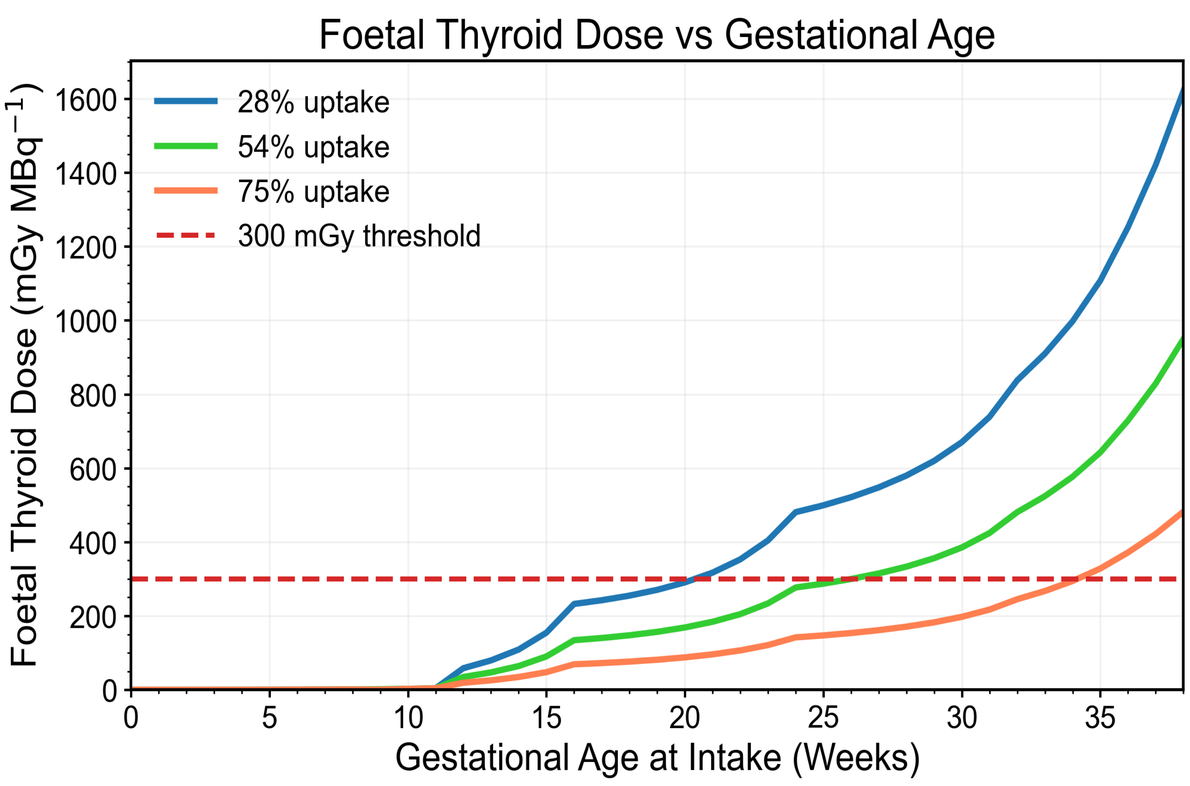


Fig4. Foetal thyroid dose coefficient (mGy MBq^{-1}) as a function of gestational age at maternal ingestion for three maternal thyroid uptake scenarios. Increased maternal uptake reduces foetal thyroid dose by increasing sequestration of iodine within the maternal thyroid. The dashed line indicates the approximate 300 mGy foetal thyroid dose threshold reported in the literature.

Conclusions

This validated, gestation-dependent maternal–foetal iodine biokinetic model quantifies foetal thyroid dose following diagnostic I-131 uptake procedures and demonstrates how maternal thyroid physiology influences foetal exposure. Model results indicate that foetal thyroid dose is negligible prior to approximately 10–12 weeks' gestation, before the onset of foetal thyroid function, but increases rapidly thereafter with gestational age. Modelled increased maternal thyroid uptake reduced foetal thyroid dose by enhancing sequestration of iodine within the maternal thyroid. Appropriate implementation of established pregnancy screening and timing policies should prevent clinically significant foetal thyroid doses during diagnostic I-131 uptake studies.

References

[1]. Iijima, S. (2021). Effects of fetal involvement of inadvertent radioactive iodine therapy for the treatment of thyroid diseases during an unsuspected pregnancy. EJO & GRB, 259, 53–59.
[2]. ICRP, 2001. Doses to the Embryo and Fetus from Intakes of Radionuclides by the Mother. ICRP Publication 88. Ann. ICRP 31 (1-3).
[3]. Rump, A., Hermann, C., Lamkowski, A., Abend, M., & Port, M. (2022). Simulations of radioiodine exposure and protective thyroid blocking in a new biokinetic model of the mother–fetus unit at different pregnancy ages. Archives of Toxicology, 96(11), 2947–2965.

A Microsoft Power Apps Solution for Radioactive Waste Inventory Management in Nuclear Medicine

Melissa Gunnoo[1] , Eamon Loughman[1], Eloise Gault[1], Courtney Kelly[2], Susan Maguire[1]

Mater Private Network

Introduction

Healthcare facilities with nuclear medicine departments must maintain detailed radioactive waste inventory ensuring full traceability from waste store entry until decay to safe levels and final disposal. Paper-based logs meet regulatory requirements but remain slow and cumbersome during audits/inspections. This Microsoft Power Apps solution provides structured, searchable records improving workflow efficiency and long-term traceability using existing hospital infrastructure at no extra cost.

Methods

App Architecture

Custom **Radioactive Waste Management** phone application built in Microsoft Power Apps (canvas)

- **Main Screen:** QR code scanning
- **Check-in Screen:** Radioactive waste intake
- **Check-out Screen:** Disposal verification
- **Gallery:** Real-time inventory list
- **Backend:** SharePoint List (existing hospital environment/cloud)

Data structure and validation

SharePoint List structured around regulatory-critical fields with mandatory app validation preventing incomplete saves:

Table A. SharePoint List Schema
Regulatory-Critical Fields with App-Enforced Validation Rules

Field	Type	Validation	Regulatory Purpose
Isotope	Choice	Mandatory	Identifies radionuclide for decay tracking
Waste Type	Choice	Mandatory	Classifies waste form per EPA disposal rules
Waste Tag Number	Single Text	Unique + Mandatory	Physical container traceability
Radiation In	Number	Mandatory, >0	Check-in activity measurement
Radiation Out	Number	On disposal	Final decay verification
Login/Disposal Dates	Date	Auto-populated	Regulatory clearance record

Configuration and Testing

Flow Chart A. App Development Process

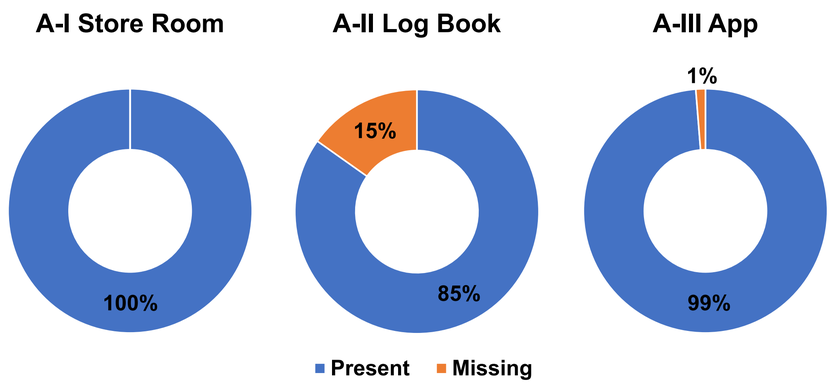


Data Analysis

Audit Data From Pilot (Oct 2025-Mar 2026):

Inventory Reconciliation: Physical store room inventory (n=79) compared against Power App (78/79, 99%) and paper log book (67/79, 85%)

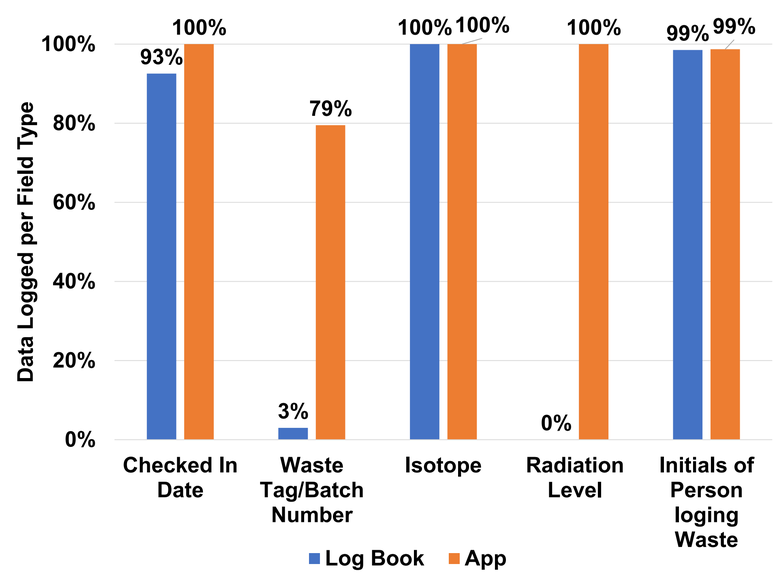
Chart A. Inventory Audit Comparison



Data Completeness : Chart B compares field-level data completeness within captured records:

- Power App (n=78 records): Achieved 100% completeness across all critical fields (Waste Tag Num, Radiation Level, Date Checked In and Isotope fields)
- Log Book (n=67 records): Recorded only 3% Waste Tag No entry, 0% Radiation Level - not standard practice, making tracking difficult

Chart B. Data Completeness by Field
n=78 App records | n=67 Log Book matches



Cost Analysis

- Commercial radiation waste tracking software costs ~€22K + recurring annual ~€2K (mid-size hospitals).
- Power App: €0 recurring - uses existing Microsoft 365 + budgeted staff time.

Table B. Cost Comparison for Radioactive Waste Tracking Solutions

Solution	Software/Hardware Cost + Annual Licence	Labour Cost	Total
Paper Log	€0*	€0	€0
Power App	€0* (existing Microsoft 365 + Staff use their own phone)	€0 (hospital staff)	€0
Commercial Software (such as Comecer)	~€20K* + 2K	~€2K (setup/training at start)	€24K

*Using existing hospital resources

Results/Discussions

Implementation Success

Power Apps deployment achieved 99% physical inventory reconciliation vs paper logs at 85% over first 5 pilot months.

Figure A. QR sticker and App Main Screen



Data Capture

Fields previously omitted (Radiation Level 0%; Waste Tag Number 3%) now enable decay tracking and audit-ready reports - previously difficult with manual logs.

Figure B. SharePoint List Interface

ScannedID	CheckedINDate	TagNo	TypeOfWaste	Isotope
RW10017	4/30/2025 1:12 AM	1427923	Sharps	Lutetium-177
RW10018	4/30/2025 1:13 AM	1427907	Bin	Lutetium-177
RW10019	7/1/2025 1:19 AM	ET12652A8	Residue	Radium-223

Staff Workflow Benefits

- On-demand data access **eliminates waste handling** for checks
- QR stickers enable **identification from a distance**, reducing radiation exposure per ALARA principles.
- Staff report **intuitive 1-tap autofill and instant total counts/lists** as faster than logbook writing

Economic & Versatility Impact

- Zero recurring cost via Microsoft 365 licenses saves significantly vs commercial software
- Scalable template enables hospital-wide radiation safety enhancements including lead apron annual testing tracking, EPD data entry and radiopharmaceutical receipt verification.

Conclusion

This in-house Power Apps solution proves low-code digital tools can transform nuclear medicine waste tracking using hospital existing Microsoft 365 licenses - no budget needed. Its versatile design supports future rollout to other radiation safety applications, eliminating commercial software costs hospital-wide.

Staff gain an intuitive mobile-first interface that simplifies compliance logging, cuts manual errors, and delivers real-time dashboards for instant audits and KPI tracking.

References

1. Radiological Protection Act 1991 (Ionising Radiation) Regulations 2019 (S.I. No. 30 of 2019). Government of Ireland.
2. Environmental Protection Agency. Guidance for undertakings on the application of the Ionising Radiation Regulations (IRR19). EPA, 2022.
3. Quote Reference: Comecer Ireland (Electramed), BH4 Light LAF Cabinet Quotation, March 2026.

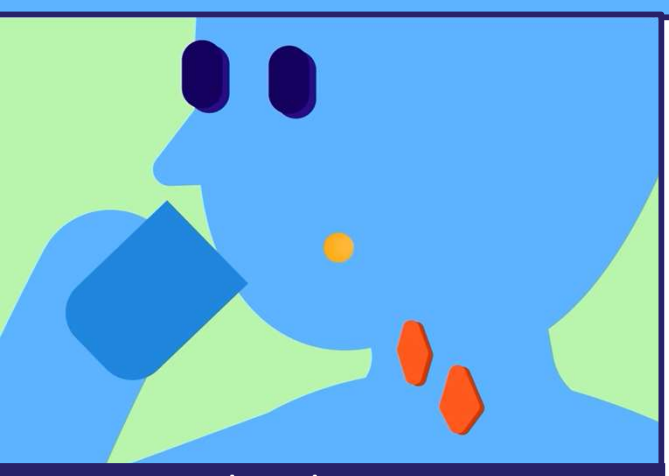
1. Department of Diagnostic Imagining and Nuclear Medicine Mater Private Network
2. School of Physics and Clinical and Optometric Sciences Technological University Dublin

From Capsule to Clearance: An Animation for Improving Radiation Safety Communication in ^{131}I Radionuclide Therapy

Hannah Reilly[1], Aoife Gaffney[1], Una O'Connor[1], Dr Laura Sinclair[1], Prof. Marie Louise Healy[1], Dr Chris Soraghan[1], Ali Asghar Ayaz[1], Ed McGinley[2], Seán King[2], Aoife FitzPatrick[2], Joseph Kenny[2]

[1] MPBE, St. James's Hospital, Dublin
[2] Moving Image Design Department, National College of Art and Design (NCAD), Dublin 8

Hannah Reilly, Physicist, St. James's Hospital; hareilly@stjames.ie



Capsule Administration

OBJECTIVE: Patients undergoing ^{131}I therapy for thyroid cancer are given written information as well as discussions with physics staff about radiation safety and their therapy pathway.
However:

- Traditional written and verbal communications can be overwhelming
- Patients are often anxious and unfamiliar with nuclear medicine procedures
- Patients are often unsure what to expect in terms of the in-patient therapy room and managing this period of isolation

AIM: To develop an animated patient information video which clearly explains the ^{131}I therapy pathway, radiation safety principles and patient expectations in an accessible and engaging format

METHOD: An animated video was designed through a collaboration with the National College of Art and Design, the MPBE Design Lab and the Nuclear Medicine Team.
A patient centred script and storyboard was co-created outlining:

- The ^{131}I treatment preparation
- Capsule administration
- Radiation safety advice
- Post treatment considerations

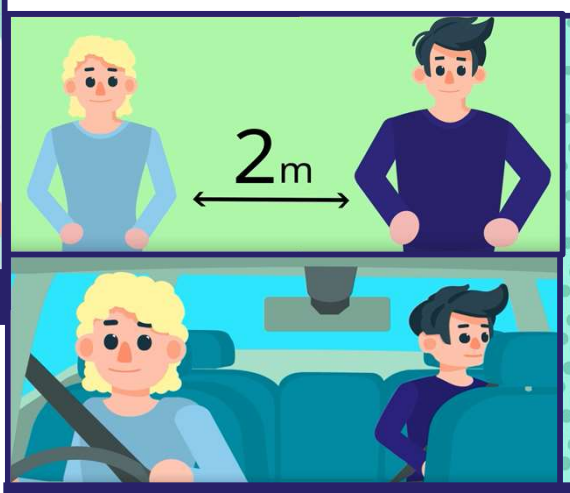


Patient Isolation Suite



Patient Uptake Measurement

RESULTS: A six-minute informative animated video was produced that visually explains the ^{131}I therapy process and associated radiation safety measures. The resource provides patients with a clear overview of what to expect before, during and after treatment, helping to reduce uncertainty and anxiety.





At Home Radiation Safety

Scan me to watch the video in full!

CONCLUSION: Animation is an effective tool for communicating complex radiation safety information to patients. This approach:

- Improves patient understanding
- Supports optimisation of radiation safety and patient compliance
- Enhances informed consent

This video will be made available to patients in advance of their ^{131}I therapy before treatment via QR codes and digital platforms.

OSPIDÉAL SAN SÉAMAS
ST JAMES'S HOSPITAL

Spark Innovation Programme

NATIONAL COLLEGE OF ART & DESIGN

DESIGN INNOVATION LAB
St James's Hospital

S.W.I.M.S.: Diving into Contamination Monitoring and Spills Response in Nuclear Medicine

OBJECTIVE: Radiation protection (RP) training is a legal requirement and spills training forms part of this. Nuclear Medicine (NM) and PET involve the use of unsealed radioactive materials. Spilling even small amounts of this creates a hazard.

In emergency situations staff must respond quickly and safely but remembering multiple procedural steps can be challenging. The S.W.I.M.S. protocol was introduced to staff outlining the steps needed to deal with a spill: **S**top, **W**arn, **I**solate, **M**inimise, **S**urvey.

AIM: To develop a simple training resource introducing the S.W.I.M.S acronym to guide a standardised response to radioactive spills.



See SWIMS in action!
Scan to watch the training video

METHOD: A script and storyboard for the video was developed based on department protocols and lessons learned from previous incidents and in-person training sessions.

Filming was carried out by the hospital medical illustrations team detailing the correct steps to follow in the event of a spill, the personal protective equipment required and the correct monitoring techniques.

This video was designed as a visual training aid to complement existing RP training.

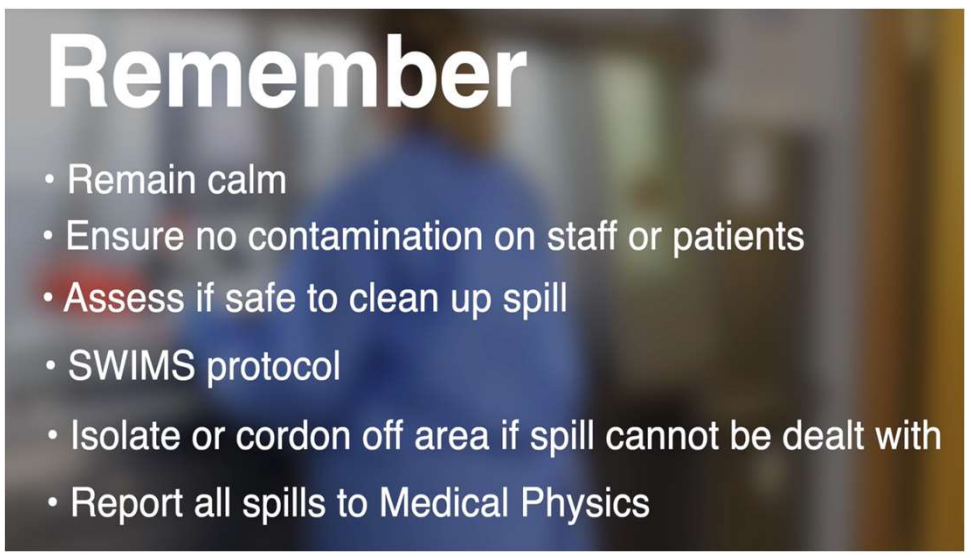
Simple Steps Save Time! – S.W.I.M.S A Clear Spills Response Acronym

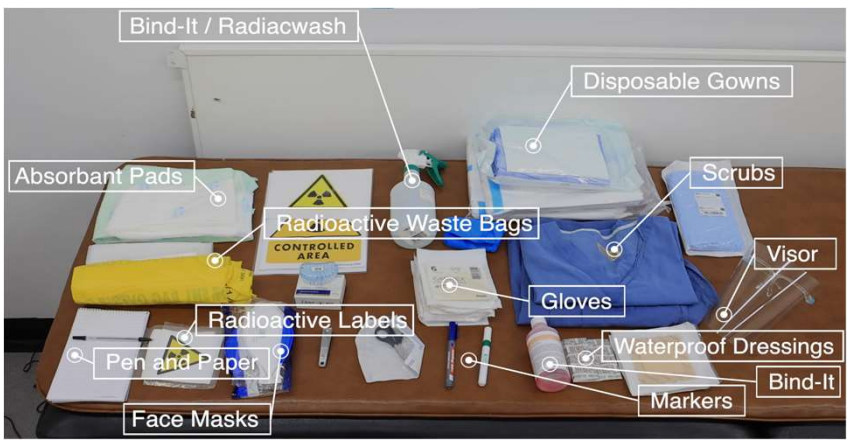
RESULTS: A short educational video demonstrating the S.W.I.M.S. spill response protocol was produced.

This resources provides:

- A clear step-by-step approach to spills
- A visual demonstration of correct response procedures
- A memorable acronym to support efficient decision making during a spill.

Following introduction of this resource staff reported improved awareness of spill procedures and were more likely to pause and report contamination incidents appropriately.





CONCLUSION: This informative and user-friendly video provides a consistent communication tool for staff working in the NM and PET department and allows for ease of access to online training for staff. The training helps staff respond quickly, safely and effectively during contamination incidents.

OSPIDÉAL SAN SÉAMAS
ST JAMES'S HOSPITAL

Hannah Reilly[1], Aoife Gaffney[1], Anna-May Woods[1], Una O'Connor[1], Laura Sinclair[1], Steve Toner [2], Paul Quinlan [3]

[1] MPBE, St. James's Hospital, Dublin 8
[2] DIAGIM, St. James's Hospital, Dublin 8
[3] SACC, St. James's Hospital, Dublin 8

hareilly@stjames.ie

Development And Validation of a Monte Carlo Simulation to Estimate Skin Dose in a Nuclear Medicine Department

Conor Lupton[1,2], Ann McCann[2], Jackie McCavana[2,3], [1]Dublin City University, [2]St Vincent's University Hospital, [3]School of physics UCD

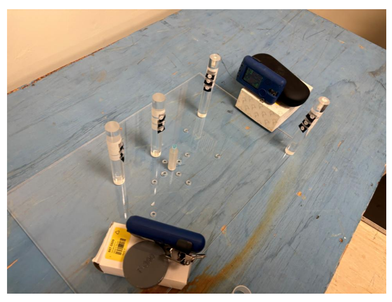
Introduction

The manipulation, dispensing and administration of radiopharmaceuticals often involves the hands of workers being in close contact to unsealed radioactive sources. This can result in significant radiation exposure to the hands especially when high energy beta emitters are involved. Routine extremity monitoring with a TLD ring can underestimate the maximum dose received by the hands. In addition, freely available skin dose software (e.g. VARSKIN+) can struggle to accurately reproduce clinical geometries, and recent publications have highlighted inaccuracies in some of it's dose calculations [1].

This project aims to develop and validate a Monte Carlo (EGSnrc) simulation model to provide real-time, geometry-specific Hp(0.07) and Hp(10) estimates for NM staff across a range of clinically relevant radionuclides.

Methods

1. Install and validate Monte Carlo (MC) software EGSnrc by reproducing known geometries and absorbed dose values from Amato *et al* [2].
2. Develop existing MC model of a radionuclide syringe source (McCann et al, 2021 [3]) to measure Hp(0.07) and Hp(10) in close proximity to the source for a range of radionuclides [3].
3. Validate the improved model by experimental measurements using in-house TLD100Hs (Thermo Scientific Harshaw) to measure Hp(0.07) and RadeyeB20-ERs (Thermo Scientific) and personal electronic dosimeters (PED, Tracerco) to measure Hp(10).
4. Compare the MC simulations results to Varskin+.



Experimental set-up



PED



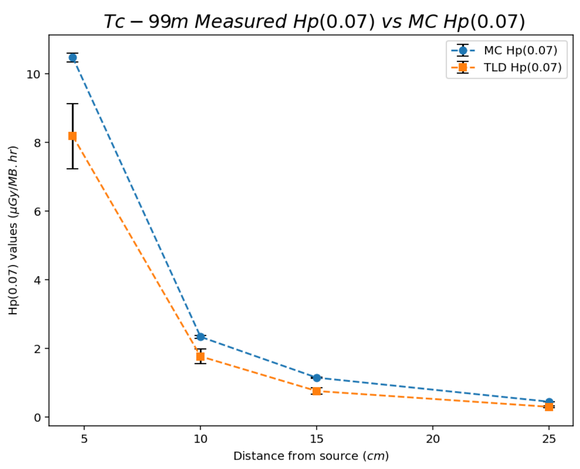
RadeyeB20

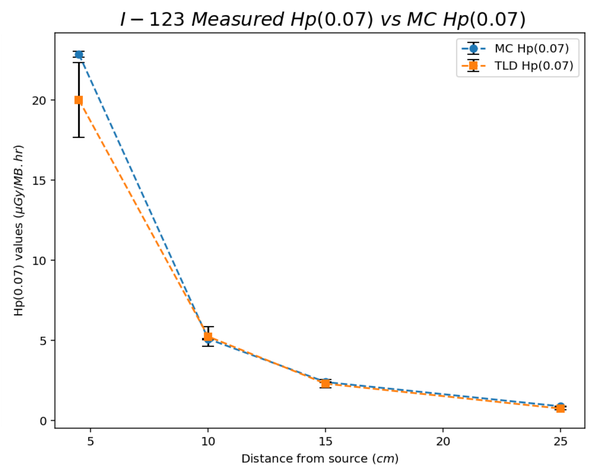


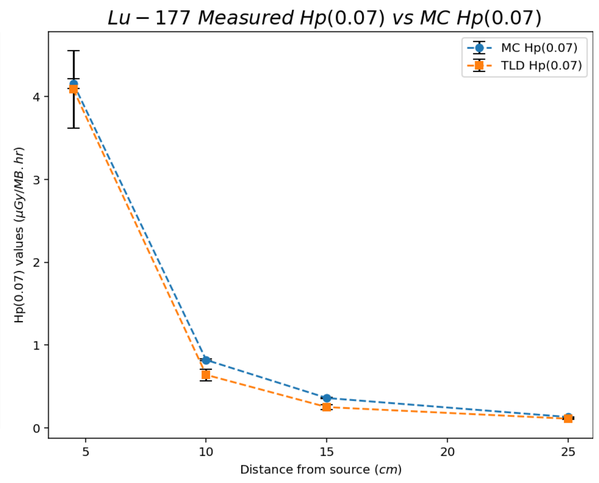
TLD100H Reader

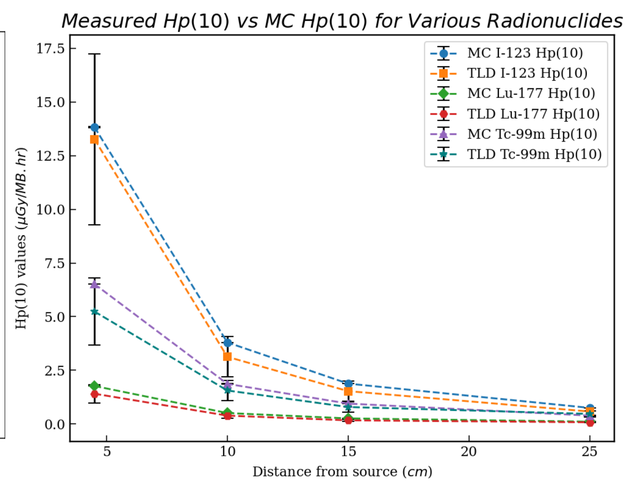
Results

Experimental Validation Hp(0.07) & Hp(10) for ^{99m}Tc, ^{123}I and ^{177}Lu



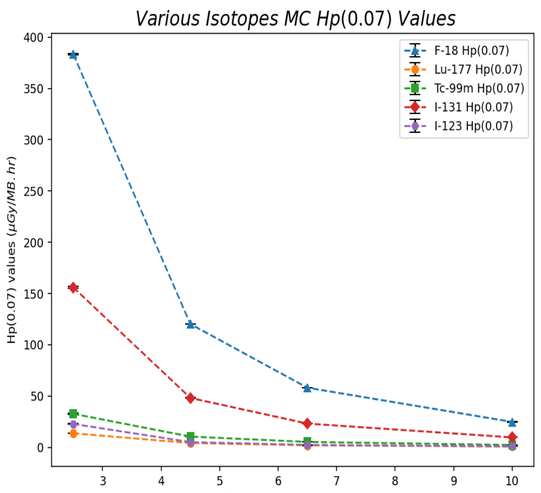


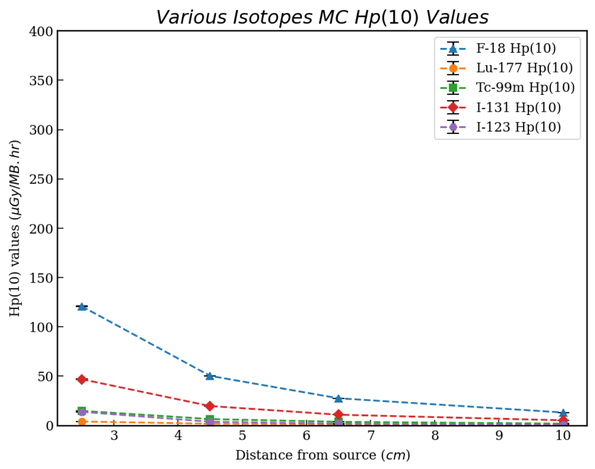




Excellent agreement (within 1.28 µGy/MBq.hr) was seen for Hp(10) for all source to detector distances (SDDs) across the three radionuclides. Deviations of up to 2.29 µGy/MBq.hr and 2.79 µGy/MBq.hr were noted for Hp(0.07) at SDDs ≤ 10cm for ^{99m}Tc and ^{123}I respectively, this was potentially due to the experimental set-up and angulation of the TLD. The deviations were considered acceptable.

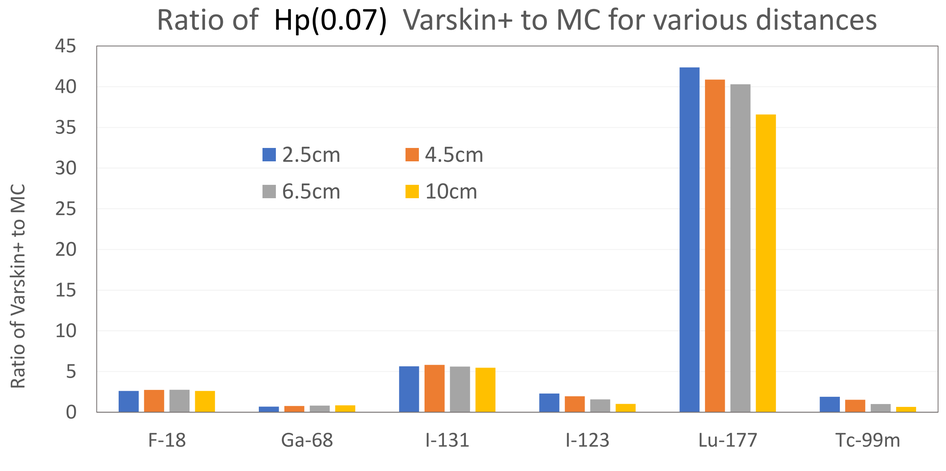
Clinically Relevant Simulations





As expected Hp(0.07) decreases rapidly as the distance from the source increases. With the exception of ^{68}Ga and ^{18}F, Hp(0.07) approaches Hp(10) for SDDs > 6.5cm. This is due to the reduced dose contribution from electrons to Hp(0.07) as distance from the source increases.

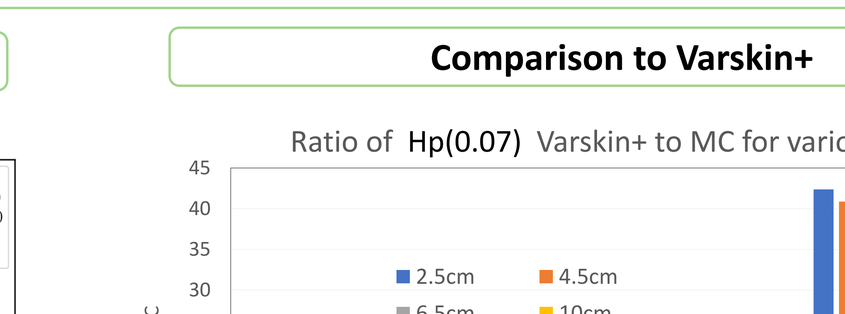
Comparison to Varskin+



While Varskin+ showed reasonable agreement for ^{18}F, ^{123}I and ^{99m}Tc, it significantly overestimated Hp(0.07) for ^{177}Lu and less so for ^{131}I. While Hp(0.07) was underestimated for ^{68}Ga.

Conclusions

A MC simulation model of occupational exposure was successfully developed and validated through experimental measurements of Hp(0.07) and Hp(10). Hp(10). Varskin+ was found to over-estimate skin dose for ^{131}I and ^{177}Lu Future work will include adapting the MC model to include more clinically relevant geometries and materials such as manipulating a 3-way tap, cannula etc.



Images of the new MC model. Image on the left shows the radiation emerging from the source while the image on the right labels the areas of the model.

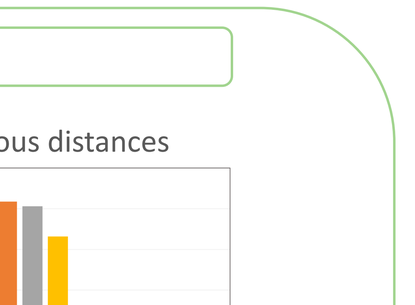


Image of the geometry used in Varskin+

References

[1] Thomas Frosio et al 2022 J. Radiol. Prot. 42 011510
[2] Amato *et al* : Radiation protection from external exposure to radionuclides: A Monte Carlo data handbook https://doi.org/10.1016/j.ejmp.2018.02.003
[3] McCann, A. *et al:* Assessment of occupational exposure from shielded and unshielded syringes for clinically relevant positron emission tomography (PET) isotopes—a Monte Carlo approach using EGSnrc doi: https://doi.org/10.1088/1361-6498/ac0df5

Comparison of scintillation meters and survey meters for the monitoring of ^{177}Lu contamination arising from nuclear medicine procedures

Cian O'Hara, Ann McCann, Jackie McCavana, St Vincent's University Hospital

Study aim – To calibrate monitors for ^{177}Lu surface contamination measurement and waste management applications

Introduction

Routine contamination monitoring is of particular importance when high activity concentrations of radionuclides are used for nuclear medicine. To confirm compliance with regulatory disposal limits and area classification, quantification of contamination in terms of Bq or Bq/cm^2 is important.

The purpose of this study was to assess the performance of commonly used Geiger-müller tubes (Rad-Eye B20) and scintillation meters (Berthold LB 124) in terms of sensitivity, linearity, and minimal detectable activity for ^{177}Lu.

Methods

Following IAEA Safety Report No. 16[1] meter calibration recommendations, four 100cm^2 squares of absorbent paper were prepared with activities of ^{177}Lu ranging from 30 kBq to 950 kBq. Sources were measured using each meter at a selection of clinically relevant distances, with various filter and meter settings. Calibration factors were established to convert detector measurements to Bq/cm^2.

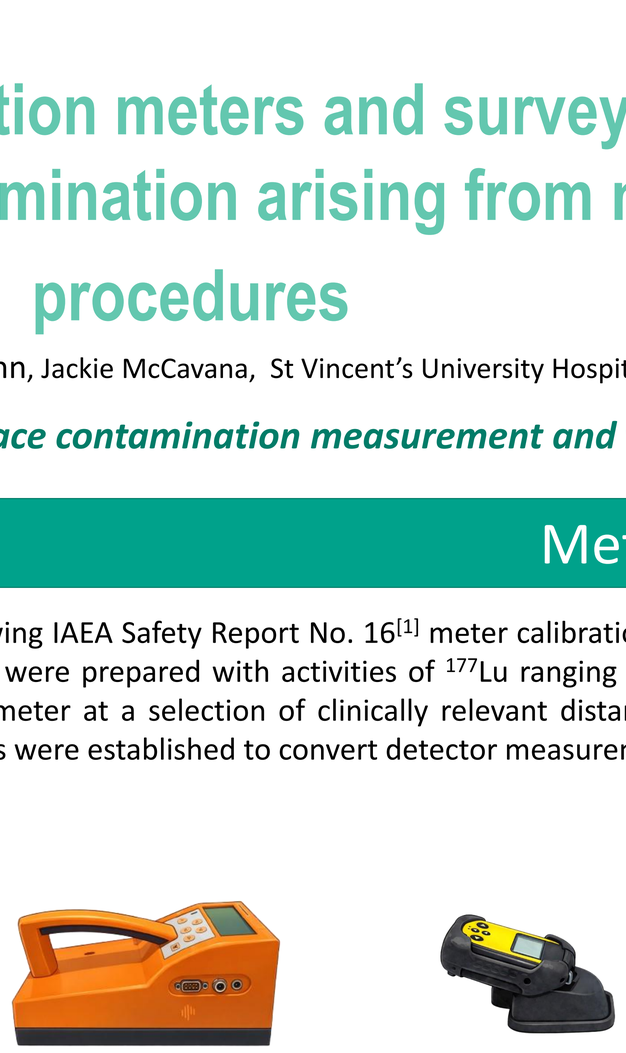


Figure 1: Berthold LB124 (Left) and RadEye B20 (Right)

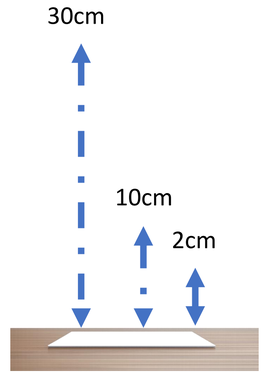
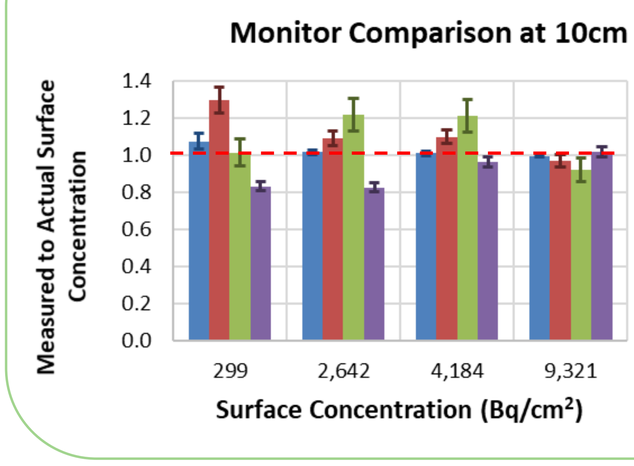


Figure 2: Measurement set-up

From the background results, the limits of detectability and quantification[2] were determined using the background and its standard deviation. The limits were compared to measurements of four 100cm^2 squares of absorbent paper prepared with ^{177}Lu activities ranging from 110 Bq to 1009 Bq.

Results

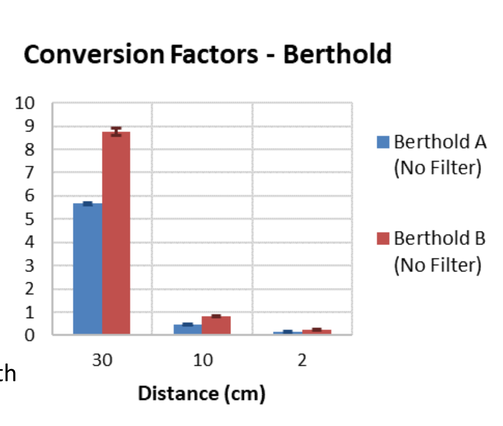
Conversion Factors

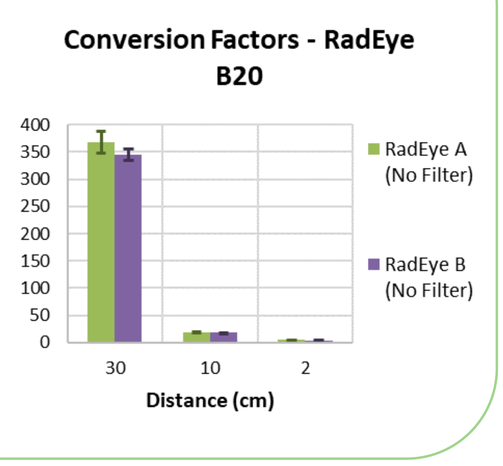


RadEye B20
- Conversion factors are equivalent within their calculated uncertainties

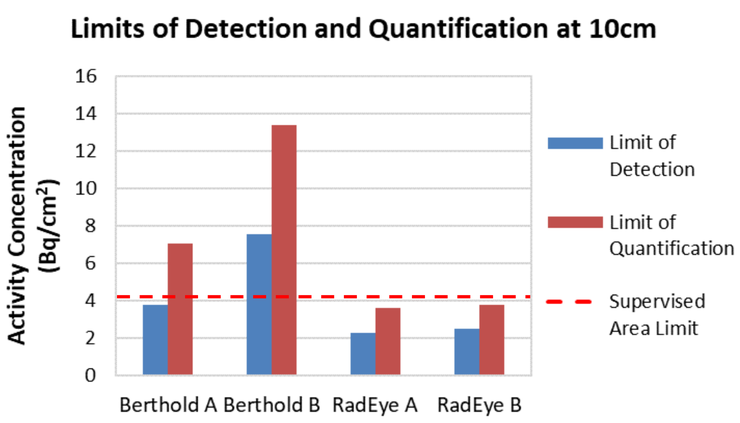
Berthold LB124
- Distinct variation in the sensitivity between both meters at all distances
- Berthold A was found to over-saturate with high concentration activities at distances of 2cm

At each distance, measurements had high correlation with the known activities (R^2>95%)



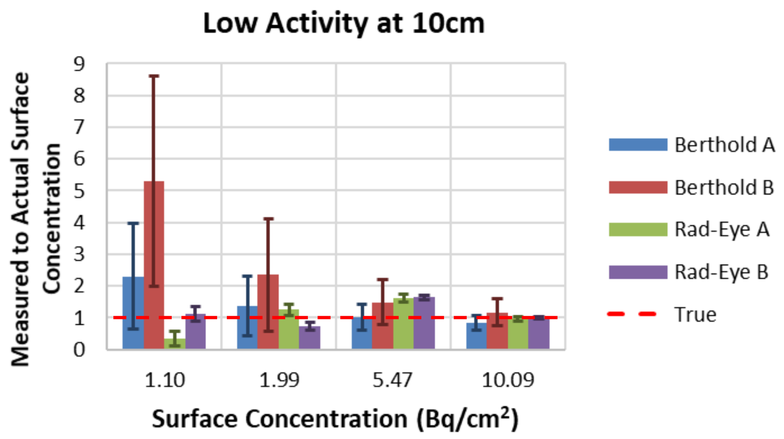


Low Activity Detection



RadEye B20 and the Berthold LB124
- Measurements at 10cm resulted in the least variation from the actual surface concentration
- Good agreement was found above 4 Bq/cm^2 (supervised area limit for beta/gamma emitters)

Berthold
- Large variation below 4 Bq/cm^2 which is in agreement with the limit of detection



Conclusions

For measurement of contamination, a distance of 10 cm is the optimal distance to prevent over-saturation at high activities and provide accurate results at low activities. Both scintillation meters and survey meters can be used for the detection of surface contamination above the supervised area limits for beta/gamma emitters published by the IAEA.
Characterisation of individual meters is recommended to prevent over-estimation of activity measurements.
All meters can accurately detect contamination of individual items a tenth of the limit for ^{177}Lu disposal (<1MBq).

Set up at 10cm (No plate/filter)	Settings	Device Units	Conversion Factor to Bq/cm^2	Limit of Detection (Bq/cm^2)	Limit of Quantification (Bq/cm^2)	1MBq*	Disposal Limit[3] 10MBq**
Berthold A	Gross	cps	0.469	3.75	7.04	21308	213076
Berthold B	Gross	cps	0.837	7.53	13.39	11953	119534
RadEye B20 A	Sr/Y90	Bq/cm^2	19.069	2.29	3.62	524	5244
RadEye B20 B	Sr/Y90	Bq/cm^2	17.915	2.51	3.76	558	5582

*Below measurable levels for scintillation meters and survey meters
**Maximum activity for disposal exceeds measurable levels for Berthold LB124

References

1. *International Atomic Energy Agency (IAEA) Safety Reports Series No. 16, Calibration of Radiation Protection Monitoring Instruments, 2000.*
2. *Ekoume, F.P. et al. (2020) 'Validation of a cost-effective alternative for a radiochromatography method to be used in a developing country', EJNMMI Radiopharmacy and Chemistry, 5(1). doi:10.1186/s41181-020-0092-1.*
3. *S.I. No. 30/2019 - Radiological Protection Act 1991 (Ionising Radiation) Regulations 2019*

ST. VINCENT'S HEALTHCARE GROUP
Advancing Healthcare Since 1834

Quality Assurance for SRS and SABR radiotherapy treatment planning with the QUASAR MRID^{3D} phantom

Lisa Rebello, Admire Dzingwa, Michael Roche

Medical Physics (Radiotherapy) Department, Cork University Hospital

Introduction

- MRI is widely used in radiotherapy planning, particularly for **SRS and selected SABR treatments**.
- High geometric fidelity is essential to prevent **target localization and dose delivery errors**.
- Planning MRI systems should maintain a **geometric accuracy within 1 mm** over the clinically relevant volume[1].
- This study evaluated the **geometric accuracy and distortion of a 1.5 T MRI scanner** for radiotherapy planning.

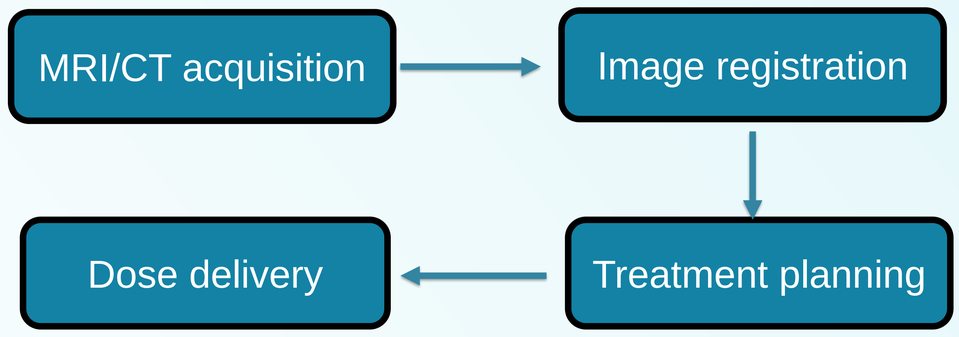


Figure 1: Schematic of MRI-based radiotherapy workflow

Methodology

Component	Details
Scanner	GE 1.5 T MRI
Analysis System	QUASAR MRID^{3D}
Phantoms Used	(1) QUASAR MRID3D Phantom (2) CIRS Stereotactic End-to-End Verification (STEEV) Phantom
RT Planning - MRI Sequences	(1) QUASAR Phantom: Axial Fast Spoiled Gradient Echo (FSPGR) (2) STEEV Phantom: 3D T1 FSPGR and 3D T2 Fast Spin Echo (FSE) Cube
Nominal Measurements	(1) QUASAR Phantom: 30 x 40 x 50 mm cuboid (2) STEEV Phantom: 30 mm spherical target
Metrics measured	(1) Geometric Accuracy (2) Geometric Distortion

Table 1: MRI Acquisition and Phantom Measurement Methodology

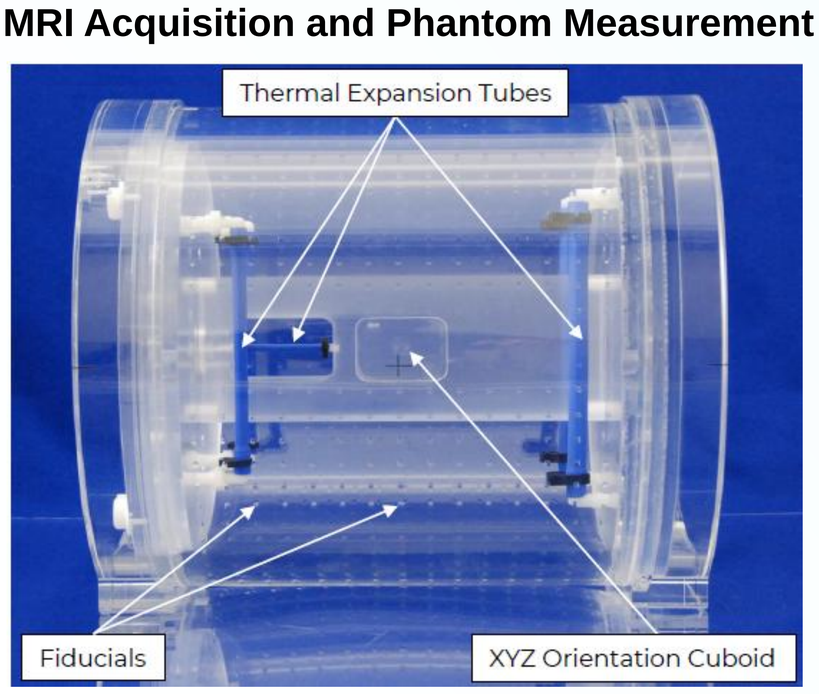


Figure 2: Components of a QUASAR MRID^{3D} phantom

Results

Phantom	Parameter	Result
QUASAR (Cuboid)	Dimensions	**± 0.2 mm** of nominal value
	Volume	**± 1.2%** of nominal value
STEEV (Sphere)	Dimensions	**± 0.8 mm** of nominal value
	Volume	**± 2.3%** of nominal value

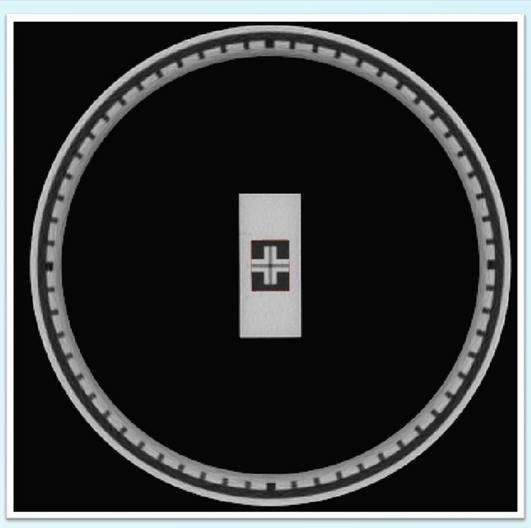


Figure 3: MRI visualization of QUASAR cuboid



Figure 4: MRI visualization of STEEV spherical insert

- **Geometric Distortion** was assessed within a **70 mm Diameter Spherical Volume (DSV)** centered at the MRI isocentre (± 35 mm)
- Mean distortion along **dx, dy and dz < 0.5 mm**
- Absolute distortion (**dr) < 0.5 mm,** Confidence rating **≥ 94.5%**

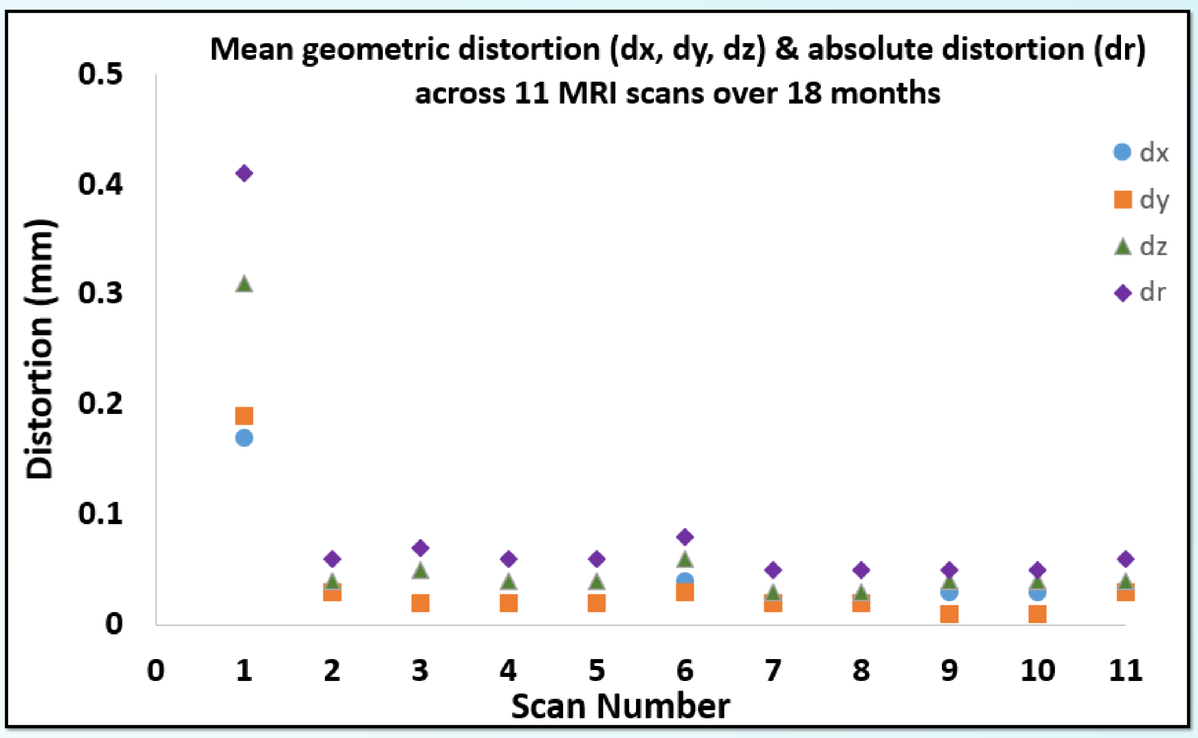


Figure 5: Plot of Mean geometric distortion and absolute distortion

Conclusion

- The **GE 1.5T MRI scanner** demonstrated **sub-millimetre geometric accuracy** with **minimal distortion** over a 18-month period.
- Results support its use in **radiotherapy treatment planning** for **SABR** and **SRS** where high geometric precision is required.
- The **QUASAR MRID3D** and **CIRS STEEV** were commissioned for **routine QA** in SABR/SRS planning.

References

1. Speight R, Dubec M, Eccles CL, George B, Henry A, Herbert T, Johnstone RI, Liney GP, McCallum H, Schmidt MA. IPEM topical report: guidance on the use of MRI for external beam radiotherapy treatment planning. Phys Med Biol. 2021;66(5):055025. doi:10.1088/1361-6560/abdc30.

Evaluation of the Effect of Rotations on Coverage of Nodal Boosts in Gynae SIB Patients

R. Smyth[1,2], C. Fleming[1], C. Malone[1,3]

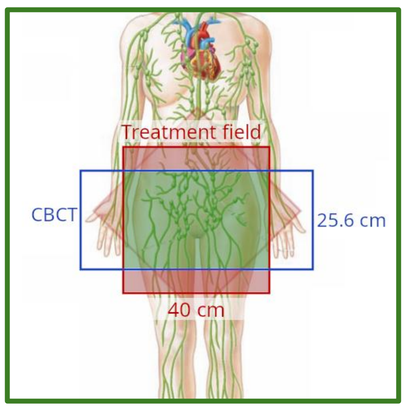
1. St. Luke's Radiation Oncology Network, St. Luke's Hospital, Dublin.
2. Centre for Physics in Health and Medicine, School of Physics, UCD, Dublin, Ireland
3. Erasmus MC Cancer Institute, University Medical Centre Rotterdam, Department of Radiotherapy.

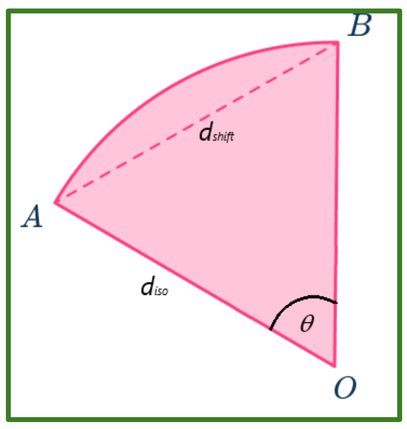
Background

Limited CBCT field-of-view (FOV) can prevent verification of distal nodal boosts in cervix SIB plans. As the distance from isocentre (d_{iso}) increases, small residual rotations create larger geometric displacements that may decrease coverage. The aim of this study was to quantify how patient rotations affect dose to boosted nodal targets, and how effects scale with nodal location, d_{iso}, rotation axis, and volume, to enable prediction of coverage loss when CBCT FOV constraints are present.

$$d_{shift} = 2 \cdot d_{iso} \cdot Sin\left(\frac{\theta}{2}\right)$$

57.5 Gy target, **52 Gy must be delivered**





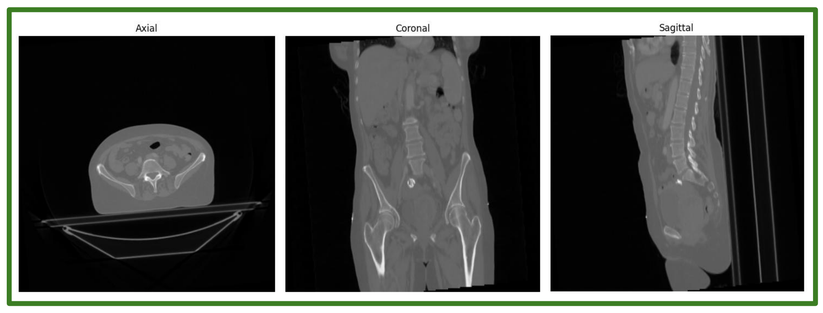
Materials & Methods

5 patients, 34 nodes, 18 rotations

Patient CT images were virtually rotated

±3° , ±5°, and ±7°

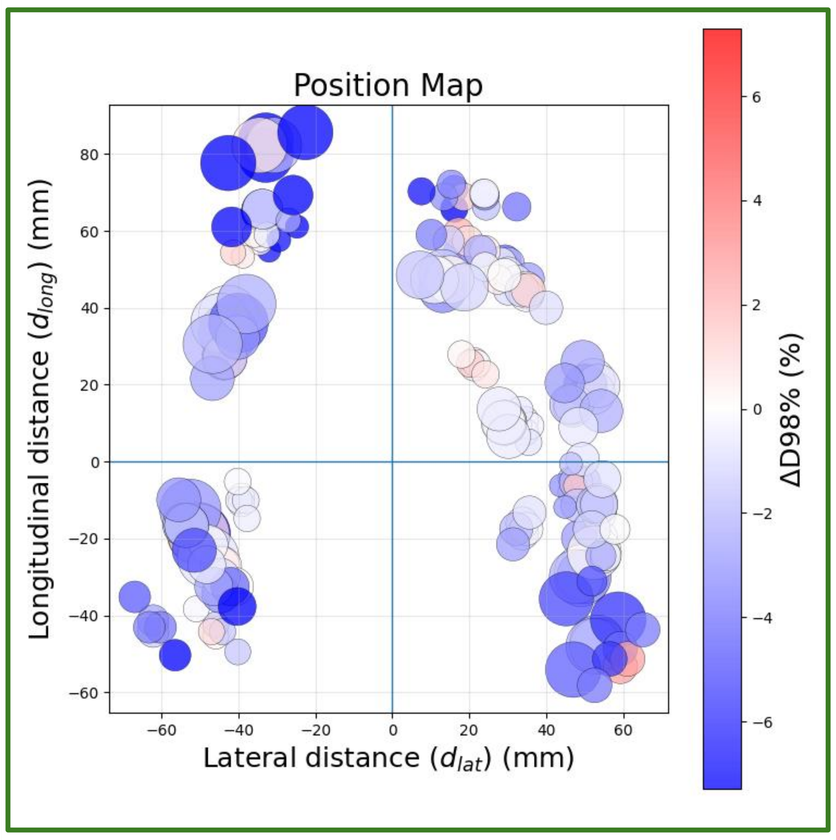
Pitch, roll, yaw



1. Plans were recalculated in Monaco
2. Dose-volume histograms exported
3. $D_{98\%}$ analysed

18 rotations of 34 nodes

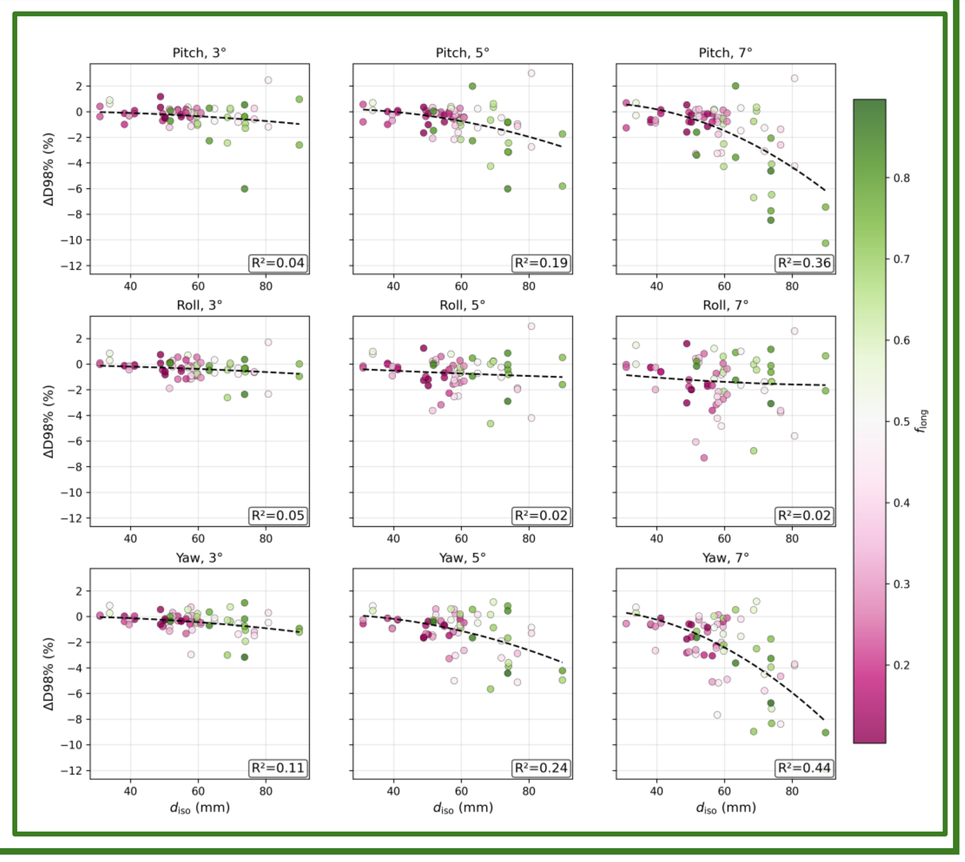
Results



Pitch and yaw produced a **quadratic loss** of coverage with increasing d_{iso} (R^2 = 0.36, 0.44), while roll produced a weak linear correlation (R^2 = 0.02).

Reductions of $\Delta D_{98\%}$ up to **6.79 ± 1.17 Gy** (12 ± 2.9%) for 5° setup error were estimated for nodes at d_{iso} of 163 mm, the distance between the edge of FOV and treatment field for the machines in this study.

Reduction below 52 Gy possible



Discussion

Across 34 boosted nodes:

When distal nodal boosts are partially or completely outside CBCT FOV, residual **rotations ≤ 5° can reduce PTV SIB coverage** below treatment requirements, scaling with d_{iso} for pitch/yaw. The distance of a given node from the axis of rotation was a strong indicator for change in dose coverage. Node volume independently modified risk - larger nodes exhibited greater absolute $\Delta D_{98\%}$, while smaller nodes showed higher variability in $\Delta D_{98\%}$.

Nodes outside CBCT FOV are at risk of underdosage

Conclusion

Uniform margins and standard IGRT protocols may be insufficient for these nodes. Findings support

1. 6DoF correction to minimize rotational residuals
2. Distance-stratified margins or tolerances for nodal boosts
3. More advanced set-up protocols such as SGRT

Remedial action recommended

References

1. Dominique L. Rash et al. "Clinical Response of Pelvic and Para-aortic Lymphadenopathy to a Radiation Boost in the Definitive Management of Locally Advanced Cervical Cancer". en. In: *International Journal of Radiation Oncology*Biology*Physics* 87.2 (2013-10), pp. 317–322. issn: 03603016. doi: 10.1016/j.ijrobp.2013.06.2031.
2. EMBRACE II Study Group. EMBRACE II Protocol. 2016.
3. Louise Vagner Laursen et al. "Residual rotational set-up errors after daily conebeam CT image guided radiotherapy of locally advanced cervical cancer". en. In: Radiotherapy and Oncology 105.2 (2012-11), pp. 220–225. issn: 01678140. doi: 10.1016/j.radonc.2012.08.012.
4. Ester Orlandi et al. "Radiobiological basis and clinical results of the simultaneous integrated boost (SIB) in intensity modulated radiotherapy (IMRT) for head and neck cancer: A review". en. In: Critical Reviews in Oncology/Hematology 73.2 (2010-02). Publisher: Elsevier BV, pp. 111–125. issn: 1040-8428. doi: 10.1016/j. critrevonc.2009.03.003.

Investigation into Feasibility of Using Varian Multi-Criteria Optimization (MCO*) to Improve Simple (Prostate) and Complex (Head and Neck) VMAT Plans in the Clinical Environment.

Western Health and Social Care Trust

Ellen Baker, Barry O'Connell, Margaret Moore
Northwest Cancer Centre, Altnagelvin, Derry

Ollscoil na Gaillimhe University of Galway

Introduction

- MCO is a plan optimization tool which allows Pareto optimally generated plans to be generated in order to facilitate finding the best fit.
- Pareto optimal plans include multiple objectives and constraints and iteratively progress through mathematical solutions to explore plan trade-offs. Clinically speaking, the aim is to give the PTV (planning target volume) the best coverage whilst minimizing the dose to organs at risk.
- Robustness is considered an important measure of MCO to investigate. A "robust" plan is one which is not clinically degraded to any great extent by daily anatomical and setup differences.
- The Plan Uncertainty tool in Eclipse can test robustness by adding perturbations to the plan.

Aims

- Test the feasibility and robustness of this tool for clinical use
- Test MCO's ability to improve tumour coverage
- Test if MCO may improve doses to OARs for better tissue sparing. Ideally the doses to all OARs should be as low as reasonably possible (ALARP).
- Assess if MCO may lead to improved patient outcomes

Methods

- 20 anonymised patient plans were selected (10 prostate, 10 head and neck). The original plan optimization objectives were exported and made available for each plan.
- The selected plan was duplicated twice (standard optimization, MCO)
- 1. Enter optimization window
- 2. Pull up objective template with pre-set priority weightings for each structure.
- 3. Click start VMAT optimization, ensuring GPUs, and calculate intermediate dose are ticked.
- 4. After standard optimization enter the MCO workspace and select all of the relevant PTV and OAR objectives to explore.
- 5. Click on "Explore Trade-Offs." This will begin the MCO calculation.
- 6. Once complete the user can now toggle the sliders to explore trade-offs and try to identify the optimal plan compromise. The mandatory PTV coverage may be "restricted" which then reduced the ranges of OAR exploration available.
- The SO and SO-MCO plans were then compared within the Plan Evaluation workspace.

Results and Discussion

Prostate:

OAR (Dmean, Gy)	Rectum	Bladder	Bowel
Difference SO vs MCO	5.2%	1.2%	1.6%

Figure 1: Prostate Averages

- On average, mean dose to OARs was lower for every clinical plan as compared to MCO plans. MCO Calculation time approx. 30mins.
- Aware of CHHiP trial – may affect OAR priority. -> outermost of 3 PTVs -> all structures ticked so rectum priority decreased (high deviation)

*DVH, visual dose comparison, and bar chart for all also analysed.

Metric	PTV	MUs	CI	Robustness
Difference	1.0%	5.6%	0.01%	-1.0%
StdDev ±	1.1%	9.5%	0.1%	0.03%

Figure 2: Prostate PTV, MUs, CI, and Robustness.

- MCO reduces MUs (decrease of 5.6%, 2 exceptions)
- MCO did not affect conformality (0.01%)
- MCO did not make any plans less robust (-1%)
- Satisfactory – PTV value and standard deviations deemed clinically insignificant.

Head and Neck:

OAR (Dmean, Gy)	Spinal Cord	ParotidCombined	Larynx	Brain Stem
Difference SO vs MCO	9.1%	2.7%	4.7%	0.5%

Figure 3: HN Averages

- On average, the mean dose to organs at risk was lower for every plan in the clinical plan as compared to MCO plans. Calculation time approx. 90mins.
- Checked Dmax Protocol for spinal cord passed.

Metric	PTV Hi D99%>95%	Mus	CI	Robustness
Difference	0.9%	5.0%	0.0%	2.5%
StdDev ±	2.5%	6.8%	0.3%	6.4%

Figure 4: HN PTV, MUs, CI and Robustness

- MCO reduces MUs (5%)
- MCO did not affect conformality - CI remained exactly the same
- MCO did not make any plans less robust (2.5%)
- Satisfactory – PTV value and standard deviations deemed clinically insignificant.
- Trade-offs not satisfactory or worthwhile – very little room to toggle OARs.

Conclusion

This concludes that MCO is case dependent and should be used as a supplementary tool rather than a replacement to conventional planning.

Acknowledgments

Thank you to all at the planning team at NWCC- especially Barry, for all your help!

Investigation into Minimum Bladder Filling Volumes for Pelvic Radiotherapy Treatments

Miriam Kennedy[1], Dr. Triona Brosnahan[2], Margaret Moore[2],

1 Physics, School of Natural Sciences, University of Galway, Galway, Ireland

2 Department of Radiation Oncology, University Hospital Galway, Galway, Ireland

Email: miriam.kennedy.0@gmail.com

Introduction – Bladder Filling for Pelvic Radiotherapy

- Bladder filling minimizes dose to organs at risk (OARs), particularly the small bowel.
- Patients are required to drink water before the initial planning CT and each treatment fraction to maintain the same bladder volume.
- Bladder filling is not sustainable throughout all fractions, if a patient's bladder is smaller than expected during the pre-treatment cone beam CT (CBCT), the patient may need get off the bed to drink more water.
- This can result delays in treatment and additional CBCTs being needed

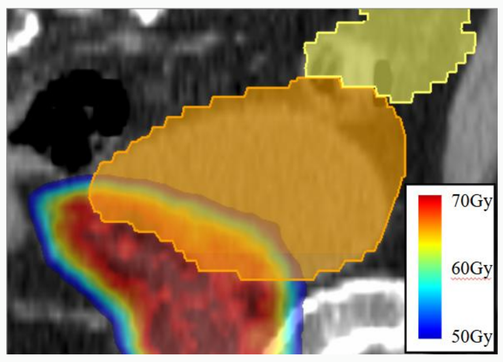


Figure 1: Orange: bladder, yellow: small bowel. A full bladder pushes the small bowl out of high dose region
[Image from Monaco TPS]

Aim

Determine a minimum bladder volume that can be used to decide if prostate treatment can proceed when a bladder is smaller than the planned volume. Essentially what is the smallest bladder that is still safe to treat

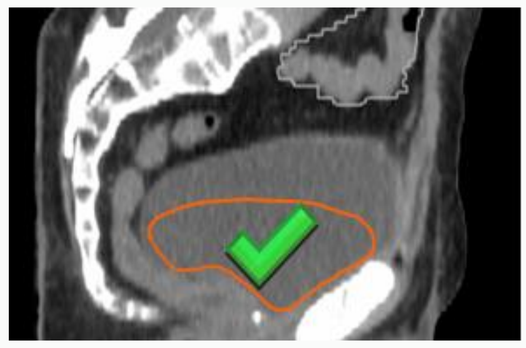


Figure 2: Sagittal view of prostate planning CT. Hypothetical "minimum bladder" drawn in orange.
[Image from Monaco TPS]

Materials and Methods

Materials: Monaco TPS and patient prostate treatment plans.

Method: The minimum bladder volume was defined as the threshold volume required to satisfy all Dose-Volume Constraints (DVCs). To calculate this, both bladder and small bowel DVCs were examined. For small bowel DVC assessment the worst-case scenario was modelled where the bladder is absent and the small bowel fills the resulting void. The minimum bladder volume was inferred by determining the minimum displacement necessary to push the small bowel out of high-dose regions and maintain DVCs.

$$V70Gy < 15\% \longrightarrow V70Gy < 0.15 \times V_{Bladder}$$

$$V_{Bladder} > \frac{V_{70Gy}}{0.15}$$

46 plans were assessed:

- SIB (68Gy in 25#, n=20)
- Prostate bed (66Gy in 33#, n=8)
- CHIiP (60Gy in 20#, n=18)

Sample DVC calculation: V70Gy < 15% is a bladder DVC. V70Gy is the volume that receives 70 Gy and was found by projecting the 70 Gy isodose line down onto the planning CT and intersecting it with the bladder contour . The bladder volume must be greater than V70Gy/0.15 for this DVC to be satisfied. This was repeated with all bladder and small bowel DVCs.

Results (I)

- Bladder showed a large ability to shrink before either bladder or small bowel go out of tolerance.
- Bladder DVCs frequently went out of tolerance before small bowel DVCs, with the minimum bladder volume only being defined by the small bowel DVCs for 3/46 plans.
- Typically, relative bladder filling "rule of thumb" to assess suitable bladder volume (with >66% full being acceptable). This not suitable for 60 Gy in 20# plans with 6/18 requiring >66% filling.
- Using relative volumes is not useful - smaller initial bladder volumes (planning CT) resulted in larger relative volume requirements.

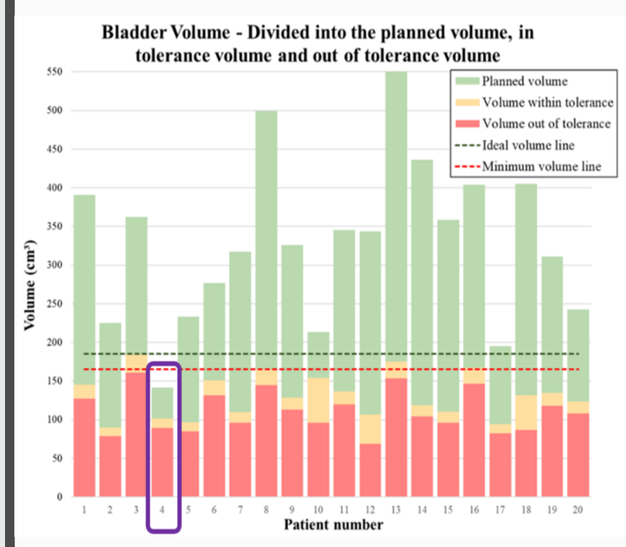


Figure 3: Volume on planning CT as a function of volumes where all DVCs are satisfied (green), at least one DVC is in tolerance (orange), at least one DVC is out of tolerance (red). Smallest initial planning bladder volume highlighted in purple.

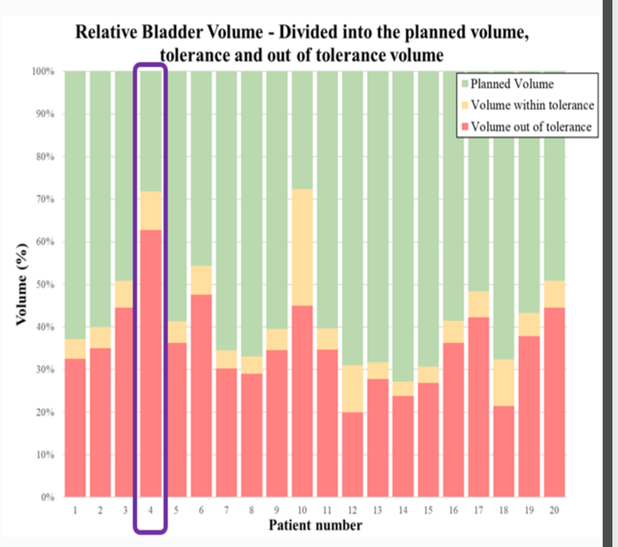


Figure 4: Volume on planning CT, colours have same meaning as Figure 3. Smallest initial planning bladder volume, despite having a small minimum bladder volume, has the largest relative bladder fill showing that relative bladder filling does not indicate a larger absolute volume

Results (II)

Table 1: Mean planned, "ideal" and "minimum" bladder volumes for SIB cohort (68Gy/25#)

Bladder Volume	Mean (cm³)	SDOM (cm³)	[min, max] (cm³)
Planned	328.8	101.0	[141.6, 550.3]
Ideal	131.3	27.6	[90.1, 184.2]
Minimum	110.5	26.1	[68.5, 161.2]

Table 2: Mean planned, "ideal" and "minimum" bladder volumes for prostate bed cohort (66Gy/33#)

Bladder Volume	Mean (cm³)	SDOM (cm³)	[min, max] (cm³)
Planned	388.1	118.8	[189.9, 526.5]
Ideal	296.2	75.7	[158.7, 405.7]
Minimum	157.4	40.5	[81.3, 204.6]

Table 3: Mean planned, and "minimum" bladder volumes for CHHiP cohort (60Gy/20#). In UHG, no tolerances were defined for bladder or small bowel DVCs, therefore the "ideal" and "minimum" bladder volumes are the same.

Bladder Volume	Mean (cm³)	SDOM (cm³)	[min, max] (cm³)
Planned	371.0	108.4	[171.6, 554.5]
Minimum	203.8	42.3	[122.1, 270.3]

- "Ideal" volumes are bladders which are large enough to ensure all DVCs are satisfied, "minimum" indicates that at least one DVC is "within tolerance" (i.e. still treatable).
- Minimum bladder volume is treatment dependent with the CHHiP protocol requiring nearly double the bladder volume compared to the SIB protocol.

To translate these minimum volumes into a clinically useful tool, "Guide Contours" were developed based on the patient's bladder contour on the planning CT. These contours represent the calculated safe-volume threshold and can be overlaid directly onto daily CBCTs. This provides Radiation Therapists with an objective "go/no-go" metric to ensure the bladder is sufficiently full before treatment.

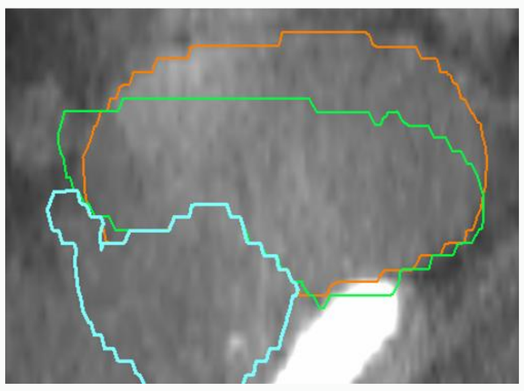


Figure 5: CBCT of bladder which was rejected due to bladder volume concerns. Blue: prostate, orange: bladder volume, green: minimum bladder volume contour. The orange bladder is larger than the green guide contour indicating that treatment could have proceeded in this case. [CBCT viewed in Monaco TPS]

Discussion and Conclusion

Table 4: Summary of mean minimum bladder volumes for each cohort examined.

	SIB 68Gy in25#	Prostate Bed 66Gy in 33#	CHHiP 60Gy in 20#
Minimum Volume (mean)	110.5	157.4	203.9
SDOM	26.1	40.5	42.3

1. Absolute volume (cm^3) is the key parameter (not the relative volume).
2. Bladder typically goes out of tolerance before small bowel.
3. Required bladder volume is treatment protocol dependent.
4. Rule of thumb 66% bladder volume acceptable is not suitable for 60Gy in 20#.

Future Work

1. Clinically viable minimum bladder volume contour generator
2. Finite element analysis bladder modelling.
3. Include others OARs.
4. Include gynaecological cancer treatments.

References

1. **Gorovets, D., Happersett, L., Elguindi, S., et al. (2021)**. Minimum Bladder Reference Contour to Guide Bladder Filling for Prostate Radiotherapy. *International Journal of Radiation Oncology, Biology, Physics*, 111, e274-e275.
2. **Kong, V., Dang, J., Wan, V., & Rosewall, T. (2023).** The dosimetric underpinning of bladder filling criteria for prostate image guided volumetric modulated arc therapy. *The British Journal of Radiology*, 96(1145), 20230020.
3. **Moore, A., & Forde, E. (2017).** A dosimetric evaluation of threshold bladder volumes for prostate cancer radiotherapy. *Journal of Medical Imaging and Radiation Sciences*, 48(3), 270–275.

Five years of radiotherapy dose reference levels: A single institution review

Authors: Christopher Walker[1], Derry McCarthy[2], Claire Harman[2]

Introduction

1997: European Directive 97/42/Euratom enshrined the general method of using diagnostic reference levels for radiological procedures

- *A facility should not exceed these dose levels consistently*

2018: This is updated into Irish law as SI 256, 332 and 413

2021: HIQA publish a guidance document on the establishment of dose reference levels (DRLs), a radiotherapy equivalent

- *National DRLs established for common procedures*
- *Local facility DRLs created by an undertaking*
  - *These are compared to National DRLs, where available*

The median value of dose-length-product (DLP) is determined annually for all relevant scans taken from each CT protocol used clinically

- *These are the local facility DRLs*
- *They are tabulated and prominently displayed at the CT scanner console*

Materials & Methods

In the Glandore centre at Cork University Hospital GE Dosewatch v3.3 (GE Medical systems) is connected to two Discovery RT CT scanners.

- *Full DICOM CT header information sent automatically following each patient examination*
- *Centrally stored - Large database available*

On an annual basis:

- *Data exported to .csv files for each CT scanner*
- *Refined to remove quality assurance data, test patients and commissioning datasets*
- *Median DLP calculated for each protocol*
- *Laminated copy of these values placed at each CT scanner*
- *Notable data discrepancies compared to the previous year are investigated*
- *Pareto principle applied to identify the 20% of protocols which have changed the most*
- *Investigations carried out and annual report completed*

For this study, core protocols were defined – those with > 15 patients scanned on each of the five years. Any trends were noted.

Results

For scans taken from 2020–2023, analysis was from October – October.
For scans taken from 2024–2025, analysis was from January – January.

In 2025, 41 protocols were in use clinically in the Glandore centre.

15 core protocols were identified for this study, with the number of patients scanned using each shown in Table 1, over five years.

Protocol name	Oct 2020 to Oct 2021	Oct 2021 to Oct 2022	Oct 2022 to Oct 2023	All 2024	All 2025
1.1 BRAIN MAR	106	160	136	127	130
3.1 HEAD & NECK MAR	56	91	86	121	131
3.2 HEAD & NECK MAR IV CONTRAST	86	99	108	100	70
5.2 THORAX	73	82	86	78	99
5.3 BREAST	150	216	145	156	187
5.4 BREAST DIBH	187	232	239	233	279
5.7 OESOPHAGUS (LWR 2/3)	46	63	30	36	35
5.9 4DCT RETROSPECTIVE CINE	15	15	33	43	70
6.1 ABDOMEN	41	35	32	51	42
7.1 SPINE	96	104	108	120	110
8.1 PELVIS SUPINE	15	131	127	185	184
8.2 PELVIS SUPINE MAR	25	32	22	31	20
8.3 PROSTATE	102	173	180	156	175
8.7 PELVIS SUPINE IV CONTRAST	142	154	162	85	81
8.10 3-D GYNAE MAR	111	103	127	120	101

Table 1: The number of patient scans – from 2020 through to the end of 2025 - for the 15 core protocols identified in the Glandore centre

Results (Continued)

The graphs in Figure 1 show the median DLP (in mGycm) for all scans taken using these 15 core protocols over five years.

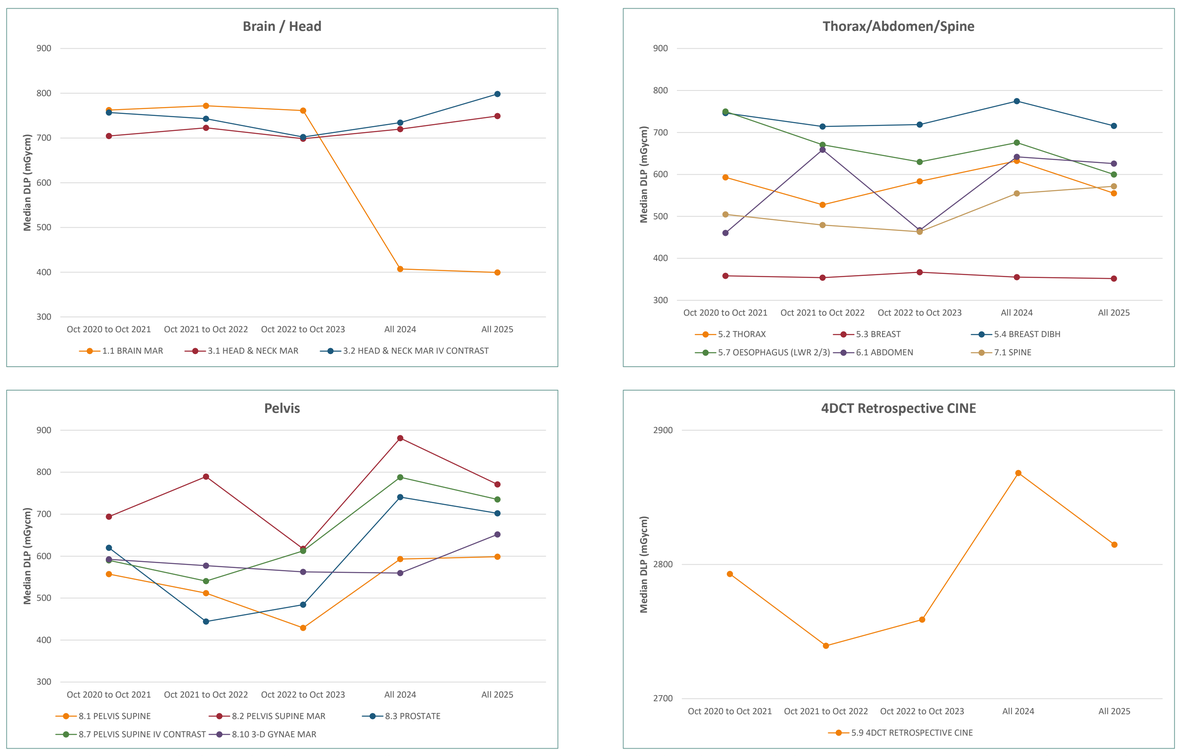


Figure 1: Four graphs depicting the change in Median DLP (mGycm) for the five annual analyses carried out on core CT scanner protocols at the Glandore centre, Cork University Hospital. They are roughly arranged by anatomical site with 4DCT data shown separately.

Discussion

This study only analyses the core protocols identified; other protocols (< 15 patients) were checked internally.

A loss of scanner-Dosewatch connectivity late in 2025 occurred. This resulted in lower patient numbers. It was discovered by this work.

A simple linear regression model was used to determine whether median DLP values were trending over time for each core protocol. Table 2 illustrates the results of this, as well as providing brief comments.

Protocol name	Slope of linear regression (mGycm / year)	Trend	Comments
1.1 BRAIN MAR	-109.1	↓	Adjustments in CT noise index significantly improved DLPs
3.1 HEAD & NECK MAR	8.6		None
3.2 HEAD & NECK MAR IV CONTRAST	7.4		None
5.2 THORAX	2.9		None
5.3 BREAST	-1.1		None
5.4 BREAST DIBH	-0.1		None
5.7 OESOPHAGUS (LWR 2/3)	-29.5	↓	Improved scan borders
5.9 4DCT RETROSPECTIVE CINE	17.2		Scan borders reduced but very variable cohort, depends also on breathing period
6.1 ABDOMEN	31.4	↑	Scanning borders increased
7.1 SPINE	20.9	↑	More patients with multiple sites - longer scans
8.1 PELVIS SUPINE	16.4		None
8.2 PELVIS SUPINE MAR	24.6	↑	Scanning borders changed from 15cm below ischium to skin level - marginally longer scans
8.3 PROSTATE	46.0	↑	Scanning borders changed from L4 to L2 for nodes
8.7 PELVIS SUPINE IV CONTRAST	53.7	↑	As per 8.2
8.10 3-D GYNAE MAR	10.1		None

Table 2: For the 15 core protocols identified, the slope generated by a simple linear regression model to identify protocols that are trending is shown. Possible reasons are also presented.

The analysis flagged a change made to 1.1 Brain MAR in 2024, where an improved CT Noise Index reduced patient scan dose.

Planned changes to scan borders or multiple palliative sites imaged in one acquisition account for other trends.

This work did not highlight any additional areas of concern.

Conclusion

The annual procedure for local facility dose reference level generation at the Glandore centre, Cork University Hospital has been extended. This work identified core protocols with a larger annual patient cohort. Any overall trends or changes in median dose length product over a five year period have been investigated, and no areas of concern noted.

References

Euratom, "Council Directive 2013/59/EURATOM of 5 December 2013 laying down basic safety standards for protection against the dangers arising from exposure to ionising radiation," Offical Journal of the European Union, 2013.
"European Union Regulations 2018, SI No. 256 of 2019," 2018. [Online]. Available: http://www.irishstatutebook.ie/2018/en/si/0256.html.
"European Union Regulations 2019, SI No. 332 of 2019," 2019. [Online]. Available: http://www.irishstatutebook.ie/eli/2019/si/332/made/en/pdf.
"European Union Regulations 2019, SI No. 413 of 2019," 2019. [Online]. Available: http://www.irishstatutebook.ie/eli/2019/si/413/made/en/pdf.
"Health Information and Quality Authority. Diagnostic Reference Levels. Guidance on the establishment, use and review of diagnostic reference levels for medical exposure to ionising radiation," July 2021. [Online]. Available: https://www.higa.ie/reports-and-publications/guide/guidance-establishment-use-and-review-diagnostic-reference-levels.

[1] Department of Medical Physics, The Glandore Centre, Cork University Hospital, Wilton, Cork, T12 DC4A
[2] Department of Radiation Therapy, The Glandore Centre, Cork University Hospital, Wilton, Cork, T12 DC4A

Corresponding Author: Christopher Walker
Christopher.Walker@hse.ie

Disclaimer: No AI has been used in the creation of this poster

FSS an Iardheiscirt
HSE South West

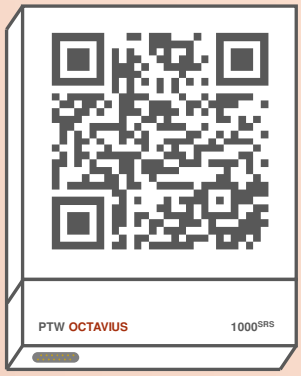
CUH Ospidéil Ollscoile Chorcaí Cork University Hospitals | UCC Coláiste na hOllscoile Corcaigh University College Cork, Ireland

CUH/UCC CANCER CENTRE

Evaluating dosimetric improvements in the PTW Octavius 1000^{SRS} array for SABR QA

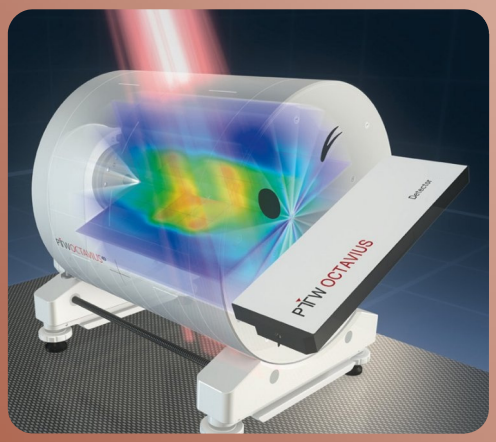
Morgan Healy, Michael Roche, Darren Coen
Department of Medical Physics, CUH/UCC Cancer Centre, Co. Cork

Scan to read the full article



INTRODUCTION

The aim of this study[1] was to characterise the PTW Octavius 1000^{SRS} array following repair and upgrade, evaluate any improvements in the detector array's performance for SABR measurements, and compare to existing literature[2,3].



INTRODUCTION

2019 SRS Array first commissioned → 2023 Clinical PSQA plans measured → 2024 Q1 PTW repair post HV Fault → 2024 Q2 Post-upgrade measurements

Work carried out by PTW involved exchanging the entire detector field and front foil of the 1000^{SRS} array with the latest version. The manufacturer provided no information as to what the latest version improved, although further information on the array's performance was subsequently identified[5].

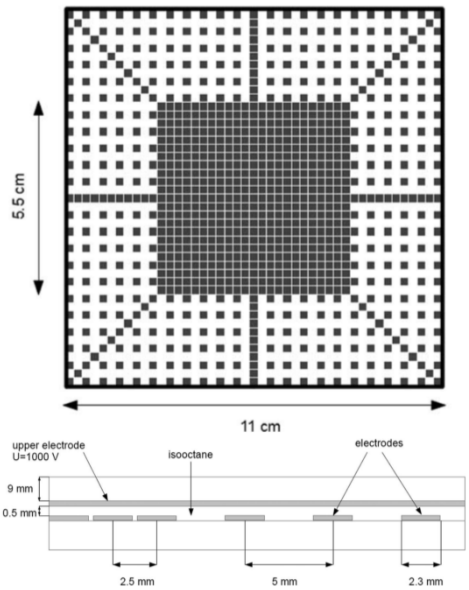
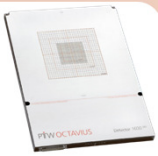


Figure 1: Schematic diagrams of the 1000^{SRS} array[3]

METHODS



Array Characterisation Measurements:

- Reference calibration 4×4 cm² field
- Peripheral chamber calibration check
- Water equivalent depth comparison
- Signal leakage over 1 to 10 mins
- Dose-rate linearity (varying MU/min (PRF))
- Dose per pulse (DPP) comparison to Poppe et al. 2019[4].
- Output factors for 1×1 to 10×10 cm²

PSQA Validation with Clinical Plans:

PSQA measurements both pre and post the array upgrade, for 10 clinical lung and liver SABR cases, were compared to evaluate any improvement in the performance of the array.

Evaluation criteria

- 3D global dose,
- Absolute gamma,
- 10% threshold
- Gamma criteria analysed:
  - 3% / 2 mm
  - 2% / 2 mm
  - 2% / 1 mm



RESULTS

Reference calibration and absorbed dose measurement under reference conditions remain unchanged pre- and post-upgrade.

Peripheral chamber calibration improved. Results of the 180° flip test are shown for X6 FFF maximum dose rate (~1300 MU/min), 0.1 mm distance-to-agreement and 1% local dose difference.

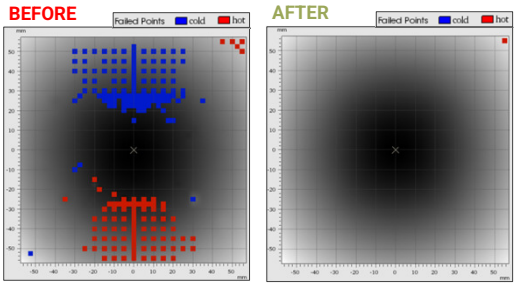


Figure 2: Results of the peripheral chamber calibration test.

Water equivalent depth of the array's effective point of measurement remains unchanged (10.5±0.3 vs 10.0±0.3 mm for X6 FFF), and is consistent with manufacturer's specified value of 10.1 mm.

Signal leakage has improved, though still not optimal performance. Out of 977 detectors, up to 17% pre- and 10% post-upgrade exceeded specification (>2 mGy/min).

Dose per pulse non-linearity was comparable to Poppe et al.[4] pre-upgrade (−2.5% vs −2.1% at DPP of 0.619 mGy) but improved post-upgrade (-1.0% versus −2.2% at DPP of 0.652 mGy). Dose rate was approximately 1300 MU/min.

RESULTS

Dose-rate linearity has improved, as shown in the graph. MU/min was varied from 100 to 1320 MU/min with DPP held constant. All values are normalised to 100 MU/min.

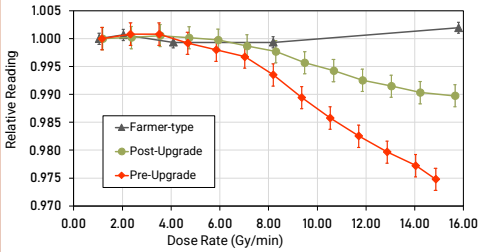


Figure 3: Dose rate linearity for X6 FFF.

Output factors post-upgrade showed a maximum difference of −0.9% for X6 CFF and −1.2% for X6 FFF, and agreed within ± 1.0 % of the TPS for fields > 1.5 × 1.5 cm^2. The field-size dependent correction factors recommended by Shin et al.[2] are not required.

Clinical PSQA deliveries showed passing rates post-upgrade 9.2% higher on average for 2%/1mm, but no significant difference for 3%/2mm and 2%/2mm.

CONCLUSIONS

The array underperforms in some areas;

- Leakage outside of specification for a large number of chambers, even after the upgrade.
- Dose rate non-linearity was still at -1.0 % after the upgrade (1320 to 100 MU/min). A technical note from the manufacturer subsequently stated the tolerance for dose rate linearity = 1.04[5].

However:

- Absorbed dose measurements under reference conditions unchanged.
- Peripheral chamber calibration improved.
- Signal leakage improved.
- Dose rate linearity improved.
- Field size output factors improved.
- 9.2% increase in gamma analysis passing rate for 2%/1mm.

REFERENCES

1. Healy M, Roche M, Coen D. Dosimetric characterization of a liquid-filled ion chamber array post upgrade and evaluation of improvements for stereotactic plan verification. J Appl Clin Med Phys. 2026;27:e70371. doi.org/10.1002/acm2.70371
2. Shin HB, Noh YY, Kim H, Kim C, Sung K, Kim DW. Correction method for depth and field size dependence in Octavius 1000 SRS patient-specific QA. Radiat Phys Chem. 2024;223:111892.
3. Poppe B, Stelljes T, Looe H, et al. Performance parameters of a liquid filled ionization chamber array. Med Phys. 2013;40(8):082106-1.
4. Poppe B, Stelljes T, Looe H, et al. Erratum: "Performance Parameters of a Liquid Filled Ionization Chamber Array". Med Phys. 2019;46(10):4708-4709.
5. PTW-Freiburg GmbH. Technical Note: Dose Rate and Dose per Pulse Dependence of PTW Solid State and Liquid-filled Detectors. [Document #: D252.200.03/03]. Physikalisch-Technische Werkstätten. Accessed online: 06/03/2026.

CONTACT

Morgan Healy
Physicist
The Glandore Centre,
Cork University Hospital, Wilton Road,
Cork. T12 DC4A
morgan.healy@hse.ie
+353-21-4234830

Michael Roche
Principal Physicist
The Glandore Centre,
Cork University Hospital, Wilton Road,
Cork. T12 DC4A
michael.roche1@hse.ie
+353-21-4234830

CUH Ospidéil Oiscoile Chorcaí Cork University Hospitals | UCC Coláiste na hOllscoile Corcaigh University College Cork, Ireland

CUH/UCC CANCER CENTRE

Feidhmeannacht na Seirbhíse Sláinte Health Service Executive

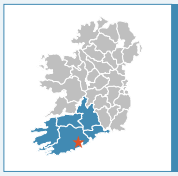
Validating Rapid Delivery of Prostate SABR with FFF Arcs using Intra-fraction Prostate Displacements

M. Healy, M. Roche, O. McKivitt, P. Collins, C. Little, M. Moran, D. Coen, A. O'Connell, D. O'Gorman, E. Hayes, M. O'Cathail, M. Higgins, S. O'Cathail

Department of Radiation Oncology, CUH/UCC Cancer Centre, Co. Cork.

INTRODUCTION

Ireland has some of the highest incidences of prostate cancer in the world[1], where it is the most commonly diagnosed cancer (exc. non-melanoma skin cancer).[2] Standard treatment regimes are resources intensive requiring 20-39 fractions.



1 in 3
invasive cancers in Irish men are prostate cancer.

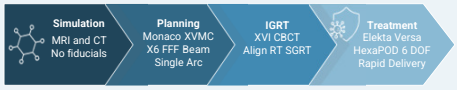
4,516
men in Ireland were diagnosed with prostate cancer in 2022.

Prostate SABR offers major efficiency gains HYPO-RT-PC[3] and PACE-B[4] trials presented large scale data proving non-inferiority of SABR treatments for prostate cancer, with 36.35Gy/5# being favourable. Due to intrafraction motion of the prostate, guidelines recommend re-imaging should occur during prostate SABR treatments at approx. 3-4 minute intervals[4].

MATERIALS & METHODS

Equipment needed for prostate SABR is readily available in a modern radiotherapy clinic. At CUH equipment utilised:

- Versa HD linac with 6 MV FFF
- XVI cone beam CT imaging
- HexaPOD 6 degree of freedom couch
- Monaco treatment planning system
- AlignRT stereo photogrammetry SGRT
- GE MRI and GE CT simulators



A prospective planning study involving a total of 40 test plans created on 10 patient datasets was carried out to determine the optimal delivery technique. 10 MV FFF, 6 MV FFF and 6 MV CFF were compared, as well as 6 MV FFF using a single and dual arc. Test cases were evaluated based on TPS predicted delivery time and plan quality, A rapid delivery time meeting all dose aims and constraints was deemed optimal.

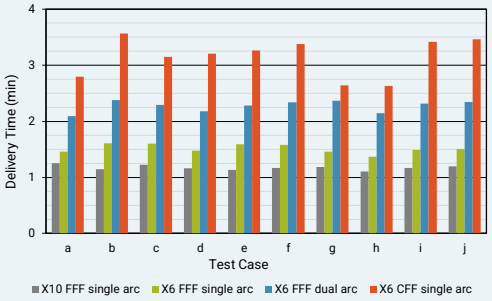
A retrospective review of the first 50 fractions was carried out for verification and quality improvement purposes. Plan quality metrics were taken from the TPS and time from beam-on to beam-off (inc. all interruptions / beam holds) was recorded from the linac log files. Intrafraction motion of the prostate was measured between the pre/post-treatment CBCTs for the first 5 patients.

RESULTS

Prospective planning study:

FFF beams enabled substantially faster delivery compared to conventional beams.
Median delivery times were:

- 70 s for 10 MV FFF single arc [IQR: 69-72]
- 90 s for 6 MV FFF single arc [IQR: 88-95]
- 138 s for 6 MV FFF dual arc [IQR: 132-141]
- 194 s for 6 MV single arc [IQR: 173-204]



Plan quality between the single arc and dual arc techniques was similar. The prescription dose spillage (PDS) for the 10 single arc 6 MV FFF test plans was 1.090 ± 0.032 -vs- 1.076 ± 0.028 for the dual arc plans. Similarly the modified gradient index (MGI) was 4.34 ± 0.43 -vs- 4.10 ± 0.45. However, the dual arc approach had significantly slowly delivery times.

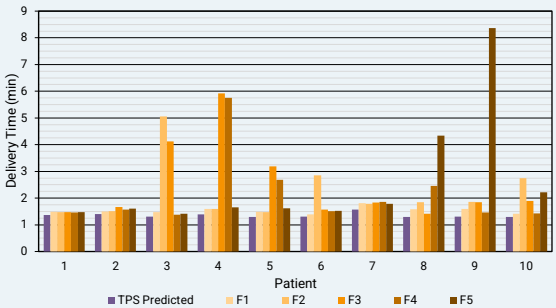
Prostate SABR delivery technique:

The approach implemented at Cork University Hospital:

- 36.25 Gy / 5# following PACE-B protocol.
- 5 mm CTV-PTV margin, option for 3mm posteriorly
- No fiducial markers[5]
- CT and T2w MRI for simulation
- CBCT and AlignRT for IGRT
- Single arc, no mid-treatment CBCT
- Dual arc, with mid-treatment CBCT

Retrospective Treatment Review:

Clinical delivery times for all 50 fractions are shown below:



The median delivery time was 96 s [IQR: 89-113] compared to a predicted delivery time of 79 s [IQR: 78-83]. Clinical delivery times include all interruptions, patient and linac related.

Retrospective Treatment Review:

Results showed:

- 76% (38/50) of fractions were delivered <2 mins
- 86% (43/50) were delivered <3 mins
- 88% (44/50) were delivered <4 mins

Prostate displacements between pre/post CBCT imaging showed:

- CTV was within PTV on every post-CBCT image
- 89.3% of the intra-fraction displacements were ≤ to 3 mm.
- max prostate translation = 4 mm
- max rotation = 1.0°
- Lateral corrections most common

CONCLUSION

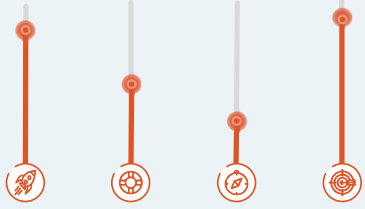
Rapid delivery of Prostate SABR at CUH

86% of deliveries completed in under 3 mins

50% reduction in PTV margins vs standard tx

35% faster delivery with FFF (6 MV)

89% of intra-fraction displacements ≤ 3mm



✓ Prospective study involving 40 test plans allowed the optimal delivery approach to be selected.

✓ Retrospective study involving 50 delivered fractions allowed the technique to be validated.

✓ Recently[5] Linac SABR without fiducials was associated with lower odds of grade 2+ urinary toxicity at 2yr versus Linac SABR with fiducials.

REFERENCES

1. G. Gandaglia, R. Leni, F. Bray and others, "Epidemiology and Prevention of Prostate Cancer," European Urology Oncology, vol. 4, no. 6, pp. 877-892, 2021.
2. NCRI, "Cancer in Ireland 1994-2022 Annual Statistic Report of National Cancer Registry," National Cancer Registry, Cork, Ireland. Accessed online: 11/03/2026.
3. A. Widmark, A. Gunnlaugsson, L. Beckman and others, "Ultra-hypofractionated versus conventionally fractionated radiotherapy for prostate cancer: 5-year outcomes of the HYPO-RT-PC randomised, non-inferiority, phase 3 trial," The Lancet, 2019.
4. D. H. Brand, A. C. Tree, P. Ostler and others, "Intensity-modulated fractionated radiotherapy versus stereotactic body radiotherapy for prostate cancer (PACE-B): acute toxicity findings from an international, randomised, open-label, phase 3, non-inferiority trial," Lancet Oncology, vol. 20, pp. 1531-1543, 2019.
5. R. Ratnakumaran, D. H. Brand, A. Sasitharan and others, "Exploring Factors Associated with Late Urinary Toxicity After Prostate Stereotactic Body Radiotherapy: Findings from the PACE-B Study," European Urology, vol. 89, pp.71-79, 2025.

CONTACT

Morgan Healy
Physicist
The Glandore Centre,
Cork University Hospital,
Wilton Road, Cork.
T12 DC4A
morgan.healy@hse.ie
+353-21-4234830

Michael Roche
Principal Physicist
The Glandore Centre,
Cork University Hospital,
Wilton Road, Cork.
T12 DC4A
michael.roche1@hse.ie
+353-21-4234830

Cross Modality Harmonization of UHDR Radiation Dosimetry

Cormac Kerins[1], Kevin Byrne[1,2], Yannick Poirier[2], Mihaela Ghita-Pettigrew[3], Oran McElligott[4], Sina Mossahebi[2], Cathy Fleming[4], Brendan McClean[4], Karl T. Butterworth[3], Mark Foley[1] and Michael Martyn[1]

[1]Physics, School of Natural Sciences, University of Galway, Ireland
[2]University of Maryland School of Medicine, Baltimore, United States
[3]Queens' University Belfast, Belfast, Northern Ireland
[4]St. Lukes Radiation Oncology Network, Dublin, Ireland

Overall Goal

Develop protocols to standardise radiation dosimetry and reporting for UHDR beams across three modalities and institutions. Utilise commercial dosimeters to ensure that the process can be readily replicated by other teams.

Dosimeters:

- Medscint RP-FLASH (Scintillation Dosimeter)[1]
- PTW flashDiamond (Schottky Diode Dosimeter)[2]
- PTW Advanced Markus
- Gafchromic EBT-XD (Radiochromic Film)
- Orthochromic OC-1 (Radiochromic Film)

Beamlines:

- XSTRAHL FLASH-SARRP (kV Photon, Queen's University Belfast)
- Varian ProBeam (MV Proton PBS, Maryland Proton Treatment Center)
- Modified Varian Clinac 21EX (MV Electron, University of Maryland Medical Center)
- Modified Elekta Precise (MV Electron, St. Lukes Radiation Oncology Network)

Specific Aims

Aim 1: Ensure the response of our dosimetry systems is self-consistent and in agreement with radiochromic film measurements. Identify possible dosimeter failure modes and their dependence on beam parameters.

Aim 2: Investigate the temporal structure of the beamlines at participating institutions. Characterise the space of possible outputs for each beamline. Identify the space of beam structure parameters which are common to all beamlines. Define a set of "FLASH standard beams" which can be produced across all beamlines.

Aim 3: Provide dosimetric support to a multi-institution study quantifying the influence of beam modality on the FLASH effect.

Significance

The influence of particle type on the FLASH effect is still an open question. There are different accelerators associated with the production of all three particles. These accelerators produce beams with vastly different time structures. Disentangling the effect of time structure from particle type will require strong standards for measurement and reporting of beam structure[3].

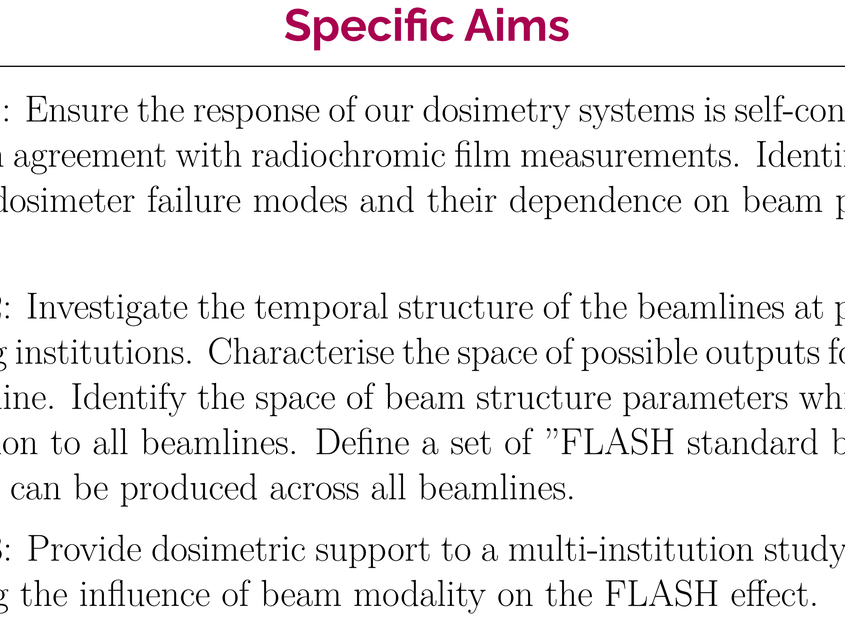


Figure 1. A lack of standardisation in UHDR dosimetry and radiobiological protocols has led to conflicting results in the literature.

Innovation

- The protocols will utilise two commercially available dosimeters with exceptional temporal resolution.
- They address the three most common beam modalities used in FLASH research (kV photon, electron, proton).
- High temporal resolution dosimetric data will be available for the in-vitro studies.

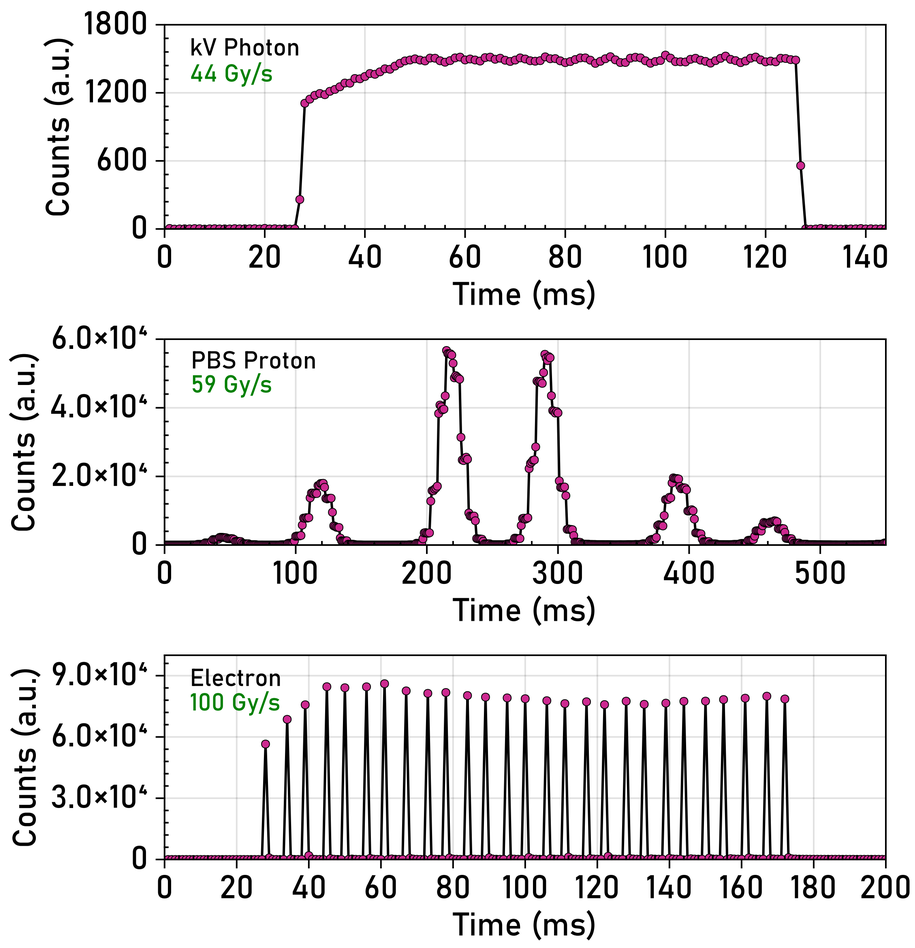


Figure 2. Scintillator measurements for kV photon, MV proton, and MV electron beams.

Approach

Aim 1: Initial Investigation with Dosimeters:

- Identification and analysis of non-ideal dosimeter behaviour.
- Implement solutions for any deviations oberved.

Aim 2: Beam Structure Characterisation:

- Characterisation of the temporal structure of each beamline.
- Harmonisation of dose rate and beam parameter definitions.

Aim 3: Application to In-Vitro FLASH Studies:

- In-vitro studies will be conducted across all four beamlines using the scintillation and diamond dosimeters.
- Film dosimetry will be used to confirm the total absorbed dose delivered.

References

1. Guo, L., Zhou, B., Tsai, Y. C., Jiang, K., Iakovenko, V., Wang, K. K. (2025). Comprehensive characterization and validation of a fast-resolving (1000 Hz) plastic scintillator for ultra-high dose rate electron dosimetry. Medical physics, 52(10), e70006. https://doi.org/10.1002/mp.70006
2. Marinelli, M., di Martino, F., Del Sarto, D., Pensavalle, J. H., Felici, G., Giunti, L., De Liso, V., Kranzer, R., Verona, C., Verona Rinati, G. (2023). A diamond detector based dosimetric system for instantaneous dose rate measurements in FLASH electron beams. Physics in medicine and biology, 68(17), 10.1088/1361-6560/acead0. https://doi.org/10.1088/1361-6560/acead0
3. Lin, B., Du, H., Hao, X., Liang, Y., Xu, H., Tang, W., Li, J., Zhang, Y., Du, X. B. (2025). The influence of beam parameters on FLASH effect. Frontiers in oncology, 15, 1431700. https://doi.org/10.3389/fonc.2025.1431700

Quality assurance tests for RapidArc Dynamic

Agnieszka Bartnikowska, Robert Nolan, Darina Hickey, Luke Rock
Radiotherapy Department, Beacon Hospital, Dublin

Introduction

- RapidArc Dynamic (RAD) (Varian Medical Systems) is a novel optimisation and delivery system that enables dynamic collimator rotation and incorporates integrated Static Angle Modulated Ports (STAMPS) within volumetric modulated arc therapy (VMAT).
- The aim of this study was to design and establish a quality assurance (QA) programme for RAD following commissioning.
- Beacon Hospital is the first to implement RAD clinically in Ireland and the UK.

Method

- The RAD technique was commissioned and validated on a Varian TrueBeam linear accelerator for four photon beam energies (6 MV, 10 MV, 6 MV FFF and 10 MV FFF).
- Monthly QA and patient-specific quality assurance (PSQA) procedures were established for RAD. A quality control test designed by Varian, the Dose Rate Collimator Speed test (DR-CS) test, was used to assess synchronisation of dynamic collimator, multi-leaf collimator (MLC) positioning, and dose rate [1].
- The DR-CS test plan consists of five gantry sub-segments designed to deliver a uniform dose to five sectors of a circular field using unique combinations of collimator speeds and dose rates using a static V-shaped MLC field (see Figure 1), as well as an open field used for normalisation. The relative dose delivered in each sector of the field is compared.
- The DR-CS test was implemented for monthly QA for the 6 MV energy, while Portal Dose Image Prediction (PDIP) and ArcCHECK (Sun Nuclear) were used for PSQA.

Results

- Calculated percentage differences between each sector in the DR-CS test, shown in Figure 2, were consistently within the tolerance of $\pm$ 3%.
- Mean absolute differences, shown in Figure 3, were within the tolerance of $\pm$ 1.5% each month.
- Average gamma passing rates for PSQA measurements for ten patients planned with RAD are shown in Table 1.

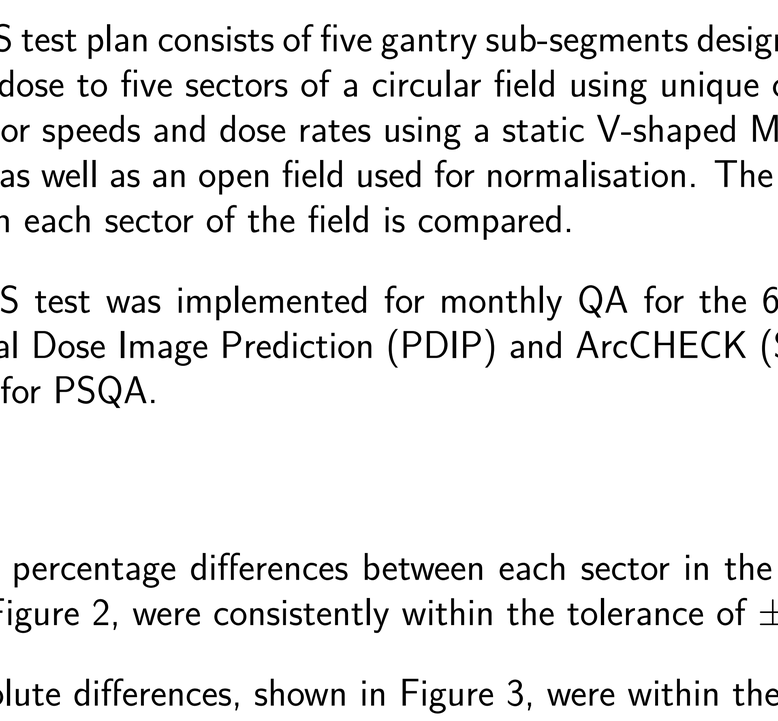


Figure 1. Integrated Portal Dosimetry image of a DR-CS test delivery taken from a Varian White Paper [1].

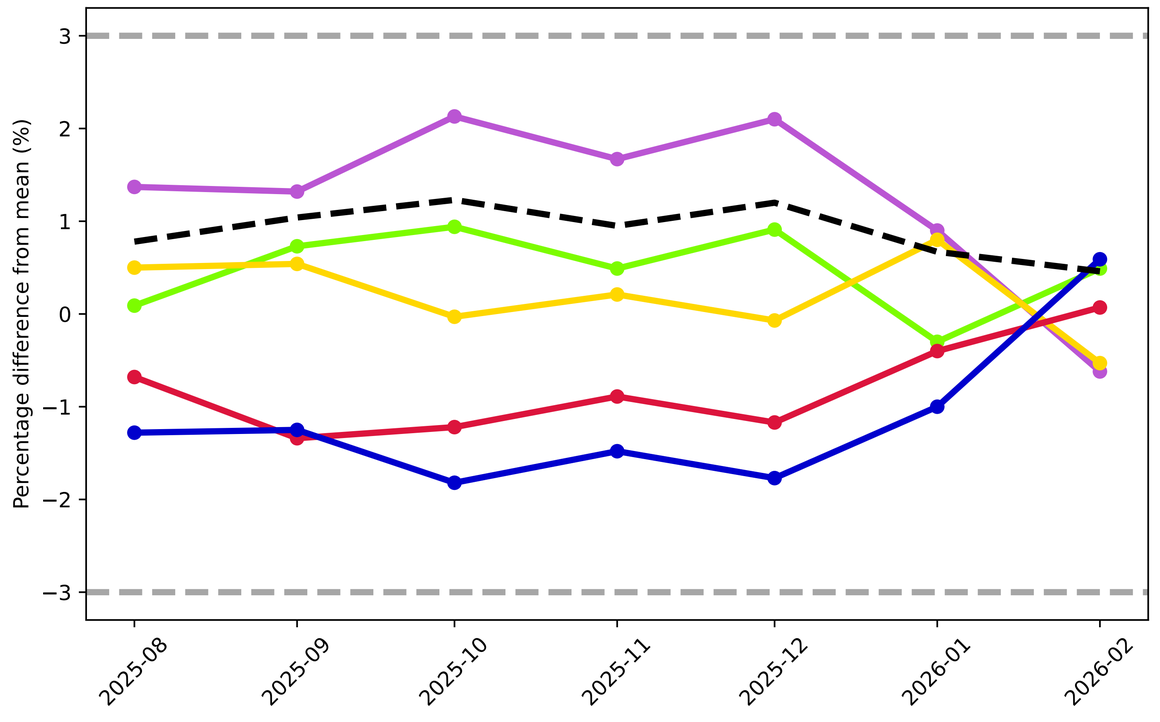


Figure 2. Calculated percentage differences from the mean for each sector by month for the DR-CS test. Sector A (blue), sector B (red), sector C (yellow), sector D (purple), sector E (green) and absolute mean value (black dashed line) are plotted. The dashed grey lines indicate the tolerance for individual sector percentage differences from the mean.

Table 1. Average gamma passing rates (2%, 2 mm, 10% threshold) for in-phantom (ArcCheck) and portal dosimetry (PDIP), with/without (full/sep) STAMPS separated into separate fields.

Patient	Site	Fields	ArcCheck	PDIP (full)	PDIP (sep)
1	Pelvis	2	93.1%	98.9%	98.4%
2	Liver	2	95.3%	98.3%	98.4%
3	Breast	3	91.1%	98.5%	99.1%
4	Breast	3	92.4%	99.4%	99.3%
5	Breast	4	94.6%	98.1%	98.7%
6	Breast	4	92.6%	98.5%	98.7%
7	Breast	4	94.3%	99.1%	98.9%
8	Breast	5	89.8%	99.1%	99.2%
9	Breast	4	93.2%	96.5%	96.8%
10	Breast	4	93.5%	97.3%	97.5%
	Average		93.0%	98.4%	98.5%

Discussion

- Monthly DR-CS test results have all been within tolerance. Recently, the spread of results across sectors has reduced. This was found to likely be due to an engineering intervention during a routine machine service. Control limits, similar to those described by Van Riet *et al.*, will be defined for this test [2].
- Portal dosimetry gamma passing rates have been consistently higher than ArcCheck passing rates. No anomalies have been detected by splitting STAMPS into separate measurement fields in portal dosimetry. Gamma passing rates are consistent with what was seen during the commissioning of RAD.

Conclusion

- This study demonstrates a practical approach to the QA of RAD. DR-CS was performed monthly and individual plans were measured using multiple methods. It is anticipated that the volume of PSQA methods used in this centre for RAD will be reduced following an initial trial period.

References

[1] M. Jennings, M. A. Ghazal, E. Onjukka, et al. RapidArc Dynamic Quality Assurance. White paper, Varian Medical Systems, Inc., 2025.

[2] Emma Van Riet, Wout Piot, Bianca Vanstraelen, Karel Aerts, Truus Reynders, Tom Depuydt, and Wouter Crijns. Initial follow-up of mechanical QC tests for RapidArc Dynamic (RAD). *Journal of Applied Clinical Medical Physics*, 27(1):e70411, 2026.

Characterization of EBT-XD Film for use in High Dose Kilovoltage Energy Applications

Austin Stricker[1], Amey Bermingham[2], Aoife Donnellan[2], Louise Fahy[2]
[1] Physics Unit, School of Natural Sciences, College of Science and Engineering, University of Galway, Ireland.
[2] Department of Medical Physics and Clinical Engineering, University Hospital Galway, Ireland.

Background:

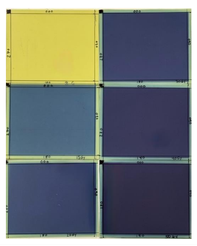
Radiochromic film is a useful dosimetry system for clinical and research applications. However, a limitation is often its designed dose range. Gafchromic EBT-XD film is a radiochromic film specifically designed to have a wider dose range than other forms of Gafchromic film such as EBT3[1]. This higher dose range makes EBT-XD valuable for high dose applications in either the kV or MV energy region. While previous literature has performed film characterization work for EBT-XD film for high dose MV applications, there is limited available work that characterizes the kV range or the difference in functionality across these energy ranges.[2-4]

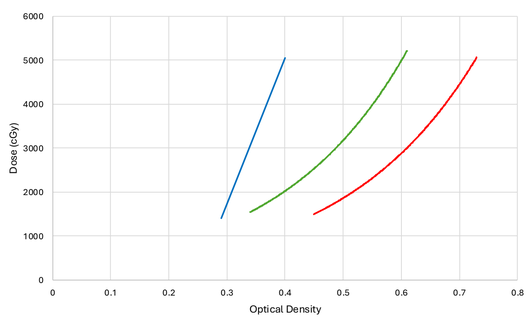
Objective:

Perform film characterization testing for EBT-XD film for high dose applications in the kV range.

Dosimeter:

- GAFChromic EBT-XD Film
  - Dynamic Dose Range: 0.1 Gy to 60 Gy.[1]
  - Calibrated with Womed T-200 kilovoltage X-ray therapy unit at 200 kV.
    - Dose Points:
      - 15 Gy
      - 25 Gy
      - 30 Gy
      - 40 Gy
      - 50 Gy



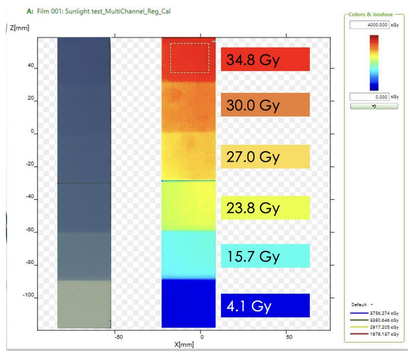


Reaction to Sunlight

- Known sensitivity to UV light.[5]
- Strip of film was left on a windowsill exposing 2-cm every other day.

Table 1 - Apparent dose after various durations of sunlight exposure

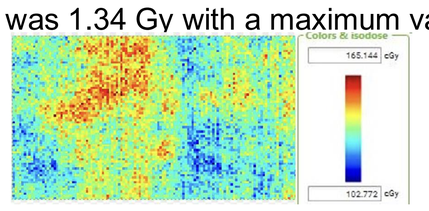
Days Exposed to Sunlight	Apparent Dose (Gy)
12	34.8
10	30.0
8	27.0
6	23.8
4	15.7
2	4.1



***Conclusion:** Sunlight exposure can have a significant impact on dose.

Reaction to Office Light:

- The resulting average apparent dose of the film was 1.34 Gy with a maximum value of 1.65 Gy and a minimum value of 1.03 Gy.



***Conclusion:** Short-term exposure to normal (non-UV) office lighting will have little to no impact on read dose.

Film Position

- Film irradiated to 10 or 15 Gy and scanned at different locations on scanner

Table 2- Average dose readout for film irradiated to 10 or 15 Gy by location on scanner

Position	Upper Left	Middle Left	Bottom Left	Upper Middle	Middle	Bottom Middle	Upper Right	Middle Right	Bottom Right
Read dose of film irradiated to 10 Gy (Gy)	13.6	12.3	13.7	13.6	12.4	14.0	13.7	12.5	14.0
Percentage Difference relative to Middle (%)	+9.2	-0.4	+10.2	+9.6	N/A	+12.4	+10.3	+0.8	+12.4
Read dose of film irradiated to 15 Gy (Gy)	19.3	17.0	20.0	19.7	17.0	19.9	19.8	17.1	20.3
Percentage Difference relative to Middle (%)	+12.7	+0	+16.2	+14.7	N/A	+15.7	+15.2	+0.6	+17.7

***Conclusion:** Clear effect on read dose based on scanner location, effect appears to increase with dose.

Film Orientation:

- Film irradiated to 10 or 15 Gy and scanned in different orientations on scanner

Table 3- Average dose readout for film irradiated to 10 or 15 Gy by orientation

Orientation	Normal	90°	180°	270°	Inverted Normal	Inverted 90°	Inverted 180°	Inverted 270°
Read dose of film irradiated to 10 Gy (Gy)	12.3	12.0	12.3	12.0	12.5	12.0	12.5	12.0
Percentage Difference relative to Normal (%)	N/A	-2.9	+0	-3.2	+0.94	-2.5	+0.9	-2.5
Read dose of film irradiated to 15 Gy (Gy)	16.9	16.5	16.9	16.5	17.2	16.4	17.2	16.4
Percentage Difference relative to Normal (%)	N/A	-2.3	+0.2	-2.2	+1.6	-2.8	+1.5	-2.9

***Conclusion:** Film orientation does have some impact on the read dose, particularly if scanned in portrait vs. landscape orientations. This finding is consistent with literature.[4]

Reaction to Repeated Scans

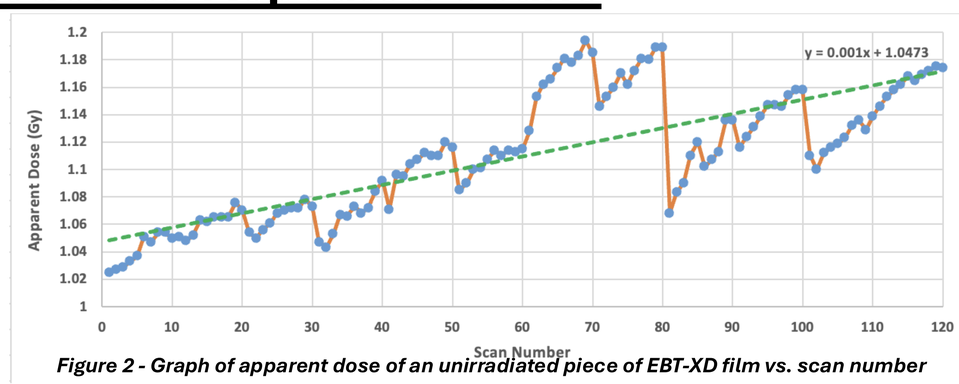


Figure 2 - Graph of apparent dose of an unirradiated piece of EBT-XD film vs. scan number

***Conclusion:** There is a small change in apparent dose as a function of the number of times the film is scanned. However, the dose added by the scanner could be considered negligible for high-dose applications as the dose added per scan is only approximately 0.001 Gy per scan. Additionally, scanner warm up appears to impact read dose, again, this only appears to be relevant at very low doses.

Energy Dependency and Readout Time:

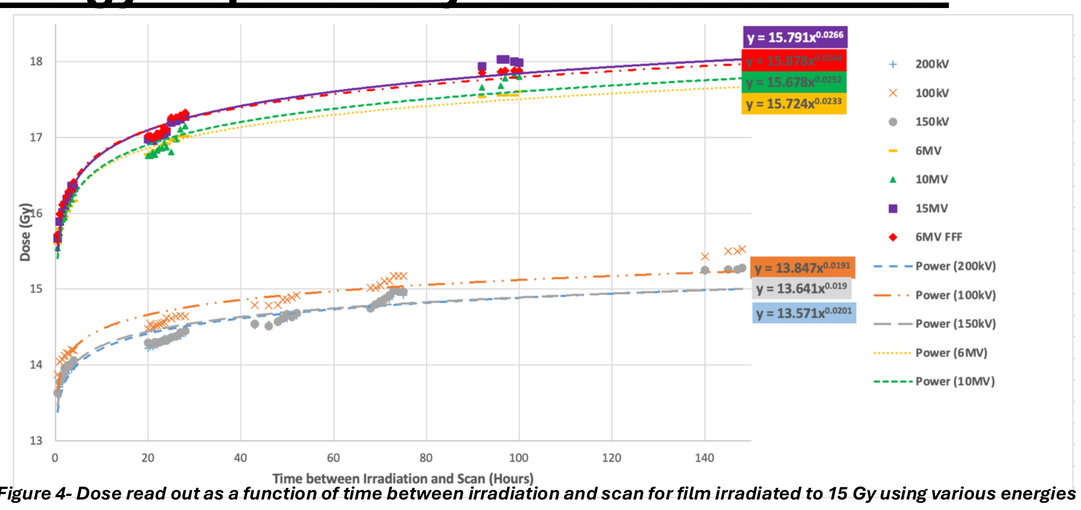


Figure 4- Dose read out as a function of time between irradiation and scan for film irradiated to 15 Gy using various energies

***Conclusion:** There appears to be some energy dependency, especially when calibrated with kV but used for MV measurements. Additionally, there is a noticeable change in dose readout as a function of time between irradiation and scan. This is especially prevalent within the first 24 hours. Consistent with other literature.[4]

Repeatability:

- Two pieces of film irradiated to 15 Gy with either 150 kV or 200 kV scanned 40x each.

Table 4- Statistics of repeatability test for both the 150 kV and 200 kV data sets

	Average Dose (Gy)	Standard Deviation (Gy)	Range (Gy)	Coefficient of Variation (%)
150 kV	15.52	0.01	0.05	0.08
200 kV	15.50	0.01	0.03	0.05

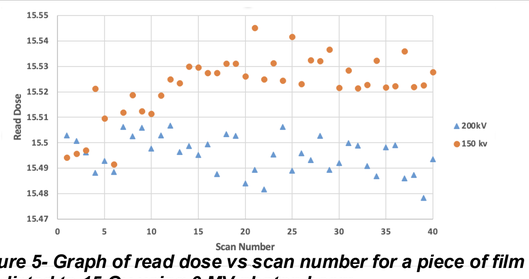


Figure 5- Graph of read dose vs scan number for a piece of film irradiated to 15 Gy using 6 MV photon beam

***Conclusion:** There is little variation in read dose over 40 scans. This shows that in high dose applications, used scanner and software repeatability is good.

General Conclusions:

- A similar shape/size of film should be used throughout the study and scanned in the same orientation in the center of the scanner, including for calibration films.
- The time film is scanned post-irradiation should be consistent and at least 24 hours.
- Though there is little indication that routine handling under non-UV office light impacts dose, best practice is to minimize exposure of film to any light.
- The beam energy that is to be measured should be the same used for calibration.
- For low dose applications, the scanner should be warmed up prior to scanning.

Clinical Impact:

High-dose kV irradiation use in a clinical setting is rare but does have specific uses such as in blood irradiation which is achieved by delivering 25-50 Gy from a kV source. Depending on the delivered dose, it could also be useful in HDR brachytherapy or orthovoltage therapy treatments. Characterization of how EBT-XD film behaves at high-doses delivered with kV energy beams is critical to understand its limitations. Additionally, many findings in this project are universal to radiochromic film best practice and can be directly applied to any QA program to benefit patient outcomes.

Acknowledgements:

The author would also like to thank the staff of University of Galway and the University Hospital Galway Department of Medical Physics and Clinical Engineering for their assistance.

References

1. Ashland Advanced Materials. *GAFCHROMIC TM DOSIMETRY MEDIA, TYPE EBT-XD.*
2. Grams, M. P., Gustafson, J. M., Long, K. M. & De Los Santos, L. E. F. Technical note: Initial characterization of the new EBT-XD Gafchromic film. *Med Phys* 42, 5782–5786 (2015).
3. Shameem, T., Bennie, N., Butson, M. & Thwaites, D. Comparative characterisation of different types of Gafchromic films for radiotherapy use. *Phys Eng Sci Med* https://doi.org/10.1007/s13246-025-01596-0 (2025) doi:10.1007/s13246-025-01596-0.
4. Miura, H. *et al.* Gafchromic EBT-XD film: Dosimetry characterization in high-dose, volumetric-modulated arc therapy. *J Appl Clin Med Phys* 17, 312–322 (2016).
5. Katsuda, T. *et al.* Comparing three UV wavelengths for pre-exposing Gafchromic EBT2 and EBT3 films. *J Appl Clin Med Phys* 16, 449–457 (2015).

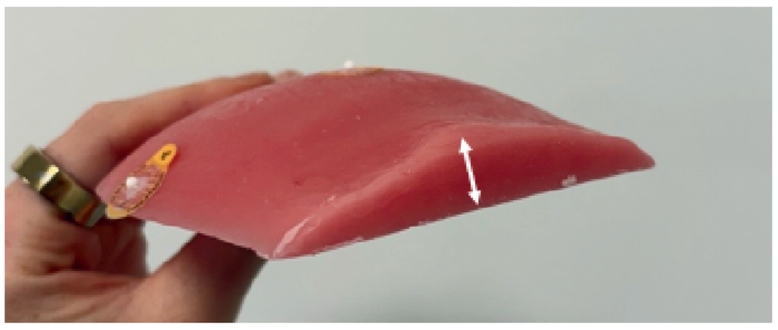
Investigation of the dosimetry of electron fields at oblique angles of incidence and non-uniform surfaces

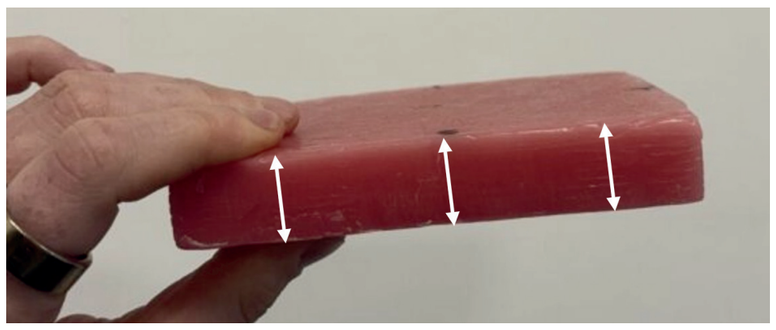
Comparison between the Monaco treatment planning system and Versa HD treatment units

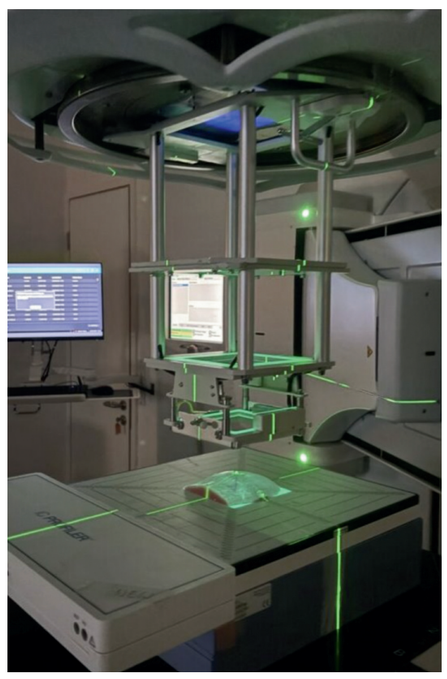
Ciara Hickey[1,2], Paul Hill[1], Darren Coen[1] and Michael Moran[1]
[1]Cork University Hospital, [2]St Luke's Radiation Oncology Network

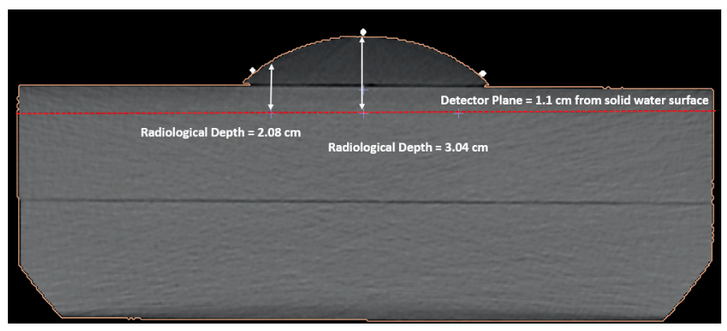
Purpose and Aims

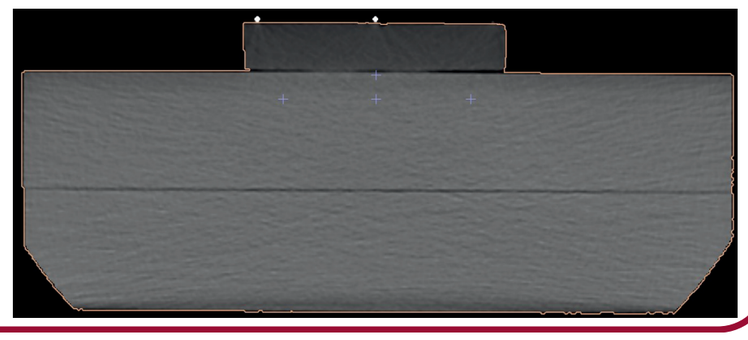
In CUH, a historical limit of 20° incident angle for electron treatments exists, based off historical planning methods using manual calculations. At present, all electron plans are calculation using eMC in the TPS. Therefore, the 20° limit may be an unnecessary limitation. The aim of this work was to investigate the accuracy of dose calculation with increasing angle of incidence on non-uniform surfaces and to compare treatment plans calculated in Monaco with measurements made on Elekta Versa HD linacs.





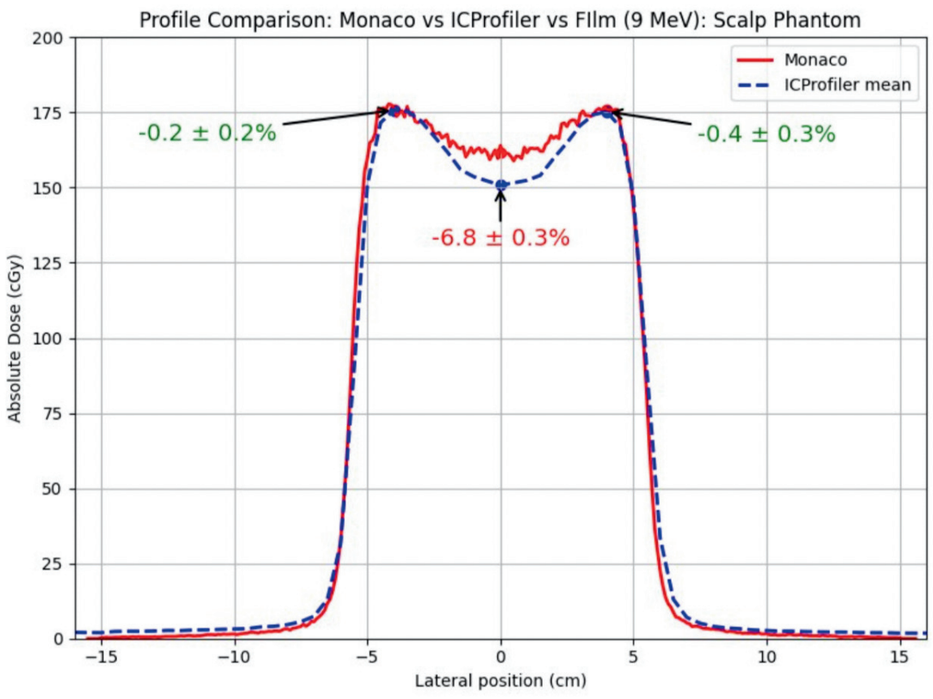




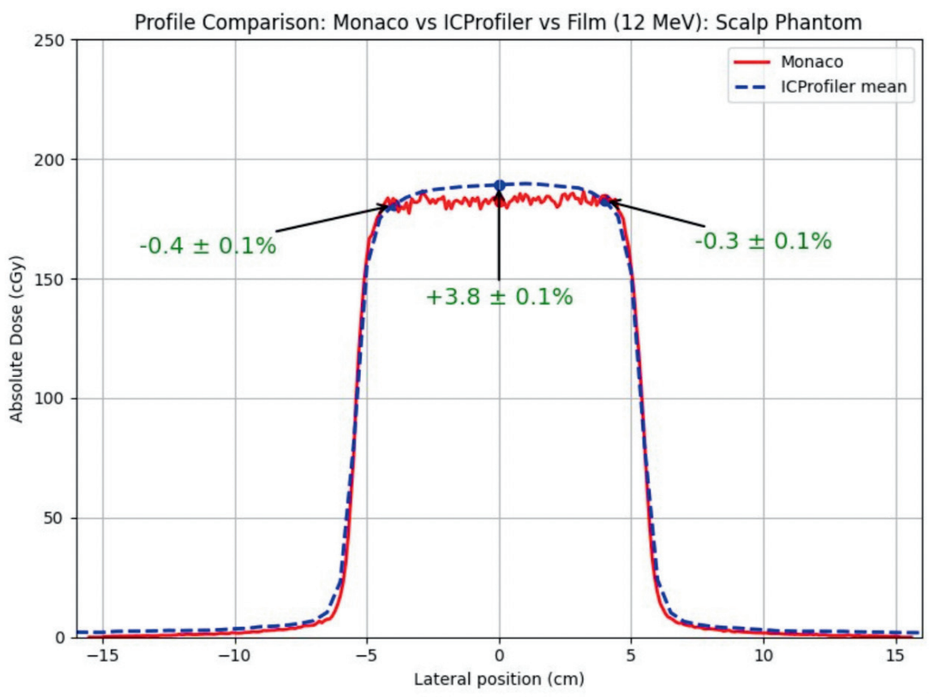


Phantom Measurements and Comparison

Scalp-shaped and a flat control wax phantoms were created to investigate the accuracy of the Monaco eMC algorithm at increasing incident angles for available electron energies in CUH; 6, 9, an 12 MeV. At ±4 cm, the incidence angle was 30°. Measurements were taken with the IC Profiler, EBT4 film and point dose measurements with a Roos parallel plate ionisation chamber.



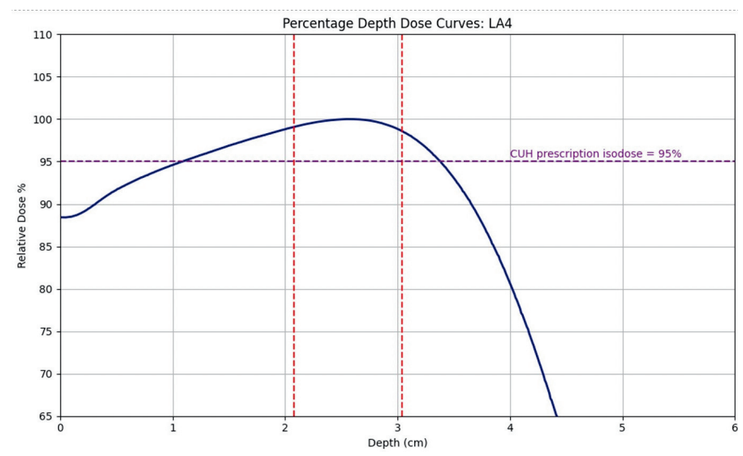
Comparison	-4 cm		0 cm		+4 cm	
	Scalp	Control	Scalp	Control	Scalp	Control
ICP v Monaco	0.2% ± 0.2%	6.6% ± 0.2%	6.8% ± 0.3%	7.5% ± 0.2%	0.4% ± 0.3%	5.8% ± 0.2%



Comparison	-4 cm		0 cm		+4 cm	
	Scalp	Control	Scalp	Control	Scalp	Control
ICP v Monaco	-0.4% ± 0.1%	2.0% ± 0.2%	3.8% ± 0.1%	3.5% ± 0.2%	-0.3% ± 0.1%	2.8% ± 0.2%
Film v Monaco	3.9% ± 1.7%	6.9% ± 2.3%	5.6% ± 2.4%	7.0% ± 2.0%	2.1% ± 2.8%	3.0% ± 7.4%
Roos v Monaco	–	–	0.8% ± 0.1%	2.2% ± 0.1%	–	–

Results and Discussion

The physical depth of the phantoms limited the investigation to 9 and 12 MeV due to the achievable depth of measurement being too far beyond d_{max} for 6 MeV. For 9 MeV, the measurement at the centre of the phantom was several cm beyond d_{max} (at a high gradient on the depth dose curve). The difference between the TPS and measurement at this point was out of tolerance (5%). For 12 MeV, all points of measurements were on the high dose/low gradient region of the depth dose curve. For these points, the TPS values and the measured values (ICP, EBT4 and Roos chamber measurements) matched within the tolerance of 5%.



Conclusion

In the high dose/low gradient region, TPS ≡ IC Profiler measurements within 5% (up to an oblique angle of ~ 30°)

Assessment of conventional geometric contour comparison metrics via correlation with dose in prostate stereotactic body radiotherapy

Owen McLaughlin[1], Stephen J. McMahon[1], Suneil Jain [1,2], Conor K. McGarry[1, 3]

1 – Johnston Cancer Research Centre, Queen's University Belfast
2 - Clinical Oncology, Northern Ireland Cancer Centre, Belfast Health and Social Care Trust
3 – Radiotherapy Physics, Northern Ireland Cancer Centre, Belfast Health and Social Care Trust

Clinical impact

This assessment will provide a benchmark for developing a radiotherapy-specific metric to improve correlations. An improved metric will allow determination of significant changes in structures if utilised in adaptive workflows.

Introduction

- Currently utilised geometric contour-comparison metrics often poorly correlate with clinically relevant quantities such as dose [1].
- This study assessed a series of common geometric metrics (figure 1) and their correlation with planned dosimetric measures.

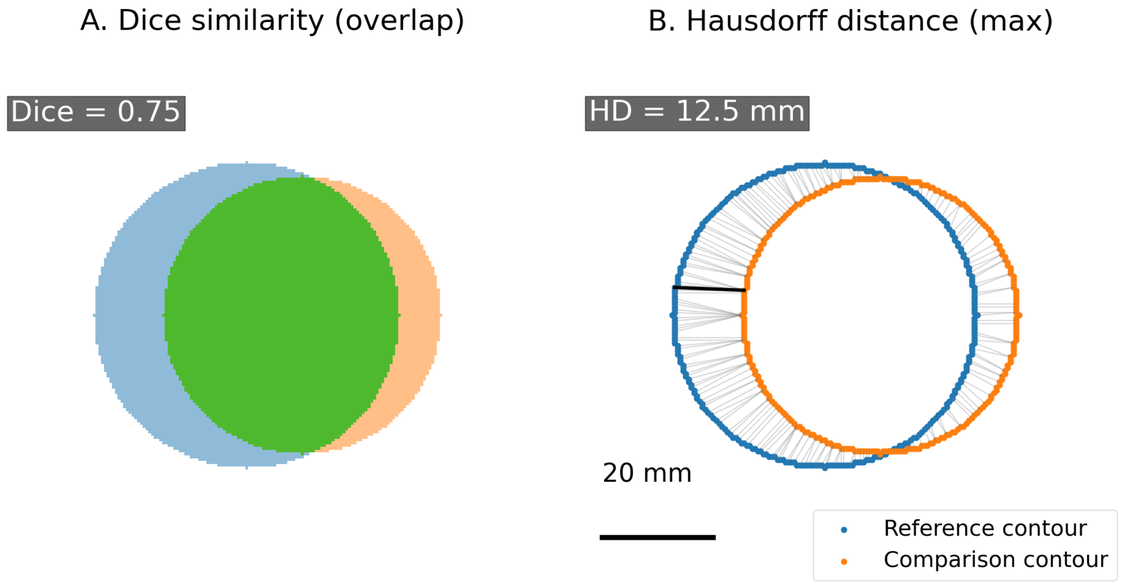


Figure 1. *Visualisations of A. DICE similarity coefficient as the proportion of overlap between structures, B. Hausdorff distance showing the maximum surface-to-surface separation.*

Methods

- Patients were treated in the SPARK trial (n=46) across 5 centres and received volume modulated arc therapy delivering 36.25 Gy in 5 fractions to the prostate planning target volume [2], [3].
- Analysis was carried out as per workflow in figure 2.
- PACE dose-volume histogram (DVH) constraints were extracted:
  - Rectum: V18.1Gy, V29.0Gy, and V36.0Gy.
  - Bladder: V18.1Gy, V29.0Gy, and V37.0Gy.

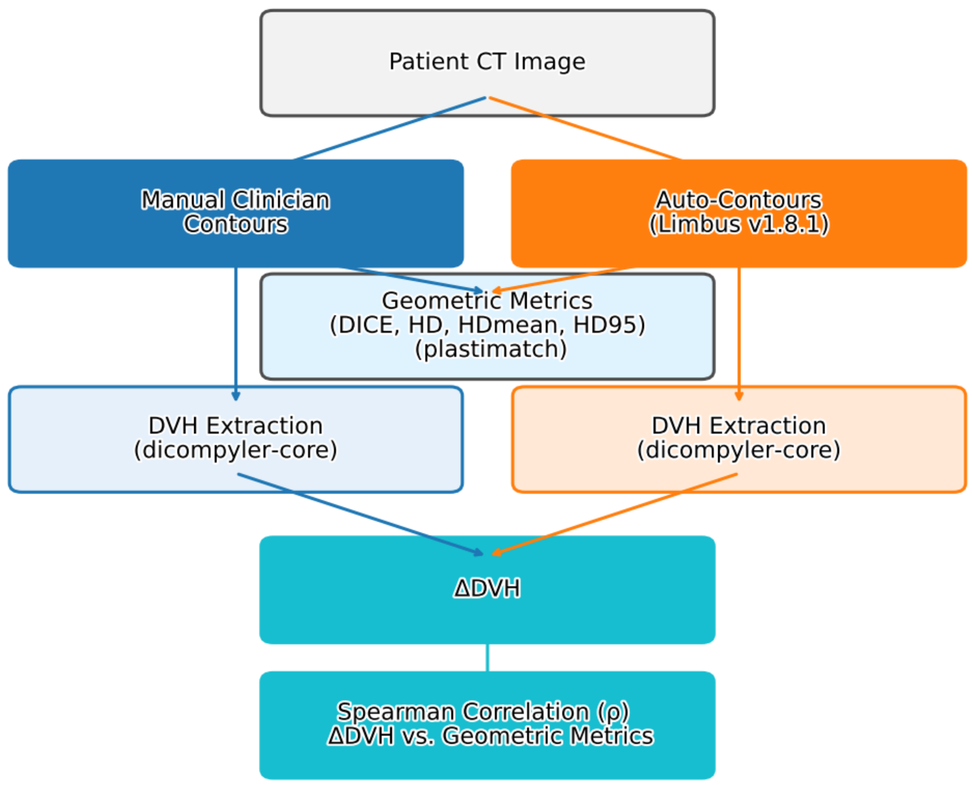


Figure 2. *Flowchart of work comparing manual and auto-contours using geometry, calculating DVHs and DVH differences at constraints and correlating these properties using a Spearman's rank correlation coefficient (ρ).*

Results

Intermediate bladder dose differences demonstrated the strongest correlations with surface distance metrics (figure 3):

- ΔV18.1Gy moderately correlated with HDmean (ρ = 0.70).
- ΔV29.0Gy moderately correlated with HD95 (ρ = 0.68).
- ΔV37.0Gy fairly correlated with HD (ρ = 0.41).

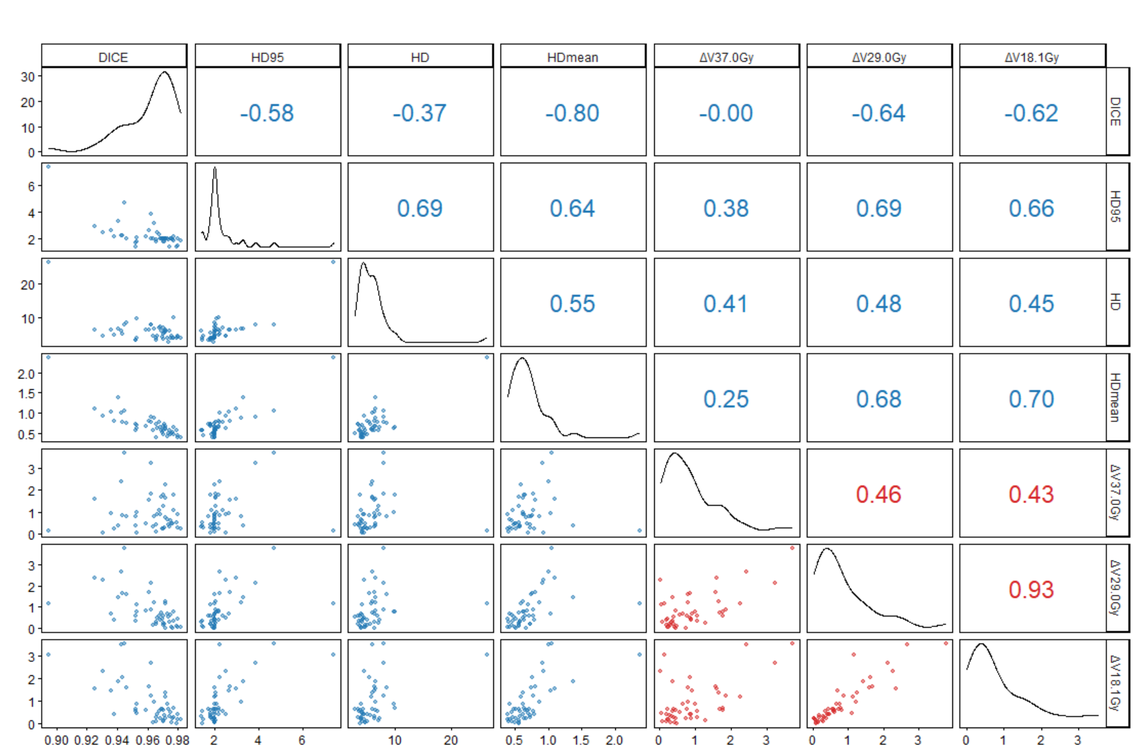


Figure 3. *Correlation table comparing bladder DVH metric differences with geometrical metrics.*

Rectum correlations (figure 4) were also dose-dependent:

- ΔV18.1Gy moderately correlated with DSC (ρ = –0.64).
- ΔV29.0Gy showed a fair correlation with DSC (ρ = –0.49).
- Correlations between ΔV36.0Gy and all metrics were poor.

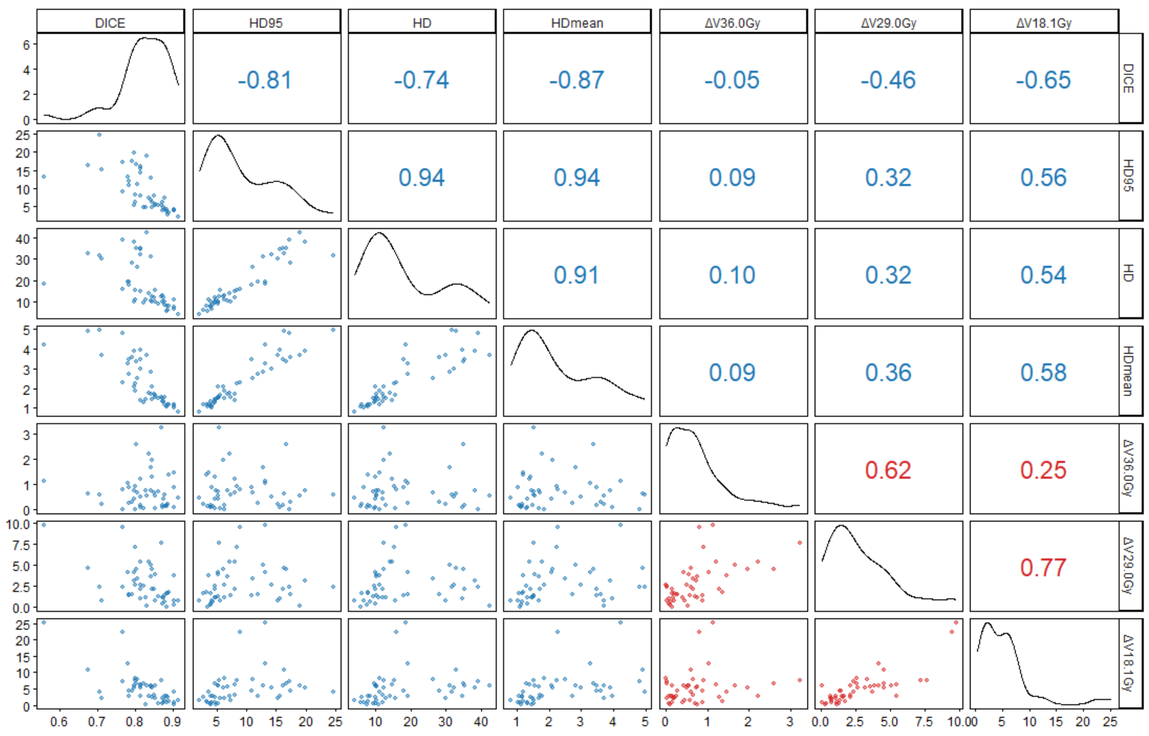


Figure 4. *Correlation table comparing rectum DVH metric differences with geometrical metrics, including total rectum height disagreement.*

Conclusion

- The performance of conventional geometric comparison metrics has been tested for prostate radiotherapy patients.
- Fair-poor correlations between conventional geometric metrics and high dose demonstrate the need for improved metrics.
- Next steps involve the development of a radiotherapy specific metric accounting for directionality in contour agreement.

References

[1] M. V. Sherer et al., "Metrics to evaluate the performance of auto-segmentation for radiation treatment planning: A critical review,", 2021
[2] C. Sengupta et al., "The TROG 15.01 stereotactic prostate adaptive radiotherapy utilizing kilovoltage intrafraction monitoring (SPARK) clinical trial database," Med Phys, 2025
[3] P. Keall et al., "Stereotactic prostate adaptive radiotherapy utilising kilovoltage intrafraction monitoring: The TROG 15.01 SPARK trial," BMC Cancer, 2017

Acknowledgements

This work was funded by the HSC Research and Development Division, Opportunity-Led Research Award (COM/5719/22). Authors acknowledge the access to Limbus Contour provided by Limbus AI.

Characterisation of an ultra-high dose rate electron beam for FLASH radiotherapy studies using a novel plastic scintillation detector

Oran McElligott[1,2], Cormac Kerins[3], Edward Maksay[2], Michael Martyn[3], Mark Foley[3], Cathy Fleming[1,2], Brendan McClean[1,2]

[1] School of Physics, University College Dublin, [2] St. Luke's Radiation Oncology Network, [3] Physics, School of Natural Sciences, University of Galway

Saint Luke's Radiation Oncology Network

Purpose

For FLASH radiotherapy studies, accurate dosimetry is paramount. In particular, temporal characterisation of ultra-high dose-rate (UHDR) beams is crucial given the uncertainty surrounding the impact of temporal beam parameters, such as dose-per-pulse (DPP), pulse repetition frequency (PRF) and mean dose-rate (MDR), on biological response.[1,2]

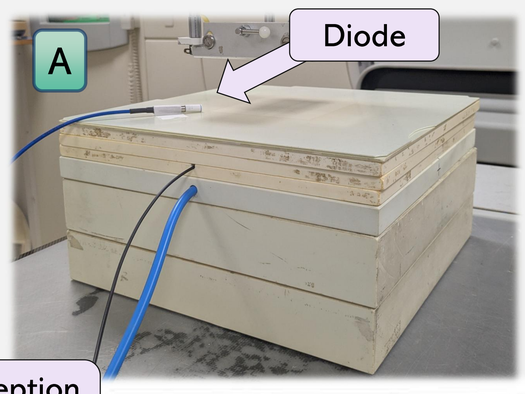
This work aimed to optimize and characterise a 10 MeV UHDR electron beam produced with a modified Elekta Precise linac, using a novel high-temporal resolution plastic scintillator, the MedScint RP-FLASH[3], with the aim of yielding a consistent, reproducible beam for pre-clinical FLASH radiotherapy studies.

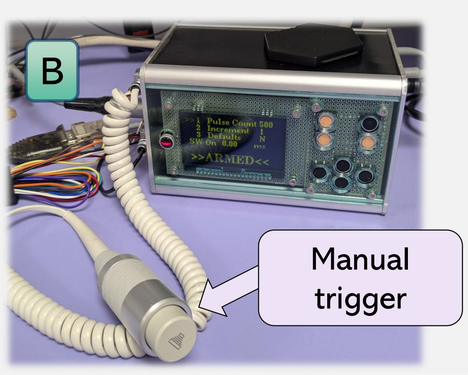
UHDR-enabled linac

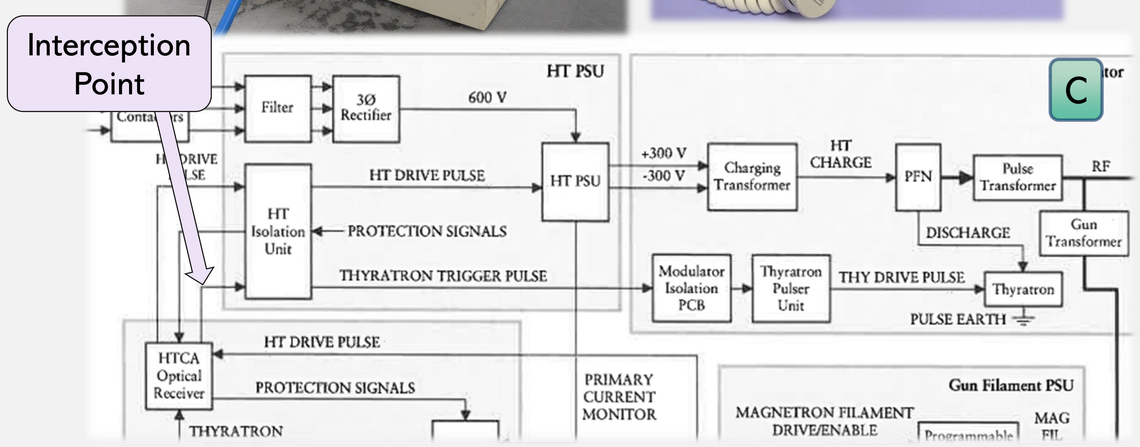
An Elekta Precise linac at our centre has been modified to operate on a pulse-controlled basis and allow production of a UHDR beam.

Modifications include:

- bypassing of monitor chamber interlocks
- removal of scattering foils
- introduction of diode-based beam-monitoring system (Fig A-C).







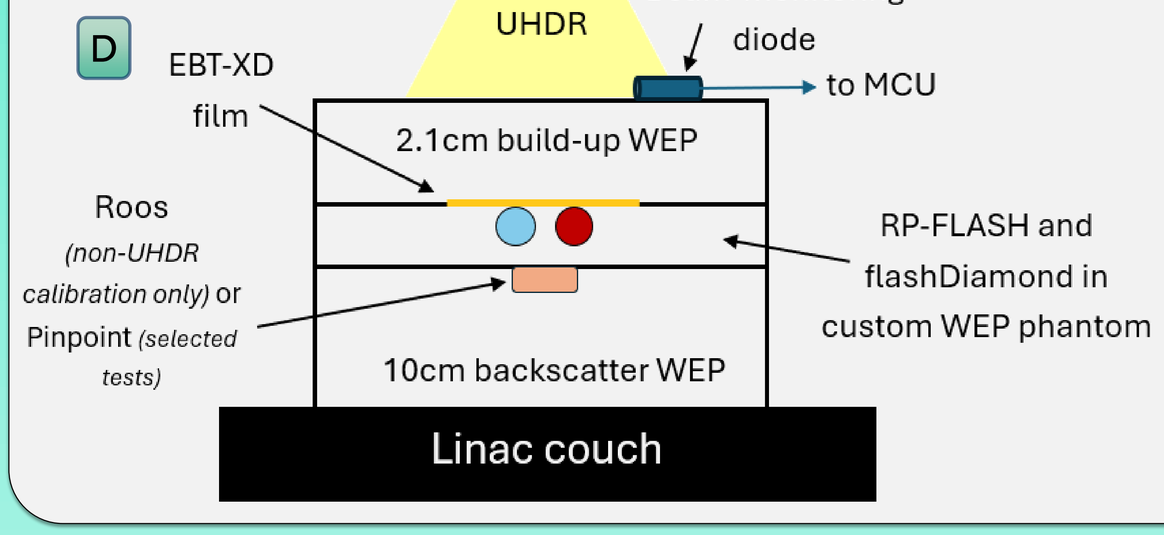
The diode connects to an Arduino microcontroller unit (Fig B), which counts pulses detected by the diode and interrupts the thyratron trigger signal between the HTCA Optical Receiver and the HT Isolation Unit (Fig C) once a set number have been delivered.

Methods

A gun warm-up procedure was developed to reproduce the same temporal profile, characterised using the RP-FLASH. Manual adjustments were made to magnetron frequency control settings to eliminate the characteristic "ramp-up" period.

Electron gun parameters were adjusted to achieve maximum output, measured in solid water by the RP-FLASH, with a pinpoint ionization chamber as reference (Fig D). The RP-FLASH and PTW flashDiamond[4], with reference EBT-XD film (Fig D), were used to measure:

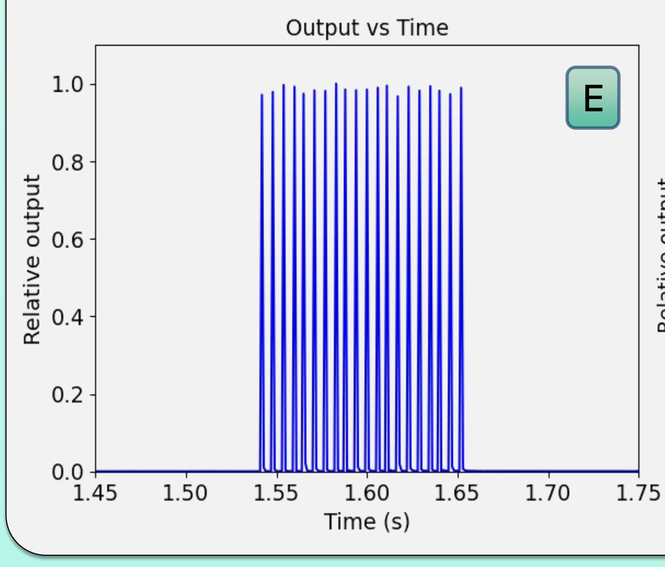
- output factors
- depth doses
- repeatability
- reproducibility
- dose-per-pulse variation with SSD
- linearity with pulse count
- constancy with pulse separation

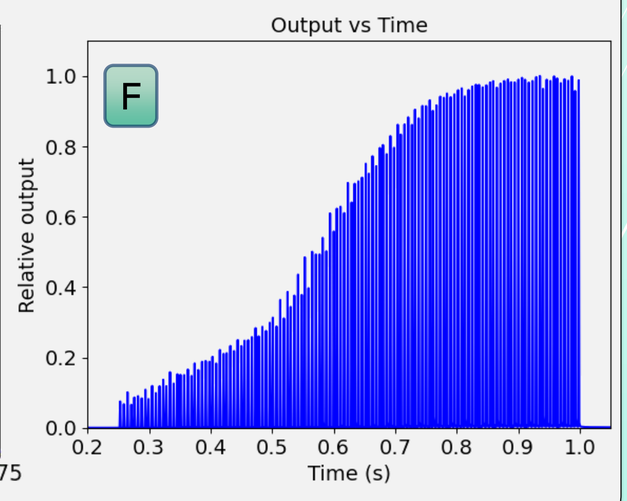


UHDR beam temporal characterisation

The 1 kHz sample rate of RP-FLASH allows interrogation of beam structure in intervals of 1 ms, allowing individual pulses to be resolved.

Manipulation of magnetron charge rate and rest value yielded a well-defined beam structure (Fig E) with consistent pulse heights, eliminating the characteristic, but undesirable, "ramp-up" period (Fig F).

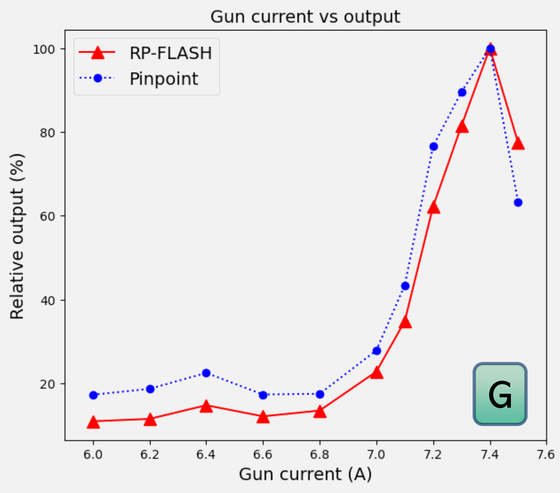


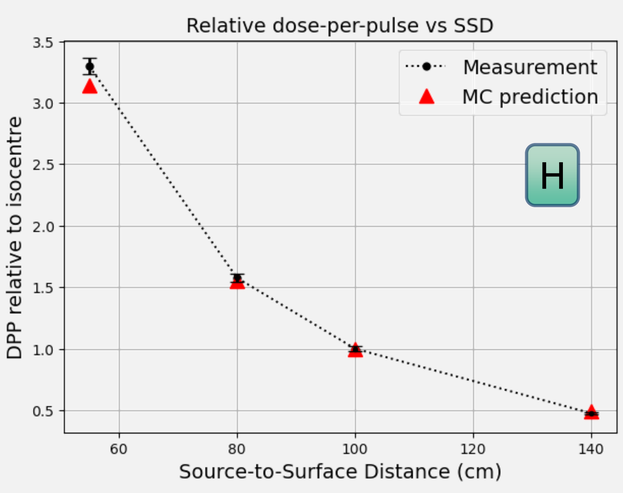


Dosimetric results

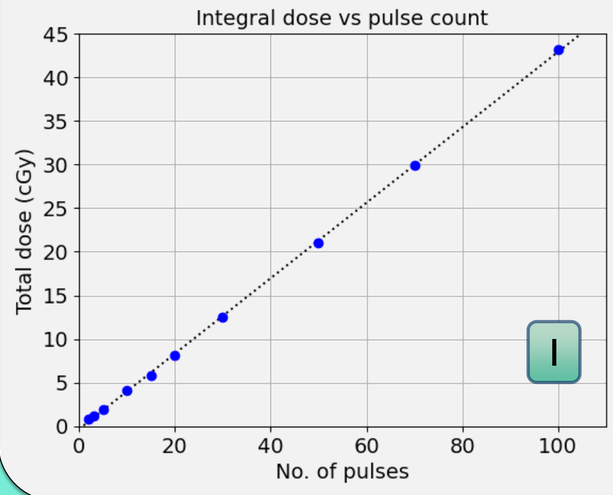
Maximum output was achieved for a gun current of 7.4 A (Fig G). Maximum mean dose-rates of 79 Gy/s and 262 Gy/s were achieved at isocentre and at minimum SSD, respectively, corresponding to mean dose-per-pulse (DPP) of 0.46 Gy and 1.53 Gy.

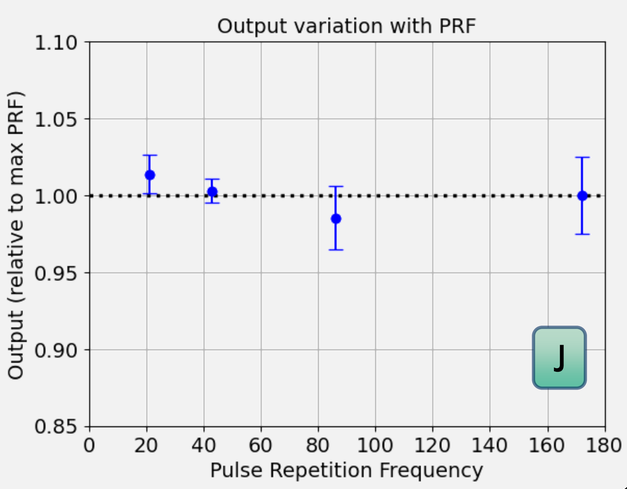
Relative DPP changes with SSD (Fig H) and field size factors agreed with Monte-Carlo predictions within 3% and 5%, respectively.





Output was linear with pulse count (Fig I) and constant with pulse repetition frequency (Fig J), varying by no more than 1.4% from 22-172 Hz. The beam is repeatable and reproducible, displaying <3% variation for repeated 20-pulse outputs over an hour post warm-up, and across 3 separate days.





Concluding remarks

Utilising the high temporal resolution of the RP-FLASH scintillator, optimal linac parameters were identified for producing a reproducible UHDR electron beam, suitable for pre-clinical FLASH studies.

A comprehensive dosimetric characterisation was performed, of which preliminary analyses are presented here. Complete analysis, including a full uncertainty analysis, is ongoing. Degradation of scintillator signal over repeated exposures (10s of kGy) required that the flashDiamond was used as the primary dosimeter (validated against EBT-XD film) and the RP-FLASH was used primarily for temporal information.

References

[1] Liu K et al. Int J Radiat Oncol Biol Phys. 2025;121:1063–1076.
[2] Grilj V et al. Int J Radiat Oncol Biol Phys. 2025.
[3] Guo L et al. arXiv. 2025; arXiv:2501.
[4] Marinelli M et al. Med Phys. 2022;49:1902–1910.

A Monte-Carlo model of standard and FLASH-enabled Elekta linacs for in vitro dose verification and prediction in pre-clinical radiobiological studies

Oran McElligott, Cathy Fleming, Brendan McClean
School of Physics, University College Dublin and St. Luke's Radiation Oncology Network

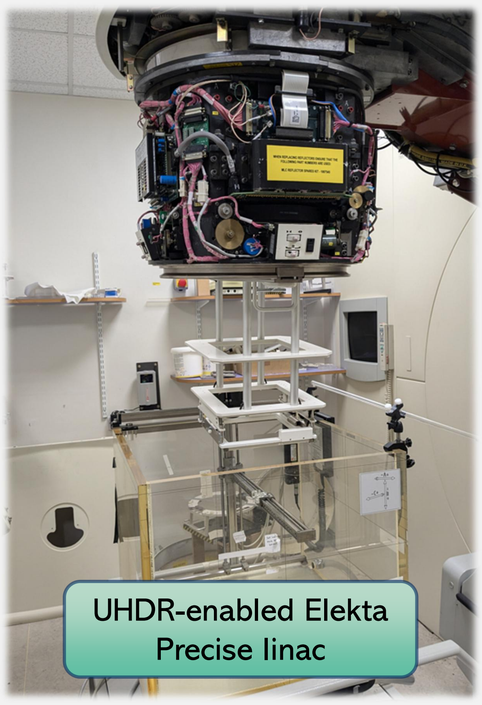
Saint Luke's Radiation Oncology Network

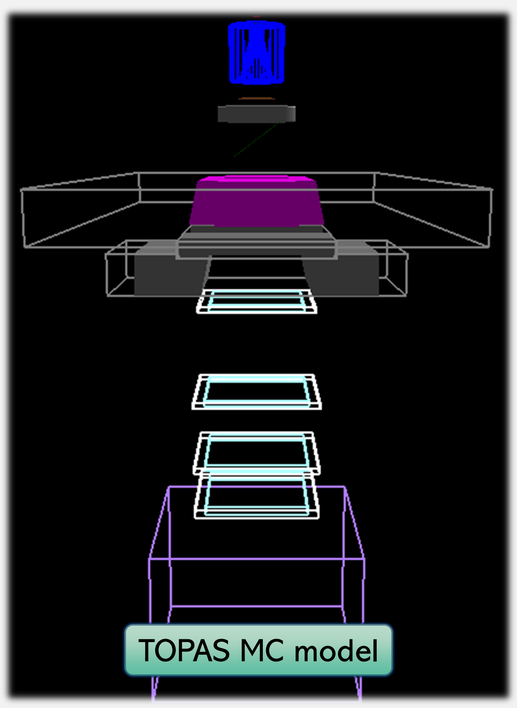
Purpose

Pre-clinical radiobiology studies at our centre require regular prediction and verification of delivered dose and dose-rate, particularly in situations where standard dosimetry methods are unreliable or impractical, such as under ultra-high dose-rate (UHDR) conditions. This work aimed to construct and validate in silico models of a standard Elekta Synergy linac and a locally modified, UHDR-enabled Elekta Precise linac using the TOol for PArticle Simulation (TOPAS) Monte Carlo (MC) toolkit, to support and enhance these studies.

Methods

MC models of both linacs were built in TOPAS for three beam models – 6 MV photons, 10 MeV conventional (CONV) and 10 MeV UHDR electrons. Source parameters and scattering foil geometries were iteratively optimized to match measured data.

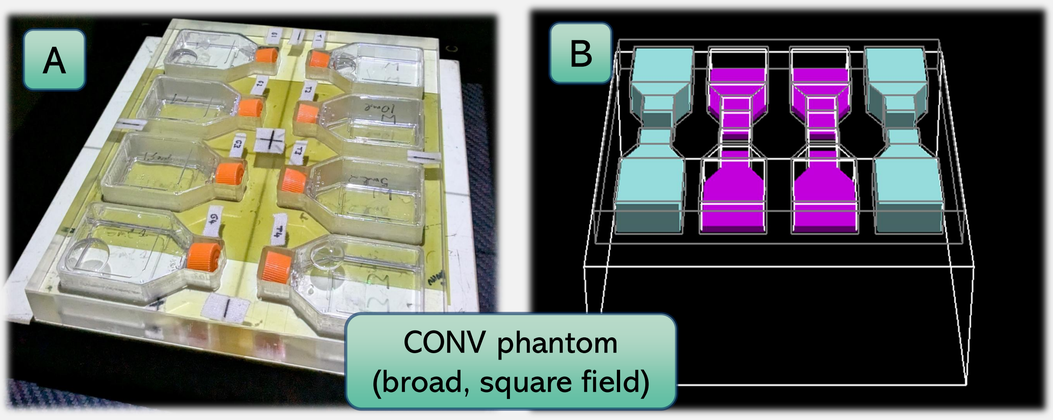


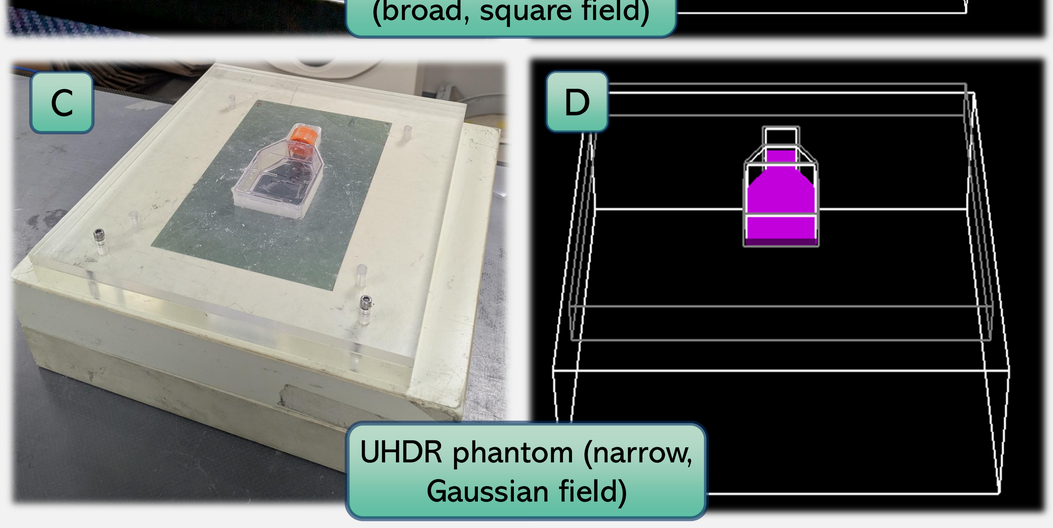


For CONV beams, validation was performed with high-resolution PTW microDiamond measurements in water. For the UHDR beam, a MedScint RP-FLASH scintillator and radiochromic film were used in solid water. Comprehensive uncertainty analyses were performed for all simulations and measurements.

Model Validation Parameters		
Percentage Depth Dose	Beam Profiles (Inplane & Crossplane)	
Output factors	$TPR_{20,10}$ (photons)	R_{80}, R_{50} , R_p (electrons)

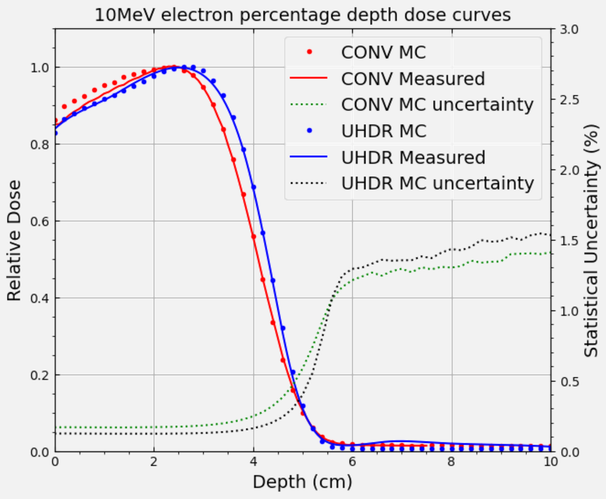
In vitro irradiations were simulated with phantom models (Fig B, D) to verify dose delivered to irradiated cells, and to predict relative dose and dose-rate changes in different configurations. Predictions were confirmed experimentally using ion chambers, film and PTW flashDiamond, and used to inform development of new custom phantom, appropriate for UHDR studies (Fig C).

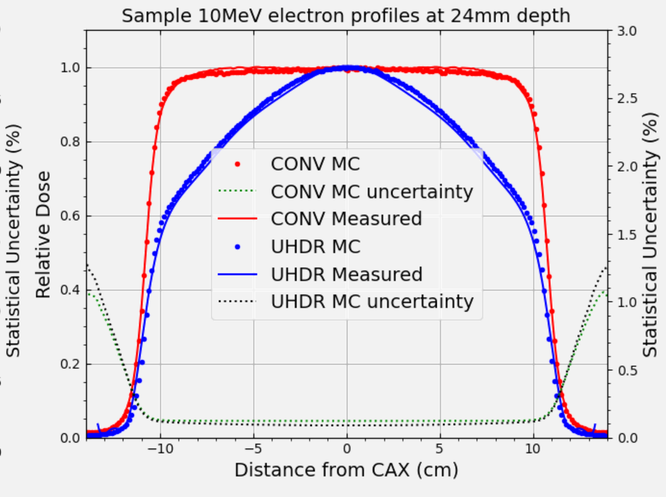


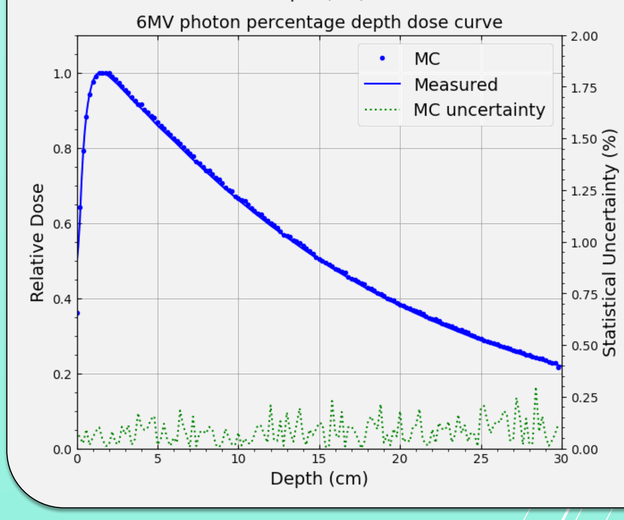


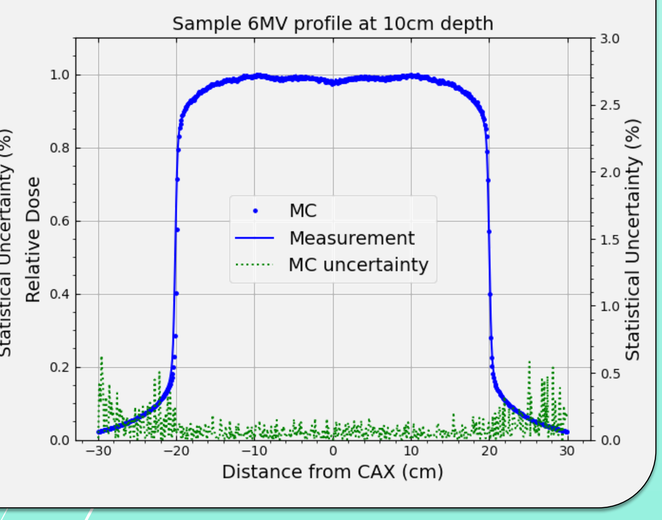
Beam Model Validation

MC-simulated percentage depth dose (PDD) curves displayed 100% gamma-passing rates (GPRs) beyond d_{max} for 1%/1 mm criteria for all beam models. All profiles exhibited >99% GPR (2%/1 mm). All output factors and quality indices agreed within 3% of measurement. Maximum MC statistical uncertainties were 0.6% (photons) and 1.6% (electrons).





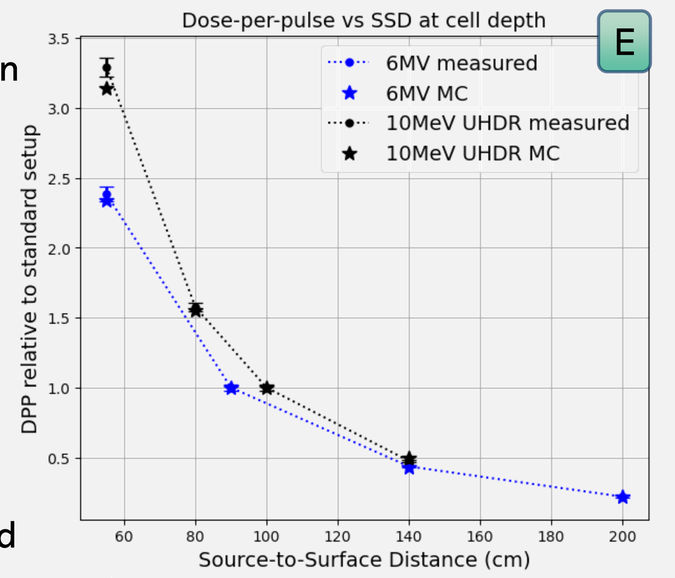


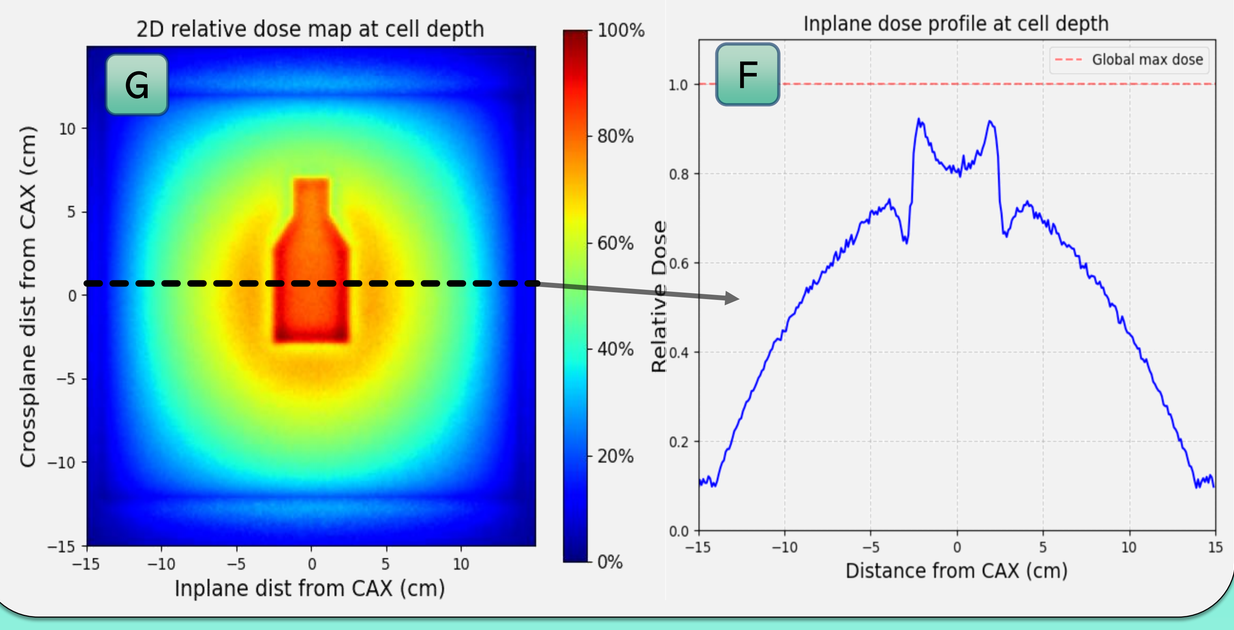


In vitro irradiation simulations

Simulated cell irradiations predicted relative dose and mean DPP changes within cell irradiation setups to within 3% (photons) and 5% (electrons) under all configurations (Fig E).

Simulated dosemaps were used to visualize and quantify flask coverage (Fig F), and to determine necessary phantom setup for UHDR (Fig G), validated against film measurement.





Summary

MC models of standard and UHDR-enabled Elekta linacs were constructed and comprehensively validated against physical measurement, and were used to develop an irradiation setup for in vitro UHDR studies. Models of in vitro irradiation geometries proved reliable for predicting and verifying delivered dose, dose-rate, and mean dose-per-pulse in different configurations. The complete model suite provides a robust toolkit for dose verification and prediction to support radiobiological studies at our centre.

COMMISSIONING OF A "Y" ENDOMETRIAL APPLICATOR FOR HDR BRACHYTHERAPY IN INOPERABLE ENDOMETRIAL CANCER

Panagiota Aresti[1,2], Amey Bermingham[2], Leanne Berrigan[2], Anysja Zuchora[2]

1. **St. Luke's Radiation Oncology Network**
2. **Dept. of Medical Physics & Clinical Engineering, University Hospital Galway**

Introduction

Endometrial cancer represents the majority of uterine malignancies, and high-dose-rate (HDR) brachytherapy is a key treatment modality for patients who are medically inoperable [1]. Applicator choice is critical to achieve adequate target coverage while sparing organs at risk (OARs). This project aimed to commission and clinically evaluate Varian's HDR Universal Endometrial Applicator Set for HDR brachytherapy in inoperable endometrial cancer, comparing its performance with the ring-and-tandem applicator.

Methods & Materials

Commissioning was performed in accordance with AAPM TG-56 and MPPG-13a guidelines, including visual inspection, geometric verification, offset (Figure 1a) and dwell position measurements using Gafchromic EBT3 film (Figure 1b,c,d), and applicator reconstruction in the Brachyvision treatment planning system (TPS) (Figure 2). Following successful commissioning, 18 CT-based volume-guided treatment plans were generated for previously treated inoperable endometrial cancer cases. Dosimetric comparisons were conducted between (i) the "Y" applicator with three tandems and a ring-and-tandem applicator, and (ii) the "Y" applicator with three versus two tandems. Planning objectives followed American Brachytherapy Society recommendations [2].

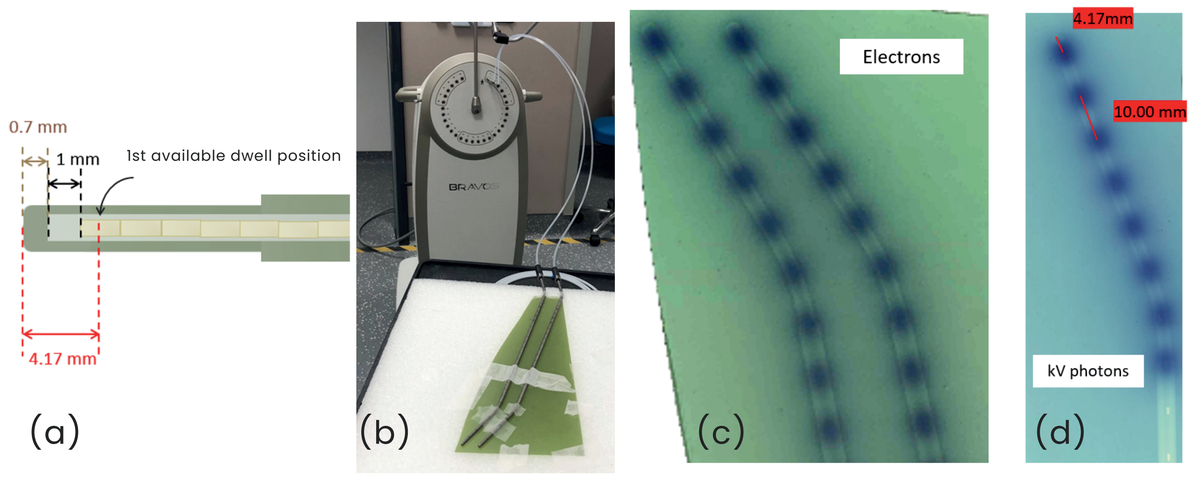


Figure 1: (a) Offset within tandem (not to scale) (b) Dwell position measurements using Gafchromic film and then exposing it to (c) electron or (d) kV photon irradiation.

Results

All commissioning tests met recommended tolerances, confirming geometric integrity, accurate source positioning, and reliable applicator reconstruction (Figure 2). Dosimetric analysis demonstrated that the "Y" applicator with three tandems achieved superior High-Risk (HR) CTV coverage (D90) and improved sparing of critical structures, particularly the rectum and sigmoid, compared with both the ring-and-tandem applicator (Table 1) and the two-tandem configuration. Figures 3 and 4 show dose distributions for one case planned using the different applicators. Clinical review by a radiation oncologist supported routine use of the three-tandem configuration with standardised insertion and planning protocols.

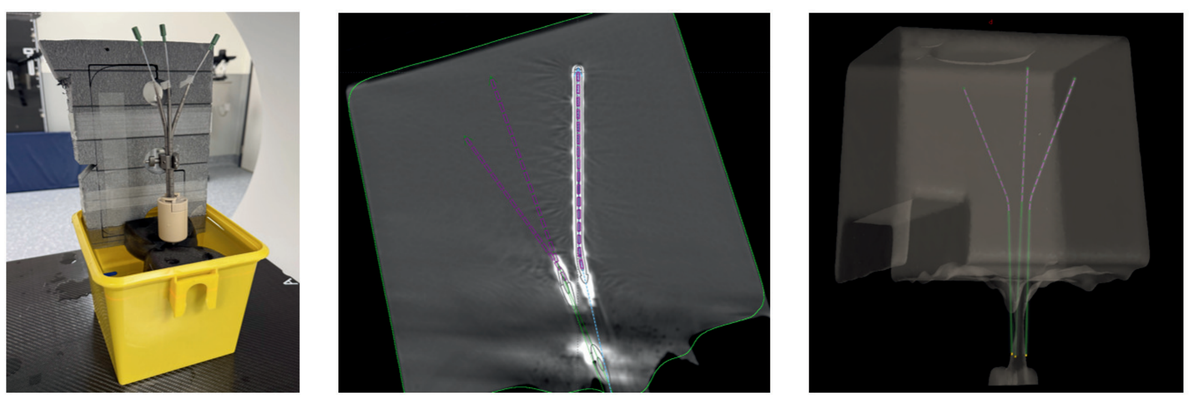


Figure 2: Applicator reconstruction in Brachyvision TPS. On the left: the setup used for the applicator CT scan.

	Ring & Tandem (Gy EQD2)	"Y" 3 Tandems (Gy EQD2)	Institutional constraints (Gy EQD2)
HR-CTV D90	68.2	68.5	65-75
Bladder D2cm^3	79.5	78.2	≤90 ≤80
Rectum D2cm^3	53.3	48.4	≤70-75
Sigmoid D2cm^3	74.6	67.0	≤65
Bowel D2cm^3	65.0	62.7	≤ 70

Table 1: Target (α/β = 10 Gy) and OARs (α/β = 3 Gy) doses in EQD2 for one case planned using the ring-and-tandem applicator and the "Y" applicator with 3 tanderms.

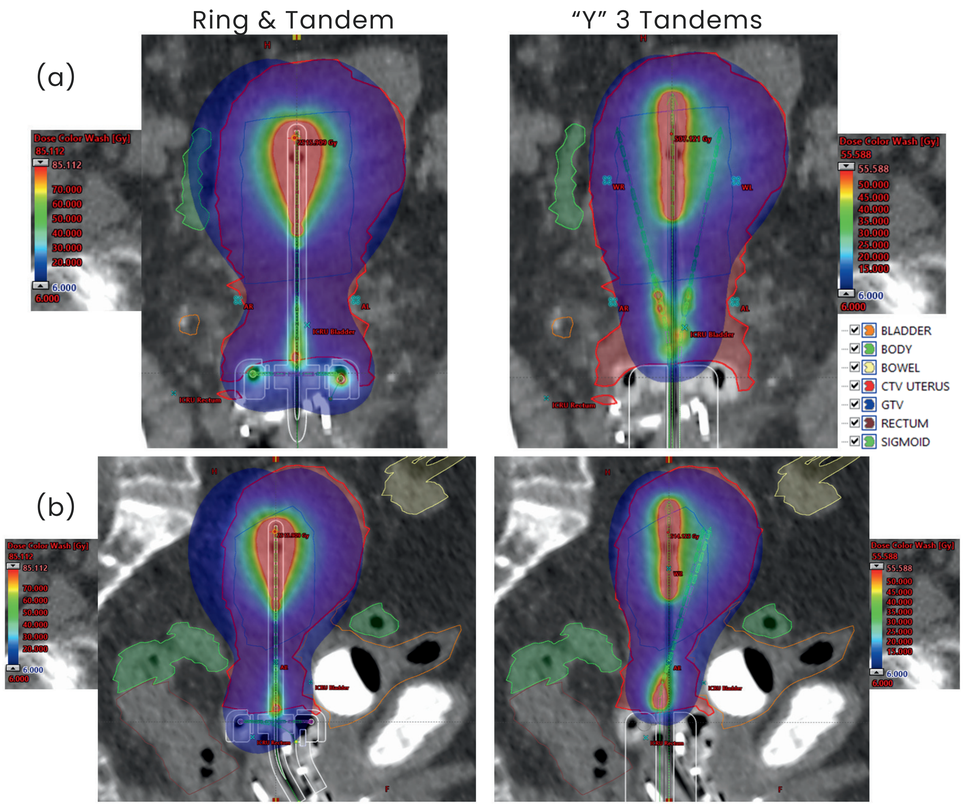


Figure 3: Dose distributions in (a) coronal and (b) sagittal view for one case planned using the ring-and-tandem applicator (left) and the "Y" applicator with 3 tanderms (right).

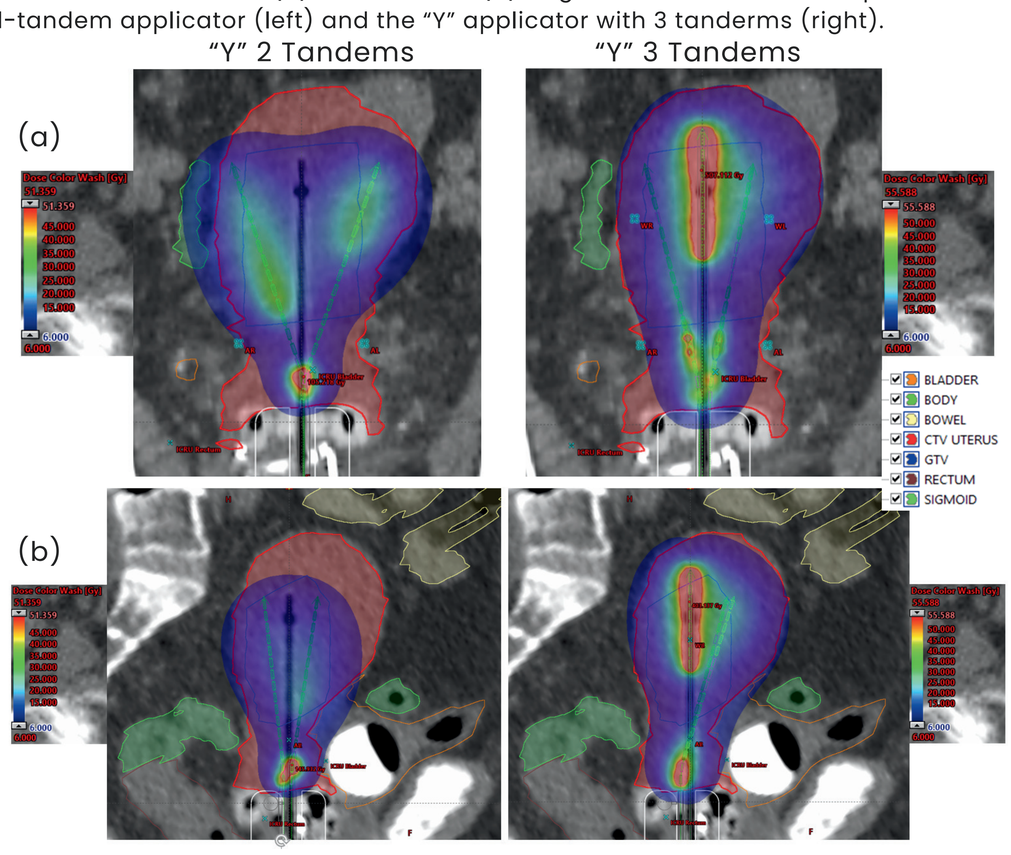


Figure 4: Dose distributions in (a) coronal and (b) sagittal view for one case planned using the "Y" applicator with 2 tandems (left) and with 3 tandems (right).

Conclusion

Varian's HDR Universal Endometrial Applicator Set was successfully commissioned and validated for clinical HDR brachytherapy. Its three-tandem configuration provides enhanced dosimetric performance and greater anatomical adaptability for inoperable endometrial cancer.

References

1. Lukez, A. et al. (2024) "National Cancer Database analysis of radiation therapy consolidation modality and dose for inoperable endometrial cancer", Brachytherapy, 23(6), pp. 623-633.
2. Schwarz, J.K. et al. (2015) "Consensus statement for brachytherapy for the treatment of medically inoperable endometrial cancer", Brachytherapy, 14(5), pp. 587-599.

EVALUATION OF ALTERNATIVE MODELLING APPROACHES FOR THE AGILITY MULTILEAF COLLIMATOR IN MONACO TREATMENT PLANNING SYSTEM

Panagiota Aresti[1,2], Dion Conlon[2], Sean Gillespie[2]

1. **St. Luke's Radiation Oncology Network**
2. **Dept. of Medical Physics & Clinical Engineering, University Hospital Galway**

Introduction

Accurate mulitileaf collimator (MLC) modelling within treatment planning systems (TPS) is essential for precise dose delivery in Intensity-Modulated Radiation Therapy (IMRT) and Volumetric Modulated Arc Therapy (VMAT). The Elekta Agility MLC incorporates complex geometric features, including tilted leaves that can compromise modelling accuracy [1]. However, excessive parameter tuning carries a risk of over-modelling [2]. This study evaluated and optimised key MLC parameters in the Monaco TPS to determine whether refinement leads to meaningful dosimetric improvements over the current clinical model.

Methods & Materials

The Agility MLC was assessed using a combination of adapted ExpressQA THREEL fields, sweeping Gap (SG) and asynchronous Sweeping Gap (aSG) tests (Figure 1). Gap sizes of 5-40 mm were used. High-resolution 2D measurements were acquired with the IBA myQA SRS detector, while SG and aSG doses were measured using a Farmer-type ionisation chamber in water-equivalent material. Tranmission Probility Filter (TPF) parameters were varied to create three optimised models, which were compared to the institution's clinical model. Three clinical plans were recalculated and evaluated against their PSQA measurements using gamma analysis.

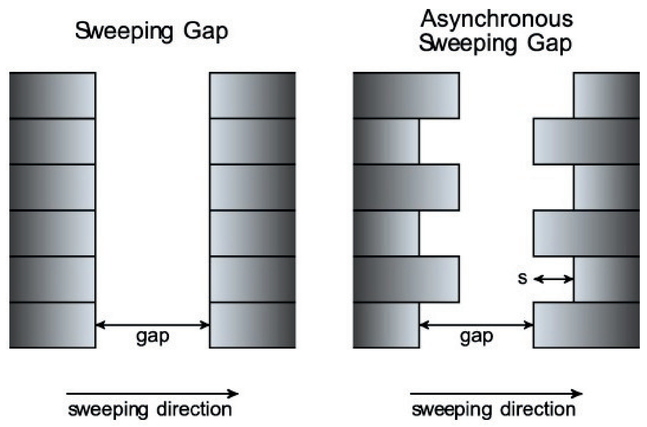


Figure 1: Schematic of the sweeping gap and asynchronous sweeping gap tests, where s=shift [3].

Results

Table 1 shows the TPF parameters used in the clinical model and the optimised models A, B, and C found from our analysis. Among the optimised configurations, model C demonstrated marginally improved agreement with measurements in transmission and groove regions for the THREEL (Figure 2) and aSG tests (Figure 3a). Linear behaviour was confirmed for SG tests (R^2>0.999), as shown in Figure 3b. Despite these local improvements, gamma analysis (Table 2) showed no substantial differences between the current and optimised models, indicating comparable overall dosimetric performance.

TPF Parameter	Clinical model	Model A	Model B	Model C
MLC offset (mm)	-0.02	-0.02	-0.02	-0.02
Leaf groove width (mm)	0.4	0.4	0.5	0.5
Leaf tip leakage	1.10	1.10	1.10	1.12
Interleaf leakage	3.00	3.00	3.00	3.00
Leaf transmission	0.0040	0.0039	0.0039	0.0039

Table 1: TPF parameters of current clinical model and optimised models A, B, and C.

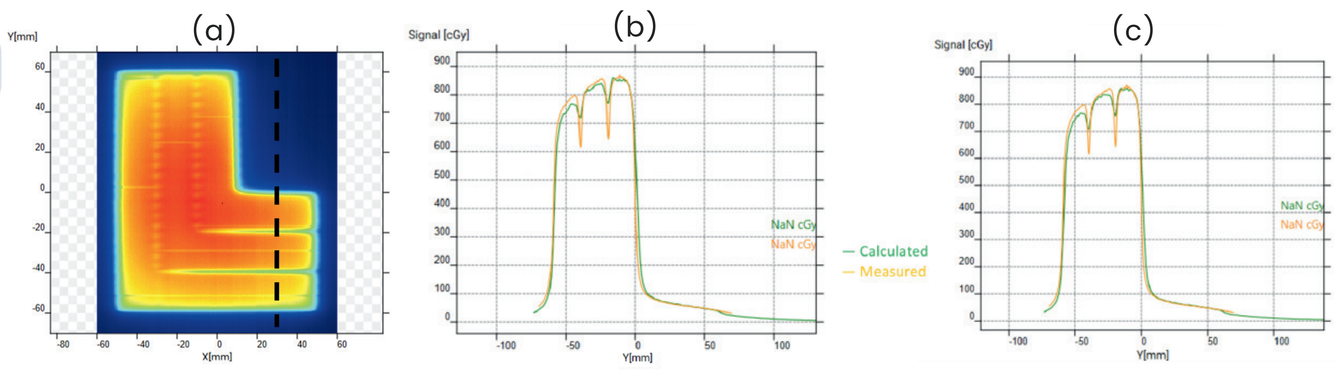


Figure 2: THREEL tests results: measured and calculated dose profiles along the dashed line in (a), shown in (b) using the clinical model and (c) using the the model C.

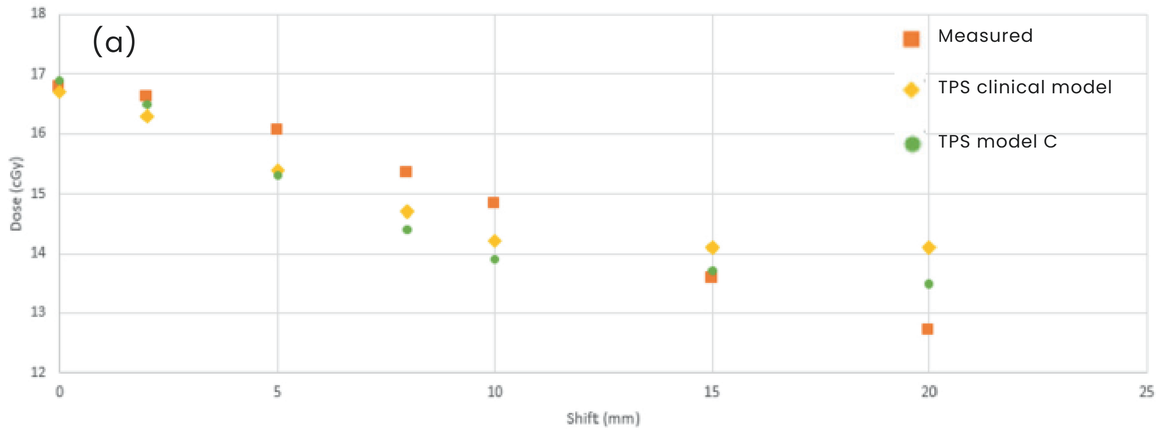


Figure 3: (a) aSG tests results when using gap 10 mm and (b) SG tests results.

(a)

Gamma criteria	Clinical model	Model A	Model B	Model C
3%/1mm	97.5%	98.6%	98.6%	98.5%
1%/1mm	96.2%	96.8%	96.8%	96.1%

(b)

Gamma criteria	Clinical model	Model A	Model B	Model C
3%/1mm	98.7%	100.0%	97.8%	98.5%
1%/1mm	91.1%	98.0%	86.9%	91.1%

(c)

Gamma criteria	Clinical model	Model A	Model B	Model C
3%/1mm	100.0%	98.7%	99.9%	100.0%
1%/1mm	98.3%	91.2%	96.6%	98.4%

Table 2: Gamma analysis results using the criteria displayed on the first collumn, 10% threshold and global analysis for (a) one stereotactic ablative radiotherapy (SABR) lung plan and (b), (c) two stereotactic radiosurgery (SRS) brain plans.

Conclusion

Modest adjustments to selected TPF parameters can marginally improve agreement in specific MLC-related regions; however, these refinements do not translate into clinically meaningful differences. This study confirms confidence in the instituiton's current clinical Agility MLC model for IMRT and VMAT, supporting safe clinical use while avoiding unnecessary parameter tuning and reducing the risk of over-modelling.

References

1. Hernandez, V. et al. (2022) "Challenges in modeling the Agility multileaf collimator in treatment planning systems and current needs for improvement", Med Phys, 49(12), pp. 7404-7416.
2. Snyder, M. et al. (2016) ". Modeling the Agility MLC in the Monaco treatment planning system", J Appl Clin Med Phys, 17(3), pp. 190-202.
3. Hussein, M. et al. (2024) "Improving the modelling of a multi-leaf collimator with tilted leaf sides used in radiotherapy", Physics and Imaging in Radiation Oncology, 29, 100543.

The impact of evolving dosimetry practices in Selective Internal Radiation Therapy (SIRT)

Niamh McArdle[1], Jackie McCavana[1,3], Gerard Healy[2], Jeff McCann[2], Colin O'Rourke[2], Ronan Ryan[2], Seán Cournane[1, 3]

[1]Department of Medical Physics and Clinical Engineering, St Vincent's University Hospital, Dublin. [2]Department of Radiology, St Vincent's University Hospital, Dublin. [3]Centre for Physics in Health & Medicine, University College Dublin (UCD).

Introduction

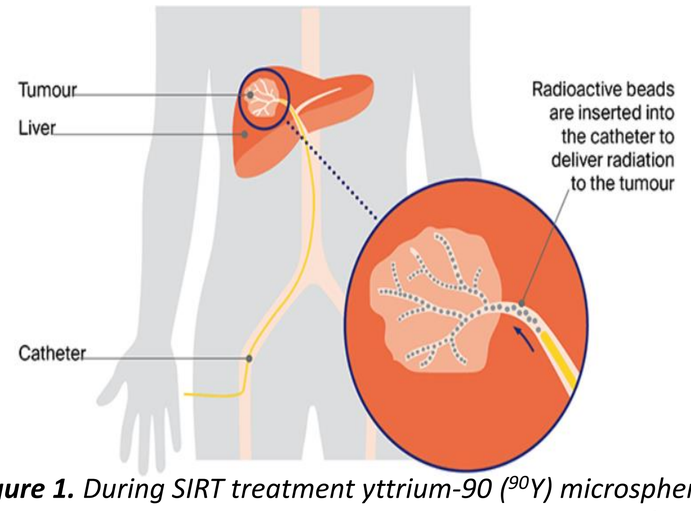


Figure 1. *During SIRT treatment yttrium-90 (^{90}Y) microspheres are injection to the tumour and tumourous arteries[1].*

[1] https://www.cancercouncil.com.au/liver-cancer-secondary/treatment/radiation-therapy/

Yttrium-90 (^{90}Y) TheraSpheres are used in SIRT for treatment of liver tumours. Previous guidance recommended a prescribed dose of 150 Gy to the target volume. The DOSISPHERE-01 trial (2020) demonstrated improved outcomes for tumour absorbed doses >205 Gy using personalised multicompartment dosimetry implemented via treatment planning software (TPS), as compared with standard single compartment dosimetry.

Aim

Given the updated guidance, a comprehensive review was undertaken comparing patient- and dose-specific metrics before and after implementation of multicompartment dosimetry, to evaluate the impact of evolving dosimetry practice.

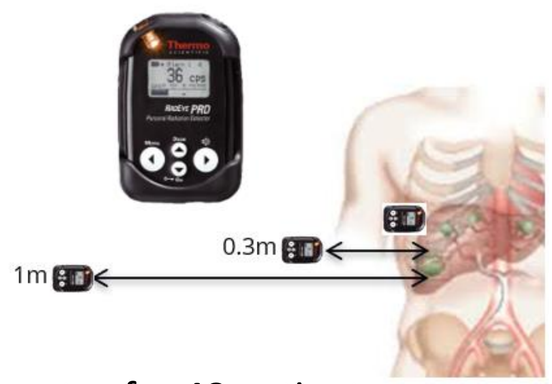
Method

1. Data Collection



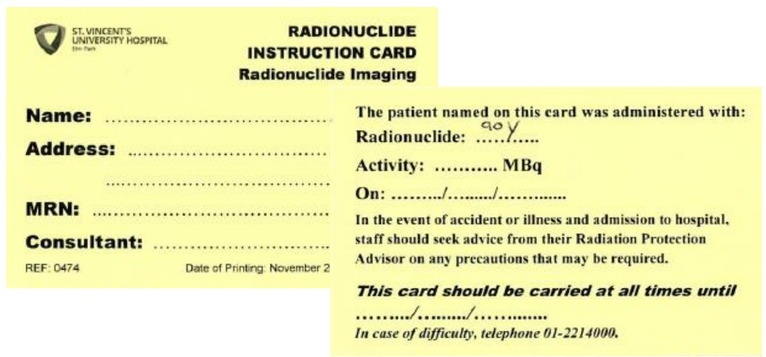
Target liver volume, dose prescription and administered activity were collected for all patients between 2016-2025 (*Figure 2*).

2. Dose Rate Measurement



Dose rates for 48 patients were measured in contact with the upper abdomen, at 0.3 m and 1 m between 2016–2025 (*Figure 3*).

3. Radiation Protection Review



Data before & after multicompartment dosimetry implementation (2016–Aug 2022 & Sept2022–2025) were compared (Mann-Whitney U Test) and radiation-protection implications assessed.

Results

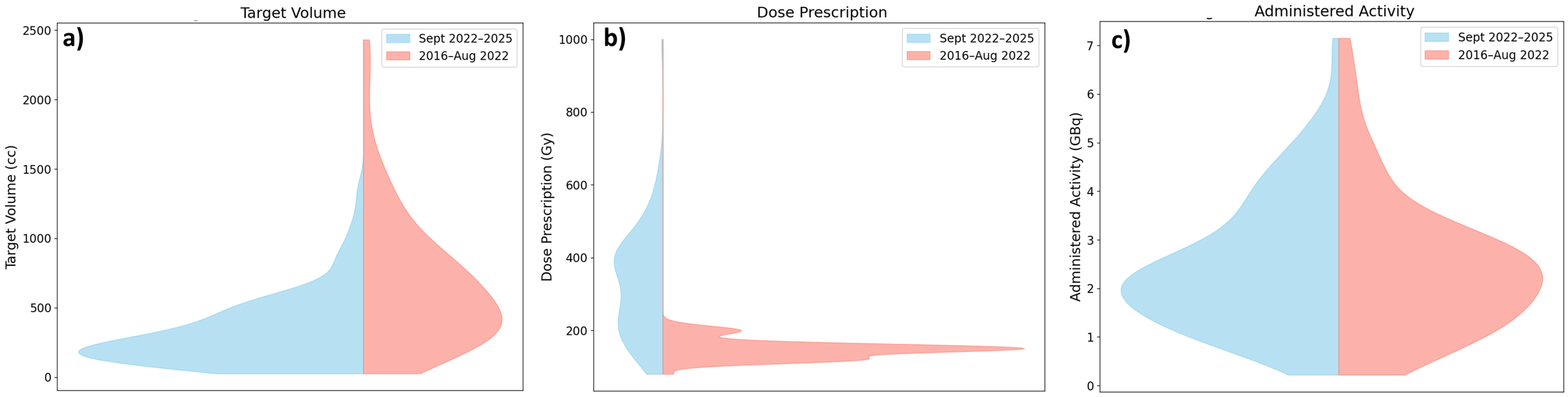


Figure 2. *Graphs showing the change in **a)** target volume, **b)** dose prescription and **c)** administered activity before and after the implementations of multi-compartment dosimetry.*

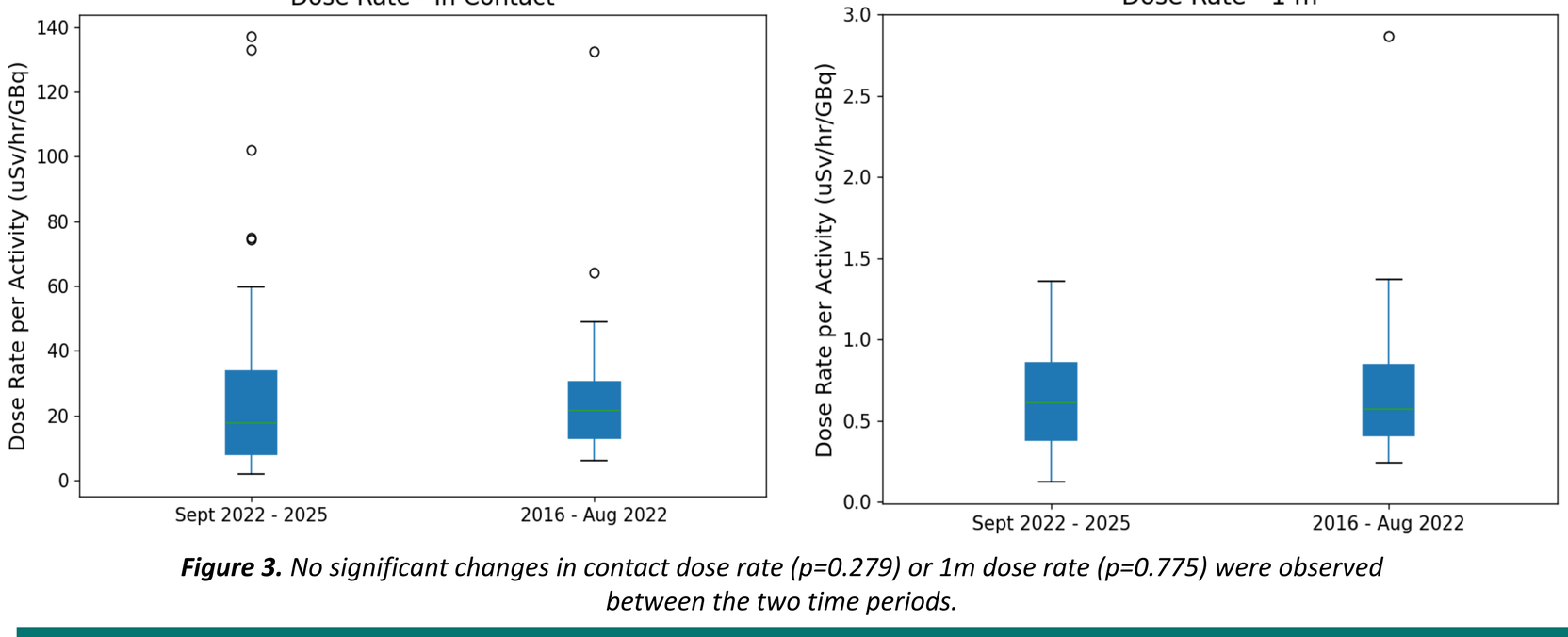


Figure 3. *No significant changes in contact dose rate (p=0.279) or 1m dose rate (p=0.775) were observed between the two time periods.*

No significant change (*p=0.887*) in administered activity was observed between the two time periods. Before TPS implementation, larger treatment volumes were prescribed lower doses, while after implementation the target volume decreased and the prescribed dose increased, resulting in comparable administered activities overall.

Conclusion

Implementation of multicompartment dosimetry facilitated planning of higher tumour and target volume doses, as supported by emerging evidence. Although the administered activity remained consistent across the two time periods, the resulting patient dose rates showed no significant changes and therefore did not necessitate any adjustment to existing contact restrictions. Continued monitoring of the data is essential, as evolving dosimetry practices may necessitate revision of radiation protection restrictions.

Questions? niamhmcardle@svhg.ie

Calculating PTV margins for abdominal SABR using the van Herk formula

Maria Babu[1], Serena O'Keeffe[1]

[1] *St. Luke's Radiation Oncology Network, St. Luke's Hospital, Rathgar*

1. Introduction

Stereotactic ablative radiotherapy (SABR) for abdominal targets demands highly accurate treatment delivery due to steep dose gradients and the proximity to Organs at Risk (OARs). Appropriate Planning Target Volume (PTV) margins ensure sufficient target coverage while minimizing normal tissue exposure. At this institution, current practice is to employ a 5 mm isotropic margin expanded to 7 mm in the superior-inferior (SI) direction for end-expiratory breath-hold (EEBH) and 5 mm isotropic margins for free-breathing (FB) SABR. This work evaluated the adequacy of these margins using the expanded van Herk formula by quantifying sources of systematic (∑) and random (σ) errors.

2. Background

This study uses the van Herk equation, (see Equation 1) which, for SABR plans, yields the PTV expansion required to cover the Gross Tumour Volume (GTV) in a given proportion of the patient population.

$$M = \alpha\Sigma' + \beta\left(\sqrt{\sigma'^2 + \sigma_{penumbra}^2} - \sigma_{penumbra}\right) \quad [1]$$

$$\text{where } \Sigma' = \sqrt{\Sigma^2 - \frac{\sigma_{total}^2}{N_{obs}} + \frac{\sigma_{total}^2}{N_{treat}}} \quad [1.1]$$

$$\text{and } \sigma'^2 = \frac{N_{treat} - 1}{N_{treat}}{\sigma_{total}}^2 \quad [1.2]$$

A description of the variables presented in equations 1-1.2 and their corresponding values, where applicable, are given in Table 1.

Variable	Description	Value
α	Population coverage confidence level	2.5 (90%)
β	Factor based on PTV covering isodose	1.28 (90% isodose)
$\sigma_{penumbra}$	Penumbral width of the beam	14.72 mm, 2.08 mm, 11.54 mm in Ant-Post (AP), Sup-Inf (SI) and Mediolateral (ML) directions
Σ^2	Summation in quadrature of all systematic uncertainties	Intrafraction motion, machine uncertainties, Image Guided Radiotherapy (IGRT), delineation
σ^2	Summation in quadrature of all random uncertainties	Intrafraction motion
N_{obs}	Median number of # used in analysis	5
N_{treat}	Number of # used in the margin calculation	3 and 5

Table 1: *an overview of the variables given in equations 1-1.2, including a brief description and their corresponding values where appropriate. The 'value' tab associated with the systematic and random errors indicate the types of errors assessed in each case.*

3. Methodology

Errors due to target intrafraction motion (Σ_{intra} and σ_{intra}) were quantified using daily CBCT imaging data from an initial cohort of 74 patients (n=31 for EEBH; n=43 for FB). The systematic component was found by calculating the standard deviation of the patients' mean movements in the AP, SI and ML directions. The random component was obtained by determining the root mean square of the standard deviation of all patients.

To ascertain the uncertainty in the treatment delivery, results of the monthly kV isocentre coincidence and picket fence tests, alongside annual static Twinkle test results were used. The standard deviation of the values taken over six months and two years, respectively, were taken to be the systematic error. The positional accuracy of the Multileaf Collimators (MLCs) was estimated from the maximum tolerance value of monthly picket fence tests.

The inherent systematic error in the IGRT system, taking into account uncertainties in the accuracy of the image registration, as well as the couch movement, was estimated as the standard error of a top-hat function [6].

The systematic error in the delineation of the GTV was estimated based on literature values [4] [5].

4. Results and Discussion

Boxplots of the patients' mean intrafraction motion in the EEBH and FB cases, respectively, are presented in Figure 1. In order to calculate PTV margins for the general patient population, the outliers values were disregarded in the final calculation. As a result, four patients were removed from the EEBH cohort and a further three from the FB group. The final values for the systematic and random intrafraction motion uncertainties are given in Table 2.

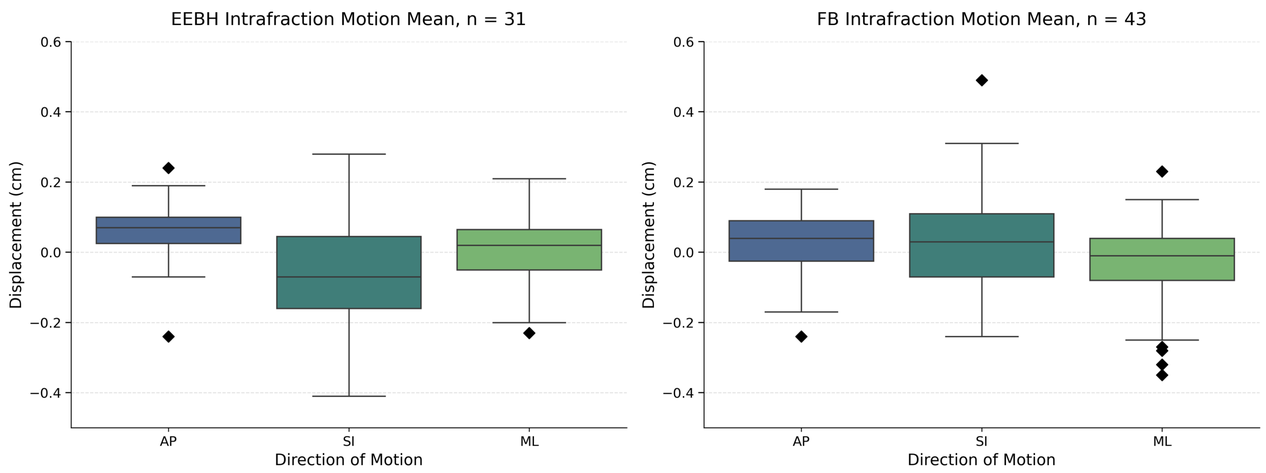


Figure 1: *Boxplots of the mean patient intrafraction motions in the EEBH and FB cases.*

Intrafraction Motion (Σ_{intra} and σ_{intra}). Without outliers.				
	$EEBH, n = 27$		FB, $n = 40$	
	Σ_{intra} (mm)	σ_{intra} (mm)	Σ_{intra} (mm)	σ_{intra} (mm)
AP	0.64	1.33	0.88	1.45
SI	1.81	2.05	1.17	2.20
ML	0.86	1.25	1.30	1.31

Table 2: *Systematic and random intrafraction motion error in three planes for the EEBH and FB patient cohorts. The values given exclude any gross outliers observed in Figure 1.*

Σ_{intra} was highest in the SI direction at 1.81 mm for EEBH, versus 1.17 mm for FB. The combined systematic error from the isocentre coincidence and Twinkle tests was 0.55 mm, 0.27 mm, 0.54 mm for the AP, SI, and ML directions respectively. Lastly, 1.5 mm delineation uncertainty and 0.58 mm uncertainty in IGRT and MLC accuracy across all three cardinal axes were noted.

PTV Margins for EEBH and FB			
		EEBH (mm)	FB (mm)
3#	AP	4.97	5.23
	SI	7.29	6.45
	ML	5.16	5.73
5#	AP	4.82	5.07
	SI	7.15	6.23
	ML	5.04	5.61

Table 3: *Calculated margins for the GTV to PTV expansion in patients treated with SABR in EEBH and FB. The values are determined based on various systematic and random errors that influence the accuracy of the treatment. Equation 1 was utilised for the margin calculation.*

The results for the EEBH cohort validated the institutional margins, while the PTV expansions calculated for the FB case indicated that the currently employed 5 mm isotropic margin may be insufficient to ensure adequate coverage of the GTV in 90% of the patient population.

5. Conclusion

Margin optimisation can help reduce toxicity risks while preserving tumour control probability. An understanding of uncertainty sources also informs protocol standardisation, improving consistency and safety across SABR treatments.

6. References

1. Tudor GSJ, Bernstein D, Riley S, Rimmer Y, Thomas SJ, van Herk M, et al. Geometric uncertainties in daily online IGRT: refining the CTV-PTV margin for contemporary photon radiotherapy. Br Inst Radiol 2020.
2. Gordon, J. J. and Siebers, J. V. Convolution method and CTV-to-PTV margins for finite fractions and small systematic errors. Phys Med Biol 2007; 52(7): 1967-90
3. Van Herk *et al.* The probability of correct target dosage: dose-population histograms for deriving treatment margins in radiotherapy, Int J. Radiation Oncology Biol. Phys 2000; 47(4):1121-1135
4. Peulen, H., Belderbos, J., Guckenberger, M., Hope, A., Grills, I., van Herk, M. and Sonke, J. J. Target delineation variability and corresponding margins of peripheral early stage NSCLC treated with stereotactic body radiotherapy. Radiother Oncol 2015; 114(3): 361-6
5. Ehrbar S, Schrader M, Marvaso G et al. Intra- and inter-fraction breath-hold variations and margins for radiotherapy of abdominal targets. Phys and Im in Rad Oncol 2023. https://doi.org/10.1016/j.phro.2023.100509
6. British Institute of Radiology Working Party. Geometric Uncertainties in Radiotherapy: Defining the Planning Target Volume. The British Institute of Radiology. 2003

Engaging radiation safety podcasts available **24/7 on any device!**

Integration of Generative AI in Radiation Safety Training

Eloise Gault, Susan Maguire, Eamon Loughman, Melissa Gunnoo
Department of Diagnostic Imagining and Nuclear Medicine, Mater Private Network

Objective

To pilot AI-generated podcast-style radiation safety refresher training on an e-learning platform and evaluate staff uptake.

Introduction

Radiation protection training is a legislative requirement for hospital staff working with ionising radiation.[1]

Conventional training relies on in-person sessions, which are constrained by clinical workload, shift patterns.

AI-generated podcasts on e-learning platforms supplement radiation safety training[2] while reducing in-person demands on medical physics staff.

The use of multimodal learning has the potential to improve knowledge retention compared to the use of traditional slide decks.[3]

Methods

Existing Training Material (Slide Decks)
↓
AI Summarisation using LLM (Perplexity AI)
↓
Podcast Generation (Google Notebook LM)
↓
Podcast Editing (Microsoft Clipchamp)
↓
Upload to E-Learning Platform (LearningMate)
↓
Staff Complete Training (Inc. Mandatory Assessment)

Large language models (LLMs) within Perplexity[4] summarised existing (non-sensitive) training materials.

The summary was imported into NotebookLM[5] to generate a two-person conversational podcast.

Audio was edited using ClipChamp[6] to produce MP3 podcasts and MP4 videos.

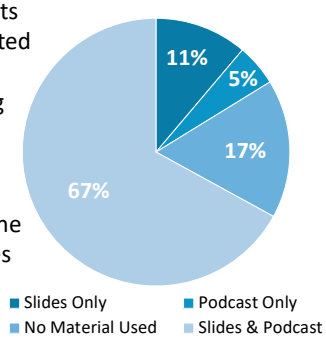
Once uploaded to LearningMate[7], staff could pick their preferred learning format (podcast, video and/or slides) and were required to complete a short assessment to pass the module.

Results

Uptake of AI-Generated Materials

72% of participants selected AI-generated content as their primary learning format.

17% did not use the training resources provided.



Learning Outcomes

Assessment pass rates were **48%** higher for participants who used AI-generated learning materials compared to those who did not use training materials provided.

User Feedback

Verbal feedback highlighted 24/7 access, availability on multiple devices and the option to learn in shorter segments as key advantages.

Workload Impact

Transitioning from in-person radiation refresher sessions to the e-learning module is projected to reduce annual medical physicist teaching time by over **60%**.*

**(based on current workload)*

Cost Analysis

By utilising free versions of generative AI software, and ClimpChamp accessed through the hospital Microsoft 365 licence, the only cost of providing these materials is included within budgeted staff time.

Conclusion

AI-generated multimedia was preferred over slide-only training and was associated with higher module pass rates.

Although initial development required staff time, the e-learning approach has the potential to substantially reduce recurring in-person teaching demands for medical physics staff.

Clinical Impact

Facilitates flexible, on-demand access to radiation safety education.

Promotes a positive radiation safety culture within the hospital while supporting regulatory compliance.

References

[1] Radiological Protection Act 1991 (Ionising Radiation) Regulations 2019 (S.I. No. 30/2019)
[2] Ramsamooj A, et al. Artificial Intelligence Versus Traditional Learning in a Medical Education Setting. Cureus. 2025;17(6):e62079.
[3] Garner K, Fang DV. Impact of Podcasting on First-Year Medical Student Note-Writing Skills. Medical Science Educator. 2015;25(3):379-384.
[4] Perplexity, Perplexity AI. Accessible at https://www.perplexity.ai/
[5] NotebookLM, Google. Accessible at https://notebooklm.google/
[6] ClipChamp, Microsoft. Accessible at https://clipchamp.com/en/
[7] LearningMate, Straive. Accessible at https://learningmate.com/

Mater Private Network

Development and Validation of a Python-Based Tool for CT Electron Density Phantom Analysis in Routine QA

Lisa Rebello, Christopher Walker, Eamonn Hayes

Medical Physics (Radiotherapy) Department, Cork University Hospital

Introduction

- **Hounsfield Units (HU)** correlate with **electron density (ED)**, enabling CT-based dose calculation in radiotherapy.
- Manual region of interest (ROI) analysis are used in routine QA .
- Automation of QA analysis can improve **efficiency, reproducibility** and **standardization** in QA workflow.
- Python **Pylinac script** was developed to automate ED analysis of the **CIRS 062M ED Phantom**.
- Study aim: **Develop and Validate** the automated workflow.

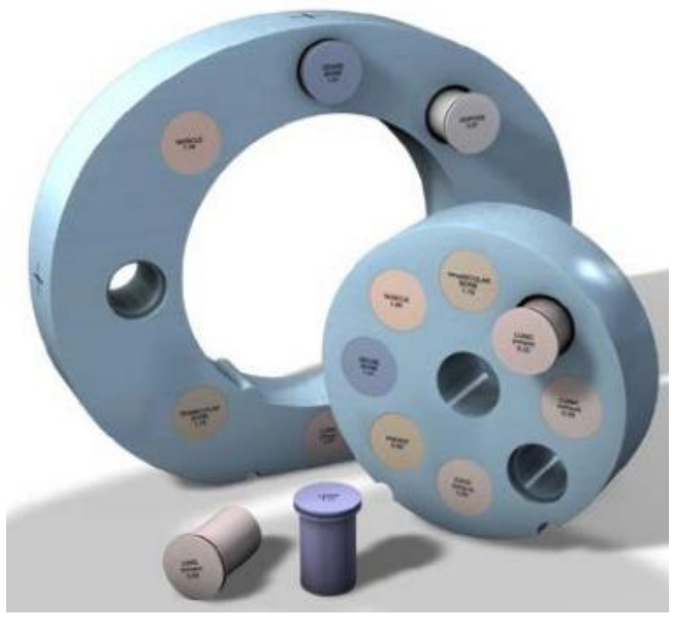


Figure 1: CIRS 062M Electron Density Phantom

Methodology

Baseline Measurement

- Established during commissioning using **manual method**
- CT **ROI tool** used ≈ **150 mm²**

Data Acquisition

- CT images acquired on **Two GE Discovery RT CT scanners**
- 6 scans performed in **Axial** and **Helical acquisition modes** per scanner
- Total **24 image-sets**, **408 ROI measurements** were analysed

Automated Analysis

- Python script using Pylinac was developed
- Automated phantom detection and roll correction
- Automated **ROI extraction**
- **Mean HU** and Standard deviation (SD) calculation for **17 inserts**

Validation

- Statistical comparison performed between:

  (1) **Manual vs Baseline** (2) **Python vs Baseline**

- Statistical significance evaluated using **p-values**

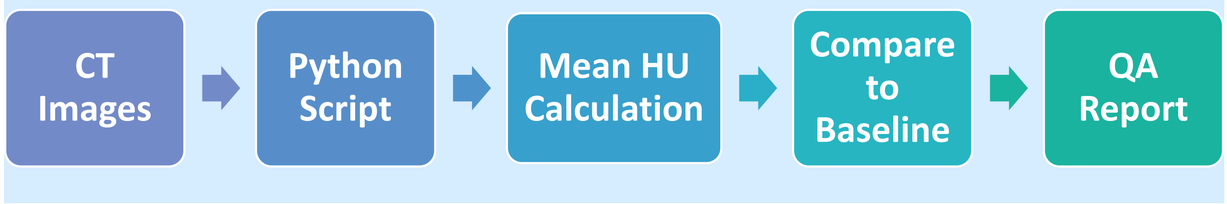


Figure 2: Automated QA Workflow

Results

- Python script successfully analysed **24 image-sets i.e. 408 ROIs**.
- One-way ANOVA produced **p-values** between **0.5 and 1.0**.
- No statistically significant differences observed between:

  (1) **Manual vs baseline** measurements

  (2) **Python vs baseline** measurements
- For all 17 ROIs, Python-derived values were within **± 20 HU** of the commissioning baseline.
- Exception observed in **Bone insert (1250 HU)** - 3/6 helical scans on one scanner exceeded tolerance by 2 HU.
- Deviation attributed to minor bias from manual ROI placement to avoid streak artifacts.

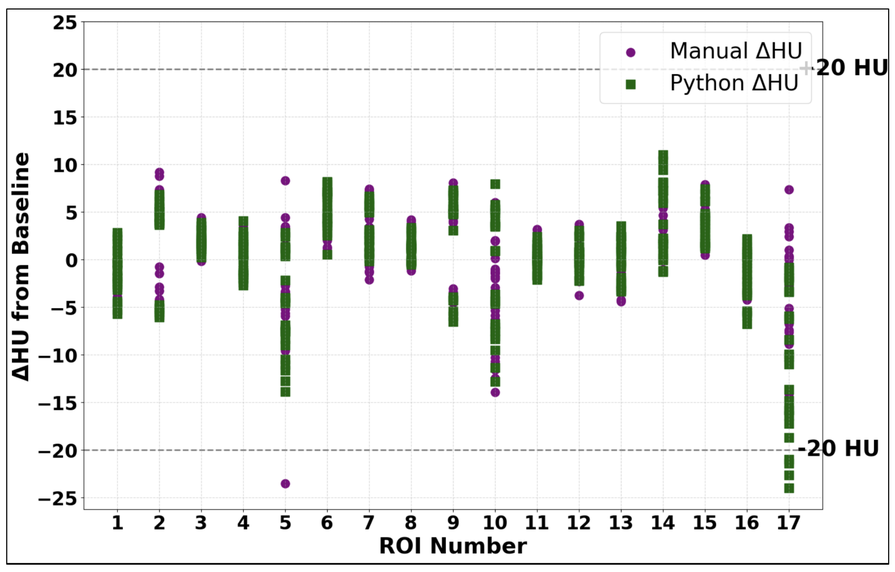


Figure 3: HU difference from baseline for manual and Python-derived measurements across 17 inserts

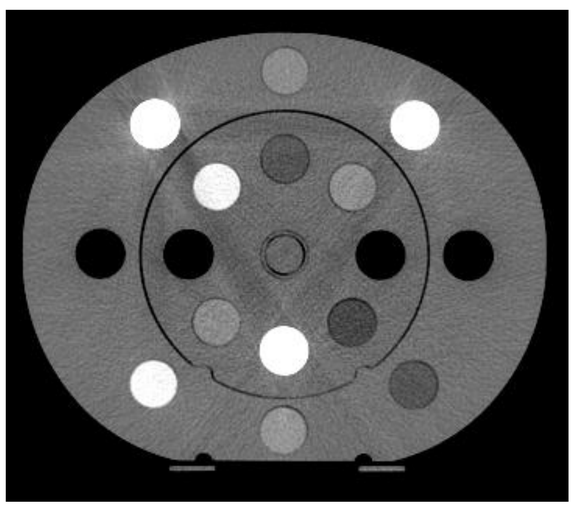


Figure 4: CT image showing streak artifact from high- density bone insert



Figure 5: Automated ROI detection using Python script

Conclusion

- The developed Python-based Pylinac script provides HU values statistically equivalent to manual ROI analysis relative to the commissioning baseline.
- Key advantages include: **(1) Reduced operator dependence**
  (2) Improved workflow efficiency
  (3) Consistent and reproducible measurements
- The validated workflow demonstrates potential as a reliable **automated tool** for **routine CT QA**.
- This supports standardized electron density verification in radiotherapy imaging.

References

1. Constantinou C., Harrington J.C., DeWerd L.A., *An electron density calibration phantom for CT-based treatment planning computers*, Med Phys, 1992.
2. Kerns J.R., *Pylinac: Image analysis for routine quality assurance in radiotherapy*, JOSS, 2023.

Department of Medical Physics (Radiotherapy), The Glandore Centre, Cork University Hospital, Wilton, Cork, T12DC4A
Corresponding Author: Lisa Rebello
Email: *Lisa.Rebello@hse.ie*

Cork University Hospital | University College Cork, Ireland Coláiste na hOllscoile Corcaigh

Feidhmeannacht na Seirbhíse Sláinte Health Service Executive

Reducing Time to Treatment in Radiotherapy Through AI-Based Auto-Contouring and Patient Scheduling

M. Roche, M. Healy, P. Coen, M. Moran, RB. Ezhilalan, E. McGrath, O. McKivitt, V. Keating, M. Hussey, M. Higgins
Department of Radiation Oncology, CUH/UCC Cancer Centre, Co. Cork.

INTRODUCTION

Real world contouring task times using AI-based systems have been published.

Improved efficiencies have been reported, in contouring task and contouring workflow times.[1,2]

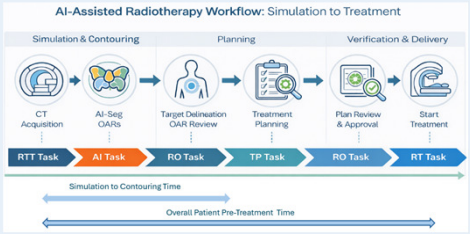


Figure 1 Tasks in an AI-assisted radiotherapy workflow.

Do these efficiencies translate into faster patient pre-treatment pathways?

This has been challenged[2]. This study aims to identify if AI-based contouring and optimised patient scheduling can be used to accelerate the treatment pathway.

MATERIALS & METHODS

Workflow Audit

Workflow data was retrospectively evaluated over three years (2023-2025), before and after the introduction of the MVision Contour+ auto-contouring software. Data evaluated included radiotherapy schedules for 3722 patients.



Elekta MOSAIQ® Quality Check List (QCLs)

Task completion times were recorded from the QCLs available from the department oncology information system (OIS) MOSAIQ®. The QCL records a timestamp for every key step in the radiotherapy workflow including:

- CT Import Complete
- Contouring Complete
- Planning Complete
- First Treatment # Complete

Evaluated Data

The contouring workflow time and the overall CT to fraction 1 completion interval were evaluated pre/post implementation of the auto-contouring software.

MVISION
- AI for Precision Radiotherapy -

RESULTS

Workflow time: CT import to contouring complete

The mean contouring time went from 5.2 ± 5.1 calendar days (95% CI 4.9 to 5.5) in 2023 before auto-contouring to 3.9 ± 3.8 days (95% CI 3.7 to 4.1) and 3.7 ± 3.7 days (95% CI 3.4 to 3.9) in 2024 and 2025 respectively, post implementation of MVision Contour+™

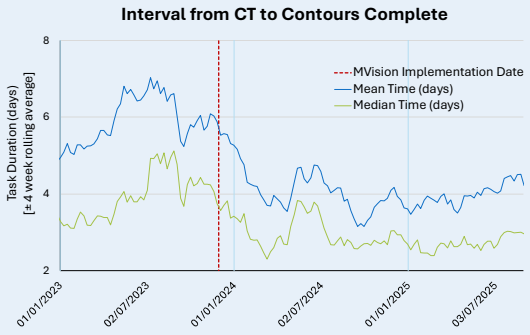


Figure 2 Workflow times from CT to completion of RO contour review. Mean time (blue), median time (green), calendar days.

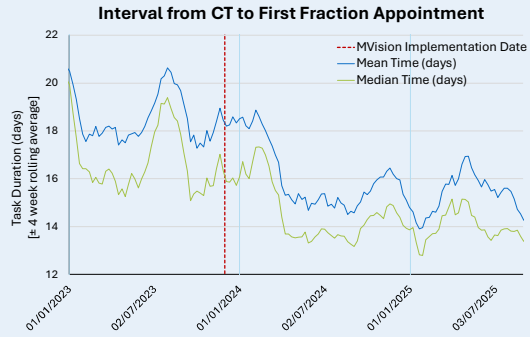


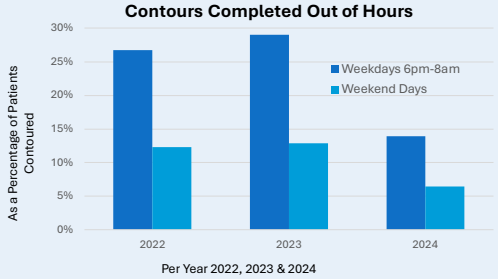
Figure 3 Workflow times from CT to first fraction completion. Mean time (blue), median time (green), calendar days.

Workflow time: CT import to #1 completion

The mean CT to treatment interval was 17.1 ± 8.1 calendar days (95% CI 16.6 to 17.6) in 2023 compared to 15.6 ± 6.8 days (95% CI 15.3 to 16) and 14.8 ± 6.7 days (95% CI 14.4 to15.2) in 2024 and 2025 respectively.

Contours completed outside of hours

The percentage of contours completed out of hours, weekdays from 6 pm to 8 am and weekend days, decreased from 42% in 2023 to 18% across 2024/2025.



DISCUSSION

Reducing time to treatment

- The mean and median contouring times reduced immediately post introduction of MVision Contour + ™.
- The mean and median time to completion of #1 reduced 4 weeks post the introduction of Mvision Contour+.

CONCLUSIONS

Delays in radiotherapy

Can be associated with an increased risk of local recurrence.

Optimising patient start dates

Patient start dates in CUH are set when treatment planning is completed.



Faster simulation to 1st # treatment

This study has shown that the overall CT to treatment interval can be reduced with AI-based OAR contouring and optimised scheduling of patient start dates post treatment planning.

REFERENCES

1. Langmack KA, Alexander GG, Gardiner J, McKenna A, Shawcroft E. An audit of the impact of the introduction of a commercial artificial intelligence-driven auto-contouring tool into a radiotherapy department. Br J Radiol.2023;96(1145):20230023.
2. Malone C, Nicholson J, Ryan S, Thirion P, Woods R, McBride P, et al. Real world AI-driven segmentation: Efficiency gains and workflow challenges in radiotherapy. Radiother Oncol. 2025 Aug;209:110977.doi:10.1016/j.radonc.2025.110977 Epub 2025 Jun 3.

CONTACT

Michael Roche
Principal Physicist - Advanced Therapies
Floor 2, The Glandore Centre, Cork University Hospital, Wilton Road, Cork
T12 DC4A

michael.roche1@hse.ie
021-4234830

Cork University Hospital | University College Cork, Ireland, Coláiste na hOllscoile Corcaigh

Feidhmeannacht na Seirbhíse Sláinte, Health Service Executive

Initial evaluation of an AI-based GTV segmentation tool for SRS treatment planning.

M. Roche, P. Hill, M. Healy, P. Coen, S. Kelleher, M. O'Cathail, M. Higgins
Department of Radiation Oncology, CUH/UCC Cancer Centre, Co. Cork.

INTRODUCTION

AI based tools for GTV delineation are becoming clinically available.

Artificial intelligence (AI) based tools are routinely used for OAR delineation[1,2] however GTV delineation is currently widely performed by ROs.



c.50 SRS
patients treated in CUH in 2025

GTVs
currently manually contoured for each patient by the RO.

AI-GTV accuracy assessment

This study assesses the accuracy of the Brainlab Elements AI-Tumor Segmentation tool on GTV delineation for SRS treatment planning.

MATERIALS & METHODS

Brainlab Elements AI Tumor Segmentation Tool

Is a AI / machine learning (ML) tool for segmentation of one or multiple cranial tumours within a patient 3D contrast-enhanced T1-w MRI scan. The algorithm does not adapt or change once deployed.

BRAINLAB

Cranial metastases AI-GTV evaluation

The AI model was used to retrospectively segment 32 cranial metastases from 19 patients treated with SRS at CUH in 2025. Contrast enhanced T1-w FSPGR MR images were used in each case.

Each GTV was automatically contoured and PTV margins were applied as per department procedures. Volume based and Dice (DSC) analysis were used to compare the AI segmented GTVs and PTVs to the original approved by the RO for the clinical treatment plan. Followed by an independent qualitative review by the RO, blinded from the original clinical GTV.

REFERENCES

1. Langmack KA, Alexander GG, Gardiner J, McKenna A, Shawcroft E. An audit of the impact of the introduction of a commercial artificial intelligence-driven auto-contouring tool into a radiotherapy department. Br J Radiol. 2023;96(1145):20230023. doi:10.1259/bjr.20230023.

2. Malone C, Nicholson J, Ryan S, Thirion P, Woods R, McBride P, et al. Real world AI-driven segmentation: Efficiency gains and workflow challenges in radiotherapy. Radiother Oncol. 2025 Aug;209:110977.doi: 10.1016/j.radonc.2025.110977 Epub 2025 Jun 3.

RESULTS

Rad. Onc. Qualitative Review Results

Results from the qualitative review of the 32 cranial metastases indicate that AI-GTVs are clinically acceptable 78% of the time. However, there were some cases where the contours drawn were not acceptable (19%). Feedback indicated that this was typically due to low contrast uptake.

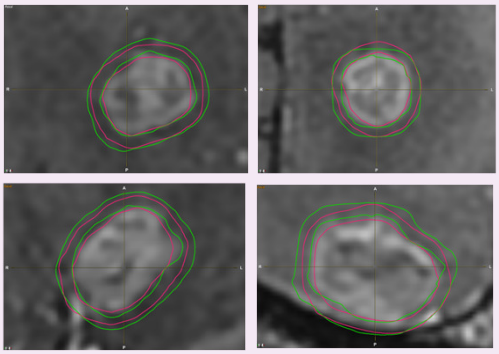


Figure 1: Independent AI-GTV/PTV structures (pink) compared to those used for clinical plans (green).

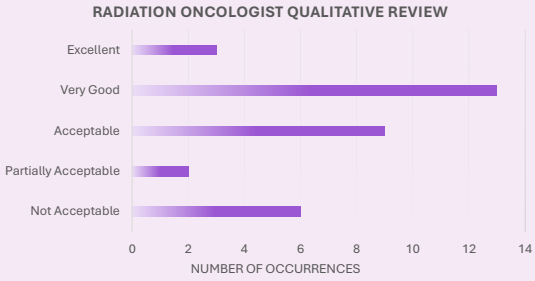


Figure 2: Score assigned to AI-generated GTVs by a Radiation Oncologist during qualitative review.

AI-Generated GTV: RO Feedback

In the majority of cases the AI-GTVs were smaller than that specified by the RO, with only 3 cases where no change to the GTV was required.

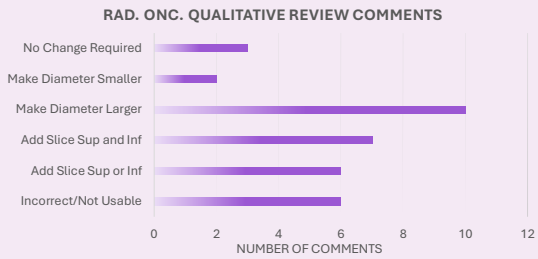


Figure 3: Recommendations provided by a Radiation Oncologist during qualitative review.

Quantitative Evaluation Results

For GTVs below 4 cc (n=27), the mean volume decreased from 1.59 cc ± 1.65 cc to 1.15 cc ± 1.20 cc with the AI-segmentation software volume smaller for every patient.

Similarly, final PTV volumes reduced from 3.27 cc ± 1.65 cc to 2.30 cc ± 1.20 cc. This is equivalent to a mean reduction in PTV diameter of 12% ± 8%

RESULTS

Quantitative Evaluation Results

or 1.91 mm ± 0.95 mm when using the AI-segmentation tool with no edits compared to RO only delineation. The mean DSC score for the AI-segmented GTVs was 0.79 ± 0.10 when compared to the RO delineation.

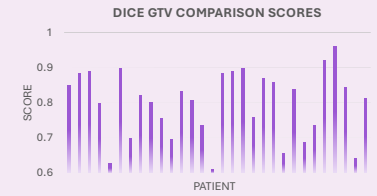


Figure 3: DICE score for AI-GTV comparison with clinically used GTVs

CONCLUSION

Is it clinically useful to have AI-generated GTVs for SRS

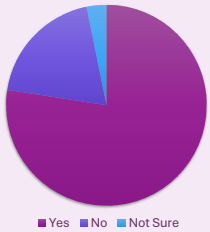


Figure 4: ROs response on the usefulness of AI-GTVs for delineation of brain metastases.

Clinical suitability of AI Cranial GTV Segmentation.

AI-based auto-segmenting tools for GTV delineation are now commercially available, although their routine clinical use is still not widespread.

Independent AI-generated contours produced consistently smaller GTVs and PTVs for SRS treatment planning compared to RO only delineation. This can lead to reduced target diameters for cranial metastases.

These findings currently support Brainlab AI Tumour Segmentation as a tool for assisting SRS GTV delineation, with clinical oversight currently remaining essential.

CONTACT

Michael Roche
Principal Physicist - Advanced Therapies
Floor 2, The Glandore Centre, Cork University Hospital, Wilton Road, Cork
T12 DC4A

michael.roche1@hse.ie
021-4234830

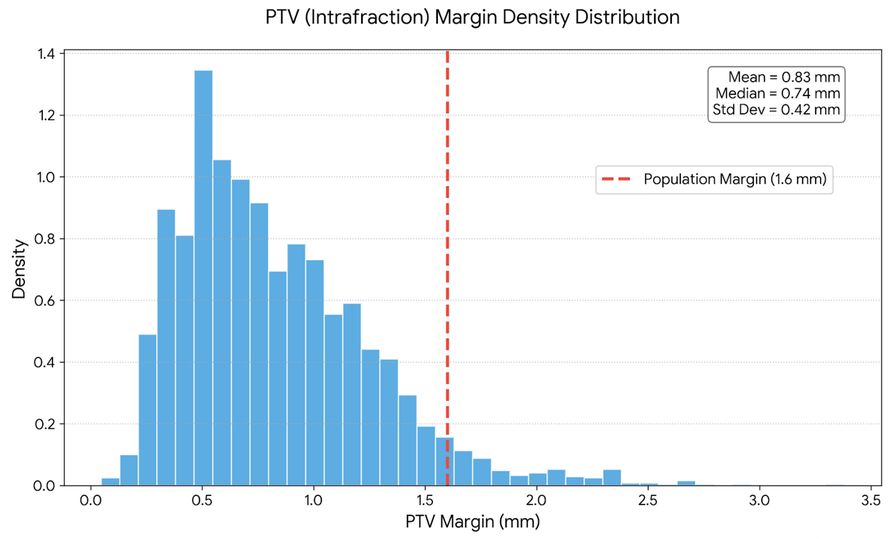
The Value of Uncertainty: Confidence-Based Individualisation of Intrafraction PTV Margins using a Bayesian Neural Network

Ciaran Malone[1,2], Jill Nicholson[2,3], Claire Fitzpatrick[2], Sinead Brennan[2,3], Orla McArdle[2,4], Pat McCavana[2], Frances Duane[2,3], Lorna Keenan[2,4], Ruth Woods[2], B.J.M. Heijmen[1], Gerard G. Hanna[2,5], Brendan McClean[2,6]

1. Erasmus MC Cancer Institute, University Medical Center Rotterdam, Department of Radiotherapy, Rotterdam, Netherlands., 2. St. Luke's Radiation Oncology Network, St. Luke's Hospital, Dublin, Ireland., 3. Applied Radiation Therapy Trinity, Discipline of Radiation Therapy & Trinity St. James's Cancer Institute, Trinity College Dublin, Ireland., 4. Beaumont Cancer Institute, Royal College of Surgeons Ireland, Dublin, Ireland., 5. Centre for Physics in Health and Medicine, University College Dublin, Dublin, Ireland., 6.Trinity St. James's Cancer Institute, Trinity College Dublin, Dublin, Ireland.

St Lukes Cancer Research Fund
Charity Ref CHY 5854

Aim: To predict the individual Systematic and Random Components of patient Intrafraction motion using early fraction SGRT data to individualize PTV margins



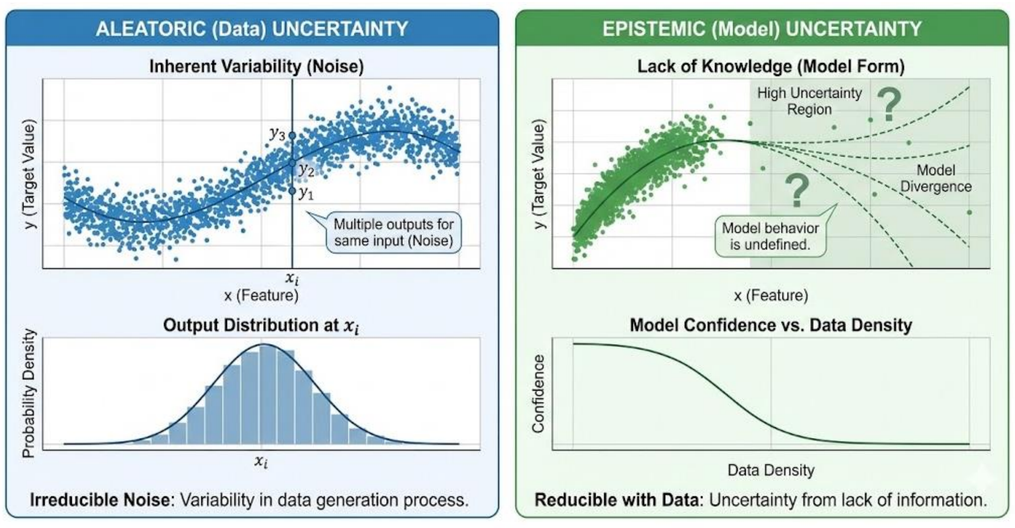


Figure 2: Left: Spread of individual margins with population based margin indicated (red dash) showing few outliers >1.6, and most margins centred around 0.8mm – what we are trying to predict. Right: definitions of Aleatoric uncertainty (e.g. measurement noise), and Epistemic Uncertainty (e.g. due to lack of data)

The problems:

1. We are predicting across a very narrow range 0.8mm +/- 0.4mm relative to the measurement noise. Difficult for the model to learn signal (aleatoric uncertainty).
2. We have a lot of data around the average, but few data to steer the model at the extremes >1.6mm (epistemic uncertainty)

The need: A human centered intuitive solution: one that indicates when the model is sure, and when it is not sure – helping effective oversight & highlighting unusual cases. End-users may not understand how models make decisions, but will understand a prediction with an error bar more intuitively.

The solution: Bayesian Neural Network (BNN) ***(Figure 3)*** consisting of an input layer accepting four standardized features, a single hidden layer (32 neurons), and four parallel output branches. **The four inputs:** The Systematic Error(Σ_n, mm) and Random Error (σ_n, mm) which are fraction aware, and 2 overall motion features across N features: Mean vector Magnitude (mm) and Standard deviation of vector magnitude. **Outputs:** the final systematic (Σ) and random (σ) components of motion and their respective patient specific noise terms (Σ_σ, σ_σ). The final output: A deterministic final margin (M = 2.5Σ + 0.7σ) delivered with a 95% credible interval of likely margins.

The benefit of this approach: Unlike traditional models that rely on fixed point-estimates for weights and biases, the Bayesian network learns a full distribution of likely parameters, explicitly capturing model confidence (epistemic uncertainty). It also learns patient-specific noise parameters (Σ_σ, σ_σ) to define a robust Student-T likelihood distribution for each component. By drawing samples from these distributions (Σ_{noisy}, σ_{noisy}) and plugging them directly into the margin formula, the model generates a comprehensive credible interval that inherently accounts for both patient (aleatoric) and model (epistemic) uncertainty.

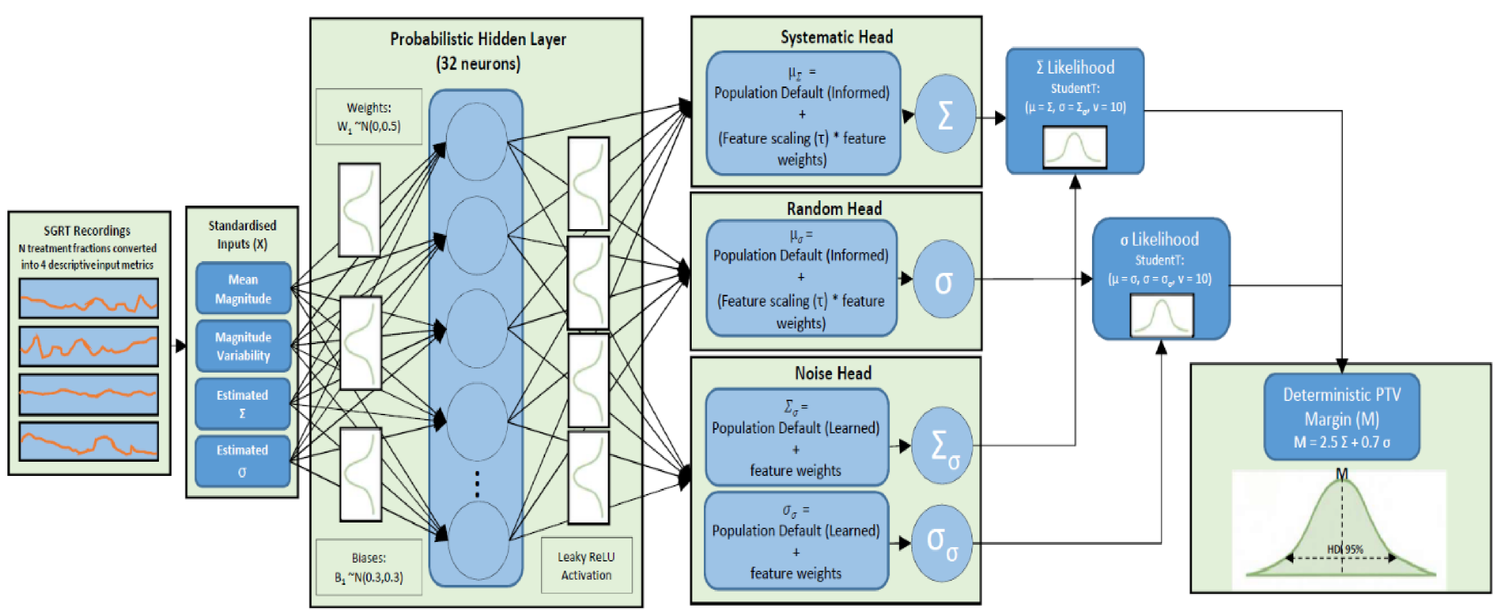


Figure 3: BNN architecture used including 4 inputs, 32 neuron hidden layer with learnable distributions for weights & bias parameters, four output heads and StudentT likelihood functions

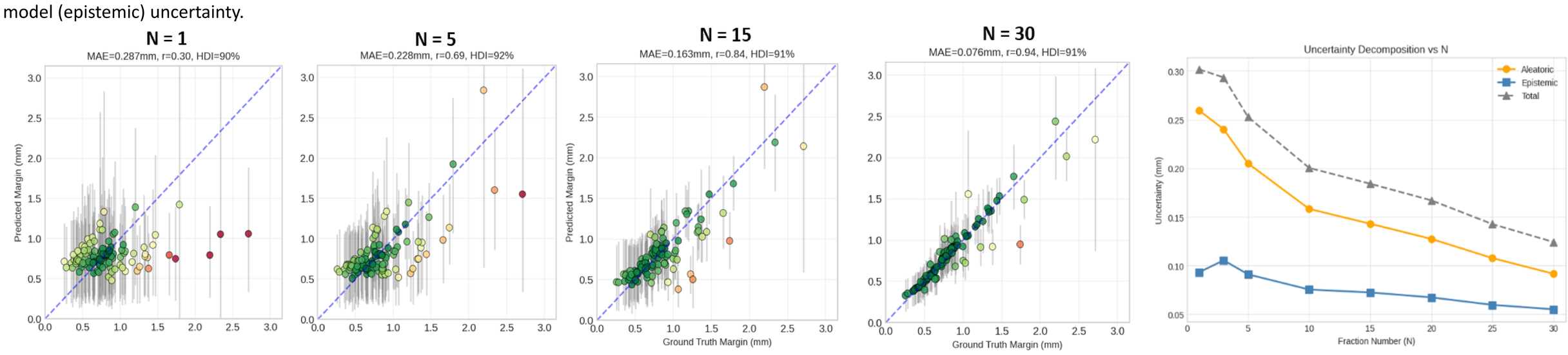
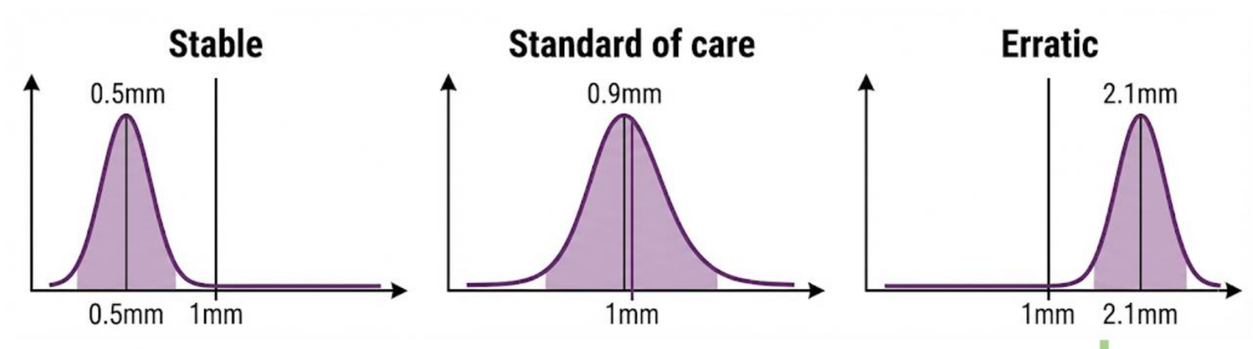


Figure 4: Left: Ground truth (x-axis) versus BNN-predicted PTV margins (y-axis) for different values of N fractions with credible intervals representing total uncertainty (Aleatoric & Epistemic), Right: Uncertainty Decomposition vs. N fractions of data.

Model Evaluation Results: At N=1: The model shows poor agreement (r=0.30), defaulting to a population-average baseline with wide uncertainty intervals. At N=5–10: Agreement improves (r=0.70–0.83) and uncertainty intervals become patient-specific. It's now possible to identify patients for potential margin reduction, and erratic patients for potential intervention. At N≥15: The model approaches deterministic accuracy (r >0.84). ***Figure 4 (right):*** Total Uncertainty (grey triangles) falls quickly with increasing number of fractions (N) and is dominated by Aleatoric uncertainty (orange circles), which drops significantly as the model learns to distinguish measurement noise from true patient instability. Epistemic uncertainty (blue squares) remains consistently low.



Clinical Category	HDI Criterion	N (%)	Accuracy	Clinical Action
Margin Reduction Possible	HDI_High < 1.0 mm	25 (24%)	84% correct	Reduced margin appropriate
Standard Margin	HDI spans 1.0 mm	74 (70%)	—	Use population margin
Margin Increase Required	HDI_Low > 1.0 mm	6 (6%)	100% correct	Increased margin needed

Total Actionable: 31 patients (30%) could receive personalised margins with high confidence.

Clinical Utility Results: Uncertainty-guided stratification for personalised margin selection is possible within 5-10 fractions. Patients were classified based on the position of their 95% credible interval relative to a 1.0 mm clinical threshold: margin reduction is recommended when the interval upper bound (HDI_High) falls below threshold; margin increase is recommended when the interval lower bound (HDI_Low) exceeds threshold; standard population margin is recommended when the interval spans the threshold. 30% of patients actionable for personalized margins.

Conclusion: We demonstrated that Bayesian neural networks offer clinical utility for personalised H&N PTV margin prediction by explicitly quantifying predictive uncertainty alongside point estimates. Our results indicate that clinically actionable predictions are achievable after just 5-10 fractions, allowing for early, confident margin reduction to reduce toxicity in stable patients, while simultaneously flagging erratic outliers for extended monitoring. This approach bridges the gap between complex AI and clinical practice: by presenting uncertainty as an intuitive credible interval, it empowers the clinical team in making risk-informed decisions without requiring specialized knowledge of neural network architectures.